

8-27-2009

Mesozoic tectonics of the Maria fold and thrust belt and McCoy basin : an examination of polyphase deformation and synorogenic response

Anthony C. Salem

Follow this and additional works at: https://digitalrepository.unm.edu/eps_etds

Recommended Citation

Salem, Anthony C.. "Mesozoic tectonics of the Maria fold and thrust belt and McCoy basin : an examination of polyphase deformation and synorogenic response." (2009). https://digitalrepository.unm.edu/eps_etds/75

This Dissertation is brought to you for free and open access by the Electronic Theses and Dissertations at UNM Digital Repository. It has been accepted for inclusion in Earth and Planetary Sciences ETDs by an authorized administrator of UNM Digital Repository. For more information, please contact disc@unm.edu.

Anthony Christopher Salem

Candidate

Earth and Planetary Sciences

Department

This dissertation is approved, and it is acceptable in quality and form for publication:

Approved by the Dissertation Committee:

Karl E Karstner

, Chairperson

Yunmei Asmussen

Thomas J. Hourin

Stephen J. Meyre

**MESOZOIC TECTONICS OF THE MARIA FOLD AND THRUST
BELT AND MCCOY BASIN, SOUTHEASTERN CALIFORNIA: AN
EXAMINATION OF POLYPHASE DEFORMATION AND
SYNOROGENIC RESPONSE**

BY

ANTHONY CHRISTOPHER SALEM

B.S., Arizona State University, 1999
M.S., Geological Sciences, Arizona State University, 2005

DISSERTATION

Submitted in Partial Fulfillment of the
Requirements for the Degree of

Doctor of Philosophy

Earth & Planetary Sciences

The University of New Mexico
Albuquerque, New Mexico

August, 2009

©2009, Anthony C. Salem

DEDICATION

For Audrey, my best friend, chief advisor, drill sergeant, sounding board, editor extraordinaire, GIS wizard, partner in crime and great love. Without her love and support, life and this work would have been a lonely endeavor.

ACKNOWLEDGMENTS

All the work that goes into conducting research and writing a dissertation may be indeed done by one person, but is actually the result of the efforts and support of many people who should be acknowledged. First of all, I would like to thank Karl Karlstrom, my dissertation advisor. Through his interactive and engaging style of advisement, his broad manner of thinking about geology, especially the disciplines of structural geology and tectonics, his seemingly never-ending supply of energy, enthusiasm and ideas and his high expectations, he challenged me to become a better geoscientist and encouraged me to bring out as much as I could about the geology of this interesting part of the Cordillera. He has been a great mentor and good friend. I would also like to thank Steve Reynolds from Arizona State University, who introduced me to the geology of the Maria Fold and Thrust Belt and was advisor for my master's thesis. I would not have made it this far without his initial encouragement and continued guidance and support throughout my studies. Thanks to the support of the rest of my dissertation committee: Yemane Asmerom and Lou Scuderi, and Tom Hoisch from Northern Arizona University, for their support, guidance and discussions. Thanks to Barry Kues for serving as outside examiner for my comprehensive exams. Special thanks to Jeff Geier and Bryan MacFarlane, for their many hours of help in the field, discussion and idea exchanges, map compilation and friendship. Special thanks also to Laurie Crossey for her kindness, warmth, help in the field and excellent photography. Thanks to Hope Johnston, Mark Tyra, David Haddad, Ryan Crow, Magdalena Sandoval and Austin Zinnser for their help in the field. Matt Heizler, Lisa Peters and Josh Feldman assisted greatly with Ar-Ar geochronology; Matt in particular deserves special thanks for all his help with obtaining and reporting Ar-Ar hornblende and biotite ages for this study. George Gehrels and the rest of Arizona LaserChron lab crew at the University of Arizona Tucson deserve thanks for making available the Laser Ablation ICP-MS facility at UA and assisting me with all stages of data collection and analyses in obtaining and reporting U-Pb zircon ages. This dissertation benefited from discussions with Paul Stone, Carl Jacobson, Dick Tosdal and Jon Spencer about the geology of the Maria Fold and Thrust Belt and McCoy Basin. Thanks to the Department of Earth & Planetary Sciences at UNM for giving me a place to work and providing financial support for my time here. Cindy Jaramillo and the rest of the office staff in the department never receive enough gratitude for helping me and my colleagues navigate the UNM bureaucracy. Finally, thanks go to my friends and family, especially my parents, Jim and Phyllis Salem, my sisters Shelley Pajak, Dana Salem-Silva and Theresa Thornburgh, my brother Marc Salem, my stepdaughter Rebecca Hamilton and my stepson Ali Al-Ali for all their love, support and patience during these past four years.

Financial support provided by the National Science Foundation (NSF GK-12 EMRGE program grant EHR-0538396 to L.J. Crossey and S. Collins, the Geological Society of America (GSA Student Research Grant, 2008 to Salem). K. Karlstrom and the Department of Earth Planetary Sciences at UNM aided in funding presented research.

**MESOZOIC TECTONIC OF THE MARIA FOLD AND THRUST BELT
AND MCCOY BASIN, SOUTHEASTERN CALIFORNIA: AN
EXAMINATION OF POLYPHASE DEFORMATION AND
SYNOROGENIC RESPONSE**

BY

ANTHONY CHRISTOPHER SALEM

ABSTRACT OF DISSERTATION

Submitted in Partial Fulfillment of the
Requirements for the Degree of

Doctor of Philosophy

Earth and Planetary Sciences

The University of New Mexico
Albuquerque, New Mexico

August 2009

Mesozoic tectonics of the Maria Fold and Thrust Belt and McCoy Basin: An examination of polyphase deformation and synorogenic response

by

Anthony Christopher Salem

B.S., Business, Arizona State University, 1999

M.S., Geological Sciences, Arizona State University, 2005

Ph.D., Earth and Planetary Sciences, University of New Mexico, 2009

ABSTRACT

Here we summarize all current knowledge about the Maria Fold and Thrust Belt and McCoy Basin tectonic provinces of southeastern California. We also present new geologic mapping, structural analysis from macroscopic to microscopic scale, U-Pb zircon ages and Ar-Ar hornblende and biotite ages from key areas in the Maria Fold and Thrust Belt and McCoy Basin to resolve kinematics and timing of polyphase deformation events related to the Mesozoic Cordilleran Orogeny in southeastern California.

The Maria Fold and Thrust Belt (MFTB) is an east-west trending belt of amphibolite grade metamorphic rocks characterized by largely south-vergent folds and ductile shear zones that place Jurassic and Proterozoic crystalline rocks over Paleozoic and Mesozoic sedimentary and volcanic rocks correlative to strata observed on the Colorado Plateau and in southeastern Arizona. Rocks in the MFTB have undergone polyphase ductile deformation and high grade metamorphism. The McCoy Basin trends subparallel with the MFTB and is defined by exposures of Jurassic-Cretaceous McCoy

Mountains Formation, a > 7 km thick siliciclastic wedge of sandstone, siltstone and conglomerate. In contrast with the MFTB, rocks in the McCoy Basin have undergone primarily brittle deformation and have undergone low grade regional metamorphism. Important questions remain regarding the tectonic evolution of these two tectonic provinces, the relationship of these two provinces to each other and their relationship to the Cordillera at large. Resolving kinematics and timing of polyphase deformation in the MFTB and assessing synorogenic response in the McCoy Basin using established and new methods of structural geology and geochronology will resolve these questions and illuminate fundamental geologic processes related to orogenesis.

This dissertation is divided into three chapters, with the goal of assessing kinematics and timing of deformation in the MFTB and McCoy Basin. A general encompassing hypothesis for investigations is that sedimentation and later deformation of rocks in the McCoy Basin can be directly linked to Mesozoic polyphase deformation in the MFTB. Structural analysis of key areas shows that there are three deformation events in the MFTB-McCoy Basin region. D_1 is characterized by initially subrecumbent isoclinal folds and shear zones and a north-dipping foliation designated S_1 . D_2 is characterized by mesoscopic and macroscopic southwest-facing isoclinal folds that refold S_1 and shear zones that imbricate and severely attenuate Paleozoic and Mesozoic strata (to less than 1% of original stratigraphic thickness). Analysis of kinematic indicators including elongate mineral lineation, stretched pebbles and concretions and microstructural textures indicates that D_1 and D_2 represent two stages of a single progressive deformation event formed by top-to-the-southeast-directed reverse and dextral shear. A diorite deformed by D_1/D_2 yields an U-Pb zircon age of 86.3 ± 1.3 Ma, indicating that D_1/D_2 represents Late

Cretaceous deformation. Published detrital zircon ages indicate that sedimentation in the McCoy Basin was coeval with middle crustal deformation in the MFTB. Kinematics of D_1/D_2 suggests that this event is related to the Sevier Orogeny and timing of deformation is consistent with other regional studies. The tectonic setting of the McCoy Basin is interpreted to have evolved from a broad Late Jurassic-Early Cretaceous rift valley to a Late Cretaceous retroarc foreland basin. The geometry of the early rift basin placed important structural controls on the geometric and spatial configurations of the Late Cretaceous MFTB and McCoy Basin. D_3 is characterized by northeast-vergent folds and shear zones and is coeval with emplacement of Late Cretaceous (79-67 Ma) granites and pegmatites, which crosscut D_1/D_2 fabrics. Strain field analysis of dikes and quartz veins and kinematic analysis of the Granite Mountains metamorphic core complex and the geometry of D_3 folds and shear zones indicates that D_3 formed as a result of northeast-directed synconvergent extension. D_3 is also coeval with peak metamorphism in the region, which is confirmed by Ar-Ar ages of hornblende of ~70 Ma. At this time, the MFTB was emplaced over the McCoy Basin along the south-vergent Maria Frontal Thrust. The kinematics and timing of D_3 deformation suggest that it is related to the Laramide Orogeny and supports the hypothesis that the change from Sevier to Laramide tectonism in the region is marked by a reorientation of the principal stress field and a change from compression to extension in the Sevier hinterland. The main phase of orogenic activity ended by ~55 Ma, based on biotite Ar-Ar ages, which is consistent with regional observations.

Compilation of previously published and unpublished mapping as well as other types of geologic data was an integral part of this investigation. Regional maps were

compiled from a single digital archive that may be readily shared and distributed to the scientific community at large.

TABLE OF CONTENTS

ACKNOWLEDGMENTS	V
ABSTRACT.....	VII
LIST OF FIGURES	XV
LIST OF TABLES	XXI
PREFACE.....	XXII
Chapter 1 : Structural evolution of the Big Maria syncline: Polyphase ductile deformation in response to progressive Sevier-Laramide tectonism in the Maria Fold and Thrust Belt, SE California	1
Chapter Abstract	1
Introduction.....	2
Tectonic Setting.....	4
Geologic background of the Big Maria Mountains	13
Paleozoic stratigraphy and degree of stratal attenuation.....	19
Structural geology	25
<i>Methods.....</i>	<i>25</i>
<i>Macroscopic structures.....</i>	<i>27</i>
<i>Area A – S₁ dominated domain along attenuated limb of the syncline</i>	<i>37</i>
<i>Area B – S₁ dominated hinge zone of the Big Maria syncline</i>	<i>47</i>
<i>Area C – D₁₋₂/D₃ overprinting</i>	<i>51</i>
<i>Microstructural analysis/Sense of shear analysis.....</i>	<i>66</i>
Discussion	72
<i>Kinematics and timing of polyphase deformation events</i>	<i>72</i>
<i>Summary of Mesozoic tectonic events.....</i>	<i>81</i>

Summary.....	84
Chapter 2 : Tectonic linkages between the middle crustal Maria Fold and Thrust Belt and upper crustal McCoy Basin, southeastern California: Implications for the Mesozoic tectonic evolution of the North American Cordillera	86
Chapter Abstract	86
Introduction.....	88
Tectonic setting.....	94
Previous Work.....	101
Regional stratigraphy and chronologic framework.....	114
<i>Proterozoic crystalline rocks</i>	<i>115</i>
<i>Cambrian Tapeats Quartzite</i>	<i>117</i>
<i>Cambrian Bright Angel Schist</i>	<i>118</i>
<i>Cambrian Muav Marble</i>	<i>119</i>
<i>Devonian Temple Butte Formation.....</i>	<i>120</i>
<i>Mississippian Redwall Marble.....</i>	<i>121</i>
<i>Pennsylvanian-Permian Supai Formation.....</i>	<i>122</i>
<i>Permian Hermit Formation</i>	<i>123</i>
<i>Permian Coconino quartzite</i>	<i>123</i>
<i>Permian Kaibab Marble</i>	<i>124</i>
<i>Triassic Buckskin Formation</i>	<i>125</i>
<i>Triassic-Jurassic Vampire Formation</i>	<i>127</i>
<i>Jurassic Aztec Quartzite</i>	<i>129</i>
<i>Jurassic volcanic rocks</i>	<i>130</i>
<i>Jurassic plutonic rocks</i>	<i>131</i>
<i>Jurassic-Cretaceous McCoy Mountains Formation.....</i>	<i>133</i>

Sediments derived from quartz porphyry and Basal Sandstone 1	134
Basal Sandstone 2	136
Mudstone Member	137
Conglomerate Member	138
Sandstone Member.....	141
Siltstone Member	142
<i>Cretaceous plutonic rocks</i>	143
<i>Cenozoic sedimentary and volcanic rocks</i>	145
Structural geology	146
<i>Overview</i>	146
<i>Methods</i>	146
<i>McCoy Mountains</i>	147
Structural overview	147
Domain analysis.....	155
Microstructures	169
Quartz vein analysis	169
Regional analysis – Little Maria Mountains to McCoy Mountains	174
<i>Palen Pass</i>	178
Structural overview	178
Domain analysis.....	188
Regional analysis – Granite Mountains to southern Palen Mountains	202
Geochronology	203
<i>Overview</i>	203
<i>Methods</i>	204
<i>U-Pb zircon ages of magmatic rocks of the Big Maria Mountains</i>	207

<i>Ar-Ar hornblende and biotite ages of magmatic rocks of the Big Maria Mountains</i>	210
<i>Discussion</i>	213
Discussion of tectonic evolution	223
<i>Late Jurassic to Early Cretaceous: Development of the McCoy rift system and synchronous widespread magmatism (170-100 Ma)</i>	224
<i>Late Cretaceous: Northwest-directed underthrusting of the miogeocline marking the onset of Sevier tectonism (100-80 Ma)</i>	228
<i>Late Cretaceous to Eocene: Laramide tectonism, widespread magmatism, deformation and metamorphism and rapid cooling (80-55) Ma</i>	231
Summary	235
Chapter 3 : A new geologic map of the Maria Fold and Thrust Belt, southeastern California: A digital repository for multiple integrated datasets	237
Introduction	237
Datasets used	239
<i>New high resolution mapping done from 2004-09</i>	240
<i>Pre-existing published and unpublished geologic mapping</i>	240
<i>TIMS and other remote sensing data</i>	240
<i>Metamorphic isograd map</i>	241
Digitization and compilation methods	242
Future directions and summary	243
References	245

LIST OF FIGURES

Figure 1.1: Regional tectonic map of the southwestern U.S.....	5
Figure 1.2: Simplified geologic and tectonic map of the Maria Fold and Thrust Belt and McCoy Basin in southeastern California showing selected important Mesozoic (shown in red) and Cenozoic (shown in black) tectonic elements, keyed in green in Figure 1.	6
Figure 1.3: Geologic map of the Big Maria and Little Maria Mountains..	14
Figure 1.4: Generalized stratigraphic column of Paleozoic metasedimentary rocks in the Big Maria Mountains from the upright and attenuated limbs compared with correlative units from the western and eastern Grand Canyon	21
Figure 1.5: Jurassic plutonic rocks (Jg) in contact with Temple Butte metadolomite (Dtb).	23
Figure 1.6: Top: Aerial photograph of the Big Maria syncline looking NE. Bottom: TIMS image of approximately the same area for comparison and illustration of units based on mineralogy.....	24
Figure 1.7: Geologic cross section along A-A' through geologic map (Figure 3; Plate 1) with no vertical exaggeration.....	30
Figure 1.8: Geologic inset map of Area B originally done at 1:6000.	38
Figure 1.9: Looking N (perpendicular to strike) at polyphase deformation in overturned Jurassic metavolcanics lower member in Area A..	39
Figure 1.10: Looking E at 2 generations of deformation in the upper member of the Jurassic metavolcanics.....	40
Figure 1.11: Looking east (up-plunge) at polyphase deformation in the lower member of the Jurassic metavolcanics (Jvl).....	41
Figure 1.12: A) Lower hemisphere equal area projection of poles to planes for S_1 from Area A (N = 65). B) Plot of stretching lineations (black squares, N = 32) fold axes (green crosses, N = 3) and stretched concretions (red triangles, N = 2) from Area A..	42
Figure 1.13: Stretched quartz concretions in the Aztec quartzite from the upright limb of the syncline.....	45

Figure 1.14: Photograph looking northwest at a Cretaceous leucogranite dike (highlighted with black lines) cutting across the composite S_1/S_2 fabric (shown in light blue) in overturned Triassic-Jurassic sedimentary rocks.....	46
Figure 1.15: Inset geologic map of Area B. 1:6,000 scale.	48
Figure 1.16: Equal area lower hemisphere stereonet plots of A) Poles to planes of S_1 . B) Trend and plunge of stretching lineation (black squares) F_2 fold axes (red triangles) and long axes of stretched pebbles (green crosses). C) The mean orientation of S_1 (dashed great circle) the beta axis of the Big Maria syncline (blue beta) and the mean orientation of stretch indicators (red star).	49
Figure 1.17: Inset geologic map of Area A.	52
Figure 1.18: Photograph looking north at contact between the Tapeats quartzite (Ct) and Proterozoic Granite (Xg).....	53
Figure 1.19: Characteristic F_2 mesoscopic fold in the Cambrian Muav marble..	54
Figure 1.20: A) Lower hemisphere equal area projection of poles to S_1 from Area C. B) Lower hemisphere equal area projection of trend and plunge of stretching lineation (black squares) and mesoscopic fold axes (red triangles) from Area C. C) Lower hemisphere equal area point density contour plot of S_3 from Area C.	56
Figure 1.21: A) F_3 folds in Jurassic granodiorite looking NW.	59
Figure 1.22: Top: Google Earth ® image of the Cretaceous leucogranite dike swarm blasting through the western part of Area C.	60
Figure 1.23: Field photograph looking east at variably deformed leucogranite dikes in the dike swarm located in the western part of Area C.	61
Figure 1.24: Lower hemisphere equal area projection of poles to planes for Cretaceous leucogranite dike swarm (left), south-central Big Maria Mountains, with corresponding point density contour plot (right).....	63
Figure 1.25: Lower hemisphere equal area projection of great circles for the mean orientation of the S_3 cleavage ($148,66^\circ W$) and dike swarm ($348,61^\circ E$) from Area C.....	65
Figure 1.26: A) High resolution scan of thin section K05 BMAR34, collected from conglomerate attenuated Triassic Vampire Formation (see Plate 1 for sample location. B) Photomicrograph in cross polarized light of feldspar delta clast at the bottom of the slide in A.	68

Figure 1.27: A) Sample K05 BMAR33 in plane polarized light and B) cross polarized light.	69
Figure 1.28: A) Plane polarized and B) cross polarized photomicrographs of sample S08 BM04 collected from the lower member of the Jurassic volcanics from the upright limb of the syncline. C) Cross polarized photomicrograph of sample S08 BM07, also collected from the lower member of the Jurassic metavolcanics, showing the same shear sense as S08 BM04.....	71
Figure 1.29: Restoration of cross section in Figure 1.7..	74
Figure 1.30: Application of crustal scale shear model for deformation in High Grade Nappe Assemblages to the Maria Fold and Thrust Belt, modified from Williams and Jiang (2005).....	77
Figure 2.1: Regional tectonic map of the southwestern U.S. with selected Mesozoic and Cenozoic tectonic elements draped over a digital elevation model of the western U.S.	90
Figure 2.2: Simplified geologic and tectonic map of the Maria Fold and Thrust Belt and McCoy Basin in southeastern California showing selected important Mesozoic (shown in red) and Cenozoic (shown in black) tectonic elements, keyed in green in Figure 1.	92
Figure 2.3: Metamorphic isograd map of the Big Maria Mountains from Hoisch et al., 1988.....	107
Figure 2.4: Generalized stratigraphic column of pre-Tertiary rocks for the Maria Fold and Thrust Belt/McCoy Basin region.	116
Figure 2.5: Looking northeast toward Palen Pass.....	126
Figure 2.6: Rounded to sub-rounded pebble to boulder size clasts in the Conglomerate Member of the McCoy Mountains Formation (Kmc).....	140
Figure 2.7: Inset geologic map of the northern McCoy Mountains (outlined in Figure 2.2).	149
Figure 2.8: Field photograph looking west at south-dipping bedding (S_0) vs. north-dipping spaced cleavage (S_1) in Jurassic Basal Sandstone 1 member of the McCoy Mountains Formation.....	151
Figure 2.9: Field photograph taken looking west at the south-dipping Mule Mountains Thrust (MMT) in the southern Palen Mountains.	152

Figure 2.10: Field photograph taken looking east at stretched pebble clast with strain tails near the foot of the Mule Mountains Thrust, southern McCoy Mountains.	153
Figure 2.11: Field photograph looking north at west-side down directed normal fault in the McCoy Mountains.....	154
Figure 2.12: Equal area lower hemisphere stereonet point density contour plots of A) poles to S_0 in Jurassic Basal Sandstone 1 member of the McCoy Mountains Formation (N = 52) and B) poles to S_1 in Jurassic volcanic rocks and Basal Sandstone 1 (N = 89).	156
Figure 2.13: Field photograph taken looking west at bedding in Jurassic Basal Sandstone 1 of the McCoy Mountains Formation.....	158
Figure 2.14: Field photograph taken looking north at two intersecting cleavages (highlighted in white) in the Jurassic volcanic upper member.	160
Figure 2.15: Equal area lower hemisphere point density contour plots of A) poles to S_0 (N = 36) and B) Poles to S_1 (N=35) from Cretaceous Basal Sandstone 2 member of the McCoy Mountains Formation.	161
Figure 2.16: Lower hemisphere equal area point density contour plots of A) poles to S_0 (N = 31) and B) poles to S_1 (N = 52) for the Cretaceous Mudstone Member of the McCoy Mountains Formation.	164
Figure 2.17: Equal area lower hemisphere point density contour plots of A) poles to S_0 (N = 16) and B) poles to S_1 (N = 11) from Cretaceous Conglomerate Member of the McCoy Mountains Formation.	165
Figure 2.18: Photomicrographs in cross-polarized light of sample M07 KS03 from Jurassic quartz porphyry (volcanics upper member).....	170
Figure 2.19: Equal area lower hemisphere point density contour plot of poles to quartz vein orientations, northern McCoy Mountains (N = 37).....	171
Figure 2.20: Looking north at network of quartz veins cross-cutting Basal Sandstone 1, northern McCoy Mountains.	172
Figure 2.21: Inset geologic map of the Palen Pass area.	180
Figure 2.22: Field photograph looking east toward Palen Pass showing the basic architecture of the northern Palen Mountains and spatial location of structural domains..	181

Figure 2.23: Field photograph taken looking north at Jurassic granite (Jg) intruding Kaibab Marble (Pk) and Supai Formation (Ps).....	182
Figure 2.24: Field photograph taken looking northwest at intrusive contact between foliated Jurassic granite (Jg) and Supai Formation (Ps).....	183
Figure 2.25: Field photograph taken looking north at F ₁ isoclinal folds with S ₁ axial plane cleavage (shown in white) from the Supai Formation.	184
Figure 2.26: Field photograph looking northwest at complex F ₁ isoclinal folds with northwest-dipping S ₁ axial plane cleavage in the Kaibab Marble	186
Figure 2.27: Field photograph looking west at imbricate set of minor, brittle, south-vergent thrust faults offsetting folded layers in the Kaibab Marble.....	187
Figure 2.28: Equal-area lower hemisphere projection stereonet point density contour plots of A) poles to S ₁ (N = 132) and B) mylonitization lineation (N = 57) from the southern Granite Mountains.....	189
Figure 2.29: Schematic cross-sectional sketch looking down-plunge at broad antiform in the Cretaceous granite in the southern Granite Mountains.	192
Figure 2.30: Equal area lower hemisphere projection stereonet plots of A) poles to S ₁ (N = 161) and B) point density contour plot of mineral elongation lineation (N = 13) from Domain II, Palen Pass area.....	194
Table 2.6: Structural data from Domain II, above Maria Frontal Thrust, Palen Pass area.	195
Figure 2.31: Lower hemisphere equal area projection stereonet plot of A) poles to S ₀ (N = 54) and B) poles to S ₁ (N = 72) from Domain III, Palen Pass area.....	199
Figure 2.32: Index map of the Big Maria Mountains showing the location of U-Pb (red filled circles) and Ar-Ar (blue filled stars) samples.....	205
Figure 2.33: ²³⁸ U/ ²⁰⁶ Pb zircon ages vs. U concentration for sample S06 B01.....	208
Figure 2.34: ²³⁸ U/ ²⁰⁶ Pb zircon ages vs. U concentration for sample S08 BM11.....	211
Table 2.9: U-Pb geochronologic analyses for Sample S08 BM11.....	212
Figure 2.35: Hornblende age spectra plots from four magmatic samples from the western Big Maria Mountains.	214
Figure 2.36: Biotite age spectra from magmatic rocks from the Big Maria Mountains. .	215

Figure 2.37: Simplified tectonic map of the southwestern U.S. during Early Cretaceous time.227

Figure 2.38: Late Cretaceous tectonic map of the southwestern U.S.229

Figure 2.39: Latest Cretaceous tectonic map of the southwestern U.S.....233

LIST OF TABLES

Table 1.1: Structural data from Big Maria Mountains, Area A.	44
Table 1.2: Structural data from Big Maria Mountains, Area B.	50
Table 1.3: Structural data from Big Maria Mountains, Area C.	57
Table 1.4: Strike and dip of dikes from the leucogranite dike swarm, western Big Maria Mountains	64
Table 2.1: Structural data for Jurassic volcanics and Jurassic Basal Sandstone 1 member of the McCoy Mountains Formation.....	157
Table 2.2: Structural data from Cretaceous Basal Sandstone 2 member, McCoy Mountains Formation.....	162
Table 2.3: Structural data from Cretaceous mudstone (Kmm) and conglomerate (Kmc) members of the McCoy Mountains Formation	166
Table 2.4: Strike and dip of quartz veins from northern McCoy Mountains.....	173
Table 2.5: Structural data from Domain I, southern Granite Mountains, Palen Pass area.	191
Table 2.6: Structural data from Domain II, above Maria Frontal Thrust, Palen Pass area.	195
Table 2.7: Structural data from Domain III, south of Maria Frontal Thrust, Palen Pass area.	200
Table 2.8: U-Pb geochronologic analyses for Sample S06-B01	209
Table 2.9: U-Pb geochronologic analyses for Sample S08 BM11.....	212
Table 2.10: Ar-Ar geochemical data for biotite and hornblende samples	216

PREFACE

This dissertation consists of three different chapters, all with the related twin goals of assessing the kinematics and timing of deformation in the Maria Fold and Thrust Belt and McCoy Basin and producing a new synthesis of the geology of this part of the Cordillera. Each chapter is written as a separate manuscript; therefore some repetition in introductory background material is unavoidable. As one of the goals is to produce a synthesis of the region, each chapter relies heavily on geologic mapping done by previous workers in the region. Also, each chapter represents a collaborative effort. However, the majority of data collection, map compilation, analytical work, data interpretation and writing were done by me and I will be lead author on each submitted manuscript.

Chapter 1 presents new high resolution (1:12,000 and 1:6,000 scale) mapping, structural analysis and stratigraphy of the Big Maria Mountains in southeastern California, with particular emphasis on the Big Maria syncline and Paleozoic rocks, and presents a refined model for Mesozoic polyphase deformation events in the region. The unpublished 1:24,000 geologic map of the Big Maria Mountains by Warren Hamilton was consulted often and relied upon heavily for publication of the 1:24,000 scale tectonic map of the mountain range. TIMS remote sensing data collected by NASA was also useful in preparing the geologic map and interpreting mesoscopic structures. Samples for microstructural analysis were collected with the help and guidance of Karl Karlstrom, Jeff Geier and Bryan MacFarlane. Steve Reynolds, Karl Karlstrom and Jeff Geier all contributed to the ideas and interpretations presented in this work. Pending revisions, this manuscript will be submitted to *Geology* for publication (Salem, Reynolds, Karlstrom and Geier in prep.).

Chapter 2 presents new 1:12,000 scale mapping and structural analysis of the northern McCoy Mountains and Palen Pass as well as new U-Pb zircon ages and Ar-Ar hornblende and biotite ages from the western Big Maria Mountains. Hope Johnston, Jeff Geier, Bryan MacFarlane, Karl Karlstrom, Laurie Crossey, Mark Tyra and David Haddad provided capable assistance in the field and assisted with sample collection for microstructural analysis and geochronology work. Matt Heizler, Shari Kelly, George

Gehrels and Josh Feldman provided assistance with sample preparation for geochronology. George Gehrels supervised and helped with use of the LA-ICP-MS at the LaserChron facility at the University of Arizona Tucson and also assisted with interpretation and report of U-Pb zircon ages. Matt Heizler at New Mexico Tech assisted greatly with timely collection and analysis of Ar-Ar geochemistry of hornblende and biotite samples, as well as with interpretation of age spectra and reporting of ages. Unpublished mapping at 1:31,250 in the McCoy and Palen Mountains by Gary Pelka and at 1:24,000 in the Little Maria Mountains by Stanton Ballard along with the published 1:24,000 map of Palen Pass by Paul Stone and Michael Kelly and the 1:100,000 map of the Blythe sheet by Paul Stone were relied on heavily for regional analysis and interpretation. Karl Karlstrom contributed a great deal to ideas and interpretations presented here. Pending revisions, this manuscript will be submitted to *Geological Society of America Bulletin* for publication (Salem and Karlstrom, in prep.).

In order to produce a regional synthesis of the Maria Fold and Thrust Belt and McCoy Basin, a new tectonic map is necessary. Chapter 3 presents a report that describes compilation methods for geologic maps produced for and accompanying Chapters 1 and 2 of this dissertation. All mapping was compiled by me from pre-existing geologic maps described above and with new mapping also described above. The personal geodatabase accompanies this volume as a CD and map files may be read by anyone with access to ArcGIS. Audrey Salem greatly aided in the compilation effort with her knowledge of ArcGIS. Karl Karlstrom contributed to interpretations presented on the published maps. Pending revisions, this manuscript, paper maps and CD will be submitted for publication as a *Geological Society of America* Map and Chart.

Chapter 1 : Structural evolution of the Big Maria syncline: Polyphase ductile deformation in response to progressive Sevier-Laramide tectonism in the Maria Fold and Thrust Belt, SE California

A.C. Salem, S.J. Reynolds, K.E. Karlstrom and J. Geier

Chapter Abstract

New mapping, stratigraphy, and structural analysis of the Big Maria syncline in the Big Maria Mountains (BMM) in southeastern California lead to a revised interpretation of the kinematics and timing of ductile deformational events at middle crustal levels in the Sevier orogenic belt. The Big Maria syncline is a kilometer-scale west-plunging fold nappe, the axial trace of which strikes NNW through the Big Maria Mountains. The structure is famous for extreme attenuation of Paleozoic cratonal strata correlative to the Grand Canyon succession. These rocks have undergone amphibolite grade metamorphism. Evaluating alternative models for its formation, this study investigates the kinematics of ductile deformation in the Maria Fold and Thrust Belt, provides new constraints on the timing of deformation and discusses implications for understanding middle crust deformation processes and the Mesozoic tectonic evolution of the Cordillera.

Three deformation events, D_1 , D_2 , and D_3 are recognized in the Big Maria syncline. D_1 is characterized by southeast-vergent, initially subrecumbent tight-to-isoclinal mesoscopic folds and shear zones and a regionally E-W striking, moderately dipping S_1 foliation that is subparallel to unit contacts. A stretching lineation on S_1 plunges to the west-northwest, and shear fabrics in deformed rocks mostly indicate a top-southeast reverse/dextral oblique shear sense. Shear strains were highest on the overturned limb, but both limbs show the same shear sense indicating that the syncline was part of a deep crustal flow system.

D_2 is characterized by southwest-vergent, km-wide ductile shear zones and associated subrecumbent macroscopic folds that refold S_1 . These folds have a weakly developed S_2 cleavage in fold hinges. We interpret the Big Maria syncline to be a macroscopic F_2 fold. The extremely attenuated Paleozoic and Mesozoic strata of the overturned limb of the Big Maria syncline are interpreted here to be due to high shear

strains in a regionally important shear zone in which Paleozoic and Mesozoic strata were underthrust northward to mid-crustal depths (12-15 km). This shear zone contains a mixture of Proterozoic basement and ~180-150 Ma Jurassic plutonic rocks in its upper plate. The shear zone, as well as the composite S_1/S_2 foliation are crosscut by Cretaceous (~79 Ma) leucogranite dikes, thus bracketing D_1/D_2 deformation between 160-79 Ma. Kinematics and timing of D_1/D_2 suggests these events were related to the Sevier Orogeny.

D_3 folds are upright to slightly overturned with north or northwest-striking axial planes (mean orientation is 328, 66° SW) and shallow plunges. They refold S_1/S_2 and contain an axial plane cleavage (S_3) that dips steeply SW. S_3 is best expressed in micaceous rocks but is also weakly expressed in some Cretaceous dikes. Variable development of S_3 and D_3 folds in dikes suggest dikes were emplaced late during D_3 . The NNE mean dike orientation suggest dikes used S_3 weakness planes then became mildly folded and boudinaged during late stages of D_3 deformation. D_3 is thus characterized by top-NE shortening that refolded D_1/D_2 structures as well as by NE-directed extension during late stage deformation. The change in movement direction from SE during D_1/D_2 to NE during D_3 is interpreted to record evolving strain fields during the change from Sevier to Laramide tectonism in the southern Cordillera.

Introduction

In this paper we present new mapping, stratigraphy, and structural analysis of the Big Maria syncline, named for the Big Maria Mountains in southeastern California, and offer a revised interpretation of the kinematics and timing of deformation events. The Big Maria syncline is a kilometer-scale, south-vergent fold nappe that deforms Proterozoic, Paleozoic, and Mesozoic metamorphic rocks. The syncline consists of an upright, relatively unattenuated southern limb, and an overturned, extremely attenuated northern limb. The syncline is unique in the region, as it is one of the best preserved Mesozoic ductile structures that has not been strongly overprinted by later brittle Mesozoic thrusting or Cenozoic extension, and therefore provides an opportunity to examine older Mesozoic ductile events.

The kinematics and timing of deformation events in the syncline are controversial, and multiple hypotheses have been advanced by different workers. One proposed model for formation of the synclines is that it formed as a synformal keel between two rising Jurassic plutons (Hamilton, 1982). An alternative hypothesis is that the syncline formed during Cretaceous north-directed underthrusting of Paleozoic and Mesozoic metasedimentary rocks beneath Jurassic and Proterozoic crystalline rocks (Ellis, 1982; Ballard, 1990). More recent tectonic models for deformation in middle crustal terranes, which would be applicable to the Big Maria syncline and the Maria Fold and Thrust Belt, invoke detachment flow (Beaumont et al., 2001) and/or channel flow (Jamieson et al., 2002; Godin et al. 2006) in crustal scale shear zones (Williams and Jiang, 2005) to explain observed features. Other workers (Spencer and Richard, 2008) have invoked critical taper theory (Dahlen, 1990) or an orogenic wedge similar to the High Himalaya Crystalline Series (e.g. Burchfiel et al., 1992) as a mechanism for explaining the tectonic origin and evolution of the MFTB. These new models might provide better understanding of the tectonics in this area. Our assessment of the kinematics and timing of formation for this structure and nearby area will allow us to address the immediate question kinematics and timing of deformation in the Maria Fold and Thrust Belt as a whole, and will allow for a more refined understanding of the tectonic evolution of the MFTB.

Understanding the processes origin and structural evolution of the syncline is also significant for advancing tectonic models of the Cordillera of the southwestern United States. Important larger implications for this project are 1) testing tectonic models for Mesozoic deformation and metamorphism in this part of the Cordillera, such as that there were evolving transport directions from the Sevier to the Laramide Orogenies prior to synorogenic collapse at the end of the Cretaceous (Hodges and Walker, 1992; Wells et al., 2005), 2) for enhancing our understanding of processes associated with middle crustal deformation, such as the effect of rock rheology on geometry and styles of deformation (Ballard, 1990; Fletcher and Karlstrom, 1990; Karlstrom and Williams, 1998; Beaumont et al., 2001), the relationship between plutonism and deformation (Fletcher et al., 1993), and the response of rocks to high strain, plastic deformation, including extreme

attenuation and channel flow (Beaumont et al., 2001) and 3) the importance of Jurassic vs. Cretaceous tectonism in shaping the Cordillera (Hamilton, 1987; Busby-Spera, 1988; Wells et al., 2005).

Tectonic Setting

The syncline is the “type structure” of the Maria Fold and Thrust Belt (MFTB, Reynolds et al., 1986), a roughly east-west trending, arcuate zone of highly deformed, amphibolite grade rocks in west central Arizona and southeastern California (Figure 1.1, 1.2). The MFTB is named for the Big and Little Maria Mountains in California and is characterized by south-vergent folds and shear zones. In addition to the Big and Little Maria Mountains, the MFTB comprises all or part of the Little Harquahala, Harquahala, Granite Wash, Plomosa, New Water, Moon and Dome Rock Mountains in Arizona and Riverside, Arica and Palen Mountains in California. Rocks in the MFTB have undergone polyphase ductile Mesozoic deformation events that have later been overprinted by brittle Cenozoic deformation events. Figure 1 shows a regional map of various tectonic elements/provinces. Modern physiographic boundaries are shown in black, Cenozoic faults are shown in yellow, identified Cenozoic metamorphic core complexes are shown in orange and Mesozoic tectonic elements are shown in red.

The MFTB likely represents a westward extension of the Late Jurassic-Cretaceous Sevier Fold and Thrust Belt (DeCelles, 2004), which formed in the foreland of the Sierra Nevada arc in response to subduction off the west coast of North America. The Sevier Fold and Thrust Belt is analogous to the Precordillera of the Andes (Verges et al., 2001; DeCelles, 2004). The basic architecture of the Sevier Fold and Thrust Belt is a foreland thrust belt in the east characterized by mostly west-dipping, east-vergent folds and brittle thrusts, and a hinterland in the west characterized by ductile deformation, high grade

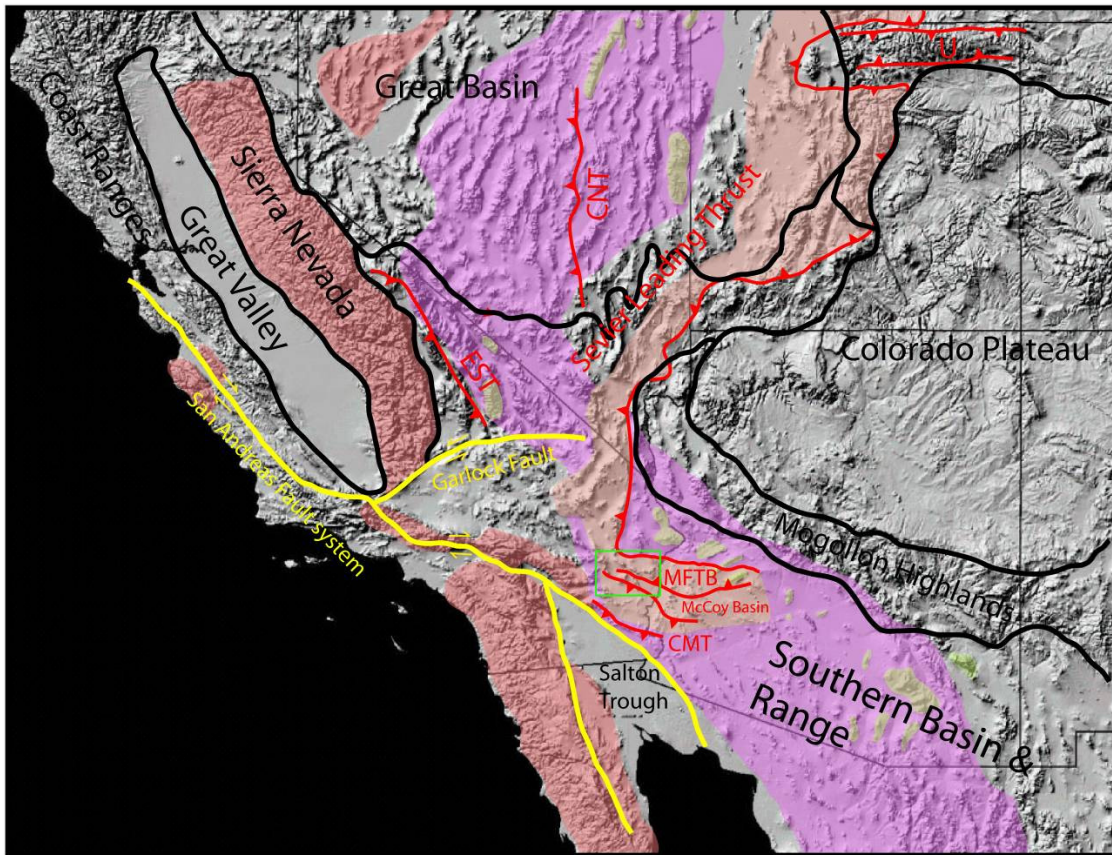


Figure 1.1: Regional tectonic map of the southwestern U.S. Selected Mesozoic and Cenozoic tectonic elements are draped over a digital elevation model of the southwestern U.S. The western half of the Maria Fold and Thrust Belt is outlined with green rectangle. Modern physiographic/geologic provinces are outlined in black. Green infill shows Late Cretaceous-Tertiary metamorphic core complexes (after Hodges and Walker, 1992; Wells and Hoisch, 2008). Purple infill shows a belt of Late Cretaceous muscovite granites (Miller and Bradfish, 1980), which largely coincides with location of metamorphic core complexes and the inferred axis of maximum crustal thickness during the Mesozoic (Coney and Harms, 1984). The Sevier Fold and Thrust Belt, shown with pink infill, is after DeCelles (2004), with the leading edge of the thrust labeled and shown in red. Late Jurassic-Early Cretaceous batholith complexes are shown in red infill. Other major Mesozoic thrust and uplifts are shown in red and labeled EST - Eastern Sierran Thrust, CNT - Central Nevada Thrust, U - Uinta Uplift (After Wells and Hoisch, 2008).

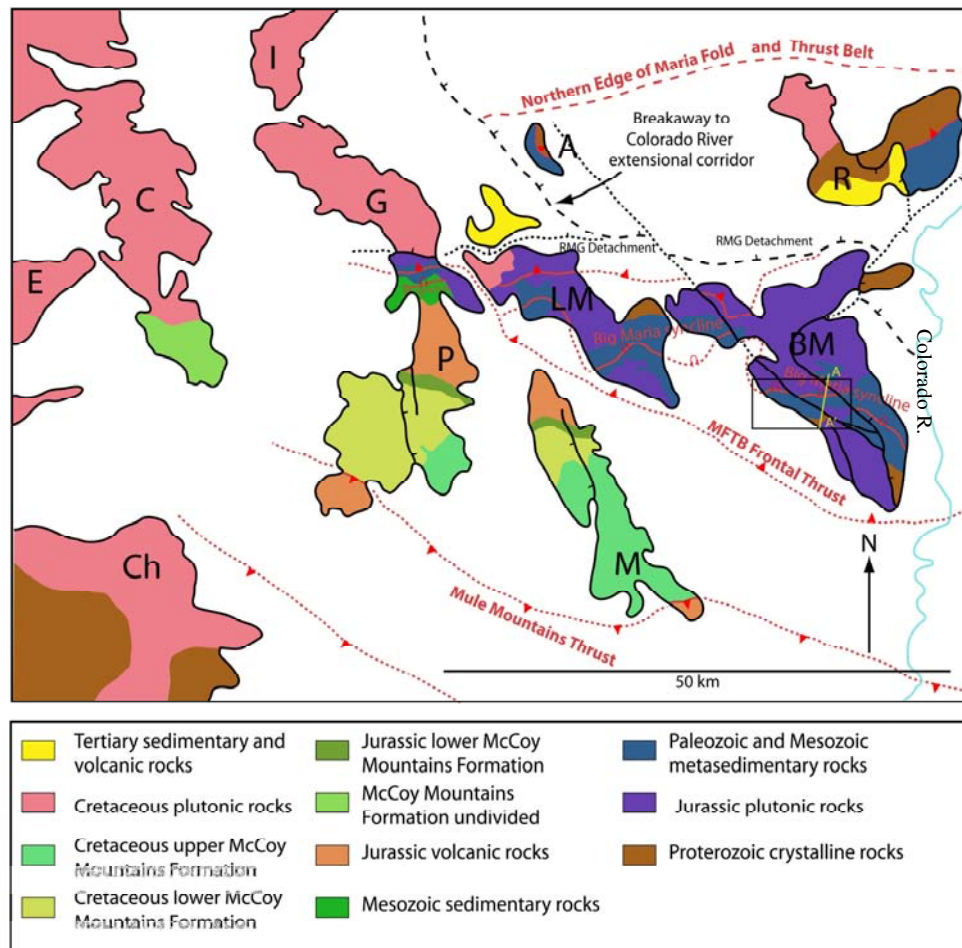


Figure 1.2: Simplified geologic and tectonic map of the Maria Fold and Thrust Belt and McCoy Basin in southeastern California showing selected important Mesozoic (shown in red) and Cenozoic (shown in black) tectonic elements, keyed in green in Figure 1. The study area is outlined with a black rectangle. Abbreviations A: Arica Mountains, BM: Big Maria Mountains C: Coxcomb Mountains, Ch: Chuckwalla Mountains, E: Eagle Mountains, G: Granite Mountains, I: Iron Mountains, LM: Little Maria Mountains, M: McCoy Mountains, P: Palen Mountains, R: Riverside Mountains, RMG: Riverside-Maria-Granite. Map compiled from Wells et al. (2005), Stone (2006), Lyle (1982), Baltz (1982) and Spencer et al. (2005)

metamorphism and metamorphic core complexes. The MFTB occupies an area that features spatial overlapping of the Sevier Foreland Thrust Belt (DeCelles, 2004) and a belt of peraluminous granites and granodiorites of Late Cretaceous age (Miller and Howard, 1985; Foster et al., 1992). This magmatic belt coincides with the Sevier hinterland and has been recognized as an area of synconvergent extension (Saleeby, 2003; Hodges and Walker, 1992). Unlike the Andean Cordillera, the Sevier-Laramide orogenic system has a hinterland that has been exhumed by extensional processes, allowing geologists to observe middle crustal ductile deformation structures (Hodges and Walker, 1992; DeCelles, 2004). Thrust faults become younger eastward (e.g. Royse et al., 1977). The approximate frontal front of the Sevier Fold and Thrust Belt is shown as the large, mostly north-south trending thrust in red in Figure 1.1. Thin skinned thrusts associated with the Sevier Foreland Thrust Belt are shown in the pink shaded area on the map. Throughout most of the Sevier belt, vergence of major folds and thrusts shows top-to-the east tectonic transport *toward* the continent, analogous with the modern Andean Precordillera. Structures that have been correlated with the Sevier belt have been documented as far southwest as the Old Woman Mountains in southeastern California (Fletcher et al., 1995; Hoisch et al., 1988). In the Old Woman Mountains, rocks have been subjected to ductile deformation and amphibolite grade metamorphism. As such, most workers have interpreted the Old Woman Range to lie in the hinterland of the Sevier belt (Fletcher et al., 1995; Hodges and Walker, 1992; DeCelles, 2004). The relationship of the Maria belt to the adjacent Sevier belt is not entirely understood. It is clear that structures that have Sevier signature kinematics, i.e., top-to-the-east shearing, are observed in the MFTB (Laubach et al., 1989; Ballard, 1990; Salem et al., 2006), so it is likely that the MFTB should be considered part of the hinterland of the Sevier Belt. However, the questions remain as to why the belt is characterized by mostly south-vergent structures, which indicate transport toward the continent, and why the belt trends E-W almost perpendicular to the main grain of the North American Cordillera. Resolving these questions is one of the goals of this investigation.

Figure 1.2 shows a regional tectonic map of the western half of the Maria Fold and Thrust Belt in southeastern California. Individual mountain ranges are outlined in black. Paleozoic and Mesozoic high grade metamorphic rocks are shown in blue; these rocks are useful for identifying Mesozoic structures. Major Mesozoic structures, including thrust faults and the Big Maria-Little Maria syncline are shown as red lines. Major Cenozoic normal and right lateral faults are shown as black lines. Exposures of the Jurassic-Cretaceous McCoy Mountains Formation are shown as shades of green and yellow. Late Cretaceous plutonic rocks are shown in pink. The green rectangle on the map shows the location of the study area. The Maria Fold and Thrust is bounded to the south by the Maria Frontal Thrust, the name designated herein for the tectonic contact between the middle crustal MFTB and the supracrustal McCoy Basin crustal blocks. The nature of the northern boundary of the fold and thrust belt is less certain. Structures characteristic of the MFTB are not observed along the Colorado River north of the Riverside and Arica Mountains. The Cenozoic Riverside-Maria-Granite (RMG) Detachment separates the Arica and Riverside Mountains block in its hanging wall from the Big and Little Maria and Palen Mountains block to the south. The RMG Detachment accommodates the breakaway to the Colorado River Extensional Corridor. The Big Maria-Little Maria syncline is a major structure that jogs northwest through the Big and Little Maria Mountains for ~ 50 km. Overall, the syncline strikes west northwest, but is disrupted by marked north deflections as the result of later refolding. The Big Maria-Little Maria syncline is truncated by the Maria Frontal Thrust in the west and appears to terminate at a hinge zone exposed in both the central and southeastern Big Maria Mountains.

The MFTB lies in the southwestern Basin and Range physiographic/geologic province. The Basin and Range stretches from northern Mexico to southern Oregon is characterized by small mountain ranges separated by broad valleys. The Basin and Range developed as a result of widespread crustal extension and associated magmatism that was coeval with the development of the San Andreas transform boundary beginning ~30 Ma and continuing to the present (Saleeby, 2003). Basin and Range extension is evident in

the form of metamorphic core complexes (regions of high extension), detachment faults, and high angle normal faults ranging in age from Oligocene through late Miocene age. Also evident are right-lateral strike slip faults associated with the San Andreas Fault system; these faults are mostly Miocene through Quaternary age. Both extensional and strike slip features overprint and modify earlier Mesozoic contractile structures. These Mesozoic structures are also overprinted in the region by Oligocene through Miocene age volcanic deposits, igneous dikes and shallow level intrusions associated with Cenozoic magmatism (Spencer and Reynolds, 1990).

Immediately south of the MFTB is the Jurassic-Cretaceous McCoy Basin (Harding, 1982; Harding and Coney, 1985), which trends subparallel with and spatially overlaps the MFTB. The McCoy Basin is defined by exposures of Jurassic-Cretaceous McCoy Mountains Formation (MMF), a >7 km thick sequence of sandstone, siltstone and conglomerate. In addition to the type section in the McCoy Mountains, exposures of MMF are found in the Little Harquahala, New Water, Granite Wash, Plomosa and Dome Rock Mountains in Arizona and in the Riverside, Palen and Coxcomb Mountains in California. The MMF is observed in most places deposited unconformably on top of Jurassic quartz porphyry, a hypabyssal intrusive unit that is part of the Jurassic Dome Rock sequence (Harding and Coney, 1985; Tosdal et al., 1989). Locally, the MMF is observed in gradational contact with Jurassic volcanic rocks in the Palen Mountains (Fackler-Adams et al., 1997) and in disconformable contact with Paleozoic strata in the Plomosa Mountains (Harding and Coney, 1985). Almost everywhere in the McCoy Basin, the formation consistently dips to the south. The MMF has a consistent internal stratigraphy that is laterally continuous for miles (Harding and Coney, 1985) and is >7300 meters thick in the type section. Although different workers (e.g., Stone and Pelka, 1989; Harding and Coney, 1985; Reynolds, Spencer and DeWitt, 1987) have mapped several members of the MMF or correlative strata, the formation may be divided broadly into a lower and upper member (Tosdal and Stone, 1994), which are separated by an intraformational unconformity. The lower member consists, from oldest to youngest, of Harding's (1982) Basal Sandstone 1, Basal Sandstone 2 and Mudstone Members. The

upper member consists of Harding's Conglomerate Member, Sandstone Member, and Siltstone Member. The upper member is constrained to Late Cretaceous age based on fossil wood and ash fall deposits (Tosdal and Stone, 1994; Stone and Pelka, 1989). The lower member is more poorly constrained, and may range in age from Cretaceous to Late Jurassic. Evidence for a Late Jurassic age for the Basal Sandstone of the lower McCoy Mountains Formation includes detrital zircon U-Pb analysis from western Arizona (Spencer et al., 2005) and southeastern California (Barth et al., 2004) and locally observed interfingering between Jurassic volcanic rocks and the basal MMF in the Palen Mountains (Fackler-Adams et al., 1997). However, Barth et al. (2004) document detrital zircons in Basal Sandstone 2 as young as 109 Ma in the type section, indicating a Cretaceous age for the much of the lower MMF. In addition, the unconformity between the lower MMF and upper MMF, while obvious in the Plomosa and Dome Rock Mountains (Tosdal and Stone, 1994) is less apparent in the McCoy and the Palen Mountains. These observations suggest that there might be an unconformity between Basal Sandstone 2 and Basal Sandstone 1 that was previously unrecognized, or that there has been miscorrelation of stratigraphy across the McCoy Basin (Stone, written comm.), or that the lower MMF becomes younger from east to west across the basin. Timing of deposition of the MMF is important because it is the youngest unit in the region to have undergone all stages of polyphase deformation.

Like the MFTB, rocks in the McCoy Basin have undergone regional metamorphism and deformation. However, in contrast with the MFTB, peak metamorphism in the McCoy Basin is interpreted to be much lower grade (sericite and albite are the main metamorphic minerals present, Pelka, 1973) and deformation in the basin is primarily brittle in character. The tectonic setting of the McCoy Basin is a matter of debate. Some workers (Dickinson et al., 1981; Spencer et al., 2005) argue that the McCoy Basin represents a westward extension of the Bisbee Basin of southeastern Arizona. Other workers argue that the MMF was deposited in a retroarc foreland basin (Barth et al., 2004). Still, other workers contend that the McCoy Basin was a transtensional basin associated with the Jurassic Mojave-Sonora Megashear (Harding and

Coney, 1985), although this view has been discredited by the evidence for a Late Cretaceous age for the upper MMF. Tosdal and Stone (1994) take the middle ground and argue that McCoy Basin has a complex tectonic history, perhaps originating as a rift basin and then evolving into a back arc basin. Understanding the tectonic setting of the McCoy Basin is important for understanding MFTB deformation, as the McCoy Basin spatially overlaps the MFTB, and as the MFTB might be a source terrane for at least the upper part of the formation.

The MFTB is separated from the stable Colorado Plateau region to the north and west by a northwest trending belt of Oligocene-Miocene metamorphic core complexes (Hodges and Walker, 1992; DeCelles, 2004). This belt of metamorphic core complexes stretches from northern Sonora at least as far as British Columbia and spatially overprints the hinterland zone of the Sevier Fold and Thrust Belt. The metamorphic core complex terrane is characterized by high degree of crustal extension and is famous for low-angle detachment faults that contain middle crustal plutonic and metamorphic rocks in their footwalls and upper crustal rocks in their hanging walls. Horizontal displacement along low angle detachment faults can be on the order of kilometers to tens of kilometers. The metamorphic core complex terrane contains excellent examples of both brittle extension, in the form of high angle normal faults, fault breccia and psuedotachylites (e.g., Reynolds and Lister, 1987) and ductile extension in the form of mylonite fabrics, and ductile, low-angle normal shear zones. Coney and Harms (1984) point out that the metamorphic core complex belt is found in the area of greatest crustal thickening during Mesozoic contractile orogeny, such that the area of maximum Cenozoic crustal extension spatially overlaps the area of maximum Mesozoic crustal thickening. The metamorphic core complex belt spatially overprints the MFTB in the east and lies immediately north of the MFTB in the west (Spencer and Reynolds, 1990). This increases the complexity of local geometries and makes palinspastic reconstruction of the MFTB to its pre-Cretaceous tectonic setting difficult. In this area, there are thus three major stages of Cenozoic extension and transtension: metamorphic core complex “hyper-extension”, Basin and Range high angle normal faulting and San Andreas transtensional (normal and dextral).

These Cenozoic events that have to be taken into account in order to unravel the kinematics of earlier Mesozoic contractile (and tensional) tectonic events, both in analyzing mesoscopic and macroscopic structures in the field and in doing regional scale reconstructions.

The Colorado Plateau and Arizona Transition Zone flank the MFTB to the north of the metamorphic core complex terrane. The Colorado Plateau is a relatively stable cratonal block, consisting of a ~ 3 km platform of Paleozoic and Mesozoic strata that overlies mostly Paleoproterozoic crystalline basement rocks of the Yavapai-Mazatzal terrane (e.g. Whitmeyer and Karlstrom, 2007). Locally there are exposures of Meso- and Neoproterozoic sedimentary strata that were deposited in rift basins that formed during the breakup of Rodinia (Timmons et al., 2005). The topography of the Plateau consists predominantly of broad tablelands and mesas that are locally incised by deep canyons, e.g. the Grand Canyon. This topography is disrupted by igneous intrusions that form high isolated mountain ranges and by large monoclinical uplifts formed as the result of reactivation of mostly Precambrian faults and shear zones during the Laramide Orogeny. The Plateau is relatively high, with the average elevation ~1500 m above sea level. Initial uplift of the Plateau took place during the Laramide Orogeny and recent studies have shown that the Plateau has remained at its elevation since the end of the Laramide (Spencer, 1996; Pederson et al., 2002; Flowers et al., 2008). Compared with the surrounding region, the Plateau has experienced relatively little internal deformation since the end of the Precambrian (Humphreys, 1995) The Arizona Transition Zone is located between the Colorado Plateau to the north and the southern Basin and Range, consisting primarily of Proterozoic crystalline rocks overlain by Tertiary volcanic and sedimentary rocks. However, Paleozoic sedimentary rocks and Cretaceous-Tertiary plutonic rocks are locally exposed. The topography of the Transition Zone consists of large mountain ranges separated by small basins. Initial uplift of Paleozoic and Proterozoic rocks in this area began during Triassic time and is believed to have been a result of local uplift along rift faults associated with the breakup of Pangea (e.g. Burchfiel and Davis, 1975; Reynolds et al., 1989). This region later became the Mogollon Highlands and was a source terrane for

Mesozoic strata on the Colorado Plateau to the north and for the MFTB/McCoy Basin terrane to the south. Compared with the Basin and Range, the Transition Zone experienced relatively little Mesozoic and Cenozoic deformation. Deformation in the Transition Zone is mostly brittle, characterized by high angle normal faults formed as a result of widespread Tertiary extension.

The Colorado Plateau region is an important reference datum for the MFTB, because the Maria belt contains extensive exposures of highly deformed and metamorphosed rocks correlative to the classic cratonal sequence of the Grand Canyon of the Colorado Plateau. Therefore, Paleozoic rocks, because of their easily recognized stratigraphy and extensive exposure, should aid in palinspastic reconstruction of the MFTB/McCoy Basin terrane to its original state prior to the onset of active margin tectonics in the Middle Jurassic. Cratonal strata are exposed with variable degree of lateral continuity throughout ranges in west-central Arizona and southeastern California (Figure 2, Stone et al., 1983) and contrast with thicker, miogeoclinal strata to the west and southwest (Stewart et al., 1990). It is our hope that detailed structural analysis of the kinematics and timing of formation of deformation events exposed in the Big Maria syncline might provide new insight into our understanding of the MFTB and explain how this important yet enigmatic tectonic element fits in with the rest of the Cordillera.

Geologic background of the Big Maria Mountains

The Big Maria Mountains (Figure 1.3) contain a diverse lithologic suite; the oldest rocks in the range are Proterozoic granitic gneisses. These granites consist chiefly of megacrystic potassium feldspar (up to 3 cm in diameter), quartz, biotite, and muscovite, and exhibit an augen texture defined by the feldspar phenocrysts. These rocks are inferred to be part of the Mesoproterozoic (~1400 Ma) suite of A-type granite (Anderson, 1989), based on lithologic correlation (Hamilton, 1982). These A-type granites extend across much of continental North America (Karlstrom et al., 2003; Whitmeyer and Karlstrom, 2007). The Big Maria Mountains lie in the eastern edge of the Mojave Proterozoic crustal block. Proterozoic basement rocks recognized in the area in

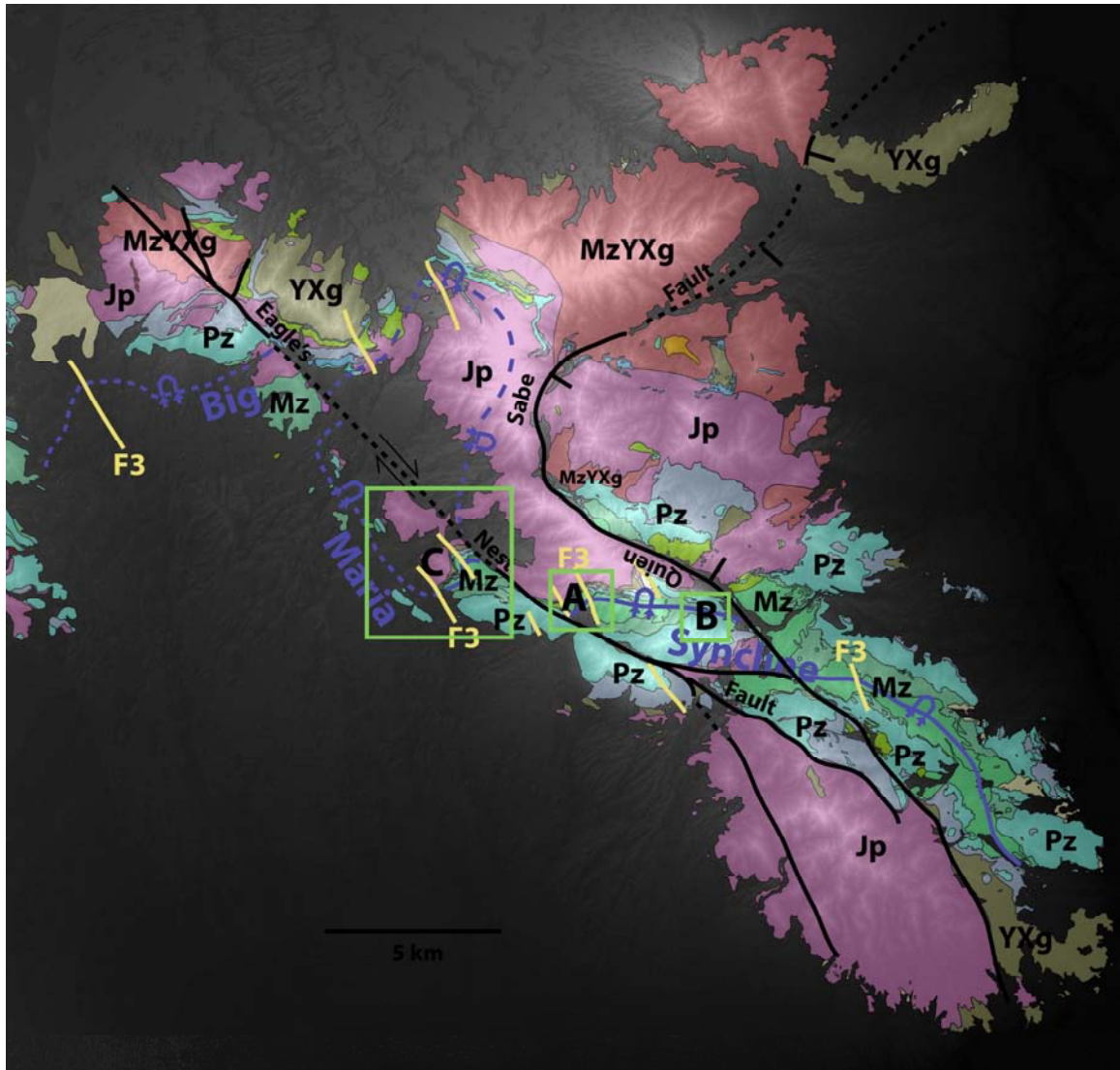


Figure 1.3: Generalized geologic map of the Big Maria Mountains laid over digital elevation model. Purple line shows axial trace of composite F_2 Big Maria syncline. Yellow lines show location of major F_3 refolds. Labeled green squares show location of domains mapped at 1:6000 scale for detailed structural analysis. Black lines show location of major Cenozoic faults. YXg: Proterozoic gneiss (brown), Pz = Paleozoic sedimentary rocks (shades of blue and purple), Mz = Mesozoic sedimentary and volcanic rocks (shades of green), Jp = Jurassic plutonic rocks (shades of pink), MzYXg = gneiss of Mesozoic or Proterozoic age (red). Tertiary rocks are shown in shades of orange or yellow.

the vicinity of the MFTB represent 1900-1800 Ma juvenile arc rocks of the Mojave Province that have been overprinted by 1720-1688 Ma granitoid rocks associated with the Late Paleoproterozoic Yavapai-Mazatzal Orogeny (Whitmeyer and Karlstrom, 2007). It stands to reason that some Proterozoic gneisses exposed in the range and nearby might be a part of this older province, but very little geochemical analysis has been done on Proterozoic rocks in the Big Maria Mountains to determine their age and origin. Also, sorting Proterozoic from Jurassic crystalline rocks is difficult in the region due to compositional and textural similarities and strong Cretaceous deformation and metamorphism.

Proterozoic basement is nonconformably overlain by Paleozoic metasedimentary rocks correlative to the classic cratonal sequence of the Grand Canyon (Noble, 1923; Hamilton, 1982). This sub-Paleozoic nonconformity is widespread throughout most of western North America and is referred to as the Great Unconformity at the Grand Canyon (Walcott, 1894). Hamilton (1982) first published these lithologic correlations and assigned formation names from the Grand Canyon for the metasedimentary rocks of the Big Maria Mountains. Paleozoic sedimentary rocks range in age from Cambrian through Permian. Paleozoic rocks consist of a basal, “dirty” quartzite designated the Cambrian Tapeats Quartzite, which is overlain by a silvery-green micaceous schist designated the Cambrian Bright Angel Schist, which is overlain by a grayish banded calcitic marble designated the Cambrian Muav Marble. Salem (2005) recognized an unconformity between the Muav Marble and a massive metadolomite, designated the Devonian Temple Butte Formation. The unconformity is marked by the presence of a green, siliciclastic metasandstone. The metadolomite is overlain by a white calcitic marble, with local chert-rich layers, designated the Mississippian Redwall Marble. Based on comparison of transposed thicknesses of units in the BMM with their respective units in the Grand Canyon (Salem, 2005), it is likely that some of the massive metadolomite may actually be dolomitized Redwall Marble, similar to what has been observed in the nearby Little Harquahala Mountains (Spencer *et al.*, 1985). However, it is difficult to resolve any stratigraphy in the massive metadolomite so, for mapping purposes, the contact between

the Redwall Marble and the Temple Butte Formation is placed at the contact between the white marble and the massive metadolomite. Overlying the Redwall Marble is a thick, distinctive sequence of quartzite, calc-silicate, and carbonate layers designated the Pennsylvanian-Permian Supai Formation. The Supai is easily recognizable, as quartzite and calc-silicate layers form resistant layers made dark by desert varnish, and carbonate layers form recessive, light-colored layers, giving the rock a banded appearance. The characteristic light and dark bands of the Supai Formation allow for easy recognition and characterization of mesoscopic folds. Much of the calcite in the Supai Formation has been metamorphosed into wollastonite, the presence of which led Hoisch et al. (1988) to conclude that metamorphism in the MFTB must have been accompanied by large amounts of water. They calculated a fluid to rock ratio for the Supai Formation in the Big Maria Mountains of ~17:1, with smaller values reported for the Kaibab and Muav Marbles (~5:1). The large volumes of water required for this metamorphism may have come from de-watering of a hydrated subducting slab during the Late Cretaceous time (Hoisch et al., 1988). In addition, the wollastonite layers also define a mineral lineation, the mean orientation of which may represent the stretching direction during polyphase deformation. The contact between the Supai Formation and the Redwall marble is marked by a layer of reddish sandstone that has been interpreted as metamorphosed terra rosa at the top of the Redwall marble (Morrissey, 1999). Terra rosa is a term for red shale that forms as a result of sub-aerial weathering of carbonate rocks, and thus the presence of terra rosa defines an unconformity (Boggs, 2000). This unconformity is recognized at the Grand Canyon and throughout the Mogollon Rim area of the Colorado Plateau (Beus, 2003b).

The Supai formation is overlain by a pale green sequence of quartzite and schist designated the Permian Hermit Formation. The Hermit is overlain by a clean, vitreous, pinkish red or grayish white quartzite designated the Permian Coconino Quartzite. The Coconino Quartzite crops out as resistant ledges and locally contains high-angle planar crossbeds. The Coconino Quartzite is overlain by a thick sequence of chert-bearing carbonate and calc-silicate rocks designated as the Permian Kaibab Marble. Like the

Supai Formation, the Kaibab includes large amounts of wollastonite. Between the Coconino quartzite and the Kaibab marble is a layer of greenish siliciclastic and calc-silicate rocks which might be correlative to the Permian Toroweap Formation of the Grand Canyon (Hamilton, 1982), however, for mapping purposes, the Toroweap Formation and Kaibab Marble are mapped together. The Kaibab is the thickest and most widely distributed of Paleozoic rocks in the Big Maria Mountains, with a maximum tectonic thickness of over 300 m. As such, the Kaibab Formation provides a useful structural marker for simplified structural/tectonic maps.

Paleozoic rocks are overlain by Mesozoic sedimentary and volcanic rocks ranging in age from Triassic through Late Jurassic. The Jurassic tectonic evolution of the region has been controversial in terms of the interplay between extension, compression, cratonal sedimentation and the influences of arc volcanism. The basal Triassic Buckskin Formation (Reynolds et al., 1989) rests disconformably above the Kaibab Marble (though the contact is locally sheared). The Buckskin Formation consists of a greenish fine-grained chloritic schist member and a massive calcareous quartzite member; the Buckskin Formation is likely correlative to the Triassic Moenkopi Formation of the Colorado Plateau. The Buckskin Formation is overlain by the Triassic-Jurassic Vampire Formation (Reynolds et al., 1987), which consists primarily of coarse grained conglomerate and volcanically derived sandstone. The Vampire Formation has been interpreted to represent stable cratonal conditions, but large, angular feldspar clasts in the conglomerate suggest localized uplift nearby during deposition and the presence of volcanically derived sediment suggests input from the Triassic magmatic arc (e.g., Asmerom et al., 1988). The Vampire Formation may record the onset of active margin tectonics on the southwestern margin of North America, possibly as rifting related to the breakup of Pangea (Reynolds et al., 1989). The Vampire Formation is overlain by the Aztec quartzite, a clean, vitreous, eolian quartzite correlative to the Aztec/Navajo Sandstone of the Colorado Plateau. This formation suggests that stable cratonal depositional conditions persisted in the region into the Early Jurassic, but that there was an interfingering of cratonal and arc-derived volcanic materials.

The Aztec quartzite is overlain by a thick sequence of volcanic rocks of Early Jurassic age. The contact between the Aztec quartzite and the volcanic rocks is gradational, with layers of Aztec quartzite interbedded with the overlying volcanic rocks. The Jurassic volcanic rocks indicate the onset of active margin tectonics during the Middle Jurassic. The volcanic suite consists of metamorphosed rhyolite, dacite, tuff (metainimbrite sequence of Hamilton, 1982), and hypabyssal quartz porphyry. In the Big Maria Mountains, the Jurassic volcanic rocks may be divided into a lower member and an upper member. The lower member is greenish-gray micaceous schist, consisting of quartz, plagioclase, potassium feldspar, muscovite and abundant epidote. The lower member, like the Bright Angel Schist, is useful for examining polyphase deformation fabrics due to its high mica content. The compositional variation between green epidote rich layers and gray quartz-mica layers makes this an important unit to study to recognize deformation fabrics. The upper member is a light tan to buff micaceous schist, which consists of abundant quartz and muscovite with lesser feldspar and sparse oxides. These rocks are likely correlative to the Jurassic Dome Rock sequence of Tosdal et al. (1989).

A suite of Jurassic plutonic rocks represent the youngest rocks in the BMM to experience all episodes of polyphase deformation. These rocks are the most aerially extensive rocks in the BMM and throughout the SW Mojave Desert region. The Jurassic plutonic rocks consist (in ascending order) of a dark greenish dioritic member, a light gray granodiorite that contains large (~1 cm. in diameter) euhedral lavender feldspars, and a leucocratic granite. The plutonic rocks are likely correlative to the Kitt Peak-Trigo Peaks Supergroup of Tosdal et al. (1989). Both the Jurassic volcanic and plutonic rocks were part of a Jurassic magmatic arc that extended along the western margin of North America from Sonora to British Columbia (Tosdal et al., 1989).

All rock units described above have been subjected to all episodes of polyphase deformation, which indicates that all deformation must post-date Jurassic magmatism. These rocks all exhibit a pervasive, predominately north-dipping cleavage designated here as S_1 . In most cases, S_1 is subparallel with relict bedding features in Paleozoic and Mesozoic strata and unit contacts and is observed to be an axial planar cleavage to

isoclinal mesoscopic folds. All older rocks in the range are intruded by Cretaceous leucogranite dikes. These dikes consist of plagioclase feldspar and quartz, but also contain books of muscovite, biotite, garnet, and epidote. They are part of a regionally extensive suite of two-mica, strongly peraluminous granitic plutons (Miller and Bradfish, 1980). These dikes are weakly deformed, locally folded or boudinaged, and are likely coeval with peak metamorphism, based on an association of increasing metamorphic grade with areas of high dike density in the range (Hoisch et al., 1988). These dikes cross-cut the S_1 fabric and must post-date most major polyphase deformation events. Although distributed throughout the range, the majority of dikes in the range are present in a swarm exposed in the southwestern part of the range. This swarm of dikes has been attributed to the presence of a nearby pluton (Hoisch et al., 1988), though this pluton is not exposed anywhere at the surface in the BMM. The dike swarm is also associated with increasing metamorphic grade in the range (Hoisch et al., 1988).

The youngest rocks in the range are Tertiary rhyolite plugs, mafic dikes and sedimentary rocks exposed in the north side of the range that are part of the late Miocene Bouse Formation. Tertiary magmatism in the range is interpreted as being coeval with polyphase Tertiary extensional and transtensional deformation. Quaternary surficial deposits flank the range and form a pediment separating the BMM from other nearby mountain ranges. Tertiary-Quaternary Colorado River terrace deposits are observed along the east flank and around the southeastern tip of the range.

Paleozoic stratigraphy and degree of stratal attenuation

Paleozoic metasedimentary rocks in the BMM were first described by Miller (1944) who grouped the rocks together as the Maria Formation. Miller assigned a Paleozoic age to the rocks based on possible correlation with rocks of the Colorado Plateau. Hamilton (1964) recognized that Paleozoic rocks had been subjected to polyphase deformation and extreme attenuation. Hamilton also recognized that metasedimentary rocks of the Maria Formation formed a distinct stratigraphy that could be correlated to the classic cratonal sequence of the Grand Canyon; however he did not

publish these correlations until much later (1982). Paleozoic rocks were subsequently assigned names from their respective correlative formation in the Grand Canyon. These rocks are the most useful for defining Mesozoic structures, as well as for palinspastic reconstruction. Once these correlations were recognized, Paleozoic rocks throughout western Arizona and southeastern California were remapped and correlated across the region (Figure 1.2, Stone et al., 1983). This recognition also allowed for the identification of large-scale fold nappes throughout the region that featured imbricated and attenuated Paleozoic sections. As one contribution of this paper, we refine the current understanding of Paleozoic stratigraphy, as described in this section.

Figure 1.4 shows a generalized stratigraphic column for Paleozoic rocks in the BMM compared to eastern (a) and western (b) Grand Canyon thicknesses. In the thick, unattenuated fold limb (c), thicknesses of units in the BMM are reasonably close to thicknesses for unaltered sedimentary correlatives in the Grand Canyon, supporting the correlation to the cratonal (non-miogeoclinal) Paleozoic section of the southwestern US as reported by Stone *et al.* (1983).

The total average thickness of the Paleozoic section in the BMM is approximately 1180 m (Salem, 2005), which is fairly close to the reported *average* thickness of the Paleozoic section at the Grand Canyon of approximately 1500 m (Beus and Morales, 2003). The observed 320 m difference in thicknesses is interpreted to be accounted for by attenuation of even the thick limb of the fold in the BMM due to flattening of units and observed shear-related transposition of original bedding during ductile deformation.

In some areas, Paleozoic rocks have been attenuated to less than 1% of original stratigraphic thickness (Hamilton, 1982). In the Big Maria syncline, Paleozoic units in the upper limb of the syncline have been attenuated on average to 8% of the thickness of corresponding units in the lower limb of the syncline (Figure 1.4d, Salem, 2005). Carbonate units and micaceous schists have been attenuated to a greater extent than quartzite and calc-silicate rocks. This is probably due to the greater competency of quartzite and calc-silicate rocks compared to carbonates and micaceous schists. Although

Generalized stratigraphic columns for Grand Canyon Paleozoic rocks and correlative sections from the Big Maria Mountains

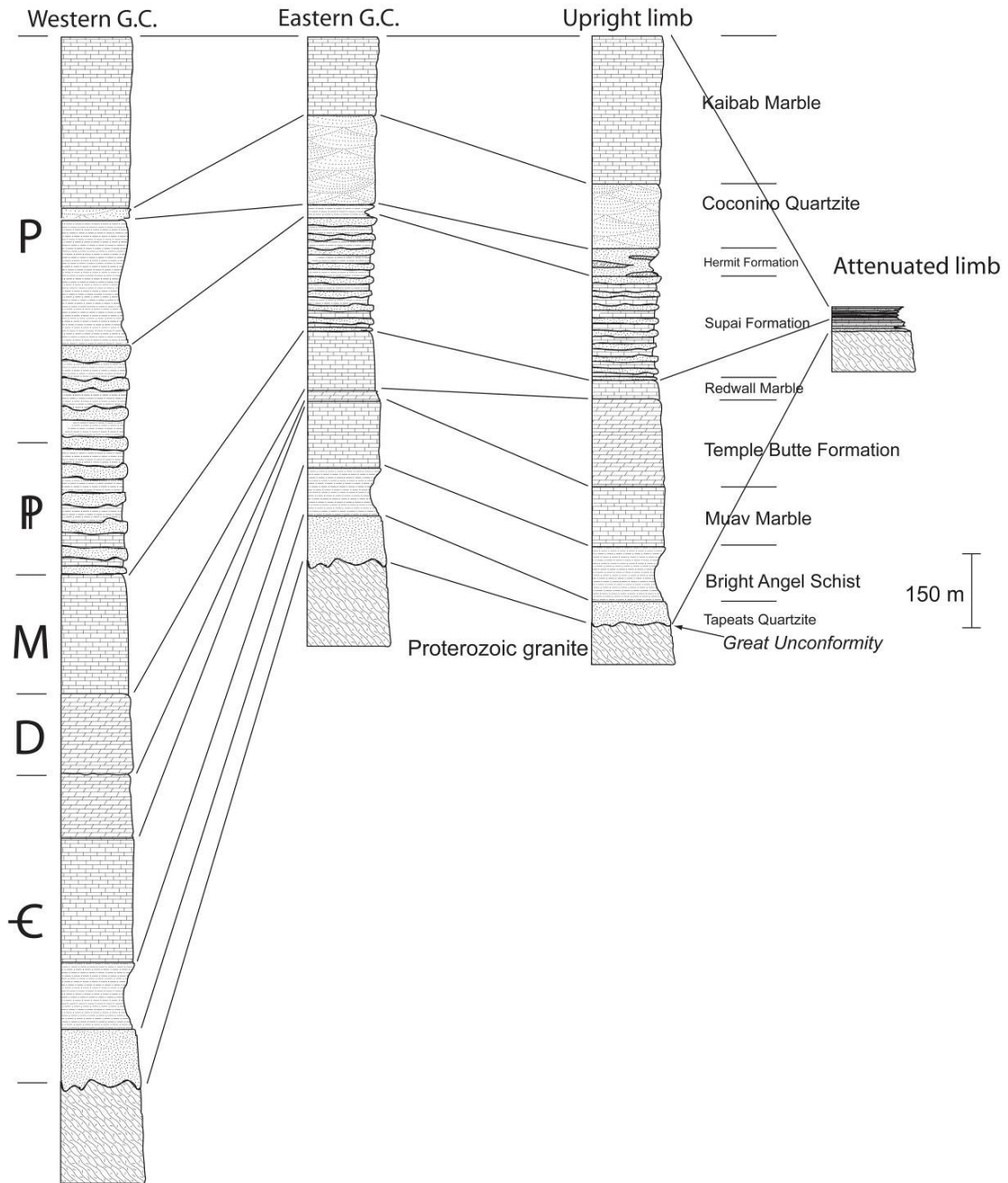


Figure 1.4: Generalized stratigraphic column of Paleozoic metasedimentary rocks in the Big Maria Mountains from the upright and attenuated limbs compared with correlative units from the western and eastern Grand Canyon (Beus & Morales, 2003). Unit thicknesses in the Big Maria Mountains (given in m) do not represent original depositional thicknesses but are instead measured transposed thicknesses (Salem, 2005). Ages (geologic periods) are assigned to units based on correlation with unmetamorphosed Paleozoic stratigraphy of the Grand Canyon of the Colorado Plateau (Hamilton, 1982).

thickness of units is variable, with some units being sheared out locally, overall Paleozoic units are continuous and in correct, though inverted, stratigraphic order. A notable exception is observed near the hinge zone of the syncline, where the lower Paleozoic section through the Cambrian Muav Marble is missing, and Jurassic granite is in contact with the Devonian Temple Butte Formation (Figure 1.5). Along strike of the syncline, both in the upright and attenuated limbs, Jurassic rocks intrude through the Paleozoic section but are never observed to intrude any higher than the Devonian Temple Butte Formation.

The geometry of stratal attenuation provides clues to deformation processes as discussed by Ballard (1990). Paleozoic rocks in the upright limb of the syncline maintain their approximate tectonic thicknesses as they come around the hinge zone (Figure 1.6). From the annotated aerial photograph of the Big Maria syncline, shown in Figure 1.6a, the geometry of the Permian Kaibab Marble is the most useful for examining the geometry of the syncline itself. The Kaibab Marble (Pk) comes around the hinge of the syncline and then is abruptly attenuated. However, note that the Kaibab Marble can be identified even in the attenuated section for a few kilometers along strike of the attenuate limb, until it reaches a constriction where the entire Paleozoic section thins to less than 20 m thick. This abrupt further attenuation of units is observed quite nicely in the TIMS (Thermal Infrared Multiscanner Spectrometer) image shown in Figure 1.6b. This cutout of the TIMS image for the central part of the range roughly coincides to the same area shown in the aerial photograph in Figure 1.6a. In this image, different lithologies show up as different red, blue or green color bands. The Kaibab Marble, from Figure 1.6a, shows up as the prominent green (carbonate) unit with blue (calc-silicate minerals) streaks that defines the shape of the syncline. The Kaibab Marble is shown to come around the hinge of the syncline, where it then becomes abruptly attenuated. Note, that the Kaibab is the top most green stripe of a multicolored band of red, blue and green that is the entire Paleozoic section (Pz).

The geometry of most folds in the area show thickening of fold hinges and thinning of limbs, similar to Class 3C folds as discussed in Ramsay (1967). However,

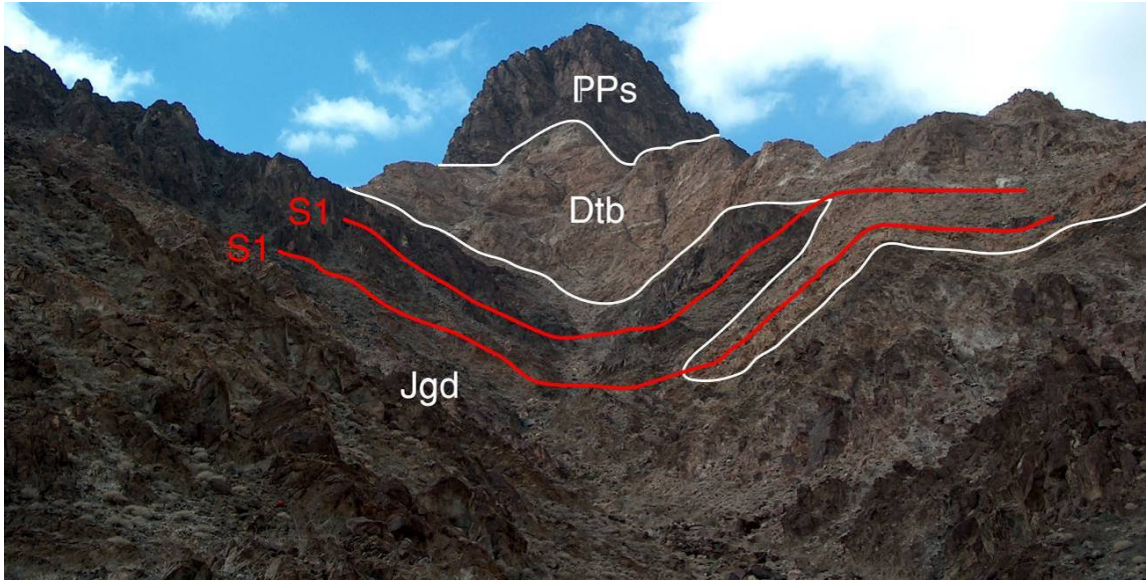


Figure 1.5: Jurassic plutonic rocks (Jg) in contact with Temple Butte metadolomite (Dtb). Plutonic rocks have inclusions of Tapeats quartzite and Bright Angel schist, although these are not distinguishable in this photograph. The contact between the Temple Butte metadolomite and Jurassic granodiorite is folded around S_1 foliation, which is penetrative through both units and which runs subparallel with contacts throughout the field area.

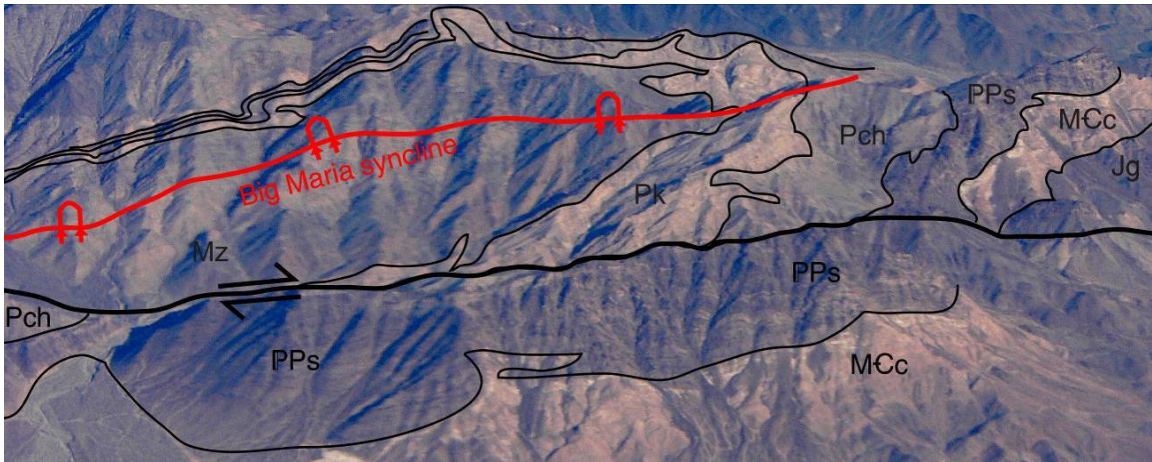
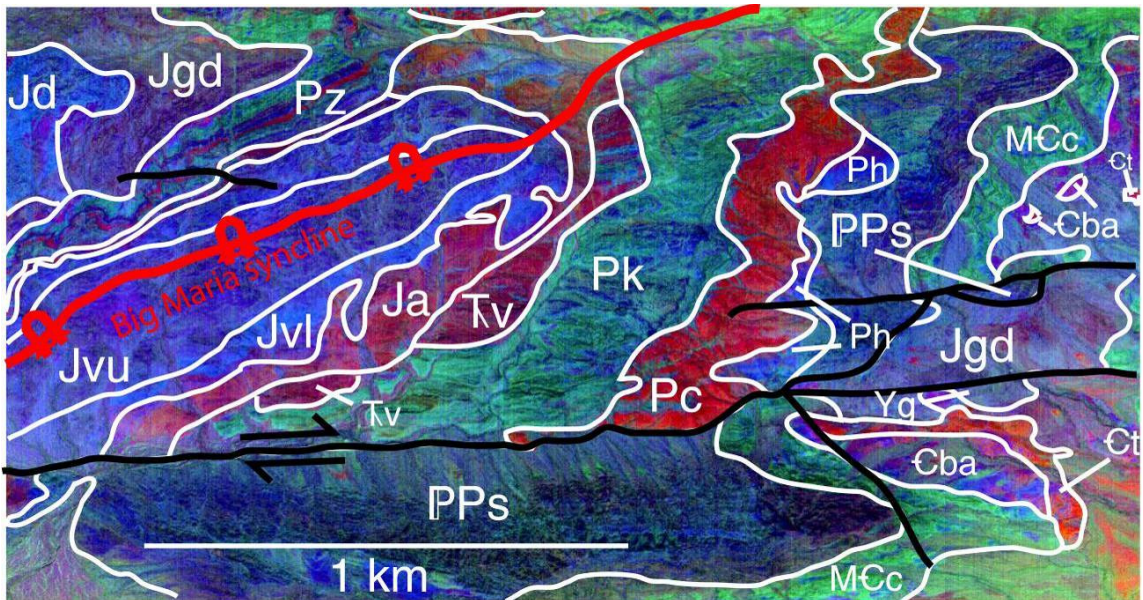


Figure 1.6: Top: Aerial photograph of the Big Maria syncline looking NE. Contacts between units have been sketched in. The syncline is best defined by the contact between the Kaibab marble (Pk) and Mesozoic metasedimentary and metavolcanic rocks (Mz). Photograph S.J. Reynolds. **Bottom:** TIMS image of approximately the same area for comparison and illustration of units based on mineralogy. Note the ease of separating different geologic units using the TIMS image. In general, quartz shows up as red, carbonates as green, calc-silicate minerals as blue, micaceous rocks as purple.



attenuation of Paleozoic units happens abruptly at the hinge zone and then the section gradually becomes even thinner to the west (down the plunge direction). As shown in Figure 1.5, deformation is characterized by ubiquitous intrafolial folds and boudinaged layers. In this field photograph, taken looking west, the intrusive contact between Jurassic granodiorite and the Devonian Temple Butte Formation has been folded into tight F_1 isoclinal folds. Intrafolial folds can be tens to hundreds of meters long on their long axes. What we observe, as shown in Figure 1.5, is that the pervasive S_1 fabric is actually axial plane cleavage to isoclinal F_1 folds of varying scale. In addition, contacts such as where the Jurassic granodiorite intrudes Paleozoic rocks are often characterized by psuedostratigraphy or “ghost” stratigraphy. In this case older Paleozoic rocks, such as the Tapeats Quartzite in the intrusive granodiorite are observed to be approximately where they would occur in a “normal” section, except for the fact that they have been intruded by younger plutonic rocks. At first glance, it appears as though the plutonic rocks have intruded through the Paleozoic section and that older Paleozoic rocks were either displaced by magma injection or that the contact between the Jurassic plutonic rocks and higher Paleozoic section rocks represents localized shear zones. The psuedostratigraphy confirms that the plutonic rocks have intruded the section as a series of sheet-like sills, preserving tens of meter scale inclusions of older Paleozoic rocks. S_1 cross-cuts contacts in this photograph, indicating that this cleavage formed after intrusion of the granodiorite. Finally, there are only a few places in the study area where the lower Paleozoic section has been removed. Where this is the case, these local areas of shear could be interpreted as being formed as the result of localized extensional shear. However, we interpret that both stratal attenuation and the local omission of strata as due to crustal flow during overall contractual deformation (see below).

Structural geology

Methods

Structural studies followed standard methods of structural analysis in polydeformed terranes (Hobbs et al., 1976; Ramsay, 1967; Davis and Reynolds, 1996).

By convention, we use the abbreviation S to refer to a tectonic fabric (i.e., cleavage) that formed as the result of a deformation event, D to refer to a deformation event, F to refer to folds that formed during a deformation event and L to refer to a mineral lineation that developed during deformation. Furthermore, we use subscripts to refer to the generation of development of a structural feature. For example, D₁, D₂, D₃ represent first deformation event, second deformation event and third deformation event. Initial and subsequent mapping efforts were built upon the excellent mapping done by Hamilton (1964; 1982; 1984). The study area was reconnaissance mapped at 1:24,000 (Salem, 2005). This work focused primarily on separating out individual Paleozoic lithologies. Subsequent mapping was done at 1:12,000. Mesozoic units were separated out and distinctions were made between Jurassic and Proterozoic crystalline rocks. Once the initial mapping was done, three areas were selected for further structural analysis. In each of these areas, macroscopic and mesoscopic folds and faults were characterized. Overprinting relationships between multiple cleavage fabrics, between cleavage fabrics and faults, and between different cleavage fabrics and igneous intrusions were also examined. Numerous measurements were taken in the Cretaceous leucogranite dike swarm at the western end of the range in order to determine the direction of finite extension during dike emplacement. Structural fabrics were then correlated across the area based on overprinting relationships to determine the kinematics and timing of deformation events on a regional scale. This data was then combined with existing geochronologic data to determine a regional chronology and model for deformation events. Mapping was aided through the use of Thermal Infrared Multispectral Scanner (TIMS) images (Figure 1.6) provided by NASA (1995) which were georeferenced using ArcGIS. As shown in Figure 1.6, different minerals will emit different colors in the red-green-blue spectrum in infrared, which aids a great deal in mapping. Comparing the TIMS to the aerial photograph, more detail can be captured from the TIMS image. Also, many mesoscopic folds can be picked out and mapped from the TIMS compared with mapping on the ground, allowing for a more complete picture of the syncline. Finally, the

TIMS image agrees very well with field mapping done in this investigation and from previous work (Hamilton, 1982; Morrissey, 1999).

Macroscopic structures

This section begins by describing the geometry of the Big Maria syncline, the major macroscopic fold of the range, and then proceeds to place this fold in the context of the overall deformational regime in the Big Maria-Little Maria Mountains, which includes multiple phases of Mesozoic contractile and Cenozoic extensional deformation. The basic structural architecture of the Big Maria Mountains consists of Proterozoic through Jurassic rocks folded in the macroscopic subrecumbent Big Maria syncline the southern part of the range, which is in the lower plate of a major south-vergent ductile thrust. In the upper plate of the thrust, in the northern part of the range, is a structurally complex zone that contains high grade Proterozoic and Mesozoic gneisses with pods and lenses of Paleozoic sedimentary rocks. The syncline is defined by a core of Paleozoic and Mesozoic sedimentary rocks flanked to the north and south chiefly by Jurassic plutonic rocks interspersed with Proterozoic crystalline basement. The syncline consists of an upright, relatively unattenuated southern limb and a moderately to extremely attenuated northern limb. The attenuated limb of the syncline defines a high strain shear zone, which we designate as the Maria Shear Zone, that trends subparallel with the syncline and is interpreted here to have formed syntectonically with the syncline. The Big Maria Syncline is exposed for several kilometers in the central Big Maria Mountains (Figs. 1.2 and 1.3). The structure is a ~2 km amplitude subrecumbent, subcylindrical, west-plunging syncline. The axial trace of the syncline trends roughly west-northwest through the range; the axial plane of the syncline strikes ~290 (WNW) and dips ~40° N. Since this large structure and associated smaller folds re-fold the pervasive S₁ cleavage, we designate them as F₂ folds. These folds might have formed during a distinct, kinematically different second deformation event or during the second stage of a progressive deformation event. In this paper, we make our case for the latter scenario. As shown in Plate 1, we mapped the axial trace of the syncline from a large normal fault in the center of the range ~3 km west

where it is offset by a major, northwest-trending transtensional (normal and dextral) fault. These two faults represent are structures formed by Miocene extension and Miocene-Pliocene transtension and, along with the Riverside Detachment Fault, are the defining structural features of the mountain range. Therefore, restoration of these Tertiary structures is key to understanding the earlier Mesozoic deformation. Brittle strain on these Tertiary faults is low enough that the older Mesozoic structures can be described and characterized. The next sections will elaborate on these Tertiary structures, and will discuss what Mesozoic structures may be observed after restoration of these later structures.

The large normal fault mentioned above strikes approximately N-S, and dips $\sim 60^\circ$ E. The fault has curvilinear geometry, based on examination of measurements taken around the fault plane by Hamilton (1982). Sense of motion along the fault is hanging wall down to the east. The Colorado River roughly parallels the strike of the fault in this area. We propose the name Quien Sabe Fault for this high angle normal fault, named for Quien Sabe Point, which is a prominent hanging-wall ridge that juts out east from the fault towards the river. The Quien Sabe Fault divides the Big Maria Mountains nearly in half and accounts for the unusual geomorphic expression of the range. It is likely the Quien Sabe Fault is a bounding fault of the Breakaway to the Colorado River Extensional Corridor (Howard and John, 1987) a narrow valley of E-W directed extension in California and Arizona named for the river that flows through it. Total displacement on the Quien Sabe Fault is unknown but must be significant, because the fault separates two distinctly different structural domains. For example, Precambrian rocks Hamilton (1982) maps in the upper plate of the Riverside detachment are juxtaposed next to Jurassic migmatite rocks that are observed in the lower plate of the Riverside Detachment. Also, the structural domain in the hanging wall (north of the fault plane) is characterized by predominately north and east dipping foliation. This is in contrast with the majority of the range (in the footwall of the fault), which is characterized by predominately north and west dipping foliation. Based on the overall down-to-the east sense of motion on the fault these rocks in the hanging wall must have originated from somewhere to the west. The

nearest place west of this area that contains a domain of east-dipping S_1 fabrics is in the eastern Little Maria Mountains (Plate 2). Assuming that these two areas represent the same east-dipping domain, then apparent horizontal offset would be on the order of 10 km. Using the spatial measuring tool in ArcGIS, the straight line distance between these matching areas is approximately 12 km. Another important marker area is the hinge zone of the Big Maria syncline, which is exposed on both sides of the fault and thus is another indicator that total displacement along the fault must be significant. Using the spatial measuring tool in Arc GIS, the straight line distance between the hinge zone exposed in the hanging wall of the Quien Sabe Fault to the hinge zone exposed in the footwall is approximately 11 km, which is in excellent agreement with the area matching measurement of the two east dipping domains. Thus, total apparent horizontal offset would be on the order of 11-12 km. However, this is only an apparent measurement and must be a gross overestimation of actual displacement along this fault. Since the fault is measured in several places by Hamilton (1982) to dip $\sim 60^\circ E$, if 11 km. were the actual horizontal displacement, then calculated vertical displacement would be 22 km., which is totally unreasonable. Based on our restorable cross section through the Big Maria syncline (Figure 1.7), we estimate approximately 1.5-2 km of vertical displacement along the fault, which is a reasonable estimate of the amount of displacement for a major high angle normal fault. To account for the difference between apparent horizontal offset on the fault with our estimation of vertical displacement, there must be a significant amount of fault block rotation along a fault plane that becomes listric at depth.

The relationship between the Quien Sabe Fault and the roughly E-W striking Riverside-Maria-Granite (RMG) detachment fault (Figure 1.2, Hamilton, 1982; Lyle, 1982; Ballard, 1990; Stone and Kelly, 1989) is unclear. The RMG detachment fault contains Tertiary sedimentary and volcanic rocks in its hanging wall and middle crustal metamorphic rocks in its footwall (Stone, 2006). Sense of motion on the Riverside Detachment is hanging wall down-to-the-north or northeast (Lyle, 1982). The RMG detachment fault partitions the Riverside Mountains and separates them from the Big

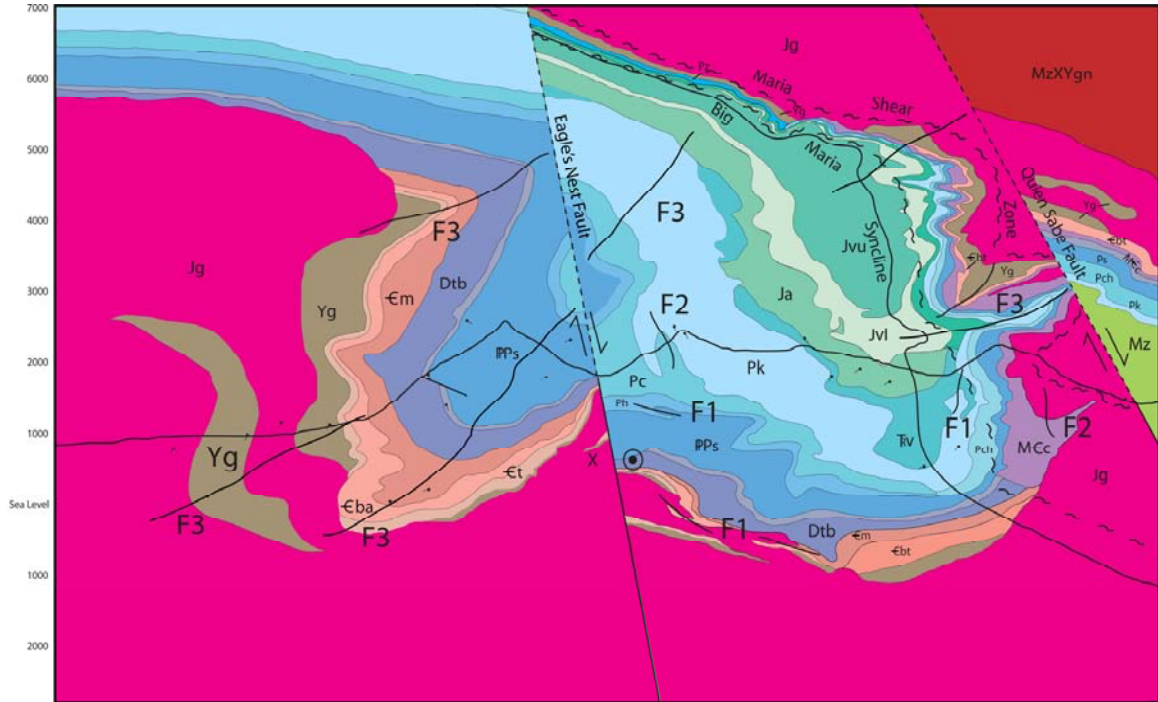


Figure 1.7: Geologic cross section along A-A' from Big Maria Mountains geologic map (Plate 1) with no vertical exaggeration. Present day erosional surface is shown as the black topographic profile. Tadpoles show strike and dip data taken from map. Elevation is shown in feet relative to sea level. Cross section constructed from placing contacts along topographic profile and using a down-plunge project of the geologic map. Polyphase folds are designated F₁, F₂ and F₃. Unit colors and abbreviations are taken from the map. Cross section shows major Cenozoic faults, axis of Big Maria syncline and Maria Shear Zone. D₃ inferred NE-directed sense of shear is based on Z-fold geometry of refolded Big Maria syncline axis and associated F₃ folds.

Maria Mountains to the south, strikes north of the Little Maria Mountains and separates the Granite from the Palen Mountains. Along most of its length, the fault represents the Breakaway to the Colorado River Extensional Corridor. Most workers, (Lyle, 1982; Stone and Kelly, 1989; Howard and John, 1987) have demonstrated this fault dips shallowly ($\sim 30^\circ$ to the north and east). It is likely that the RMG Detachment Fault developed during formation of the Colorado River Extensional Corridor and that development of the RMG detachment took place syntectonically with development of the Quien Sabe Fault.

In the hanging wall of the Quien Sabe Fault, the overturned attenuated limb of the Big Maria syncline can be traced southeast for several kilometers. Stratal attenuation of Paleozoic and Mesozoic sedimentary and volcanic rocks defines a high-strain ductile shear zone which we name the Big Maria shear zone. The Big Maria shear zone strikes sub-parallel with the trend of the Big Maria syncline and is interpreted to have formed syntectonically with the syncline. Intrafolial folds present within even the high strain zone are ubiquitous and indicate continuous folding and refolding during polyphase deformation. Attenuation of Paleozoic units mapped in the Big Maria syncline exposed in the hanging wall of the Quien Sabe Fault is not as great as is observed in the west-central portion of the Big Maria Mountains. The southeast strike of the syncline in the hanging wall of the Quien Sabe fault is in contrast with the east-west trend of the syncline in the central part of the range, where our study was focused. We interpret this change to represent a deflection of the overturned limb from an overall E-W orientation to a NW-SE orientation. Large-scale deflections such as this are interpreted to be the result of a significant refolding event that must post-date formation of the Big Maria syncline and associated structures. Since the Big Maria syncline is interpreted here as an F_2 fold, these folds are designated F_3 as they refold the syncline. The axes of antiforms and synforms associated with this deformation event are shown as F_3 fold axes (in yellow) on Figure 3.

In the southeastern part of the range, the syncline is overprinted by large, southwest-vergent ductile thrust faults. However, taking these faults into account, the overturned limb can be traced around the hinge zone of the Big Maria syncline exposed near the southeastern tip of the range. The hinge zone of the syncline is defined by the

presence of the Jurassic metavolcanics unit. Units strike SE and are deflected around an isoclinal fold hinge and then strike back toward the NW. The overturned limb strikes around the hinge line and becomes right side up on the southwestern limb. Finally, it is likely that hinge zone of the Big Maria syncline as exposed in the southeastern portion of the range represents the eastern termination of the structure, as is indicated by the geometry of the hinge zone in the footwall of the fault. The Big Maria syncline cannot be correlated across the Colorado River, though similar structures are present in the eastern Maria Fold and Thrust Belt (Laubach et al., 1989; Richard et al., 1994).

In the footwall of the Quien Sabe Fault, the Big Maria syncline strikes almost due west from the fault plane. The fault truncates the hinge zone such that only the Mesozoic sedimentary and volcanic units and the Kaibab Marble actually are observed come around the hinge. The hinge zone of the syncline is exposed immediately underneath the fault. In the hinge zone of the syncline, the Kaibab Marble and Mesozoic section maintain their thickness coming around the hinge of the syncline and then become severely attenuated, as shown in Figure 1.6. The attenuated limb of the syncline can be traced for ~2 km from the fault and individual units (or groups) can be separated out from each other, even at 1:24,000 scale. The attenuated limb is observed to come around a mesoscopic (hundreds of meters) scale F_3 antiform, at which point the entire Paleozoic section is constricted into a narrow band less than 30 m wide. The internal stratigraphy of the Paleozoic section, while inverted, is still preserved. Individual units can be discerned but cannot be mapped separately from each other except at really low scale (1:6000) mapping. From here, the attenuated section strikes southwest then west and is truncated by a large, right-lateral fault, designated here as the Eagle's Nest Fault, named for the Eagle's Nest Mine in the northwest part of the range.

The transtensional (dextral and normal) Eagle's Nest Fault bisects the field area and slices northwest along the western margin of the Big Maria Mountains. The fault has approximately 1.5 km of apparent right-lateral separation and approximately 340 feet of vertical (down to the northeast) displacement. Vertical displacement is determined from our restorable cross section (Figure 1.7). Based on its sense of motion, we interpret this

fault to be sympathetic with the larger San Andreas Fault System. Upon inspection of the map, there are two sets of points that might be matched on both sides of the fault that allow for rough fault reconstruction. Both sets of points represent axes of macroscopic F_3 folds. These points are highlighted in Plate 1. The greatest degree of stratal attenuation of Paleozoic and Mesozoic rocks is observed in the Big and Little Maria Mountains is observed here. In fact, the entire syncline is observed to undergo a major constriction in this area (Plate 1; Figure 1.3). For the sake of simplicity, we label this area the “constriction” zone. Later in this paper, we reconstruct the Big Maria syncline and discuss the significance of the constriction zone and the implications it has for overall evolution of the structure. Paleozoic units are thinned to less than 1% of original thickness, though the entire stratigraphy is still preserved. Lower Paleozoic units (Redwall and older) are covered by surficial deposits in this area, but, in keeping with the geometry of the rest of the structure, we depict these units thinning as well through the constriction zone. The axial trace of the syncline continues on the west side of the fault and trends west-northwest for approximately 2 km until it reaches the west end of the range, where unit contacts are deflected to the north (Figures 1.2 and 1.3) around another macroscopic F_3 fold in the vicinity of Black Hill. North of here, the syncline is observed to widen back to its “normal” width. For our purposes, the width of the structure is defined by exposures of Paleozoic and Mesozoic cratonal strata, though Jurassic plutonic and Proterozoic crystalline rocks are involved in the structure as well so the actual “width” of the syncline is unknown. This widening is based on the degree of attenuation of Paleozoic units, which is consistent with that observed further east in the range. Mesozoic metasedimentary rocks are exposed in scattered outcrops, but occupy a much larger spatial domain than in the constriction zone.

Beginning near Black Hill, the axial trace of the syncline is interpreted to trend NNW for approximately 7 km before it is deflected westward around yet another macroscopic F_3 fold. Unit contacts continue to strike roughly ESE across the Midland Road and can be traced and connected with units exposed in the Little Maria Mountains (Figure 1.3). Hamilton (1982) and Ballard (1990) proposed that the Little Maria syncline

is a westward continuation of the Big Maria syncline and inspection of the two maps confirms this idea. Therefore, the Big Maria syncline is large structure that is laterally continuous for ~50 km. In the northwestern Big Maria and in the Little Maria Mountains, the structure is observed to be about as wide as at is observed in most of the Big Maria Mountains. Jurassic volcanic units, which make up the core of the syncline in the Big Maria Mountains, are not exposed in the core of the syncline in the Little Maria Mountains. This might be explained as the result of change in overall direction of plunge of the syncline from the Big to Little Maria Mountains. For all of its exposure in the Big Maria Mountains, the structure plunges either west or northwest. In the eastern Little Maria Mountains, the structure plunges east or northeast. The syncline continues to plunge east until ~ 2 km west along the trace of the fold axis in the Little Maria Mountains. At this point, the structure reverses back to a westward plunge and remains so until the structure can no longer traced at the west-central margin of the range. This change in the plunge of the fold is likely accounted for by F_3 folding, which would have reoriented mineral lineation from westward to eastward plunging. Ballard (1990) argued that NE-plunging lineations exposed in the eastern Little Maria Mountains were evidence of a kinematically distinct SW-directed deformation event. However, given the comparatively small exposure of NE-plunging lineation and east-dipping foliation, and the widespread refolding of earlier structures by F_3 folds, our interpretation seems more consistent with field observations. Assuming that the syncline continues along its trajectory at the western edge of the Little Maria Mountains, the structure would strike west or northwest into supracrustal Jurassic volcanic rocks exposed in the northern McCoy and central Palen Mountains. This juxtaposition of middle crustal ductile deformed rocks next to supracrustal brittle deformed rocks represents an important tectonic contact that separates the Maria Fold and Thrust Belt from the McCoy Basin (Figure 1.2), which we designate the Maria Frontal Thrust.

Figure 1.7 shows a true-scale cross section (i.e., no vertical exaggeration) of the Big Maria syncline made near the hinge zone of the structure. This cross section was generated combining structural constraints in the field with a down-plunge projection of

our geologic map. Tadpoles indicate actual strike and dip measurements and contact lines along the topographic profile are constrained by the map. To create the down plunge projection, we first restored movement on the Eagle's Nest Fault. Then, using the average plunge of the syncline, 30° toward 280, we created the down plunge view of the syncline from the map by scaling the map along 280-100 (the plunge direction) by $\sin(30^\circ)$, which is 0.5. Thus, every feature along azimuth 280-100 was shortened by 0.5. This down plunge projection was then overlain over a primary cross-section drawn using field constraints to help complete the picture. The result is a powerful tool that illustrates all of the major deformation features described above and will be referred to frequently during each of the discussion on the various domains analyzed in detail. Colors and unit abbreviations depicted in the cross section are taken from our geologic map of the syncline (Plate 1). Restoration of this cross section will be used to unravel Cenozoic and Mesozoic deformation events and will lead to a new regional model for deformation in the area.

Because the cross section was drawn near the hinge zone of the syncline, the structure does not go very deep into the subsurface here; instead most of it projects up into space. From the cross-section, the axial plane of the syncline is observed to have an overall average dip of $30-40^\circ$ N; however, the axial plane dip at any location can be quite variable. For instance, toward the Eagle's Nest Fault in the central part of the cross section, the dip of the axial plane is shallow. Moving north (to the right) the dip of the axial plane becomes steep to sub-vertical, with a few bends, and then becomes shallow again in the subsurface before being cut off by the Quien Sabe Fault near the north end of the section. We interpret these variable dips of the axial plane to be the result of significant F_3 refolding. As is illustrated in this and subsequent sections, F_3 refolding is pervasive in the Big Maria Mountains and significantly modifies earlier structures. Major F_3 macroscopic folds are shown on the cross section. The refolding of the Big Maria syncline axis around F_3 folds shows a Z-fold geometry (Figure 1.7). Although slip along fold planes as an indication of shear sense is not always reliable, the sense of motion suggested by the Z-fold indicates that F_3 folds formed as a result of northeast-directed

normal ductile shear. Ballard (1990) documents NE-vergent folds in the Little Maria Mountains and argues that these folds formed by NE-directed normal ductile shear based on microstructural evidence. Although we document no NE-directed normal shear sense indicators in thin sections from the Big Maria Mountains, the observation that macroscopic F_3 folds here formed as the result of NE-directed normal shear agrees with Ballard's interpretation for those formed in the Little Maria Mountains. In subsequent sections, we further support this argument with field photographs of mesoscopic F_3 folds and the mean orientation of the leucogranite dike swarm as a kinematic indicator of the finite direction of extension during D_3 deformation.

As mentioned earlier, we interpret the Big Maria syncline and associated folds to represent composite F_2 macroscopic folds that refold S_1 and F_1 isoclinal folds, also labeled on the cross section. The cross section also illustrates the attenuated limb of the syncline as defining the Big Maria shear zone. Degree of attenuation is variable, but overall attenuation of units is sharp just as units bend around the axial plane of the syncline and then the attenuated limb gradually tapers, becoming thinner further upwards. The attenuated limb is easy to recognize as the thin multi-colored band north of the axial plane. Degree of attenuation increases further up, so the number of individual units that can be mapped decreases. However, even in these areas where units are lumped together in a single color, it is important to remember that in most places, stratigraphic continuity is preserved. In most places, units are observed in their correct stratigraphic order (though inverted) and individual units can still be distinguished in the field, but are simply too thin to show on a map, even at 1:6,000 scale. Just before the Eagle's Nest Fault, units become so thin that the entire Paleozoic section is shown as a single blue stripe and Jurassic and Triassic sedimentary rocks are shown as a single green stripe.

Once the initial mapping of the syncline was complete and the overall architecture of the range was determined, three areas were selected for additional structural analysis. These areas were mapped at 1:6,000 scale and are designated A, B and C. A is the central subarea – a F_2 limb region of the syncline. B is the hinge zone of the syncline. C is a limb

region that has been strongly refolded by F_3 . They are chosen as representative of the main fold and fabric generations: S_1 , S_2 and S_3 .

Area A – S_1 dominated domain along attenuated limb of the syncline

Area A (Figure 1.8) may be the best place to understand the kinematics of thrust-sense movement on S_1 . Area A is located toward the center of the study area and includes Proterozoic and Jurassic crystalline rocks that are thrust over the entire attenuated Paleozoic and Mesozoic sections, the synclinal hinge region, the entire Mesozoic upright section and upright Kaibab Formation. From point matching across the Eagle's Nest Fault, there are two points in Area A (an area of extensive D_3 refolding) that we can reasonably match with points in Area C. Therefore, Area A is a region that has been displaced down and to the right of Area C. Therefore, we expect that there will be strong parallels between the two domains. However, we also expect that there will be parallels between Areas A and B, as Area A may contain features of Area B (the hinge zone area) as well.

The area is characterized by a pervasive composite S_1/S_2 foliation that is subparallel to contacts between units and original bedding. S_1/S_2 is generally north, west, or south dipping (Figure 1.8), with an average orientation of $\sim 204, 22^\circ$ W. Although S_1/S_2 and unit contacts are observed to strike east-west through the syncline as a whole, the mean N-S striking, westward orientation of S_1/S_2 is likely accounted for due to extensive refolding. S_1/S_2 is axial plane foliation to F_1/F_2 composite isoclinal folds (Figure 1.9). These isoclinal folds and S_1 have been extensively refolded about mesoscopic F_3 folds (Figures 1.10 and 1.11). These folds are moderately to tightly folded, generally plunge west or northwest, and are characterized by a south dipping cleavage, S_3 . This cleavage is weakly expressed as an axial plane cleavage to F_3 folds. These folds have a Z-fold geometry, as shown in Figure 1.10, which resembles the refolding shown in the cross section in Figure 1.7. Figure 1.11 shows ptygmatic folding of the S_1/S_2 foliation around S_3 axial plane cleavage in the lower member of the Jurassic volcanic unit. Figure 1.12a shows an equal area, lower hemisphere plot of poles to planes of S_1 measurements in

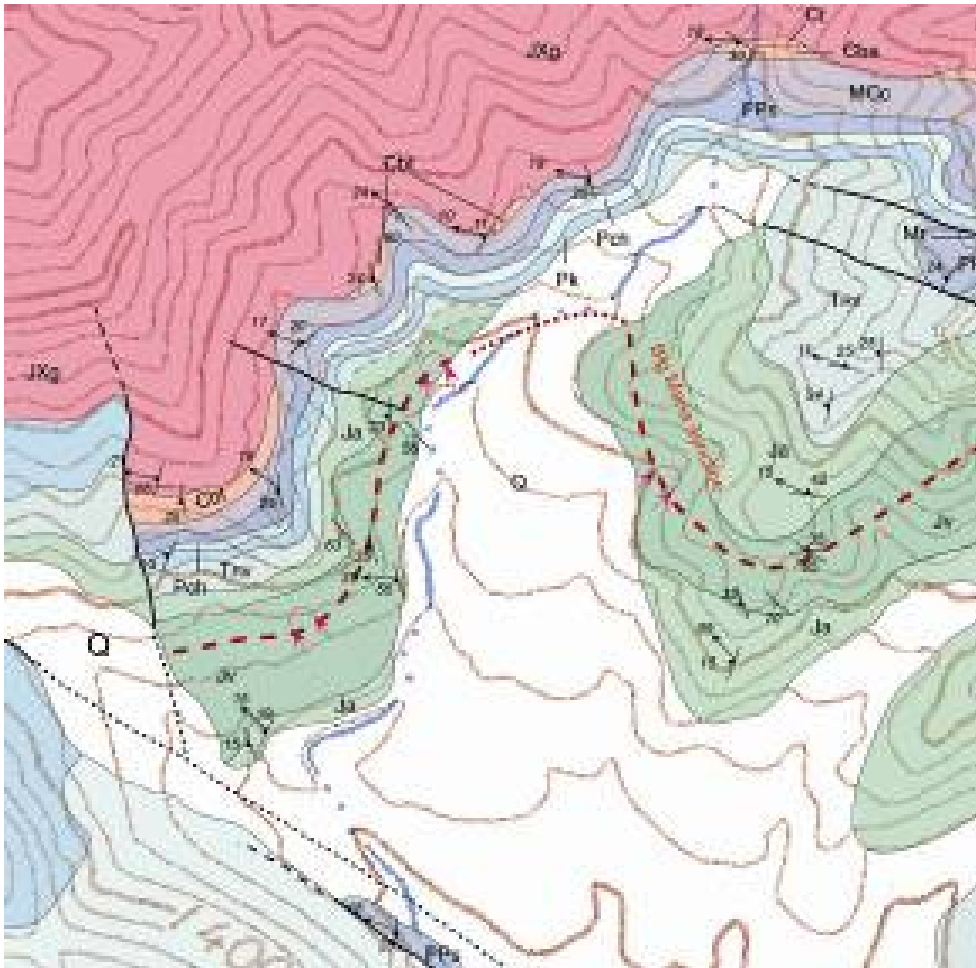


Figure 1.8: Geologic inset map of Area B originally done at 1:6000. Refer to geologic map for unit descriptions and abbreviations

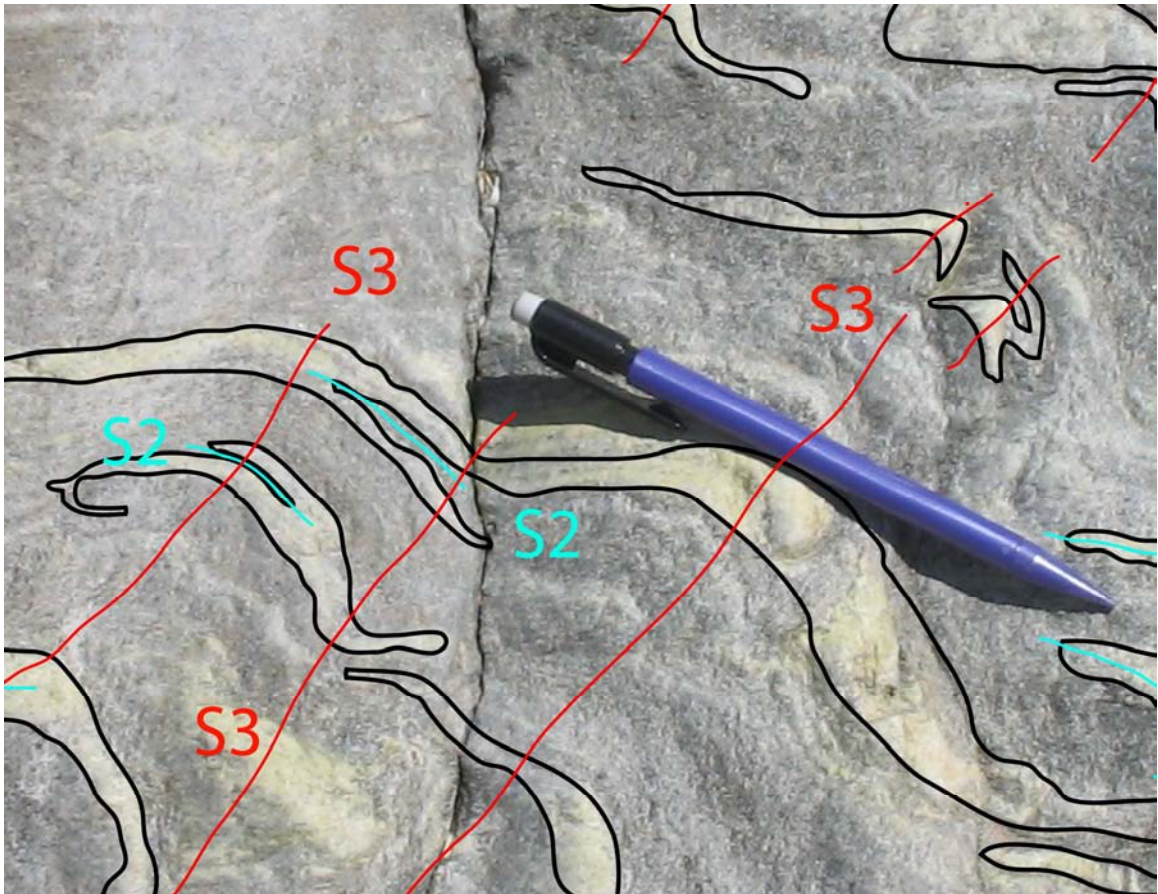


Figure 1.9: Looking N (perpendicular to strike) at polyphase deformation in overturned Jurassic metavolcanics lower member in Area A. Folds of layers of different composition (quartz and epidote) which define S_1 are isoclinally folded around S_2 (shown in blue) which is subparallel to compositional layering. S_1 and S_2 are refolded about the axial-plane cleavage S_3 (shown in red).

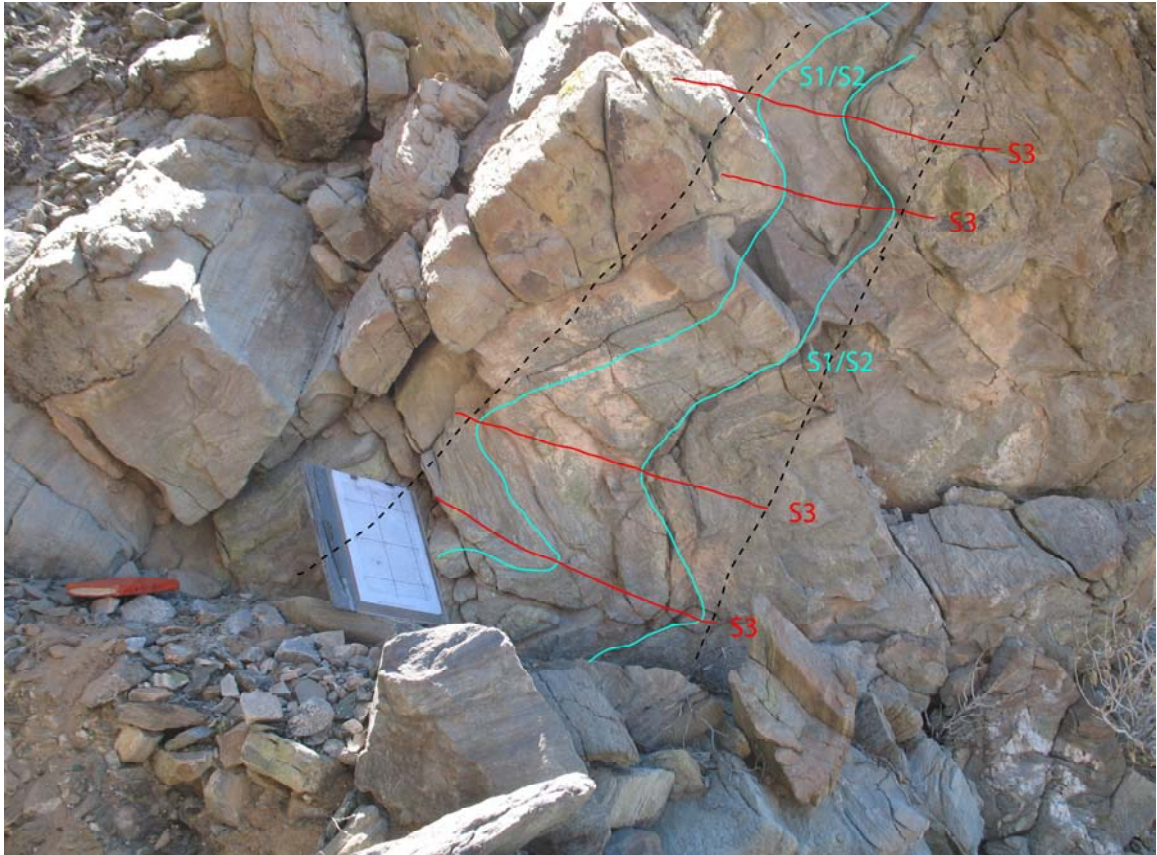


Figure 1.10: Looking E at 2 generations of deformation in the upper member of the Jurassic metavolcanics. The main composite foliation fabric, S_1/S_2 highlighted in blue, is predominately north dipping, and is refolded about a south-dipping axial-plane cleavage, S_3 . The average orientation (enveloping surface shown as black dashed line) of S_1/S_2 at this outcrop is $110, 58^\circ$ N.



Figure 1.11: Looking east (up-plunge) at polyphase deformation in the lower member of the Jurassic metavolcanics (Jv1). S_1 is defined by layering of light and dark minerals. S_1/S_2 composite foliation is primarily north-dipping. S_3 (blue) is defined as fold axes of ptygmatic folds of S_1/S_2 . S_3 primarily dips south.

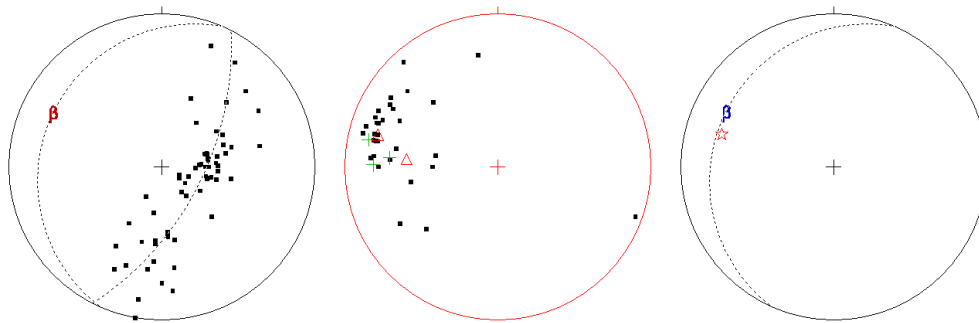


Figure 1.12: **A)** Lower hemisphere equal area projection of poles to planes for S_1 from Area A ($N = 65$). Poles to S_1 define a best-fit great circle girdle for a F_2 fold axis plunging 22° toward 297 . **B)** Plot of stretching lineations (black squares, $N = 32$) fold axes (green crosses, $N = 3$) and stretched concretions (red triangles, $N = 2$) from Area B. The average trend and plunge of lineation is 16° toward 291 . **C)** Plot of the average S_1 (dashed great circle, $204, 22^\circ W$), beta axis of F_2 fold (blue beta) and mean orientation of the stretch direction (red star).

Area A (see Table 1.1 for data). Poles to S_1 define a best fit great circle girdle that shows S_1 has been refolded about a macroscopic F_2 fold that plunges 22° toward 297. The geometry of this F_2 fold closely resembles that of mesoscopic F_2 fold axes (22° toward 276) in the area.

Figure 1.12b shows a lower hemisphere equal area plot of a pervasive mineral lineation on S_1 (see Table 1.1 for data). Plunge of lineation has a statistically significant mean orientation of 25° toward 288. We interpret this to be a L_1 stretching lineation (movement direction) because it is seen as elongated minerals in Jurassic and Proterozoic rocks as well as the long dimension of ellipsoidal stretched concretions in the Aztec quartzite (Figure 1.13). The photograph of these stretched concretions and samples collected from this area are found in the upright limb of the syncline. This indicates that shearing is present in both the upright, “normal” limb of the syncline as well as in the highly attenuated upper limb of the syncline, which means that ductile shear is prevalent throughout the rocks in the syncline. The mean orientation of the trend and plunge of the long axes of these stretched concretions is 30° toward 281, which is in good agreement with the mean orientation of the trend and plunge of the stretching lineation defined by elongated minerals.

The close agreement between the trend and plunge of the mineral elongation (stretching) lineation, long axes of stretched concretions, the trend and plunge of later mesoscopic F_3 folds is interesting and may have resulted from anisotropy control of the F_3 folds by the S_1 fabric as has been observed in the Old Woman and Piute Mountains (Fletcher and Karlstrom, 1990). This relationship is shown in Figure 12c. The alternative interpretation, that these are L_3 intersection lineations is negated by the multiple indications that these are elongation features and the evidence for shear sense on S_1 .

Leucogranite dikes are observed in this area, and the dikes are observed to continue northwest through the range. The dikes in this area have been offset from the main dike swarm exposed in the western part of the range by the Eagle’s Nest Fault. Dikes in this area generally cross-cut S_1 (Figure 1.14), which indicates that emplacement of the dikes must post-date D_1 and D_2 deformation. The dikes in this area typically strike

Table 1.1: Structural data from Big Maria Mountains, Area A. Planes reported in azimuth notation as strike, dip, sense. Lines reported in azimuth notation as plunge, trend.

S1/S2 Composite foliation

349,30,W	275,40,N	290,58,N	230,20,N
356,21,W	280,77,N	263,56,N	163,24,W
344,39,W	285,42,N	225,38,N	163,25,W
352,25,W	275,52,N	265,37,N	180,23,W
052,17,N	298,18,N	265,70,N	260,40,N
344,24,W	152,37,W	295,63,N	147,35,W
032,11,W	205,10,W	280,90,N	300,50,N
344,25,W	193,30,W	225,38,N	194,25,W
032,24,W	135,50,W	270,65,N	113,40,S
000,25,W	190,38,W	265,35,N	177,20,W
012,24,W	150,62,W	280,25,N	179,30,W
095,42,N	182,18,W	128,30,S	
085,38,N	192,27,W	168,55,W	
340,35,W	184,30,W	168,35,W	
020,15,W	300,35,N	215,15,W	
318,63,W	125,72,S	170,25,W	
348,35,W	112,74,S	195,25,W	
200.15,W	278,57,N	176,29,W	

Mineral elongation lineation

21,282	15,292
20,292	38,229
10,284	56,280
18,285	27,350
18,282	5,110
11,287	18,274
15,295	24,310
23,299	17,290
9,318	18,303
33,280	55,270
20,275	40,315
42,260	27,240
30,274	40,315
18,290	20,300
23,270	20,285
30,295	
20,282	

Fold axes

30,275
20,271
15,282

Stretched Concretions

40,275
20,285



Figure 1.13: Stretched quartz concretions in the Aztec quartzite from the upright limb of the syncline. **Top:** Looking down the long axes of stretched concretions (at the YZ plane). Long axes of concretions plunge 30° toward 281 and indicate the stretching direction (X). The YZ plane has a near circular shape, indicating that the magnitudes of Y (intermediate) and Z (shortening direction) were equal during stretching. **Bottom:** Looking perpendicular to the long axes (X direction) of stretched concretions.



Figure 1.14: Photograph looking northwest at a Cretaceous leucogranite dike (highlighted with black lines) cutting across the composite S_1/S_2 fabric (shown in light blue) in overturned Triassic-Jurassic sedimentary rocks. The dike strikes 090, and dips 50° N. In general, dikes are undeformed and crosscut composite S_1/S_2 fabric.

north or northwest and dip steeply to the east, though some dike are observed to strike subparallel with the S_1 fabric, suggesting that dike emplacement exploited pre-existing weaknesses associated with development of S_1 .

Area B – S_1 dominated hinge zone of the Big Maria syncline

Area B (Figure 1.15) includes the hinge of the Big Maria syncline. In this area, S_1 is folded along with contacts of Paleozoic and Mesozoic units around the Big Maria syncline. This is evidence that the syncline itself is an F_2 fold. Refolded mesoscopic F_1 folds are observed in the hinge zone of the syncline. The axial plane S_2 cleavage is weakly expressed as is common in progressive, steady state refolding that is observed in domains of extreme shearing (Means, 1976). Figure 1.16a shows a lower hemisphere equal area plot of poles to S_1 from Area B (see Table 1.2 for data). This plot shows that poles to S_1 defines a great circle girdle for a macroscopic F_2 fold axis (The Big Maria syncline) plunging moderately nearly due west (beta axis 25° toward 283). Based on the distribution of poles to planes, the fold may be characterized as sub-cylindrical, as most of the poles fall within 20° of the best-fit great circle girdle (Ramsay, 1967). A best fit fold axial plane of $280, 50^\circ\text{N}$ is defined by limb measurements, the map axial trace and the calculated F_2 fold axis.

Figure 1.16b shows an equal area lower hemisphere stereonet plot of lineation measurements, the long axes of preferentially stretched pebbles in the Vampire Formation (designated stretched pebbles based on similarity to stretched elements in Area A) and the trend and plunge of mesoscopic F_2 fold axes are plotted (see Table 1.2 for data). The close agreement between the mean orientation of lineation measurements (37° toward 270) and that of the stretched pebbles (32° toward 261) suggests that the hinge line of the syncline has rotated into parallelism with the bulk transport direction during progressive ductile flow. This is consistently observed in folds that have formed in areas of high ductile strain (Means, 1981) and the stretching lineation observed here may have formed as the result of mid-crustal flow during peak deformation conditions (e.g. Beaumont et al., 2001). One reason why axial plane cleavage may not be observed here

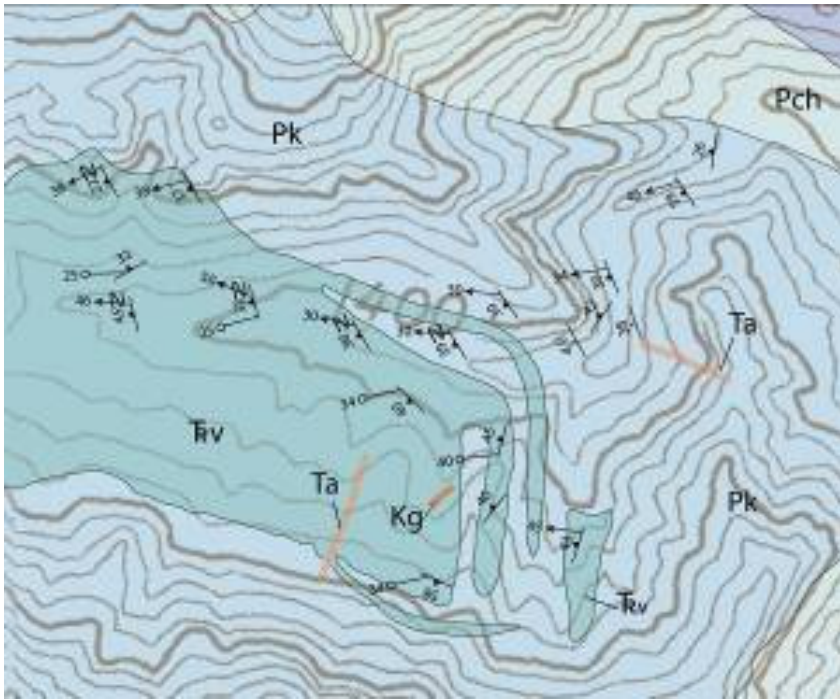


Figure 1.15: Inset geologic map of Area B. Geologic mapping originally was done at 1:6,000 scale.

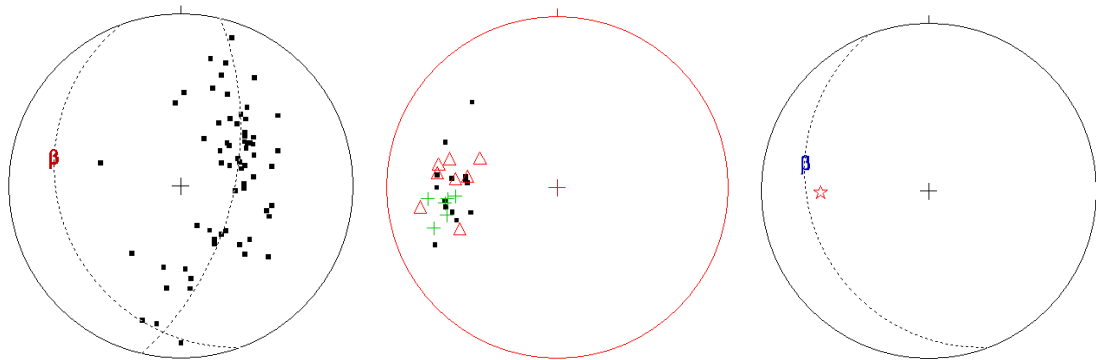


Figure 1.16: Equal area lower hemisphere stereonet plots of A) Poles to planes of S_1 . The mean orientation of S_1 is $159, 29^\circ W$. Poles to S_1 define a best fit great circle girdle for a macroscopic F_2 fold axis (Big Maria syncline) that plunges 25° toward 283 . B) Trend and plunge of stretching lineation (black squares) F_2 fold axes (red triangles) and long axes of stretched pebbles (green crosses). The mean orientation of stretch indicators is 36° toward 269 . C) The mean orientation of S_1 (dashed great circle) the beta axis of the Big Maria syncline (blue beta) and the mean orientation of stretch indicators (red star).

Table 1.2: Structural data from Big Maria Mountains, Area B.

S1 Foliation

005,26,W	230,30,N	150,22,W	116,25,S
324,59,W	016,40,E	117,50,S	138,25,W
338,30,W	108,50,S	140,40,W	137,30,W
337,38,W	164,30,W	160,50,W	092,45,S
038,42,N	225,30,N	267,40,N	130,45,S
330,40,W	173,35,W	264,45,N	168,45,W
322,39,W	148,39,W	124,65,S	219,55,W
016,43,W	199,45,W	280,70,N	130,50,S
012,45,W	140,30,W	178,30,W	238,30,N
225,40,W	086,40,S	306,40,N	282,40,N
146,42,W	110,65,S	278,50,N	182,30,W
290,58,S	227,45,W	265,50,N	237,25,N
312,40,W	248,20,N	270,80,N	
330,36,W	237,25,W	286,70,N	
342,32,W	134,45,W	121,35,S	
060,32,N	168,45,W	154,30,W	
325,37,W	109,80,S	157,25,W	
327,38,W	103,65,S	126,40,S	

Long axes of stretched pebbles

- 34,262
- 40,265
- 34,256
- 36,264
- 25,252
- 25,265

Mineral elongation lineation

- 38,252
- 38,275
- 46,273
- 22,245
- 30,292
- 30,276
- 30,270
- 34,260
- 46,254
- 45,275

Fold axes

- 20,262
- 50,291
- 38,247
- 46,277
- 30,281
- 30,277
- 40,275
- 35,285

may be the same reason that multiple fabrics are not observed in Paleozoic and some Mesozoic rocks. The low mica concentration in the Vampire and Kaibab formations and the relative strong competency of these units compared to other units in the BMM are such that only the main fabric, S_1 , is recorded. In addition, nappe-type folds are often characterized by high proportions of simple shear and rotation of steady-state fabrics during progressive simple shear.

Cretaceous leucogranite dikes are sparse here, and the S_3 cleavage recognized in Areas A and C (NW-striking, steeply SW-dipping) is not observed at all here. This tends to support a spatial correlation between development of the S_3 fabric and emplacement of the Cretaceous leucogranite dikes.

Area C – D_{1-2}/D_3 overprinting

Area C encompasses the area from west-central edge of the range to the Eagle's Nest Fault (Figure 1.17). This area includes the entire attenuated overturned limb of the syncline, the upright section from Jurassic metavolcanic rocks down to Pennsylvanian-Permian Supai Formation, Jurassic plutonic rocks and the Cretaceous leucogranite dike swarm. This area is especially good for examining F_3 folds and their spatial relationship to the Cretaceous leucogranite dikes.

All rocks in this area, except the Cretaceous leucogranite dikes, are strongly foliated with the S_1/S_2 composite fabric which is defined by metamorphic minerals and strained grains. The S_1/S_2 composite foliation is subparallel to contacts between Paleozoic and Mesozoic metasedimentary and metavolcanic units as well as primary bedding features, such as flat beds and tabular cross beds in the Tapeats quartzite (Figure 1.18). The geometry of mesoscopic structures observed in the field is a clue to deciphering the deformation history of the Big Maria syncline. A beautiful example is shown in Figure 1.19, which shows successive generations of folding and refolding by the same progressive simple shear event in the overturned Cambrian Muav Marble. This photograph was taken looking perpendicular to strike of S_1/S_2 composite foliation, which is the axial plane cleavage to the mesoscopic recumbent fold shown in the photograph.

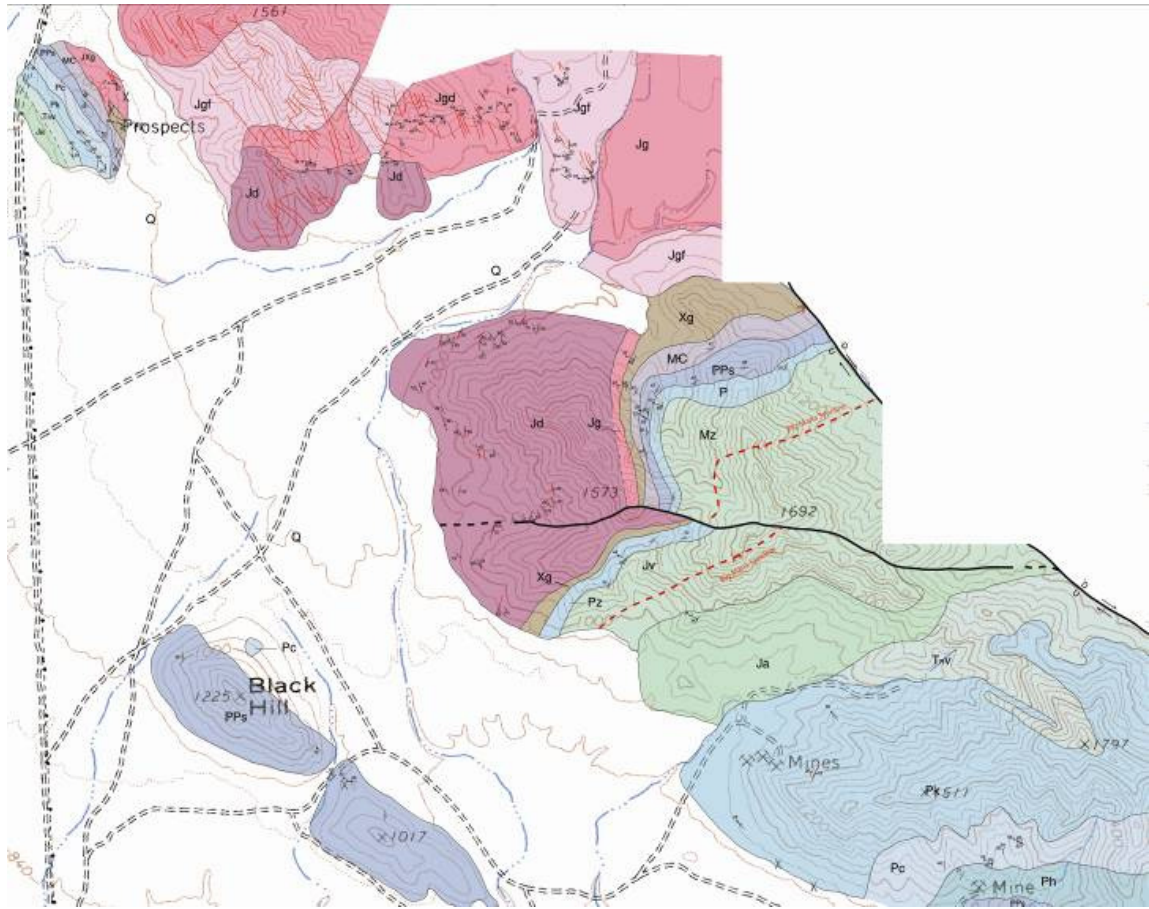


Figure 1.17: Inset geologic map of Area C. Geologic mapping originally done at 1:6000 scale.

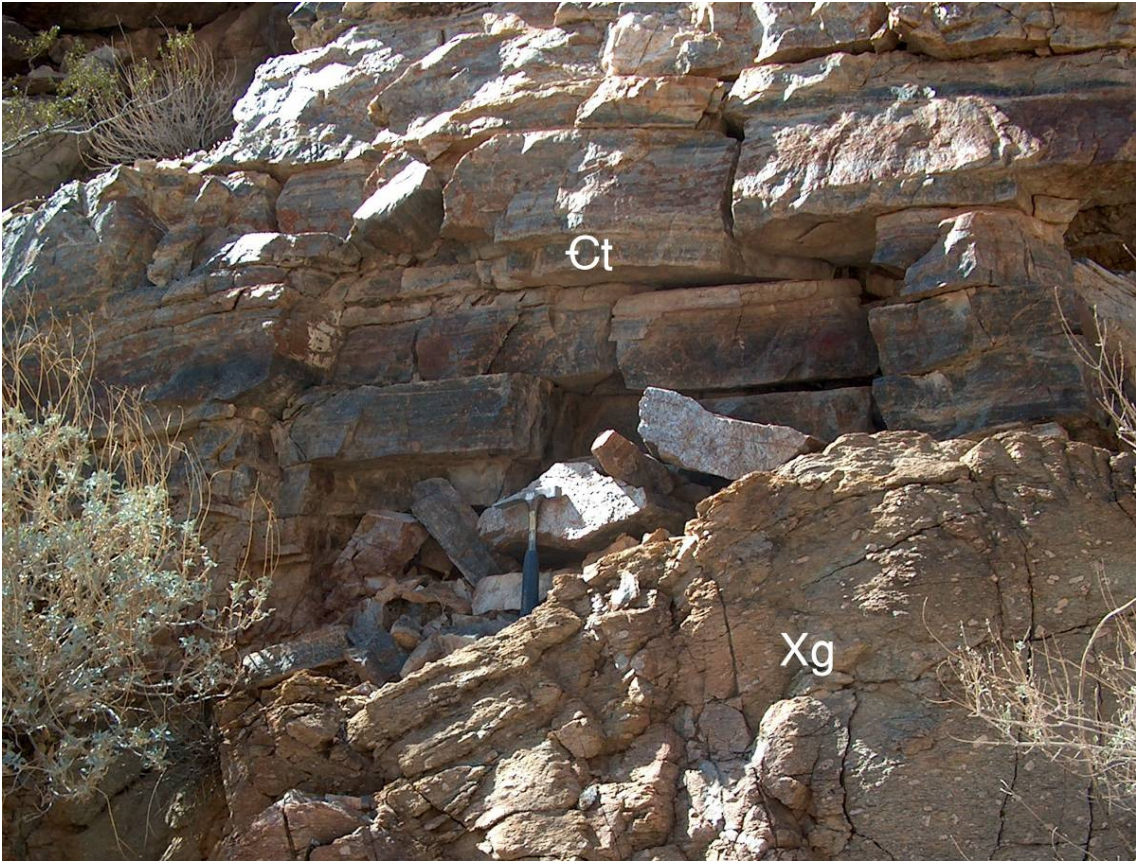


Figure 1.18: Photograph looking north at contact between the Tapeats quartzite (Ct) and Proterozoic Granite (Xg). S_1 is apparent in the basement and is parallel to original bedding structures observable in the Tapeats quartzite and the contact between the two units, which is recognized as the Great Unconformity at the Grand Canyon.

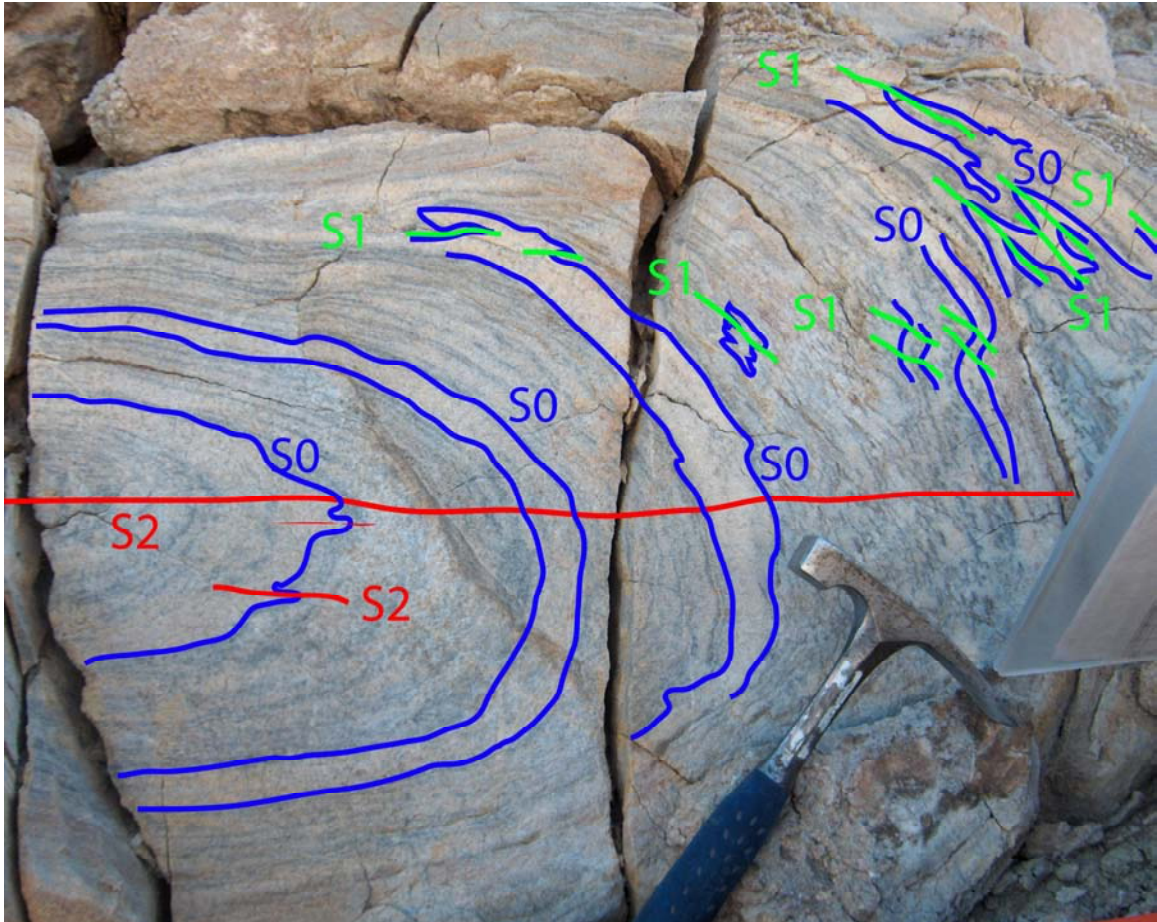


Figure 1.19: Characteristic F_2 mesoscopic fold in the Cambrian Muav marble. The Muav is an excellent unit to see polyphase deformation due to the light and dark compositional layering. S_2 is defined as the axial plane cleavage to the F_2 fold. S_1/S_2 trends subparallel with contacts between metamorphosed Paleozoic and Mesozoic units and is the dominant fabric throughout the Big Maria syncline. Note smaller folds coming around the hinge of the larger recumbent fold with fold axes antithetic to the axis of the larger fold in the right-hand side of the photograph.

The photograph shows smaller folds that are parasitic to the recumbent fold but also shows folds that have axes antithetic to the recumbent fold. These folds must have formed earlier during deformation and then were subsequently refolded around the larger structure. In the photograph, we annotate the axial plane cleavage to these earlier folds as S_1 and the axial plane cleavage of the recumbent fold as S_2 . We group the earlier folds and the recumbent folds as F_1 group folds and conclude that both generations of folding were a result of a progressive deformation event that involved steady-state shear foliation development and folding and refolding in shear-related folding as discussed for sub-area B in the hinge region. Furthermore, we interpret that composite F_1/F_2 folds as shown in this field photograph, are analogous the Big Maria syncline and associated structures.

Figure 1.20a shows an equal area, lower hemisphere stereonet plot of poles to planes of S_1 from Area C (see Table 1.3 for data). Poles to planes of S_1 define a best-fit great circle girdle, the pole to which is the beta axis of a set of sub-cylindrical F_3 folds, indicating that the S_1/S_2 composite fabric has been refolded around fold axes that plunge moderately to the northwest (28° toward 301) in this area. Mesoscopic F_3 folds are observed in Area C. Also, macroscopic (kilometer-scale) folds in this area are F_3 folds, an example of which is the large antiform, which is defined on the map by a refolding of the attenuated limb (forming downward facing folds), but also refolds the upright section as well (forming upward facing folds). As in the antiform depicted in Area A, the antiform in Area C is marked by a relatively “thick” section of the attenuated limb that becomes severely attenuated as it comes around the hinge of this antiform. We interpret that this is the same antiform on both sides of the Eagle’s Nest fault. It is also in Area C that the Paleozoic and Mesozoic core of the syncline passes through the constriction zone and is abruptly deflected northward (Plate 1). The same pervasive mineral lineation observed in Areas A and B is also observed in Area C. As in Areas B and C, this lineation is interpreted to be a stretching lineation. Figure 1.20b shows an equal area lower hemisphere stereonet plot of lineation measurements and the trend and plunge of F_3 fold axes from Area C. There is a parallelism between F_3 fold axes with the mean attitude of

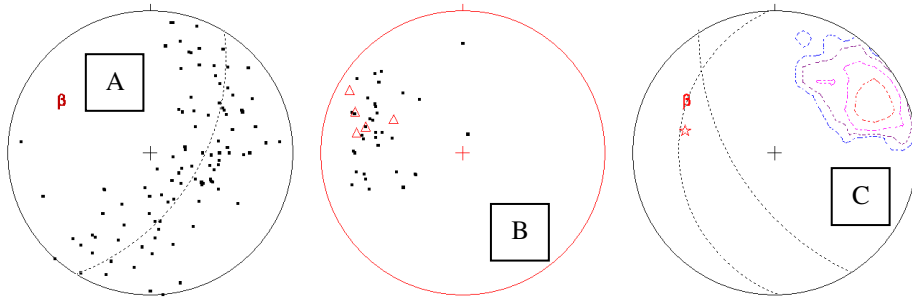


Figure 1.20: **A)** Lower hemisphere equal area projection of poles to S_1 from Area C. Poles to S_1/S_2 define a best-fit great circle girdle defining a macroscopic F_3 fold axis plunging 28° toward 301 . The mean orientation of S_1/S_2 is $178, 33^\circ W$. **B)** Lower hemisphere equal area projection of trend and plunge of stretching lineation (black squares) and mesoscopic fold axes (red triangles) from Area A. Mean orientation of stretching lineation is 34° toward 284 . **C)** Lower hemisphere equal area point density contour plot of S_3 from Area A. Mean principle orientation = $148, 66^\circ W$. Also shown are the mean orientation of S_1 (dashed great circle), beta axis of F_3 folds (red beta) and the mean trend and plunge of stretching lineation (red star).

Table 1.3: Structural data from Big Maria Mountains, Area C.
S1/S2 Composite Foliation

290,70,N	306,65,W	150,50,W	182,35,W	206,20,W	330,80,W	330,45,W
000,30,W	024,38,W	155,60,W	170,40,W	198,25,W	345,80,W	335,45,W
280,82,S	015,38,W	005,80,E	192,35,W	225,40,W	345,73,W	338,58,W
290,84,S	000,40,W	338,70,E	212,35,W	312,90,N	338,80,W	338,50,W
270,87,N	210,34,W	321,34,E	240,50,N		333,73,W	338,75,W
292,65,S	025,39,W	300,70,N	210,35,W		319,71,W	340,66,W
000,59,W	030,30,W	130,60,S	164,50,W		330,86,W	335,65,W
030,60,W	312,70,W	099,82,S	250,30,N		333,36,E	315,65,W
299,34,N	300,87,N	180,30,W	243,30,N		305,79,W	325,65,W
076,56,N	275,56,N	098,65,S	128,30,S		335,63,W	315,82,W
290,55,N	125,78,S	085,90,N	089,60,N		345,84,W	020,74,W
077,83,N	000,46,W	303,60,N	115,70,S		331,60,W	299,53,W
290,80,N	355,70,W	166,65,W	279,20,N		338,73,W	350,73,W
290,53,S	262,40,N	123,30,S	271,25,N		330,73,W	315,70,W
305,60,N	210,34,N	308,45,N	208,45,W		331,66,W	314,77,W
290,45,N	006,40,W	278,70,N	255,25,N		330,73,W	315,52,W
322,34,N	330,30,W	111,65,S	119,60,S		333,63,W	310,60,W
307,70,N	350,20,W	126,40,S	232,20,N		336,61,W	309,45,W
312,70,N	355,20,S	153,50,W	144,50,W		333,66,W	327,78,W
319,80,S	010,13,W	156,60,W	271,35,N		330,63,W	280,80,S
001,55,W	176,45,W	152,70,W	205,40,W		336,61,W	300,49,W
325,60,W	147,40,W	175,80,W	248,10,N		333,60,W	315,75,W
285,70,S	136,35,W	215,20,W	266,40,N		330,58,W	290,70,W
315,58,S	264,45,N	190,40,W	206,20,W		330,75,W	299,53,W
320,60,W	148,50,W	267,50,N	225,25,W		335,70,W	310,57,W

S3 Cleavage

L1 Measurements

Fold axes

29,280	30,249	45,296
50,321	30,278	25,281
24,000	30,258	20,291
25,260	50,240	10,299
25,270	37,283	30,285
40,275	60,245	
79,015	20,254	
30,255	24,271	
24,300	48,282	
30,299	60,246	
31,290	41,284	
18,290	50,254	
31,298	40,315	
30,285	10,305	
34,295	20,315	
33,290		
38,280		
24,310		
20,290		
18,312		

the stretching lineation. This parallelism is also observed in Area A and further supports the idea that the orientation of F_3 folds may have resulted from anisotropy control of these folds by the S_1 fabric as has been observed in the Old Woman and Piute Mountains (Fletcher and Karlstrom, 1990). A third variably expressed cleavage, S_3 , is observed in Area C that strikes northwest and dips steeply to the southwest. This cleavage is also observed in Area A and is not observed in Area B. Earlier deformation fabrics are refolded into tight, upright F_3 folds about S_3 . Figure 1.20c shows a lower hemisphere, equal area point density contour plot of poles to planes of S_3 . The point density contour plot shows a maximum, hence statistically significant, mean orientation of S_3 of 148, 66°W (see Table 1.3 for data). In the field, S_3 is expressed more strongly in the Jurassic volcanic and plutonic rocks in contrast with the Paleozoic and Mesozoic metasedimentary units. In the Jurassic magmatic rocks, “penciling” of rocks, as the result of intersecting cleavages (Figure 1.21a), is common; whereas in Paleozoic rocks, F_3 folds are defined as the folding of S_1 and S_2 cleavage planes, with no well-developed S_3 axial plane cleavage apparent (Figure 1.21b). This is likely because Jurassic magmatic rocks in the BMM have greater concentrations of mica than Paleozoic rocks, with the exception being the Bright Angel schist. Because of its high mica content, the Bright Angel develops new S_3 cleavage easily in contrast with other Paleozoic rocks, which are predominately quartzites, calc-silicates, and marbles. In the field in Area C, in micaceous rocks where both fabrics are observed, S_3 appears to be the more developed fabric. The further NW in Area C, the more dominant the S_3 fabric seems to be.

The intensity of expression of the S_3 fabric is spatially correlative with the location of a swarm of leucogranite dikes in the western part of Area C (Figure 1.22). The dikes generally strike north-south, and dip steeply to the east. S_3 overprints all units in this area, including weak development in the leucogranite dikes. Most dikes appear relatively undeformed but locally dikes are folded or boudinaged (Figure 1.23). The fact that S_1 and S_2 are crosscut by the dikes and the fact that S_3 overprints many (but not all) of the dikes, indicates that the dikes were emplaced after the formation of S_1 and S_2 and

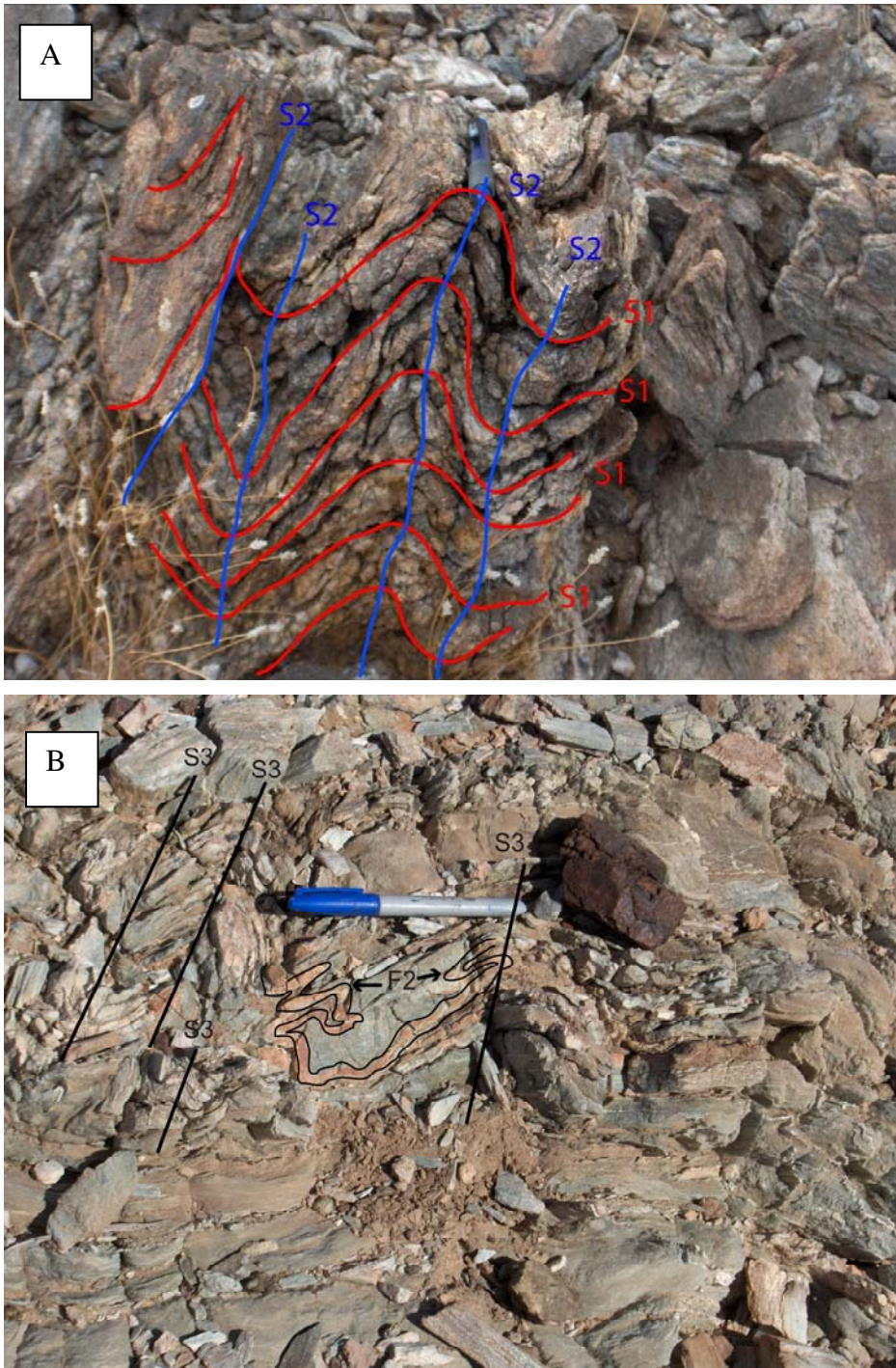


Figure 1.21: **A)** F₃ folds in Jurassic granodiorite looking NW. S₁ fabric in granodiorite is folded into tight, upright fold about SW-dipping S₂ cleavage creating “penciling” interference effect. **B)** Multiple generations of folds in a siliceous layer in the Permian Kaibab marble. F₂ isoclinal folds are defined by red and green layers. F₃ folds are shown as refolding of the main S₁/S₂ fabric; note that S₃ is defined as axial planes of these refolded folds.



Figure 1.22: Top: Google Earth ® image of the Cretaceous leucogranite dike swarm cutting through the western part of Area A. The dikes appear as thin white stripes. **Bottom:** Looking north at the Cretaceous leucogranite dike swarm on the ground. Host rocks are Jurassic plutonic rocks.



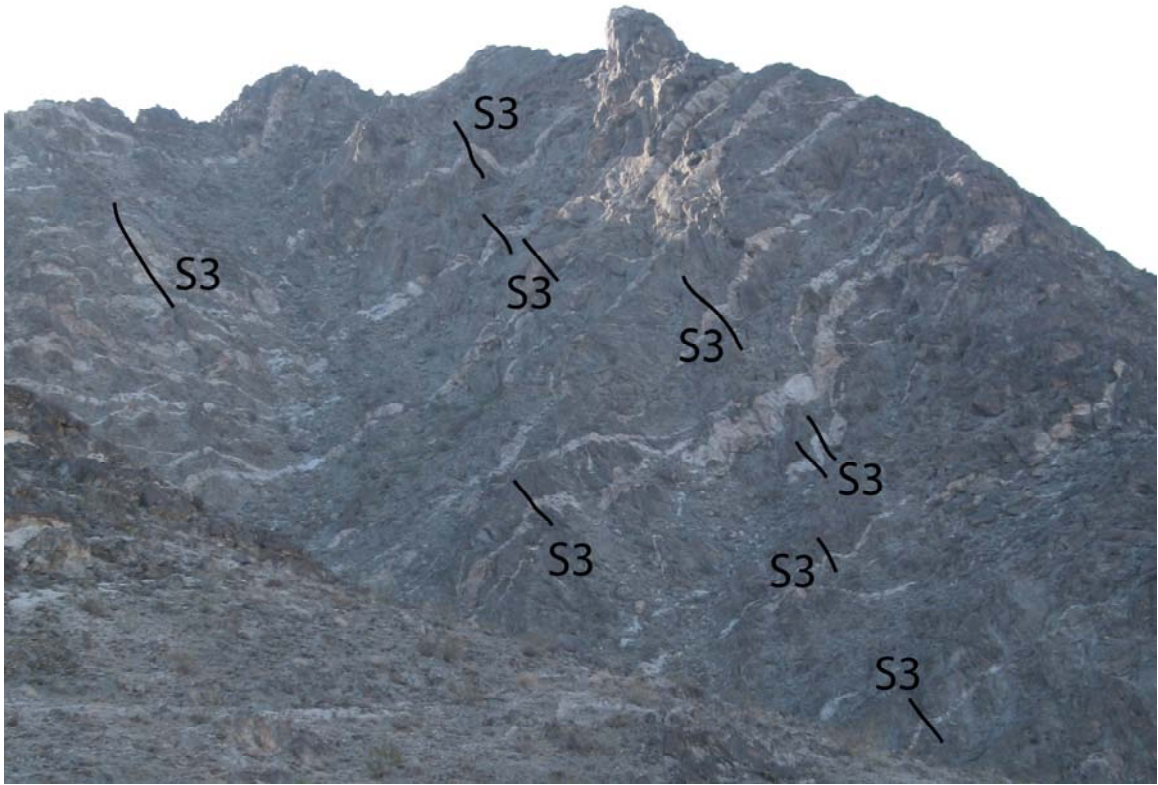


Figure 1.23: Field photograph looking east at variably deformed leucogranite dikes in the dike swarm located in the western part of Area A. Consistent folding of dikes takes place around southwest dipping cleavages.

before formation of S_3 finished. The observations suggest that emplacement of the dikes is syntectonic with respect to the formation of S_3 .

Figure 1.24 shows an equal area lower hemisphere point density contour plot of the leucogranite dike swarm from Area C (see Table 1.4 for data). The point density contour plot shows a single maximum at $348, 61^\circ E$, which we interpret is the mean orientation of the dikes. The plot also indicates that dikes have been weakly folded around a fold axis that plunges shallowly to the southeast (23° toward 151 , Figure 1.25). This weak refolding of the dikes suggests folding about an F_3 fold axis. The contradiction between the southeast plunge determined for folding of the dikes and the observed northwest plunge of F_3 folds observed in Areas A and C lends support to the hypothesis that the geometry of F_3 folds is controlled by pre-existing S_1/S_2 anisotropy. Since the dikes post-date development of the composite S_1/S_2 fabric, they would not have this anisotropy.

Assuming that dikes were emplaced during development of the S_3 fabric, the dike-perpendicular extension is sub-parallel to least compressive stress during D_3 deformation. Thus, the mean orientation of the dikes gives an extension direction of 29° toward 258 for D_3 deformation. Figure 1.25 shows a lower hemisphere equal area projection point density contour plot of the leucogranite dikes overlain by two great circles, one showing the mean orientation of the dikes and the other showing the mean orientation of S_3 . A red star shows the orientation of the extension direction determined by analysis of the dike swarm. A blue cross shows the pole to the mean orientation of S_3 , and the red letter beta shows the trend and plunge of the beta axis determined for refolding of the dikes. Note that the beta axis plots at the intersection of the mean orientation of the dikes and S_3 , indicating that S_3 could be axial plane of refolding of the dikes, as also is indicated in the field photograph in Figure 1.23. The Y direction is taken as the intersection of the S_3 (XY plane of strain) with the average dike and the shortening direction Z (and σ_1) is 90° from σ_3 which in this case suggests that Z plunges steeply to the north. The inferred Z direction for the far-field tectonic strain, based on the orientation of S_3 , is inferred to be the pole to

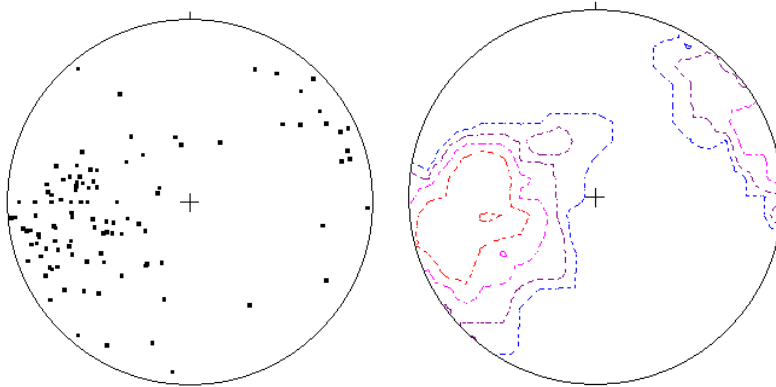


Figure 1.24: Lower hemisphere equal area projection of poles to planes for Cretaceous leucogranite dike swarm (left), south-central Big Maria Mountains, with corresponding point density contour plot (right). Mean orientation of dikes is 348, 61°E. Pole to plane of this mean orientation, 29° toward 258, defines the direction of maximum extension (σ_3) for the stress field during emplacement of the dike swarm.

Table 1.4: Strike and dip of dikes from the leucogranite dike swarm, western Big Maria Mountains
Orientations of leucogranite dikes

012,57,E	225,30,E	310,85,E	300,80,E
345,36,E	012,45,E	315,75,W	342,80,W
340,42,E	006,53,E	325,48,E	340,76,E
355,55,E	077,30,E	334,73,E	340,84,E
347,39,E	019,45,E	296,70,W	345,80,W
340,40,E	000,50,E	001,60,E	297,30,W
010,53,E	025,55,E	334,70,E	025,15,E
009,43,E	000,55,E	335,34,E	295,30,E
012,57,E	000,65,E	345,79,E	325,73,E
018,55,E	010,50,E	276,83,N	345,29,E
337,25,E	032,34,E	355,86,E	333,78,E
015,15,E	048,40,E	349,64,E	007,68,E
310,90	330,55,E	003,65,E	305,34,E
015,65,E	345,45,E	050,85,S	345,80,W
010,60,E	330,47,E	340,84,E	000,74,E
018,48,E	353,55,E	325,83,E	342,58,E
327,24,E	009,43,E	340,60,E	320,56,W
338,38,E	285,69,N	320,65,E	325,76,W
350,45,E	313,46,E	340,60,E	336,60,E
030,75,W	350,78,E	320,65,E	340,66,E
008,53,E	300,90	004,67,E	347,74,E
013,52,E	000,83,E	000,33,E	355,88,E
305,35,E	351,82,E	335,85,W	335,74,E
081,26,E	350,80,E	342,72,E	304,74,W
105,46,E	060,55,N	345,75,W	355,74,E
237,60,E	315,85,W	335,80,W	350,65,E
000,47,E	340,90	002,87,W	345,76,E
008,47,E	330,75,W	315,60,E	348,74,E
325,63,W	010,63,W	330,90	344,66,E

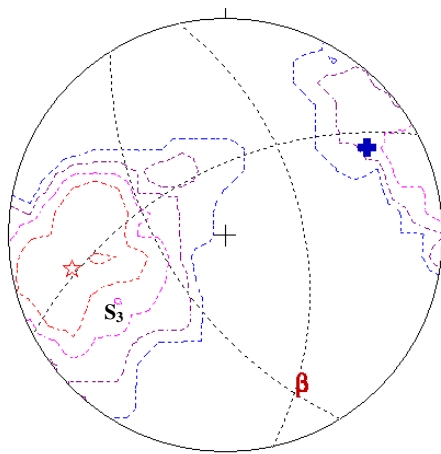


Figure 1.25: Lower hemisphere equal area projection of great circles for the mean orientation of the S_3 cleavage ($148,66^\circ W$) and dike swarm ($348,61^\circ E$) from Area A. Point density contour plot of the dikes define a great circle girdle defining a F_3 fold axis that plunges SE (25° toward 153). The red star shows the pole to the plane of the mean dike orientation (29° toward 258), which defines the σ_3 direction of maximum extension during D_3 deformation. The inferred shortening direction for D_3 is shown (blue cross) to be the pole of the mean orientation of S_3 (24° to 058). The angle between the planes is 58° .

plane of the mean orientation of S_3 , which is 29° toward 058, or northeast-directed shortening, which is inconsistent with, and is in fact nearly parallel to, the extension direction determined from emplacement of the dike swarm. A resolution to this is that F_3 folds formed during northeast-directed shortening early on during D_3 and then the dikes formed during extension parallel to shortening as crust was overthickened toward the end of D_3 . Analogs for this hypothesis include the present Himalayan orogen (Burchfiel et al., 1992) and in Proterozoic rocks of northern New Mexico (Salem et al., 2007). Although northeast-extensional shear fabrics have not been documented for the Big Maria Mountains, they were documented in the Little Maria Mountains by Ballard (1990) around the edge of the Little Maria pluton in the northwest part of the range and through examination of microstructures from other areas. Ballard also argued that northeast-directed extension modified earlier structures.

Microstructural analysis/Sense of shear analysis

Microstructural analysis of rocks from the Big Maria syncline yields important observations regarding the sense of shear during polyphase ductile deformation. As stated earlier, the mineral elongation lineation observed in the Big Maria syncline, as well as other indicators of strain such as stretched pebbles and concretions, consistently plunges at $\sim 30^\circ$ to the northwest. As such, we interpret that this represents the mean direction of transport during polyphase D_1/D_2 deformation. We also have observed that fold axes of mesoscopic and macroscopic refolds of the S_1 fabric trend subparallel with the stretching lineation, indicating that fold axes have been reoriented into the stretching direction during deformation by pervasive mid-crustal ductile flow. What is left to be resolved then is the sense of shear during deformation. Salem *et al.* (2006), in a preliminary structural analysis of the Big Maria syncline, documented some field evidence for reverse shear sense, such as “fish flash” of micas (Reynolds and Lister, 1987) in the Jurassic volcanic rocks and Aztec Quartzite and sigma clasts of feldspars observed in Proterozoic basement rocks and in the Triassic Vampire conglomerate. These observations would indicate top-southeast directed sense of shear (reverse and dextral).

In this section, we document shear sense further by examining thin sections from oriented hand samples to determine sense of shear in the Big Maria syncline (Simpson and Schmidt, 1983). Samples were cut parallel to the stretching lineation and perpendicular to S_1 foliation. We focus primarily on samples from the attenuated limb of the syncline but also present results from the upright limb of the syncline. The first sample we present is from the Vampire conglomerate in Area A (Figure 1.26). In general, this unit is excellent for examining shear sense as it consists of large (2-5 mm) quartz and feldspar deformed phenocrysts that serve as good kinematic indicators. In the hand sample this thin section was taken from, S_1 has an orientation of 056, 18°N and the stretching lineation plunges 18° toward 285. This observation suggests that shear sense is mostly dip slip with some strike slip component. This shear could either be reverse and dextral (top-southeast) or normal and sinistral (top-northwest). From Figure 1.26 it is apparent that shear sense in this sample is clearly dextral (top-left) as evidenced by the feldspar delta clast toward the bottom of the slide, quartz sigma clasts and mica fish that have been recrystallized with strain tails indicating shearing to the right. In cross polarized light (Figure 1.26b), recrystallized feldspar tails show sub-grain development indicating dynamic recrystallization due to dislocation creep; e.g. regime 1 for feldspar as characterized by Hirth and Tullis (1992). Finally, it is important to note the extent of recrystallization in this sample. Examination of the feldspar clast shows that feldspar has been partially recrystallized and annealed indicating that peak temperature during deformation had to have exceeded 450-500°C (Passchier & Trouw, 2004), which supports that deformation took place at mid-crustal levels. When reoriented to the hand sample, the dextral shear observed in the slide goes up the lineation, indicating reverse shear sense (top-southeast).

Figure 1.27 shows other samples from which show similar characteristics to the Vampire conglomerate in Figure 1.26. In general, S_1 in these samples strikes either east or north and dips to the north or west. The stretching lineation typically plunges moderately (between 15-40°) to the northwest. Shear sense indicators in these thin sections, when reoriented to their respective hand samples consistently show top-to-the-southeast

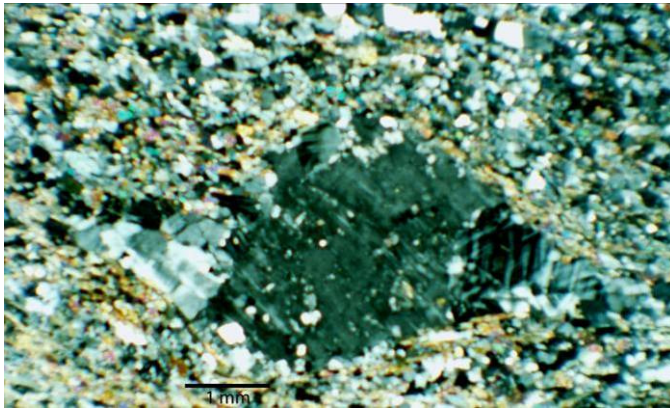
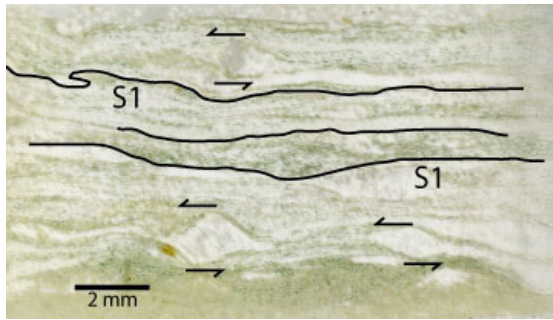


Figure 1.26: A) High resolution scan of thin section K05 BMAR34, collected from conglomerate attenuated Triassic Vampire Formation (see Plate 1 for sample location. S_1 is defined by aligned micas, epidote blades and elongated quartz veins. Sinistral shear sense is defined by sigma clasts at the top and at the bottom right part of the slide and by a feldspar delta clast at the bottom left part of the slide. **B)** Photomicrograph in cross polarized light of feldspar delta clast at the bottom of the slide in A. Note extensive recrystallization of the feldspar clast and the strain tails on both sides of the clast. Also, the matrix has been extensively recrystallized as well.

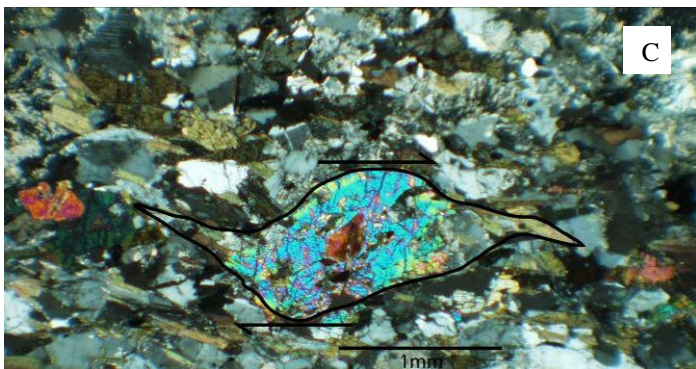
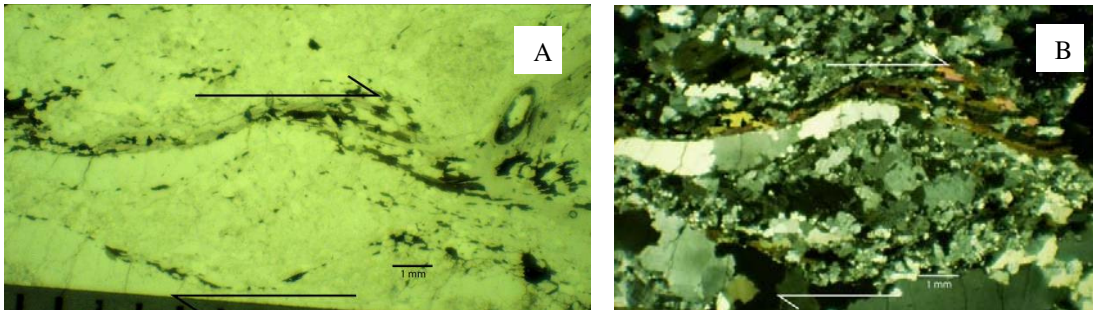
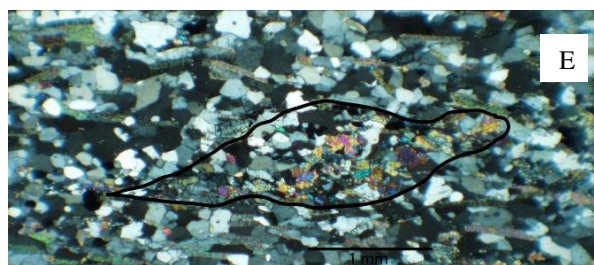
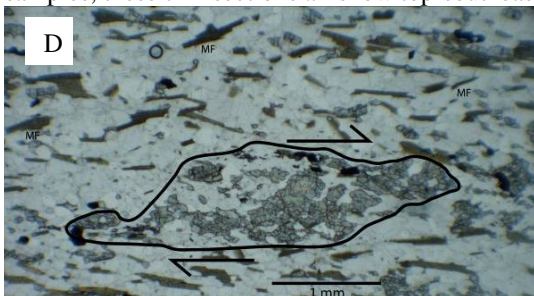


Figure 1.27: **A)** Sample K05 BMAR33 in plane polarized light and **B)** cross polarized light. Sample collected from Proterozoic granite in Area C showing dextral shear sense. Note the extensive recrystallization of the potassium feldspar megacryst in the bottom of the slide. **C)** Sample S08 BM11, collected from Jurassic diorite intrusive sill in attenuated limb of syncline from Area B. Clinopyroxene sigma clast shows dextral shear. **D)** Sample S08 BM05 collected from Jurassic volcanics lower member in upright limb of syncline from Area B. Sigma epidote clast and mica fish (MF) shows dextral shear sense. **E)** Same sample in cross-polarized light, showing dissolution of epidote clast and replacement by recrystallized quartz and feldspar. Note quartz and mica strain tails in the clinopyroxene clast. When reoriented to hand samples, these thin sections all show top-southeast reverse shear sense.



directed shear sense (reverse and dextral). Also, just as in the Vampire conglomerate, most of these samples have been extensively recrystallized (especially note Figure 1.27b). In fact, shear sense indicators, such as sigma clasts, are often best shown by relict grain boundaries, rather than individual grains themselves.

Finally, Figure 1.28a shows a sample taken from the lower member of the Jurassic metavolcanics from Area B. S_1 in this sample is oriented $350, 40^\circ W$ and the stretching lineation plunges 30° toward 285 . Unlike the previous slides shown in this section, these rocks come from the upright limb of the syncline. What is observed in the upright limb is similar to what has been documented in the overturned limb. A nicely developed S-C fabric indicates dextral shear; when reoriented to the hand sample, this sample show shear going up lineation, indicating reverse (top-southeast) directed shear. Figures 1.28b and c show other samples from the Jurassic volcanics that also have well developed S-C fabrics that indicate reverse shear sense. The crenulation of S_1/S_2 composite foliation into F_3 folds shown in microstructure provides a microscopic analogue for mesoscopic and macroscopic F_3 folds observed in the field area. As noted earlier, many F_3 folds have axial planes that dip south (Figure 1.10). These folds show up well in the Jurassic volcanic unit, especially the lower member, due to the high mica content in these rocks. Thus, refolding of the S_1/S_2 composite foliation around S_3 axial plane cleavage is observable at all scales, including microscopic. The microstructural analysis supports preliminary observations regarding top-southeast directed reverse shear sense. Furthermore, these observations indicate that most structures observed in the field area formed as the result of continuous folding of geologic units and refolding of these earlier structures by southeast-directed shearing during a single protracted progressive D_1/D_2 deformation event, which was the result of pervasive contractile ductile crustal flow. These earlier structures were then refolded around F_3 folds during a pervasive, regional D_3 deformation event.

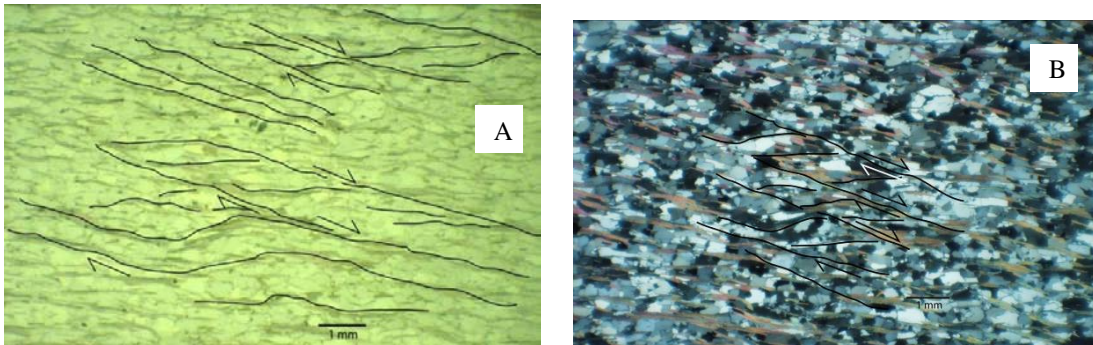
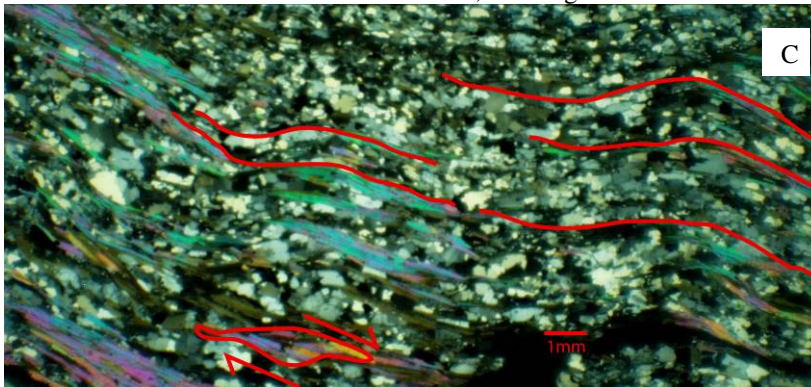


Figure 1.28: **A)** Plane polarized and **B)** cross polarized photomicrographs of sample S08 BM04 collected from the lower member of the Jurassic volcanics from the upright limb of the syncline. Thin section displays well developed S-C fabric showing dextral shear. When reoriented to hand sample, this S-C fabric shows top-southeast directed shear. Crenulated cleavage folds are analogous to mesoscopic F_3 folds observed in the field. **C)** Cross polarized photomicrograph of sample S08 BM07, also collected from the lower member of the Jurassic metavolcanics, showing the same shear sense as S08 BM04.



Discussion

Kinematics and timing of polyphase deformation events

Based on the above data, at least three Mesozoic deformation events are recorded in the Big Maria syncline, and are herein designated D_1 , D_2 , and D_3 . D_1 is characterized by tight-to-isoclinal folds and a pervasive, mostly north-dipping fabric designated S_1 , which is the main foliation fabric observed in the Big Maria syncline and vicinity. This fabric is consistently parallel to subparallel with contacts between stratified Paleozoic and Mesozoic metamorphic rocks, indicating that original bedding of Paleozoic and Mesozoic rocks has been transposed into the S_1 fabric. The presence of earlier folds with axes antithetic to S_1 indicates that strain during D_1 was accommodated through continuous folding and refolding of earlier fabrics (including original bedding) and flattening and thickening of lithologic units.

D_2 structures are characterized by south-vergent folds that refold D_1 structures and shear zones that extremely attenuate Paleozoic and Mesozoic metasedimentary and metavolcanic units. D_2 is also characterized by a weakly expressed axial plane cleavage, designated S_2 about which S_1 is refolded. In most areas, S_2 trends nearly subparallel with S_1 . Mesoscopic folds and the macroscopic Big Maria syncline are interpreted here to be F_2 folds because they refold S_1 . The trace of the fold axis of the Big Maria syncline, and associated mesoscopic folds, trends subparallel with unit contacts and S_1 except in the hinge areas of these folds. S_1 and S_2 are recorded in all units in the field area older than the leucogranite dikes, and the contact between Jurassic plutonic rocks and the attenuated limb of the syncline is also subparallel with S_1 and S_2 . The attenuated limb defines a zone of high shear strain which we have designated the Big Maria shear zone, which trends subparallel with the axial plane of the Big Maria syncline. Units in both the upright and attenuated limb of the syncline show evidence of polyphase ductile deformation and southeast-directed reverse shearing, however, so we argue that the Big Maria shear zone is a zone of highest shear strains within a several kilometers wide ductile shear zone defined by the core of the Big Maria syncline and similar structures. Locally, Paleozoic

units are observed to be intruded by Jurassic plutons. Further north in the range, Jurassic plutonic rocks are documented to intrude almost the entire Paleozoic section, and lenses and “pods” of Paleozoic rocks are preserved as roof pendants. Wherever Paleozoic rocks can be mapped with continuity, however, the rocks are observed to be in correct, upright or inverted, stratigraphic order; hence the rocks record “ghost” stratigraphy. We further interpret that S_1 represents planes of shear parallel to the Maria shear zone and that the greater degree of attenuation observed in carbonate and micaceous rocks versus that observed in rocks containing high amounts of quartz and calc-silicate minerals is the result of rheologic contrast between these units as well as preferential layer-parallel slip on S_1 shear planes in more mica and carbonate rich lithologies.

In all structural domains, we observe that S_1 has been refolded into macroscopic F_2 folds with axes that trend northwest or west-northwest. These fold axes are subparallel to the stretching direction, which is defined by a northwest or west plunging stretching lineation and other kinematic indicators, such as stretched pebbles or concretions. This indicates that fold axes of F_2 folds were rotated into the stretching direction during D_2 deformation. Furthermore, even though two major generations of folds are observed in all three structural domains, we consistently observe only stretching direction. Therefore, the trend and plunge of the stretching lineation indicates the direction of transport during both D_1 and D_2 . We interpret here that F_2 folds were formed as refolding of F_1 folds during one protracted progressive deformation event and that the Big Maria syncline actually represents a composite D_1/D_2 structure. Based on microscopic and mesoscopic shear sense indicators, shearing during D_1 and D_2 deformation is reverse. As such, D_1 and D_2 structures formed as the result of southeast-directed reverse and dextral shear. We propose that D_1/D_2 deformation were two separate stages of a steady state progressive deformation event that formed as the result of southeast-directed reverse and ductile shear. Although strains were highest in the area of the Maria shear zone, defined by the attenuated overturned limb of the syncline, both limbs showed the same shear sense and stretching lineation direction. This interpretation is confirmed by analysis of structures at all scales from microscopic to macroscopic.

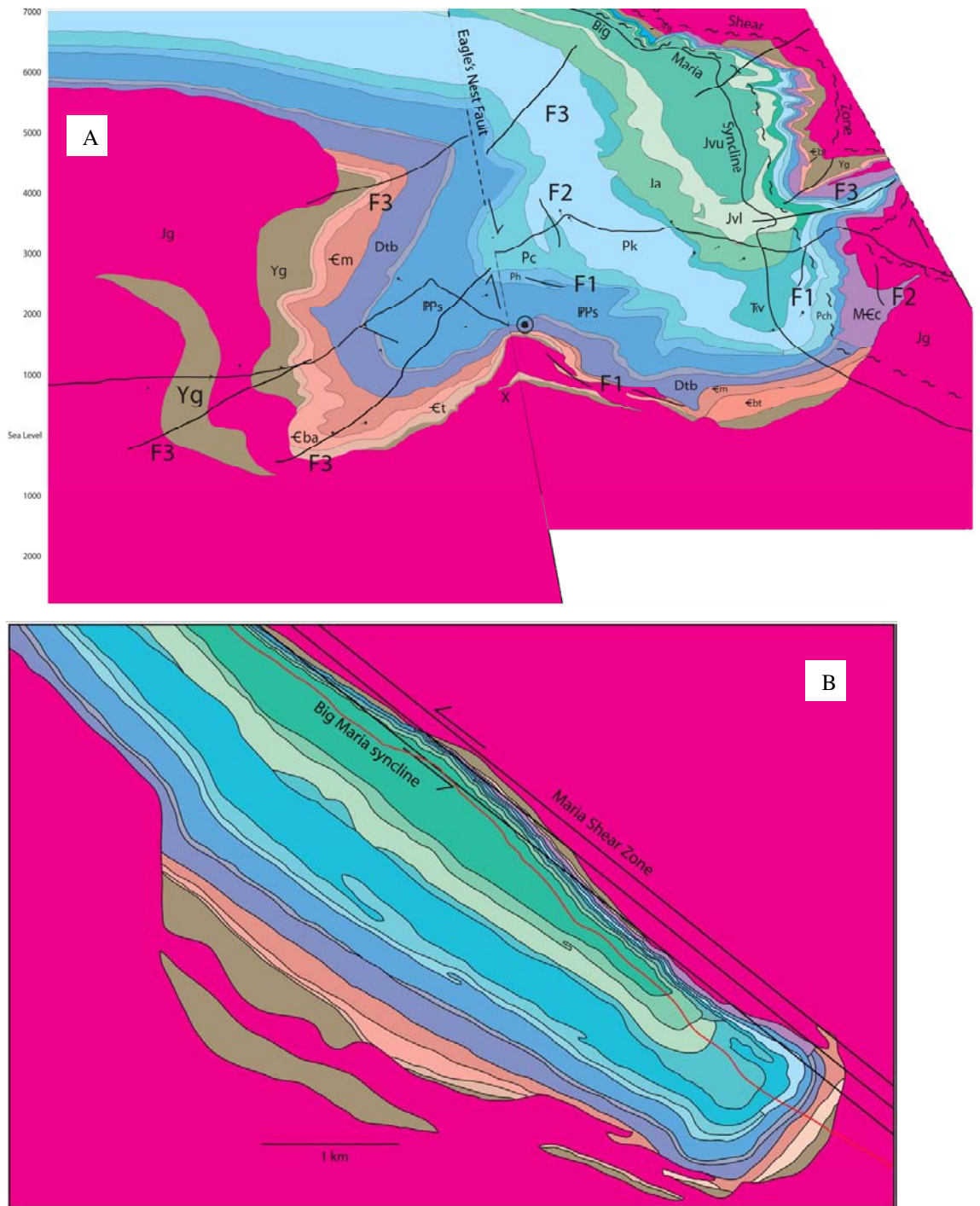


Figure 1.29: Restoration of cross section in Figure 1.8. **A)** Movement along Cenozoic Eagle's Nest and Quien Sabe Faults restored. **B)** F₃ macroscopic folds unfolded to depict Big Maria syncline in D₁/D₂ state.

The cross section shown in Figure 1.8 is a true scale cross section of the Big Maria syncline. In Figure 1.29, we restore the cross section to its original D_1/D_2 deformation state. We begin by restoring motion normal and right lateral motion along the Eagle's Nest Fault and by restoring normal movement along the Quien Sabe Fault (Figure 1.29a). Finally, we unfold major F_3 macroscopic folds (Figure 29b). We estimate that restoration of the Cenozoic faults shortens the lateral extent of the syncline by approximately 0.5 km, or about 20%. We estimate that removal of the F_3 folds extends the syncline laterally approximately 1.5 km or by about 37.5%. Once this restoration is done, the geometry of the syncline becomes clear and relatively easy to interpret. The high degree of stratal attenuation apparent in the upper limb of the syncline defines the high strain Maria Shear Zone. The shear zone trends parallel with the axis of the Big Maria syncline and is laterally continuous throughout the Big and Little Maria Mountains for approximately 40 km. We interpret that the shear zone, as evidenced by microstructures and the prevalent stretching lineation direction, formed as the result of top-southeast-directed reverse and dextral shear. The syncline is boudinaged on a macroscopic scale, with zones of constriction and expansion apparent from the cross section. The structure likely formed as a result of both pure and simple shear, with flattening of units accomplished by pure shear and high degrees of stratal attenuation accomplished by progressive, non-coaxial simple shear.

Since top-southeast-directed reverse shear sense and pervasive foliation are observed in all rocks in the range, one could argue that not just the Big Maria syncline, but the Big Maria-Little Maria Mountains as a whole were part of a crustal scale ductile shear zone during deformation, similar to High Grade Nappe Assemblages (HGNA) discussed by Williams and Jiang (2005). There are striking parallels between what Williams and Jiang discuss for HGNA and the Big Maria-Little Maria terrane. Some of these parallels include pervasive foliation and ductile shear indicators, inverted metamorphic grade (demonstrated by Hoisch et al., 1988), and zones of extreme attenuation marked by apparent crustal discontinuities. One of the problems with understanding the Maria Fold and Thrust Belt as a whole is how the high degree of stratal

attenuation, as documented here, was accomplished without unreasonably high shear strains. Figure 30 shows how the high degree of stratal attenuation observed in the MFTB could have been accomplished as a result of simple shear with reasonable shear strain values on the order of $\gamma = 5$ or 10. High strain zones, instead of being major thrust faults, may actually be pre-existing high angle normal faults that were rotated during middle crustal ductile flow. This is an intriguing idea for the MFTB region. Most workers contend that the McCoy rift basin extended northwest from southeastern Arizona into southeastern California (Dickinson et al., 1989; Tosdal and Stone, 1994; Spencer et al., 2005). Therefore, prior to deformation in the MFTB, high angle normal faults, as found in a rift setting, should have been present in this region. This possibility is considered in Figure 30a, which represents a schematic reconstruction of part of the McCoy Basin prior to Maria Fold and Thrust Belt deformation adapting a model figure from Williams and Jiang (2005). High-angle normal faults associated with the earlier McCoy Basin rift system are shown to be steeply dipping to the south. Fault blocks are rotated north and drag folds are depicted with each normal fault. In Figure 1.30b, southeast-simple shear is applied, using shear strain of $\gamma = 5$. Even at this shear strain, folds with geometries resembling the Big Maria syncline are produced. Fault drag folds and the faults themselves become zones of high strain, and syncline-anticline pairs are generated, with both “normal” and attenuated limbs. In addition, steeply south-dipping normal faults are rotated into the plane of strain and are now shallowly north-dipping faults. Axial planes to anticlines and synclines are also north dipping. In Figure 1.30c, shear strain of $\gamma = 10$ is applied. At this point, fold axial planes and high-strain zones are rotated nearly sub-parallel with the plane of strain. Based on this analysis, it is possible that the Maria shear zone could represent one of these paleo-rift faults associated with opening of the McCoy Basin. However, this does not need to be the case, and our proposed model of the Big Maria syncline and other deformational features in the Maria Fold and Thrust Belt forming as a result of southeast-directed crustal channel flow is not dependent on this idea, though it is consistent with regional models advanced by the above mentioned workers. An additional wrinkle of this application is that even though crustal-scale ductile

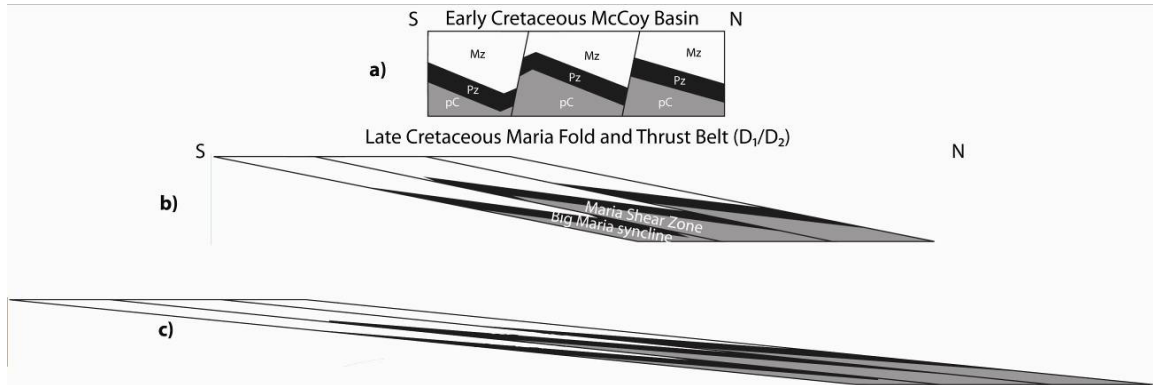


Figure 1.30: Application of crustal scale shear model for deformation in High Grade Nappe Assemblages to the Maria Fold and Thrust Belt. Modified from Williams and Jiang (2005). Mz = Mesozoic metasedimentary and volcanic rocks, Pz = Paleozoic metasedimentary rocks and pC = Precambrian basement. **A)** Schematic depiction of Early Cretaceous McCoy rift basin with south-dipping high angle normal faults. **B)** Rotation of these earlier structures during crustal scale simple, applying a shear strain of $\gamma = 5$. **C)** Rotation applying shear strain of $\gamma = 10$.

flow shows reverse shear, the terrane is actually stretched (not shortened) in the direction of ductile flow, as shown in Figures 1.30b and c. This could be useful for palinspastic reconstruction of the Maria Fold and Thrust Belt, however this type of reconstruction is difficult for the entire belt due to overprinting of older structures by younger features, such as Cenozoic normal faulting and metamorphic core complexes and Cretaceous plutons. This reconstruction is also difficult due to complex deformation within the belt and the uncertain nature of the northern boundary of the belt. Additionally, for this model to be applicable to the Maria Fold and Thrust Belt, it depends on the presence of earlier drag folds formed as a result of high angle normal faults prior to burial to mid-crustal depths. However, the interpretation of the structural evolution of the Big Maria Syncline presented here is not dependent on this model being valid.

Another problem with the Maria Fold and Thrust Belt that this study resolves is how SE-directed ductile flow could produce an apparently SW-vergent F_2 fold, such as the Big Maria syncline. Although previous workers (Ballard, 1990) have argued for two distinct deformational events with different kinematics and timing, we argue that D_1 and D_2 temporally overlap and were formed in the same progressive deformational event, even though they appear to have different kinematics. We base our argument on the prevalence of west or northwest plunging mineral lineations, stretched pebbles and concretions with long axes subparallel with this lineation (indicating that it is a stretching lineation) and microstructural and mesoscopic indicators indicating reverse, southeast-directed shear. In our model of deformation, southeast-directed thrusting (D_1) during the Sevier Orogeny subducted a large region of the cratonal section of the Cordilleran miogeocline. This crustal subduction allowed for cratonal rocks to reach middle crustal depths (12-15 km). Once this happened, fabric development (composite S_1/S_2) foliation developed and progressive folding and refolding of earlier fabrics eventually formed kilometer scale nappes. Progressive simple shear deformation with strains on the order of $\gamma = 10$ rotated the axes of F_1 and F_2 composite folds into the shear direction and accounts for extreme attenuation of Paleozoic and Mesozoic cratonal strata. The overall trend of mesoscopic and macroscopic F_2 fold axes would be northwest, which could easily be

misinterpreted as being a southwest-vergent structure based on the inferred shortening direction of the fold. D_1/D_2 in the Big Maria Mountains is correlative to D_1 in the Granite Wash Mountains model for deformation in the Maria Fold and Thrust Belt (Laubach et al., 1989) and D_1/D_2 in the Little Maria Mountains (Ballard, 1990).

The timing of D_1 is controversial, and is broadly constrained by the age of the Jurassic plutons (~160 Ma) and the Cretaceous leucogranite dikes (~75 Ma), which crosscut the S_1 fabric and the Big Maria syncline. We propose that D_1/D_2 structures were formed during the Sevier Orogeny based on kinematics and available time constraints. Further east in west-central Arizona, timing of deformation may be constrained by highly deformed and metamorphosed rocks equivalent to the Jurassic-Cretaceous McCoy Mountains Formation, the youngest unit in the area to experience all episodes of polyphase deformation. In the Big and Little Maria Mountains, however, no rocks equivalent to the MMF have been observed. However, many workers have suggested that the McCoy Basin formed as a rift basin. If our interpretation as advanced in Figure 1.29 is correct, formation of the McCoy Basin during the Early Cretaceous must pre-date middle crustal deformation in the Late Cretaceous Maria Fold and Thrust Belt. As discussed earlier, McCoy Mountains Formation is exposed in the supracrustal McCoy Basin terrane to the south. If deformation fabrics correlative to those observed in the Maria Fold and Thrust Belt are observed in the McCoy Basin, then timing of D_1/D_2 deformation would be constrained to Late Cretaceous, which is the age of most of the McCoy Mountains Formation based on detrital zircon, igneous intrusions and fossil evidence (Barth et al., 2004; Tosdal and Stone, 1994; Pelka, 1973). Furthermore, although most plutonic rocks in the Big Maria Mountains are assumed to be Jurassic in age, geochronology data in the range is sparse. Additional geochronology data from the range would be useful in further constraining the timing of deformation.

D_1/D_2 structures are subsequently refolded about F_3 folds in the BMM during D_3 deformation. D_3 refolds earlier structures around NE-vergent folds, and is characterized by a steeply SW-dipping cleavage, designated S_3 . Based on structural analysis at all scales, we interpret D_3 to be a significant regional deformation event. As discussed above,

most of the numerous significant bends and jogs that disrupt the overall WNW trend of the syncline that are observable at 100-meter and kilometer scales are demonstrably F_3 refolds and are ubiquitous in the Big Maria and Little Maria Mountains. However, these are best defined by exposures of Paleozoic and Mesozoic strata. Furthermore, field observations indicate that F_3 folds in area developed before significant development of the S_3 cleavage. In Areas A and C, we observe that F_3 folds refold earlier fabrics about folds with northwest-trending axes. These axes are also sub-parallel with the extension direction indicated by mineral elongation lineation and other kinematic indicators of finite extensional strain. This observation is likely explained by the geometry of F_3 folds being controlled by S_1/S_2 anisotropy (Fletcher and Karlstrom, 1990). F_3 folds were likely formed as the result of NE-SW directed shortening. This change in geometry represents a rotation of the principal strain field from top-southeast to NE-SW-directed shortening. The geometry of F_3 folds and the timing of formation suggest that these structures correlate with D_2 structures in the Granite Wash Mountains model for deformation in the Maria Fold and Thrust Belt.

S_3 cleavage development is most strongly expressed in micaceous rocks in an area that overlaps spatially with emplacement of the Cretaceous leucogranite dike swarm. Based on field observations, strong development of the S_3 cleavage fabric, as is observed in Area C must have taken place during emplacement of the leucogranite dikes. Locally, dikes are folded and boudinaged and contain the S_3 fabric. The dikes, however, are only weakly deformed by D_3 deformation. Therefore, we interpret that the dikes were emplaced near the end of D_3 . The orientation of the S_3 cleavage is similar to SW-dipping cleavage observed in the Granite Wash Mountains. In the model of deformation in the Maria Fold and Thrust Belt advanced by Laubach et al. (1989), this cleavage formed during a separate episode of deformation (D_4). In our model of deformation, we propose that development of this fabric accompanied emplacement of the leucogranite dikes toward the end of D_3 . Analysis of the dike swarm suggests NE-SW directed extension. Ballard (1990) also records evidence for NE-directed extension in the Little Maria Mountains. We interpret that the late stage of D_3 deformation records evidence of both

NE-directed shortening *and* extension. We interpret this NE-directed extensional event to be the result of synorogenic collapse of overthickened crust (Hodges and Walker, 1992). The channel flow model of middle crustal deformation predicts that as crust is sufficiently overthickened, sense of shear in the channel will begin to reverse, showing both compressional and extensional shear sense (Godin et al., 2006; Jamieson et al., 2002). This reversal of flow may have accounted for exhumation of the Maria Fold and Thrust Belt southward from beneath the Colorado Plateau.

Timing of D₃ is constrained to Late Cretaceous time based on the inferred timing of placement of the leucogranite dikes. Although the dikes themselves do not have reliable age constraints, a pluton exposed in the Little Maria Mountains, with a Late Cretaceous age of ~75 Ma (Hoisch et al., 1988) is chemically similar to the pegmatite swarm in the Big Maria Mountains and also contains NE-directed extensional shear bands on its margins (Ballard, 1990). Thus NE-directed was accompanied by emplacement of Late Cretaceous granites. The age of the leucogranite dikes is ~79 Ma based on K-Ar whole rock analysis (Martin et al., 1982), but more geochronologic data is needed for a more accurate age for the dikes. Granites and granodiorites of similar ages are found in the nearby Coxcomb Mountains (Barth et al., 2004), Old Woman Mountains (Foster et al., 1992) and Iron Mountains (Wells et al., 2002). Finally, sufficient regional evidence exists that supports the idea that this episode of deformation and plutonism was coeval with peak metamorphic conditions (Hoisch et al., 1998; Foster et al., 1992; Miller and Howard, 1985).

Summary of Mesozoic tectonic events

Stable cratonic depositional conditions existed in this region prior to onset of explosive volcanism in the Middle Jurassic, evidenced by metamorphosed volcanic rocks. Although these rocks have not been dated in the BMM, based on regional correlation with rocks of similar composition and stratigraphic position, these rocks are deposited between 160-150 Ma (Tosdal et al., 1989; Fackler-Adams et al., 1997). Deposition of these rocks was concomitant with, but not directly related to, an episode of plutonism in the Late Jurassic at ~170-150 Ma. Field observations indicate that these plutons intruded as sheets

and sills, evidenced by concordant contacts between plutons and “ghost stratigraphy” of Paleozoic rocks found *in situ* in the middle of the plutons. Some workers (Hamilton, 1982; Yeats, 1985; Boettcher et al., 2002) propose that the onset of deformation in the Maria Fold and Thrust Belt took place during Jurassic time and persisted through the Cretaceous. Although not enough geochronologic data has been recorded in the Maria Fold and Thrust Belt to rule out initiation of D_1 during Jurassic time, most workers conclude that deformation and peak metamorphism were coeval and that peak metamorphism is Cretaceous in age (Asmerom et al., 1988; Laubach et al., 1989; Hoisch et al., 1988). Direct evidence that deformation is entirely Cretaceous, though, could be obtained through 1) resolving the timing of deposition of the McCoy Mountains Formation and establishing tectonic links between the McCoy Basin and the Maria Fold and Thrust Belt and 2) placing further geologic constraints on the timing of pluton emplacement and metamorphic history.

Jurassic plutonic rocks and older rocks have all been subject to upper greenschist to lower amphibolite-grade metamorphism (Hamilton, 1982). P-T conditions of peak metamorphism have been determined to be 550-600°C and approximately 3-5 kbar, suggesting a burial depth of ~12 km (Hoisch et al., 1988), evidence of which is discussed earlier in the paper. Deformation is interpreted to have been coeval with peak metamorphism. Contractile deformation may have begun as early as the latest-most Jurassic, based on field evidence in the BMM, however, sufficient regional evidence exists to suggest that all contractile deformation is Cretaceous.

We favor a model of deformation in the BMM where D_1/D_2 is a polyphase, progressive deformation event. Structures formed during this event were likely the result of south-to-southeast-directed deformation beginning in the Early Cretaceous. We suggest that these structures formed as the result of northwest-directed underthrusting of the North American craton during the Sevier Orogeny, in contrast with the hypothesis that these structures formed as the result of Jurassic plutonism (Hamilton, 1982; 1987). We propose that tectonic burial to mid-crustal levels of Paleozoic and Mesozoic cratonal rocks accompanied the onset of D_1/D_2 deformation. An implication of this model is that

the MFTB is a southeastward continuation of the Sevier Fold and Thrust Belt (SFTB). Most Sevier structures are east-vergent (toward the continent) and structures we propose as correlative in the MFTB are southeast-vergent, which is consistent with overall east directed transport. However, the overall eastward trend of the MFTB across the grain of the Cordillera is somewhat of an anomaly. One possible explanation for this observed difference is that the style of deformation in a back arc region on continental crust reflects not only the stress field, but the nature of the crust being deformed (Burchfiel and Davis, 1975; 1981). In Utah and Nevada, where east-vergent Sevier structures are observed, the presence of a thick miogeoclinal crust allowed for the structural evolution of the Sevier system to develop vergence toward the continent. This is analogous to the modern Andean fold and thrust system. In contrast, the thick miogeoclinal wedge is absent in the BMM and deformation impinged on the thin Paleozoic craton of North America (Laubach and others, 1989). The absence of a thick miogeoclinal section may have been due to truncation of the southwestern margin of the North American craton (Burchfiel and Davis, 1975). Laubach and others (1989) propose that compression of young, presumably thinned crust beneath the young, deep McCoy basin could have led to underthrusting of the basin beneath the North American craton. Howard (1986) also suggests that thermal softening of continental lithosphere southwest of the MFTB by arc-related heating and plutonism may also have contributed to crustal underthrusting. We favor the HGNA model proposed by Williams and Jiang (2005), the implications of which are that high strain shear zones can form in zones of simple shear strain on the order of $\gamma = 10$. Our observations from the Big Maria Mountains tend to support the idea that high strain zones in HGNA might represent earlier discontinuities, such as high angle normal faults, although our observations may also be explained by critical taper theory.

Finally, we propose that D_3 represents an orientation of the principal strain field from southeast-directed shortening to NE-SW-directed shortening. Observed structures indicate that NE-directed shortening and extension occurred syntectonically toward the end of D_3 . This deformation is coeval with the emplacement of leucocratic pegmatites and plutons in the region. This is also consistent with the hypothesis that there were evolving

transport directions as Sevier thrusting (top-to-the-southeast) changed to Laramide thrusting (top-to-the-northeast) prior to the change from contraction to extension during the Late Mesozoic (Hodges and Walker, 1992).

Summary

The Big Maria syncline is an important structure to examine as it records evidence of multiple contractile deformation events in an important part of the North American Cordillera. Metamorphosed Paleozoic sedimentary rocks are useful for recognizing large fold nappes, examining extreme attenuation, multiple deformation fabrics, and palinspastic reconstruction. In the Big Maria syncline, Paleozoic units are attenuated to less than 1% of original stratigraphic thickness. This attenuation is the result of simple shear in a regional crustal shear zone. Three deformation events are recognized in the vicinity of the Big Maria syncline. D_1 is characterized by isoclinal folds and north-dipping shear zones that trend parallel to a pervasive north-dipping fabric, S_1 . D_2 is characterized by tight to isoclinal folds that refold S_1 about west or northwest-trending axes subparallel to the stretching direction and by extreme attenuation of Paleozoic and Mesozoic metasedimentary and metavolcanic rocks. We interpret D_1 and D_2 to represent two major generations of folding and shearing as the result of a protracted polyphase, progressive ductile deformation event, involving southeast-directed ductile reverse and dextral simple shear and middle crustal channel flow. We propose that extreme attenuation of Paleozoic rocks is the result of south-to-southeast-directed (reverse and dextral) shearing during D_1/D_2 deformation and the Big Maria syncline represents a composite D_1/D_2 structure. These early deformation events are likely the result of north-directed underthrusting of the North American craton during Sevier Orogeny. Sevier-involved conjugate thrusts on a large scale to the north show west-directed underthrusting of the craton beneath the thick marine miogeocline wedge. In the Maria Fold and Thrust Belt to the south, cratonal strata are thrust westward under themselves, such that the Colorado Plateau was adjacent to the Sevier orogenic belt in the east; ductile deformation in this area was facilitated by tectonic burial and thermal softening related to pluton emplacement. Based on regional correlation with the timing of Sevier structures as a

whole, and evidence that deformation was coeval with peak metamorphism, timing of D_1/D_2 is Late Cretaceous age. D_3 is characterized by the refolding of earlier fabrics around northeast-verging, northwest or southeast plunging folds. D_3 represents a significant regional refolding event, and is likely syntectonic with emplacement of a Cretaceous leucogranite dike swarm. The age of the dikes constrains D_3 to a Late Cretaceous event. D_3 is likely the result of NE-SW directed shortening, with evidence of extension taking place toward the end of D_3 . Extension is related to synorogenic collapse of overthickened continental crust toward the end of the Cretaceous. This extensional event allowed for extrusion and exhumation of the middle crustal Maria Fold and Thrust Belt channel and was coeval with emplacement of Late Cretaceous leucocratic granites and pegmatites in the region. Structures observed in the Big Maria Mountains correlate well with structures observed in western Arizona and in the adjacent Little Maria Mountains.

Chapter 2 : Tectonic linkages between the middle crustal Maria Fold and Thrust Belt and upper crustal McCoy Basin, southeastern California: Implications for the Mesozoic tectonic evolution of the North American Cordillera

A.C. Salem and K.E. Karlstrom

Chapter Abstract

Here we present new mapping, structural analysis and U-Pb and Ar-Ar geochronology from key portions of the Maria Fold and Thrust Belt (MFTB) and McCoy Basin in southeastern California. We correlate structural fabrics based on kinematics and relative timing of polyphase deformation events across the enigmatic tectonic boundary that separates the middle crustal MFTB terrane in the north from the upper crustal McCoy Basin terrane to the south. We then incorporate this data with existing geologic, geophysical, and geochemical data in order to constrain kinematics and timing of Mesozoic deformation events in the MFTB and present a comprehensive review of post-Jurassic tectonism in the southern Cordillera. Our hypothesis is that synorogenic sedimentation in the McCoy Basin is directly related to middle crustal polyphase deformation in the MFTB.

Structural analysis of fabrics shows that the MFTB and McCoy Basin have shared part of the same deformational history. The MFTB shows three distinct Mesozoic orogenic deformation events, designated D_1 , D_2 and D_3 . D_1 is characterized by east and southeast-vergent isoclinal folds and ductile shear zones in the MFTB and a pervasive north-dipping foliation fabric, S_1 . D_2 structures include large fold nappes that refold earlier fabrics and shear zones that emplace Jurassic and Proterozoic crystalline rocks over Paleozoic and Mesozoic metasedimentary rocks. High strain shear zones are characterized by imbrication and extreme attenuation (locally to less than 1% of original stratigraphic thickness) of Paleozoic strata. Field and microscopic kinematic indicators suggest that the D_1/D_2 was the result of pervasive crustal-scale shearing during SE-directed ductile middle crustal flow and that D_1 and D_2 temporally overlap and represent multiple stages in a complex progressive deformation event. The top-to-the-SE kinematics of D_1/D_2 is consistent with Sevier Orogeny deformation. No correlative fabrics to D_1/D_2 in the MFTB are observed in the McCoy Basin. D_3 is characterized by

NW-trending folds, SW-directed thrusts and associated SW-dipping cleavage in the MFTB. In the McCoy Basin, D_3 is characterized by southwest-vergent folds and thrust faults and north or northeast-dipping cleavage. Late Cretaceous age plutons and dikes are syn- to postkinematic with respect to D_3 .

New geochronology builds on published work in establishing a Cretaceous deformational history for both terranes. A deformed diorite containing the composite S_1/S_2 fabric in the Big Maria Mountains yields a U-Pb zircon age of 86.3 ± 2.1 Ma, which places a time constraint on D_1/D_2 middle crustal deformation. Based on youngest detrital zircon dates of 97-84 Ma from the upper McCoy Mountains Formation, deposition of the upper MMF temporally overlaps D_1/D_2 deformation in the MFTB supporting the interpretation that D_1/D_2 deformation initiated at ~ 97 Ma. The kinematics and timing of D_1/D_2 is consistent with Sevier Orogeny deformation. Ar-Ar ages of hornblende indicate that rocks cooled through $\sim 500^\circ$ C at ~ 70 Ma, agree well with crystallization ages of Late Cretaceous plutons and confirm the hypothesis that peak metamorphic temperature conditions were coeval with Late Cretaceous magmatism. Ar-Ar analysis of biotite constrains cooling of rocks through 300° C from 60-54 Ma, which is consistent with regional observations of a Paleocene-Eocene thermal event.

Identifying the temporal and tectonic linkages between the MFTB and the MMF provides new constraints on the tectonic evolution of the southern Cordillera. D_3 in the MFTB and McCoy Basin is characterized by NE-vergent folds in the MFTB and S-vergent folds and fabric development in the McCoy Basin. We interpret the MFTB structures to have formed during a progressive middle crustal flow regime during crustal thickening, channel extrusion and near simultaneous exhumation during synorogenic collapse in the region. The strain field recorded by D_1 - D_3 rotated from NW-SE to SW-NE, which we interpret to mark the change from Sevier crustal thickening to Laramide crustal overthickening and subsequent collapse of the orogen. This change is inferred to result from change in subducting slab geometry. Pre-existing geometry of the Jurassic-Cretaceous McCoy rift basin is inferred to have influenced the geometry of the Cretaceous Maria Fold and Thrust Belt and the McCoy retroarc foreland basin and that

sedimentation in the McCoy Basin is a passive record of Late Jurassic and Cretaceous orogenic events.

Introduction

The Maria Fold and Thrust Belt (MFTB) and McCoy Basin are adjacent but contrasting Mesozoic tectonic domains within the southern Cordillera. Here we present new mapping, structural analysis and U-Pb and Ar-Ar geochronology from key portions of each domain. The purpose is to characterize deformation fabrics and history in each domain and relate them to each other and to Mesozoic contractile deformation of the southern Cordillera. The goal of this research is to understand the kinematics and timing of Mesozoic deformation events in the middle crustal domain of the MFTB and to evaluate any tectonic linkages that may have existed between it and the upper crustal McCoy Basin. Better understanding of this different crustal levels and styles of deformation should help refine models for the Mesozoic tectonic evolution of the region.

The Maria Fold and Thrust Belt (MFTB, Reynolds et al., 1986) is a roughly east-west trending belt of highly deformed and metamorphosed rocks that extends from the Harquahala Mountains in west-central Arizona to the Palen Mountains in southeastern California (Figure 2.1). The MFTB, named for the Big and Little Maria Mountains in southeastern California, is characterized by basement-cored fold nappes (Burchfiel and Davis, 1981), south-vergent folds, thrust faults and ductile shear zones. The belt is famous for severe attenuation of Paleozoic and Mesozoic cratonal strata, with local attenuation to less than 1% of original stratigraphic thickness (Hamilton, 1982; Salem, 2005). The MFTB contains a diverse lithologic suite including Proterozoic basement, Paleozoic and Mesozoic cratonal strata equivalent to those observed in the Grand Canyon and the southwestern Colorado Plateau region and Jurassic and Cretaceous magmatic rocks. Rocks in the MFTB have been metamorphosed at upper greenschist to lower amphibolite (600° and 3-5 kbar, Hoisch et al., 1988) grade and have undergone primarily ductile deformation. Deformation in the Maria Fold and Thrust Belt is polyphase, with as

many as four deformation events recognized in the region (Laubach et al., 1989; Ballard, 1990).

The MFTB is flanked to the south by the McCoy Basin (Harding and Coney, 1985), which trends subparallel with the MFTB. The McCoy Basin is defined by exposures of Jurassic-Cretaceous McCoy Mountains Formation (MMF), an approximately 7 km thick sequence, which consists largely of weakly metamorphosed sandstone, siltstone and conglomerate. Exposures of MMF and equivalent facies are observed from the Coxcomb Mountains in the west to the Little Harquahala Mountains in the east and as far south as the Castle Dome Mountains in southwestern Arizona (Fig. 2.1 and 2.2). In most places in the McCoy Basin, McCoy Mountains Formation is observed to rest nonconformably on Jurassic volcanic rocks. In the Palen Mountains, the contact between the MMF and Jurassic volcanics has been interpreted to be gradational (Fackler-Adams et al., 1997). In the Plomosa Mountains, MMF has been observed deposited disconformably over Paleozoic sedimentary rocks (Harding and Coney, 1985). Rocks in the McCoy Basin, in contrast with the MFTB, have undergone mostly brittle deformation and have been metamorphosed at low greenschist grade. However, in the eastern part of the McCoy Basin, where the basin outcrop belt overlaps the Maria Fold and Thrust Belt, rocks equivalent to the McCoy Mountains Formation have undergone high strain ductile deformation. Such highly deformed rocks have been documented in the Riverside (Stern, 1998) Granite Wash and Little Harquahala Mountains (Spencer et al., 1985; Laubach et al., 1989). This suggests that the McCoy Basin had to have existed prior to some or all of the deformation events in the MFTB. The only area of contact exposed between these two terranes in the area of Figure 2.2 is in the northern Palen Mountains, which is discussed below.

Although much work has been done to characterize and develop the geologic framework of both the Maria Fold and Thrust Belt and McCoy Basin, fundamental questions still exist about the relationship of these two tectonic regimes to each other and to other parts of the Cordillera. The purpose of this investigation is to assess the kinematics and the relative and absolute timing of deformation events across a key

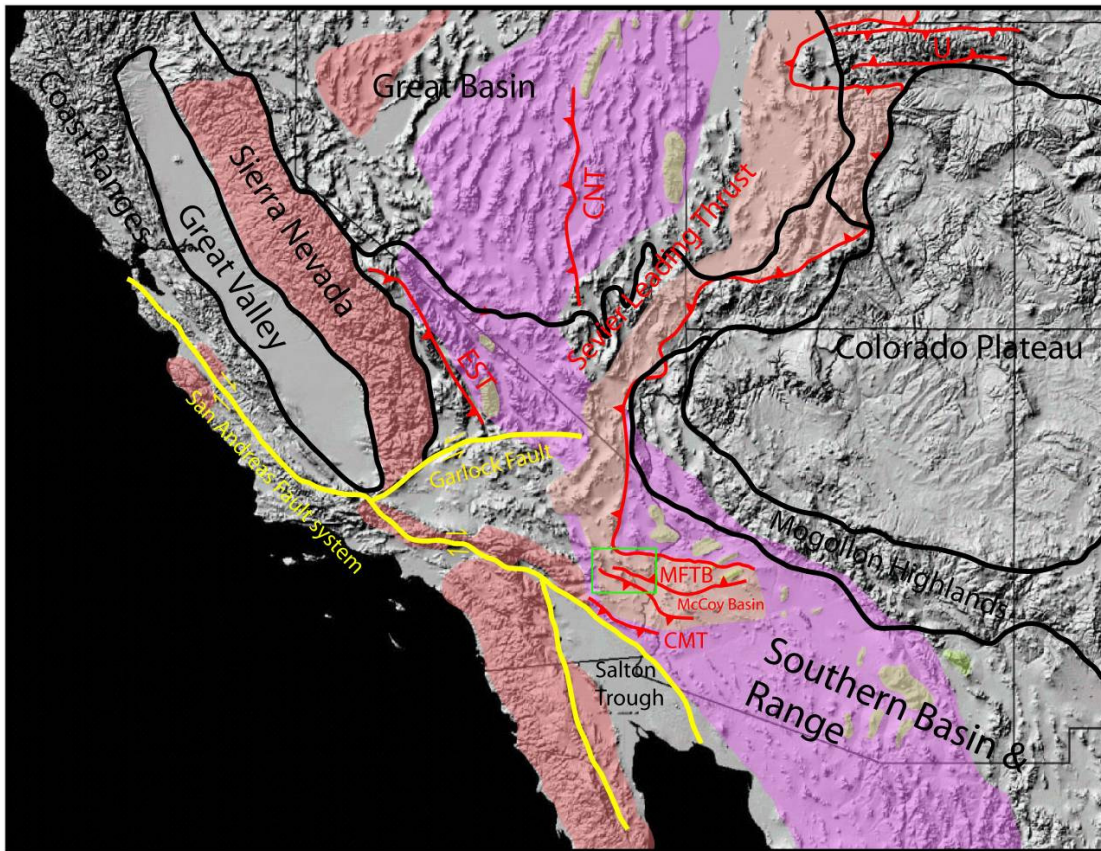


Figure 2.1: Regional tectonic map of the southwestern U.S. with selected Mesozoic and Cenozoic tectonic elements draped over a digital elevation model of the western U.S. The western half of the Maria Fold and Thrust Belt is outlined with green rectangle. Modern physiographic/geologic provinces are outlined in black. Green infill shows Late Cretaceous-Tertiary metamorphic core complexes (after Hodges and Walker, 1992; Wells and Hoisch, 2008). Purple infill shows a belt of Late Cretaceous muscovite granites (Miller and Bradfish, 1980), which largely coincides with location of metamorphic core complexes and the inferred axis of maximum crustal thickness during the Mesozoic (Coney and Harms, 1984). The Sevier Fold and Thrust Belt, shown with pink infill, is after DeCelles (2004), with the leading edge of the thrust labeled and shown in red. Late Jurassic-Early Cretaceous batholith complexes are shown in red infill. Other major Mesozoic thrust and uplifts are shown in red and labeled EST - Eastern Sierran Thrust, CNT - Central Nevada Thrust, U - Uinta Uplift (After Wells and Hoisch, 2008)

portion of the MFTB and the McCoy Basin in southeastern California. This study seeks to directly address the relationship of these two terranes to each other. Specifically, can deformation events in the Maria Fold and Thrust Belt be correlated with deformation events in the McCoy Basin, thereby establishing a link between the geologic histories of these two geologic provinces? An encompassing general hypothesis to be tested is that synorogenic sedimentation in the McCoy Basin can be linked in space and time to middle crustal ductile deformation events, leading to improved understanding of the regional tectonic history and orogenic processes. The study area includes key regions of the Big and Little Maria and McCoy Mountains and Palen Pass (Figure 2.2). This investigation will combine geologic mapping in the field, analysis of mesoscopic and microscopic structures, regional stratigraphy, and radiometric dating of key igneous and sedimentary units. Spatial analysis of multiple layers of georeferenced datasets should 1) lead to the development of a relative sequence of deformation events in this part of the MFTB and McCoy Basin, 2) provide important age constraints for each deformation event, 3) allow for a better understanding of the conditions of deformation and metamorphism in the area (including changes in rheology and P-T-t path), 4) quantify strain and allow for a determination of magnitude and direction of movements of crustal blocks during multiple deformation events, and 5) decipher aspects of the stress history via analysis of dikes and plutons.

This study has implications for understanding the dynamics of orogenic systems, which has been one of the fundamental processes that have intrigued geologists since the formalized study of geology began. One of the most essential relationships in this process is that between the development of orogenic belts and synorogenic basins. One approach to studying this process is to examine an actively developing mountain belt and synorogenic basin, such as the Andes, Alps, and Himalayas. This allows geologists to examine active processes behind the development of the mountain belt and accompanying basin, and to develop geodynamic models. For example, insights on near-surface processes, short-term rates of change, and fluxes of material are well studied in young mountain belts (e.g., Cloetingh et al., 2006, for the Alps, Banakar et al., 2003

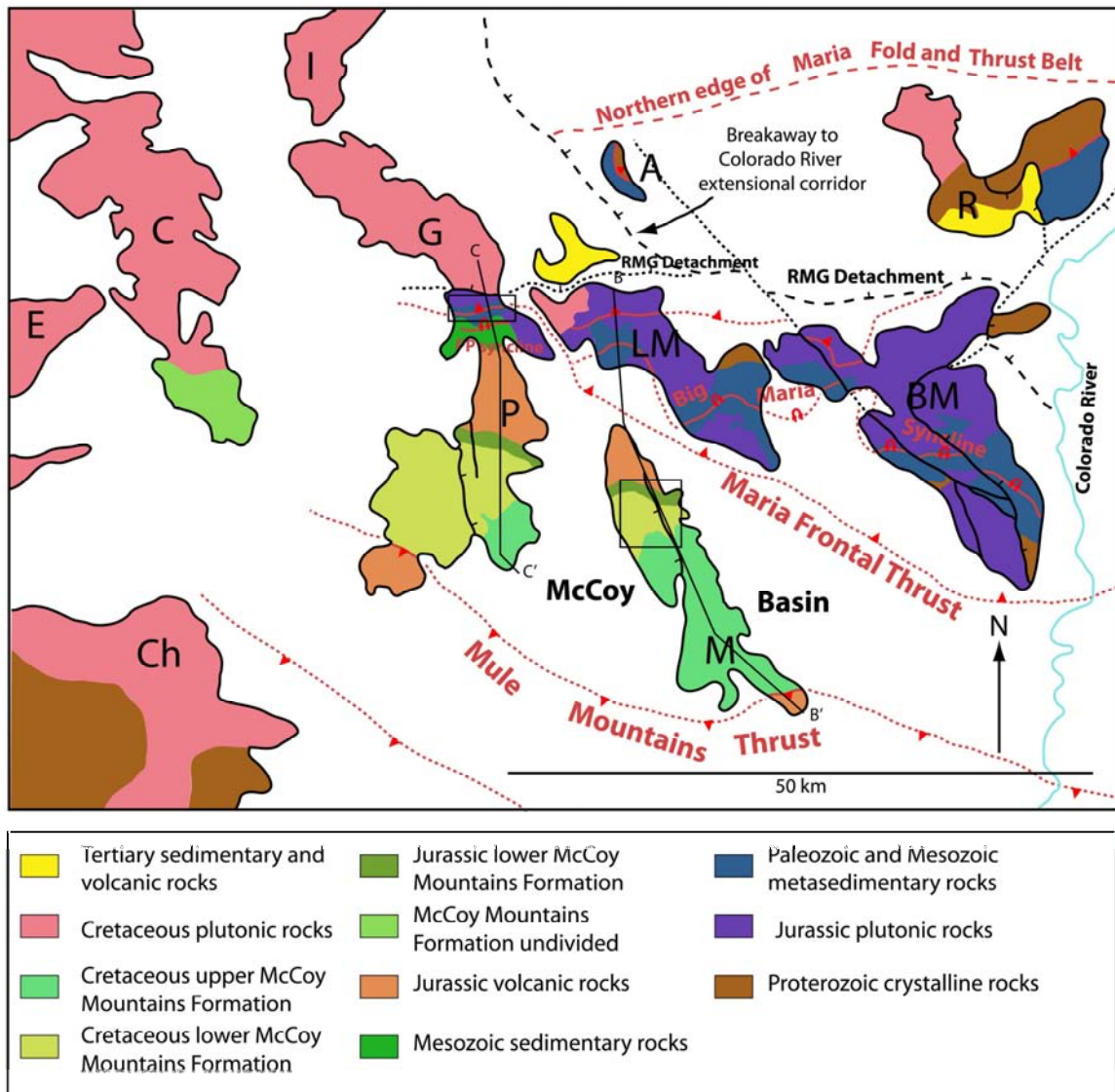


Figure 2.2: Simplified geologic and tectonic map of the Maria Fold and Thrust Belt and McCoy Basin in southeastern California showing selected important Mesozoic (shown in red) and Cenozoic (shown in black) tectonic elements, keyed in green in Figure 1. Study areas for structural analysis are outlined with black rectangles. Location of cross section lines B-B' and C-C' are shown. Abbreviations A: Arica Mountains, BM: Big Maria Mountains C: Coxcomb Mountains, Ch: Chuckwalla Mountains, E: Eagle Mountains, G: Granite Mountains, I: Iron Mountains, LM: Little Maria Mountains, M: McCoy Mountains, P: Palen Mountains, R: Riverside Mountains, RMG: Riverside-Maria-Granite. Map compiled from Wells et al. (2005), Stone (2006), Lyle (1982), Baltz (1982) and Spencer et al. (2005)

for the Himalayas, Hilley and Strecker, 2005, for the Andes, Horton, 2005 for a global survey). More complete understanding of the evolution of mountain belts also requires examination of the remnants of ancient orogenic belts and basins. This allows geologists to observe the long-term “real” effects of orogenic processes, including depth-dependent changes in processes (e.g., Karlstrom and Williams, 1998), coupling (or lack thereof) between rheologic layers (e.g. Klepeis and others, 2004), and longer-term, finite strain accumulation in an orogen (e.g. Kassem and Ring, 2004). These multiple datasets allow geologists to develop a more complete understanding of orogenic events, and provide constraints for geologic models of the evolution of an orogenic system. However, deciphering the history of ancient orogenic belts is difficult for many reasons: outcrops are sparse, often broken up by faulting, or wiped out by erosion; correlation of isolated outcrops to make complete ancient orogenic terranes is difficult. The MFTB and McCoy Basin provide an excellent field laboratory for studying an ancient orogenic belt juxtaposed next to its hypothesized synorogenic basin.

This study also will focus on regional tectonic events and will examine crustal-scale response and modification in response to temporally changing plate boundary dynamics. As will become apparent in subsequent sections, the MFTB and McCoy Basin are in their present spatial configuration as a result of a complex history of temporally changing tectonic settings accommodated by reactivation of pre-existing crustal weaknesses. Located on the southwestern margin of cratonal North America, southeastern California and western Arizona, this region has been undergoing continuous crustal scale deformation events since Late Triassic time (Burchfiel and Davis, 1975; Reynolds et al., 1989; Dickinson, 1981; Saleeby, 2003; DeCelles, 2004). In this paper we discuss how early Mesozoic intraplate boundaries and weaknesses, formed in response to plate margin dynamics, may have governed the development of the McCoy Basin and MFTB and, in turn, how these Mesozoic provinces influenced the development of later Cenozoic provinces and boundaries.

The results from this analysis combined with regional synthesis will be used to test two specific hypotheses. First, that there were evolving transport directions as Sevier

thrusting (top-to-the-southeast) changed to Laramide contraction, which was represented by east or northeast directed extension in the hinterland region of the Sevier orogenic belt during the late Mesozoic (Hodges and Walker, 1992; Wells and Hoisch, 2008). Aspects of this hypothesis have been proposed for the Granite Wash Mountains (Laubach and others, 1989) and Piute Mountains (Fletcher and Karlstrom, 1990). A corollary of this hypothesis is that the MFTB represents an eastward extension and the middle crustal roots of the Sevier Foreland Thrust Belt (SFTB), which would be confirmed by the presence of structures formed by similar transport directions and timing to the Sevier Orogeny. Second, that tectonic setting of the McCoy Basin changed over time from a syn-rift basin in the Late Jurassic-Early Cretaceous correlative to the Bisbee Basin, to a retroarc foreland basin until nearly the end of the Late Cretaceous. This model combines and integrates aspects of hypotheses advanced for the formation of the McCoy Basin by several workers (e.g., Harding and Coney, 1985; Dickinson et al., 1989; Tosdal and Stone, 1994; Barth et al., 2004). The results of this investigation will have important implications for reconstructing the Mesozoic tectonic history of this important part of the Cordillera, as well as for understanding the dynamics of the development of orogenic systems both at near-surface and mid-crustal levels, understanding the long-term response of the crust to subduction zone processes (e.g., inboard transmittal of deformation from the plate margin), and will provide an ancient analog for understanding and modeling the development of actively evolving orogenic belts and synorogenic basins.

Tectonic setting

The western portion of the Maria Fold and Thrust Belt in southeastern California comprises all or part of several mountain ranges, including the Big Maria, Little Maria, Palen, Arica and Riverside Mountains (Figure 2.2). McCoy Mountains Formation is observed in the Coxcomb, Palen, McCoy and Riverside Mountains. The Maria Fold and Thrust Belt lies in the Basin and Range Province (Figure 2.1), a physiographic/geologic province characterized by small, fault bounded mountain ranges and large valleys formed by widespread crustal extension. The province also contains a diverse geologic suite with

rocks of various age exposed encompassing almost all of geologic time. The Basin and Range Province extends from northern Mexico to southern Oregon and comprises all or part of Sonora, Chihuahua, California, Arizona, New Mexico, Nevada, Utah, Oregon and Idaho. Crustal extension in the broader Basin and Range began in Oligocene time (Stock and Atwater, 1997; Saleeby, 2003; Spencer and Reynolds, 1990) and is currently ongoing. However, the timing of the onset and end of crustal extension is locally variable. Extension initiated after subduction of the East Pacific Rise underneath southwestern North America and development of the modern San Andreas plate boundary (Stock and Atwater, 1997; Saleeby, 2003). The Basin and Range Province encompasses numerous Precambrian and Phanerozoic tectonic provinces, including the Cretaceous Maria Fold and Thrust Belt and Jurassic-Cretaceous McCoy Basin.

To the northwest of the Maria Fold and Thrust Belt, structures identified as being part of the Sevier Fold and Thrust Belt are found in the eastern Mojave Desert region (Fletcher and Karlstrom, 1990; Howard, 2002; Wells et al., 2005;). These mountain ranges contain rocks similar to those found in the MFTB to the south and with mountain ranges further north in the Death Valley region. The New York Mountains region represents the southernmost extent of Paleozoic rocks correlative to the thick marine facies of the Cordilleran miogeocline (Stone et al., 1983). In the MFTB to the southwest, exposed Paleozoic rocks are entirely of cratonal affinity. Many workers have suggested that this change in facies thickness and affinity resulted in a change in structural styles from brittle overthrusting to ductile underthrusting (DeCelles, 2004; Burchfiel and Davis, 1979; Laubach et al., 1989). Rocks in the Old Woman Mountains region have undergone upper greenschist to lower amphibolite grade metamorphism and intense polyphase ductile deformation during the Late Cretaceous (Hoisch et al., 1988; Fletcher and Karlstrom, 1990). Sense of vergence of most major structures is top-southeast (Miller et al., 1982; Howard et al., 1987). In this respect, the Old Woman Mountains region is similar to the MFTB. Structures observed in the Old Woman Mountains region are interpreted to be correlative with Sevier Fold and Thrust Belt structures. Because of this, this area has been identified as the southernmost extent of the Sevier Fold and Thrust

Belt. The Old Woman Mountains region is part of the hinterland zone of the Sevier Fold and Thrust Belt (Figure 1, Hodges and Walker, 1992), a region defined by high grade metamorphism and ductile deformation. The hinterland is the westernmost part of the Sevier Fold and Thrust Belt system. It contains the oldest thrust faults and shear zones and is spatially overlapped by Cenozoic metamorphic core complexes. Thus, the Sevier hinterland zone contains both compressional and extensional structures. It is argued that extension in the hinterland coupled with erosional denudation has exhumed middle to lower crustal rocks of the Cordilleran Thrust Belt (Hodges and Walker, 1992; Applegate et al., 1992; Wells et al., 2005). Deformation in the Sevier hinterland began during Late Jurassic time and persisted through the Late Cretaceous (Hodges and Walker, 1992, DeCelles, 2004). The Maria Fold and Thrust Belt may represent a southwestward continuation of the Sevier hinterland. Resolving kinematics and timing of deformation in MFTB will test this idea.

As shown in Figure 2.1, the MFTB and McCoy Basin lie in an area where a belt of Late Cretaceous peraluminous granites (Miller and Bradfish, 1980) convergence with the Sevier Fold and Thrust Belt (DeCelles, 2004). This convergence also coincides with the axis of greatest crustal thickening during Mesozoic contractile events (Coney and Harms, 1984). This belt of Cretaceous peraluminous granites also coincides with the hinterland of the Sevier Fold and Thrust Belt further north (Hodges and Walker, 1992). Thus, it has been widely argued that extension and Late Cretaceous magmatism were coeval in this segment of the Cordilleran Thrust Belt (Saleeby, 2003; Wells et al., 2005)

Spatially overlapping much of the Sevier hinterland and the belt of Late Cretaceous granites are a belt of metamorphic core complexes (shown as green infill on Figure 2.1), which trends parallel with and are largely identified on the eastern edge of the Sevier hinterland (Coney and Harms, 1984; Hodges and Walker, 1992; DeCelles, 2004). Metamorphic core complexes are areas that experienced extreme extension whereby rocks below the brittle-ductile transition have been exhumed as the lower plate of detachment faults, i.e., low angle normal faults (e.g., Rehrig and Reynolds, 1980). The metamorphic core complex terrane is characterized by features of both brittle

deformation, such as fault breccia and psuedotachylites (Reynolds and Lister, 1987) and ductile deformation, such as mylonitic fabrics and ductile normal-sense shear zones. Typically, detachment faults in the metamorphic core complex terrane in Arizona and southeastern California contain Proterozoic and Cretaceous-Tertiary crystalline rocks in their footwalls and Proterozoic crystalline and Tertiary sedimentary and volcanic rocks in their hanging walls. Rocks in the hanging wall of detachment faults have been transported tens of kilometers of horizontal displacement from their original source (Spencer and Reynolds, 1990). Most metamorphic core complexes in western Arizona and southeastern California have formed as the result of NE-SW directed extension. Metamorphic core complexes comprise all or part of the nearby Chemehuevi, Whipple, Buckskin, Harcuvar and Harquahala Mountains in the study area. Coney and Harms (1984) argue that metamorphic core complexes spatially overlap areas of greatest crustal thickness during the Cretaceous a hypothesis that has been confirmed by several workers in the region (Hodges and Walker, 1992; Wells et al., 2005). Metamorphic core complexes in the Cordillera have been identified as far north as British Columbia and as far south as northern Sonora with older extension to the north.

North of the Arizona and southern California portion of the metamorphic core complex terrane lies the Arizona Transition Zone. This province is characterized by relatively large mountain ranges separated by small valleys and basins. The Transition Zone extends from the big bend in the Colorado River that constitutes the Arizona-Nevada border to eastern New Mexico, where it overlaps with/terminates at the Rio Grande rift. Proterozoic rocks in the northwestern Transition Zone are of Yavapai-Mazatzal affinity (Karlstrom and Bowring, 1993; Whitmeyer and Karlstrom, 2007) and range in age from 1800-1400 Ma. Although these rocks have been ductilely deformed and metamorphosed during Proterozoic orogenic events they do not record evidence of Cretaceous deformation and metamorphism, unlike their equivalents in the MFTB. In the southeastern part of the Transition Zone there are exposures of Mesoproterozoic supracrustal sedimentary rocks designated the Apache Supergroup. These rocks are, in part, temporally correlative with the Unkar Group of the eastern Grand Canyon

(Timmons et al., 2005). There are no rocks correlative to Grand Canyon/Apache Supergroup rocks recognized anywhere in the MFTB. Meso- and Neoproterozoic rocks are exposed further north in the Death Valley region as part of the Pahrump Group. Outcrops of Paleozoic sedimentary rocks correlative to the sequence exposed in the southwestern Colorado Plateau are scattered throughout the central and southeastern Transition Zone but are not observed in the northwest portion adjacent to the Maria Fold and Thrust Belt. Tertiary and Quaternary sedimentary and volcanic rocks are observed in unconformable contact with Proterozoic and Paleozoic rocks. Rocks in the Mogollon Highlands have been deformed by Oligocene-Quaternary extensional brittle faulting. The modern Transition Zone encompasses the Mesozoic Mogollon Highlands (Reynolds et al., 1989) Initial uplift of the Mogollon Highlands is thought to be the result of uplift related to the breakup of Pangea and rifting along the southwestern margin of Laurentia (Burchfiel and Davis, 1975; Reynolds et al., 1989). The Mogollon Highlands are one of the source terranes for Mesozoic sedimentary rocks found in the Colorado Plateau to the north and in the MFTB and McCoy Basin to the southwest (Harding and Coney, 1985; Reynolds et al., 1989).

Northeast of the Transition Zone is the supracrustal Colorado Plateau province (Figure 2.1), a stable rigid lithospheric block that has experienced relatively little internal deformation since the Neoproterozoic despite multiple Phanerozoic tectonic events that have deformed adjacent regions. The geology of the Plateau in general consists of a ~4 km thick veneer of Paleozoic and Mesozoic sedimentary rocks draped over Proterozoic metamorphic crystalline rocks. Most of the Plateau was at sea level until at least approximately 90 Ma, which is the youngest age of Cretaceous marine sediments of the Mesa Verde Group. Initial uplift of the Plateau took place during the Laramide Orogeny (80-40 Ma), which is characterized by basement cored foreland uplifts, (e.g. the Front Ranges of the Rocky Mountains). On the Plateau, relict structures of the Laramide Orogeny include a few large mostly northwest trending monoclines, which were formed by reactivation of mostly Proterozoic faults and shear zones (Figure 2.1), and adjacent basins, (e.g. the San Juan Basin of the Four Corners region). Aside from these local

uplifts, the Plateau could be characterized as an area of “passive uplift” during the Laramide Orogeny, wherein this tectonic province simply rose isostatically without major amounts of tilting or folding. However, unlike the Transition Zone, the Plateau itself has experienced relatively little Cenozoic crustal extension, with most deformation again being the result of reactivation of ancient faults and shear zones. Miocene-Quaternary volcanism is evident on the southern and western margins of the Colorado Plateau. Not coincidentally, these are areas where the Plateau has been detached from the adjacent Basin and Range Province. Faults on the edge of the Plateau act as conduits that allow magma to reach the surface (Livaccari and Perry, 1993). The Colorado Plateau provides a stable reference point for understanding the geology of the southwestern U.S. For example, correlation of metamorphosed strata in the Big Maria Mountains to the classic cratonal sequence of Paleozoic rocks exposed in the western Grand Canyon (Hamilton, 1982) led to a complete re-understanding of the southern Mojave Desert region. Exposed Paleozoic sections define Mesozoic contractile structures, such as isoclinal fold nappes and ductile shear zones. Paleozoic strata of cratonal affinity are not exposed anywhere between the southwestern Colorado Plateau and the Maria Fold and Thrust Belt, a distance of approximately 200 km (Spencer and Reynolds, 1990). This large lack of lateral continuity is accounted for by the presence of the Mogollon Highlands as an ancient geographic barrier, and tectonic transport along Mesozoic and Cenozoic faults and shear zones.

To the south of the Maria Fold and Thrust Belt are exposures of the Pelona-Rand-Orocopia schist and correlative rocks. These rocks have been interpreted as a broad correlative of the Franciscan Complex that was thrust beneath North American continental crust during low-angle east dipping subduction related to the Laramide Orogeny (Dickinson, 1981; Saleeby, 2003). Restoration of the San Andreas Fault shows that the Pelona-Rand-Orocopia schist and Franciscan Complex define a northwest trending belt of marine rocks (Grove et al., 2003) that were subjected to ultrahigh pressure and high temperature metamorphism (Figure 2.1). These rocks are shown to be in tectonic contact underneath rocks of North American cratonal affinity to the north and

the Sierra Nevada-Peninsular Range batholith complexes and correlative rocks to the south. The Orocochia schist and correlative rocks are exposed as far west as the central coast of California, where they are known as the schists of Portal Ridge and Sierra de Salinas and as far east as the Slumgullion and Castle Dome Mountains in southwestern Arizona. U-Pb detrital zircon analysis suggests that these rocks were deposited from Late Cretaceous to Paleocene time (Grove et al., 2003; Jacobson et al., 2007); further geochemical studies indicate that these rocks were metamorphosed from Late Cretaceous to Eocene time and then were rapidly exhumed (Barth et al., 2003; Grove et al., 2003). Based on metamorphic mineral assemblages, rocks of the Pelona-Rand-Orocochia schist underwent high temperature (700°C) and ultrahigh pressure (~ 1 GPa) during peak metamorphism, which was Late Cretaceous-Paleocene age (Barth et al., 2003). These rocks likely represent underplating of marine facies of an accretionary wedge complex or a forearc basin during Laramide subduction of the Farallon slab underneath southwestern North America (Barth and Schniederma, 1996; Jacobson et al., 1996; Saleeby, 2003). In the southern Mojave Desert Region, the Orocochia schist and equivalent rocks are in the lower plate of the northeast-vergent Chocolate Mountains fault. In the upper plate of the fault are rocks of cratonal North America. The thrust system may be traced through the Orocochia, Chuckwalla and Chocolate Mountains. It might be possible to trace this system further southwest into Arizona, but it has been overprinted by Tertiary sedimentary and volcanic rocks. The kinematics of deformation on the Chocolate Mountains fault remains controversial. The structure is regionally correlative with the Vincent Fault of the Transverse Ranges, which also contains exposures of Pelona-Rand-Orocochia schist in its footwall. The Vincent Fault has been demonstrated to be a ductile thrust fault, with top to the southwest-directed sense of shear (Ehlig, 1981; Jacobson, 1997). However, along strike of the Chocolate Mountains Thrust appears to be more complicated. Most kinematic studies demonstrate that the Chocolate Mountains thrust has a top-northeast sense of shear (Simpson, 1990; Jacobson and Dawson, 1995), opposite that of the Vincent Thrust and opposite of what would be predicted by northeast-directed subduction of the Farallon Plate during the Laramide Orogeny (Dickinson, 1981; Burchfiel and

Davis, 1981). To resolve this, some workers have called for the fault to be a northeast-directed extensional fault (Jacobson et al., 2007), which would partially exhume the underlying schist, whereas others have invoked a passive roof model thrust (Yin, 2002), where the Chocolate Mountains fault would be a northeast-directed back thrust similar to development of the South Tibetan detachment system. Both models call for significant exhumation of the schist during Miocene extension. Resolving kinematics of the Chocolate Mountains fault is beyond the scope of this study, but it is important to discuss the Pelona-Rand-Orocopia schist and Franciscan Complex, as these units were deposited, deformed and metamorphosed around the same time as other rocks in the Mojave Desert region. Therefore, understanding these rocks is critical for evaluating the Mesozoic tectonic setting of the Maria Fold and Thrust Belt and McCoy Basin.

Just south of the Chocolate Mountains is the main strand of the San Andreas Fault Zone and magmatic rocks of the Transverse and Peninsular Ranges (Jennings, 1967; Saleeby, 2003). The San Andreas slices through and segments the Transverse and Peninsular Ranges. These rocks constitute part of the North American Jurassic-Cretaceous magmatic arc, which stretches from Baja California to northern California and includes the Sierra Nevada Batholith. This magmatic arc is analogous to the Andean arc of South America. Magmatism associated with the Jurassic-Cretaceous arc is evident as outcrops of felsic plutons in the vicinity of Joshua Tree National Park. The Coxcomb Mountains, which make up the westernmost extent of the McCoy Basin, contain outcrops of McCoy Mountains Formation that have been intruded by plutons related to the Cretaceous arc. The Cretaceous arc also overlaps the Maria Fold and Thrust Belt and vicinity in the Granite, Little Maria, Old Woman and Piute Mountains (Figure 1). A leucocratic pegmatite swarm exposed in the northwest Big Maria Mountains also is related to the Jurassic-Cretaceous arc.

Previous Work

Initial geologic mapping in the region began as a series of reconnaissance mapping efforts in the late 1930's and 1940's. Miller (1944) was the first geologist to

assign names to some of the various stratigraphic groups. For example the name Maria Formation was assigned to metasedimentary rocks exposed in the Big Maria and Little Maria Mountains. Miller tentatively assigned a Paleozoic age to these rocks based on their lithology, though no evidence such as fossils existed to confirm this age. Another example includes the McCoy Mountains Formation, a >7 km thick sequence of sandstones, siltstones and conglomerates named for the McCoy Mountains.

The first published mapping of mountain ranges in the region was by Jennings (1967) who compiled a 1:250,000 scale map of the Salton Sea 1° x 2° sheet from previously unpublished data. Shklanka (1963) studied the geology of the Little Maria Mountains and characterized polyphase deformation and metamorphism. Hamilton (1964) published a geologic map at 1:24,000 scale of the Big Maria Mountains NE quadrangle, which includes the northeastern Big Maria Mountains and the southern Riverside Mountains. In the report accompanying that map, Hamilton describes isoclinal folds of Paleozoic sections and thrust slivers. In addition, Hamilton's geologic map shows the Riverside detachment, which contains middle crustal rocks of the Riverside and Big Maria Mountains in the lower plate and contains sedimentary and volcanic rocks in its upper plate. Movement along the Riverside detachment is down-to-the-northeast (Hamilton, 1982; 1987).

The McCoy and Palen Mountains were first mapped in detail by Gary Pelka (1973) at 1:48,000 scale. Pelka separated out the McCoy Mountains Formation into 14 different members. He also recognized a sequence of metamorphosed sedimentary rocks near Palen Pass that consisted of sandstone, siltstone, conglomerate and calcareous sandstone and shale. Pelka assigned these rocks the name Palen Formation and a Mesozoic age based on its lithologic correlation to highly deformed and metamorphosed strata of the Maria Formation. Pelka also published the first qualitative descriptions of the geology of the Palen and McCoy Mountains. Pelka found that rocks of the McCoy Mountains Formation had undergone relatively low grade (upper greenschist) metamorphism and brittle deformation. A pervasive, mostly north-dipping cleavage fabric is found throughout the Palen and McCoy ranges. Pelka also was the first to recognize

that the contact between highly deformed and metamorphosed rocks of the Maria Formation and the less deformed and metamorphosed strata of the Palen Formation exposed at Palen Pass represented some kind of important tectonic boundary. Additionally, Pelka concluded that at least the upper half of the McCoy Mountains Formation must be Cretaceous in age based on fossil wood in the type section.

A major wave of geologic investigations into the region took place during the 1980's beginning with several students from San Diego State University. Tucker (1980) examined pressure and temperature conditions of metamorphism in the Big Maria Mountains. Miller found that peak pressure was 5 kbar and peak temperature conditions were 550-600°C. Emerson (1982) did a structural analysis of the Little Maria Mountains and concluded that most major folds and thrusts in the range were formed by north-directed underthrusting during Cretaceous time. Ellis (1982) reached the same conclusion regarding structures in the Big Maria Mountains (Figure 6). Additionally, similar conclusions were reached regarding deformation in the Arica (Baltz, 1982) and Riverside Mountains (Lyle, 1982) and at Palen Pass (Demaree, 1981). Martin et al. (1982) investigated the timing of magmatism, deformation and uplift in the region and concluded that major contractile deformation ended by 79 Ma, the age of an undeformed pegmatite from the Big Maria Mountains. In addition, K-Ar data on magmatic rocks in the region yielded ages of 59 and 52 Ma; these have been interpreted as cooling ages and constrain the earliest stage of uplift (Martin et al., 1982).

Hamilton published the results of his many years of work in the region in a synthesis paper on the geology of the Big Maria Mountains (1982), a 1:48,000 scale map of the mountain range and accompanying report (1984) and a summary of the geology of the region (1987). The main conclusions of these works were that rocks in the region underwent upper greenschist to lower amphibolite-grade metamorphism and ductile deformation. Hamilton (1982) interpreted that the Big Maria syncline and similar structures formed as a synformal keel between rising Jurassic plutons. In addition, Hamilton (1982; 1987) recognized small scale NE-vergent folds and concluded that most deformation observed in the Big Maria Mountains in nearby mountain ranges were the

result of top-to-the-northeast directed reverse shear and that south-facing structures were artifacts of local geometry. Hamilton, although he was the first one to formally recognize that metasedimentary rocks were correlative to Paleozoic and Mesozoic strata on the Colorado Plateau (1964) did not formally publish these correlations until much later (1982). Chiefly, Hamilton recognized that the succession of quartzite, schist, carbonate and calc-silicate rocks were stratigraphically correlative with the classic cratonal sequence of the western Grand Canyon region. As such, he assigned Paleozoic rock formations the same geologic age and formation name as their Grand Canyon equivalent (Noble, 1923); e.g., the basal quartzite in depositional contact above Proterozoic crystalline rocks he assigned the name Tapeats quartzite and so on up to the Permian Kaibab Formation. Hamilton (1982, 1987) also attempted to resolve some Mesozoic stratigraphy. He recognized a green calcareous schist in the Big Maria Mountains above the Kaibab Formation that he designated the Triassic Moenkopi Formation. He also recognized a quartzite above the Moenkopi as the Jurassic Aztec quartzite and a volcanic unit above the Aztec that he assigned a Jurassic age. Once this was established, similar rocks were observed throughout the Mojave Desert region of southeastern California (Stone et al., 1983) and this led to a fundamental reinterpretation of the Mojave Desert region. Stone et al. (1983) also distinguished between Paleozoic rocks of cratonal affinity, similar to the Grand Canyon region, and rocks of miogeocline affinity and noted that the transition between these two different groups of rocks occurs near the Old Woman Mountains. Burchfiel and Davis (1975) argued that this change in affinity influences the style of structures present in the region.

Harding (1982) and Harding and Coney (1985) characterized geology and the stratigraphy of the McCoy Mountains Formation in the Palen, McCoy and Dome Rock Mountains and in the Livingston Hills. They divided the unit into six stratigraphic members and assigned the following names (from oldest to youngest): Basal Sandstone 1, Basal Sandstone 2, Mudstone Member, Conglomerate Member, Sandstone Member and Siltstone Member. Harding and Coney (1985) concluded that there was an unconformity between the Mudstone Member and the Conglomerate Member and noted that Paleozoic

clasts were present in the Conglomerate Member but not below it. They also concluded that the McCoy Mountains Formation rests depositionally (but not conformably) on Jurassic volcanic substrate in most places, although locally it disconformably overlies Paleozoic and Mesozoic strata in the Plomosa Mountains. Based on the lateral continuity of members of the McCoy Mountains Formation, Harding and Coney (1985) coined the term McCoy Basin to describe the outcrop belt of McCoy Mountains Formation. Based on paleomagnetic data, they concluded that the McCoy Basin formed as a transtensional basin as a result of the Jurassic Mojave-Sonora Megashear, and contended that this was the origin for similar sedimentary outcrops in southern Arizona and northern Mexico. This stands in contrast with the fossil wood evidence that gave a Late Cretaceous age for the upper portion of the McCoy Mountains Formation. Harding and Coney (1985) dismissed the fossil wood evidence as being inconclusive as the fossil wood could not be precisely identified or dated. Stone et al. (1987) later demonstrated that the fossil wood was in fact of Late Cretaceous age and were able to reconcile this with the paleomagnetic data presented in Harding and Coney (1985), thus further establishing a Cretaceous age for at least the upper part of the formation.

Hoisch (1985) and Hoisch et al. (1988) did detailed studies of the conditions and timing of metamorphism during deformation in the Big Maria and Old Woman Mountains. These workers concluded that peak temperature and pressure conditions of metamorphism were between 500-600°C and ~3-5 kbar. A considerable amount of fluid flow was involved during peak metamorphism. For instance Hoisch et al. (1988) calculated a fluid to rock ratio of approximately 17:1 during peak metamorphism in the Supai Formation and approximately 5:1 in the Kaibab and Muav Formations. Based on this Hoisch et al. (1988) concluded that peak metamorphism must have been accompanied by the dewatering of a down-going subducting slab. An isograd map made of the Big Maria Mountains also shows metamorphic grade increasing from southeast-to-northwest in the range (Figure 2.3). Hoisch et al. (1988) attribute this to the presence of a subsurface pluton near the northwestern end of the range; the surficial expression of the pluton would be the dike swarm present throughout the central and northern part of the

range. Also these studies determined that peak metamorphism, which coincided with most polyphase deformation events, must have taken place at or around 75 Ma, based on K-Ar thermochronology (Hoisch et al., 1988).

Investigators from the Arizona Geologic Survey in the late 1980's used the new understanding of Paleozoic rocks and the recognition of McCoy Mountains Formation stratigraphy to remap several mountain ranges in western Arizona (Spencer et al., 1985; Reynolds et al., 1986; Reynolds, Spencer and DeWitt, 1987; Reynolds et al., 1987; Laubach et al., 1989; Spencer and Reynolds, 1990). Results of these investigations included more detailed mapping, separation out of several Mesozoic metasedimentary units and resolution of Mesozoic stratigraphy, and reinterpretation of the geologic history of western Arizona. The stratigraphy of the Mesozoic rocks will be discussed in further detail in the next section. New units previously unrecognized in the Mojave Desert region include the Triassic Buckskin Formation, which is time correlative to the Moenkopi and Chinle Formations and the Triassic-Jurassic Vampire which is time correlative to the Chinle Formation and lower Glen Canyon Group (Reynolds, Spencer and DeWitt, 1987). Reynolds et al. (1986) recognized Mesozoic polyphase deformation in western Arizona, characterized mostly by south-vergent folds and thrust faults. They recognized that these structures stretched across from western Arizona into southeastern California, that rocks involved in these structures had been subjected to high grade (upper greenschist to amphibolite grade) metamorphism and that these scattered exposures defined a roughly east-west trending tectonic terrane that they designated the Maria Fold and Thrust Belt. Structures recognized as part of the Maria Fold and Thrust Belt (MFTB) are recognized in the Little Harquahala, Harquahala, Granite Wash, Harcuvar, New Water, Moon, Plomosa and Dome Rock Mountains in Arizona and in the Big Maria, Little Maria, Riverside, Arica and Palen Mountains in California. Laubach et al. (1989) concluded that four phases of Mesozoic contractile deformation are observed in the western portion of the MFTB, which they designated D₁, D₂, D₃ and D₄. D₁ is characterized by south and southeast-southeast vergent isoclinal folds and reverse shear zones; D₁ structures are interpreted to have formed during the Sevier Orogeny. If this is the case, then the front of

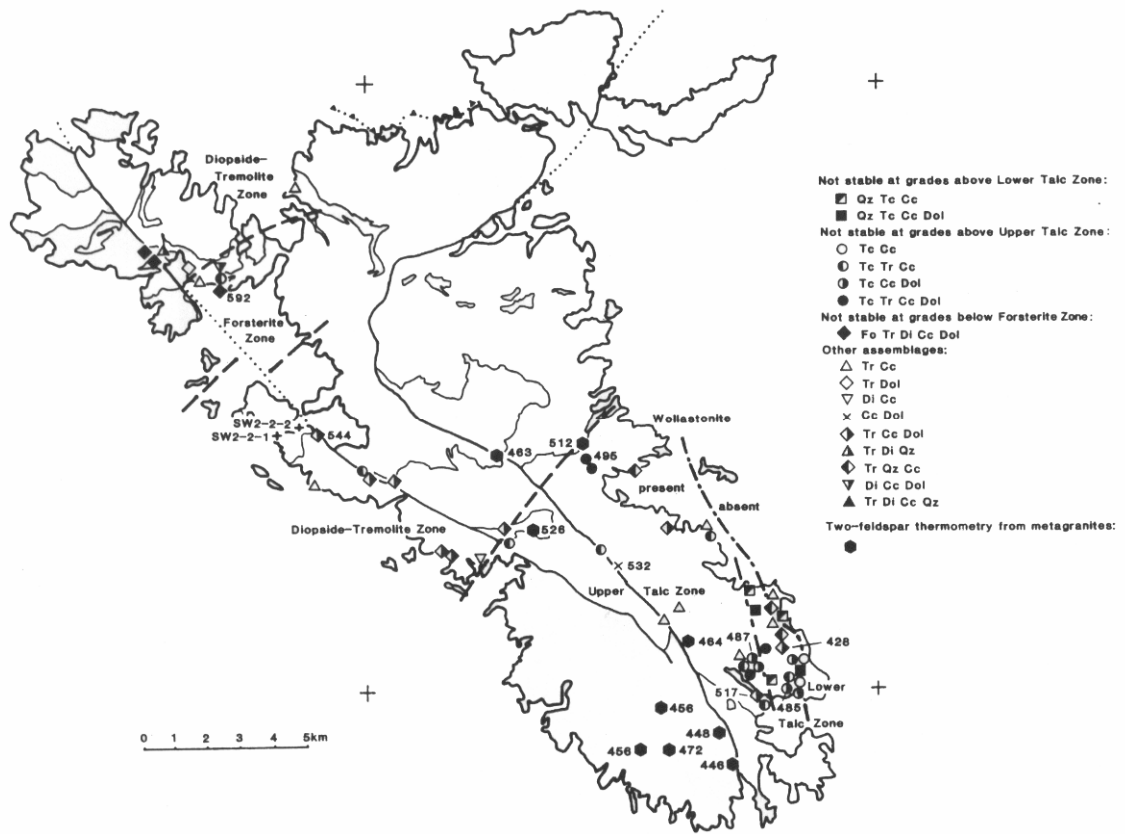


Figure 2.3: Metamorphic isograd map of the Big Maria Mountains from Hoisch et al., 1988. Symbols show mineral assemblages. Numbers by dark hexagons indicate cooling temperatures determined by two feldspar thermometry. In general metamorphic grade increases from southeast at the lower talc zone to northwest near the forsterite zone.

the Sevier Fold and Thrust Belt would be located less than 50 miles west of Phoenix, Arizona. D₂ is characterized by southwest-vergent reverse shear zones and thrust faults that emplace Proterozoic and Jurassic crystalline rocks over Paleozoic and Mesozoic cratonal strata and is responsible for imbrication and attenuation of Paleozoic and Mesozoic strata. Laubach et al. (1989) suggested that D₁ and D₂ have different kinematic signatures but might be multiple stages in the same progressive deformation event. D₃ is characterized by east-west trending open folds. D₄ is characterized by a steeply southwest-dipping cleavage that is best expressed in micaceous rocks. The youngest rocks in the region to experience polyphase deformation are strata equivalent to the McCoy Mountains Formation, so these rocks provide an upper-bound age constraint to deformation. All deformation fabrics are cross-cut by Late Cretaceous (80-70 Ma) plutons, so polyphase deformation had to predate these Late Cretaceous plutons. Based on these constraints, these workers concluded that all deformation events had to take place during the Cretaceous; however, they acknowledged that the age constraints on the McCoy Mountains Formation allowed for the possibility that deformation may have begun in the Late Jurassic.

Tosdal et al. (1989) published a regional synthesis of the Jurassic geology of the Sonoran Desert region, which includes northern Mexico, southern Arizona and southeastern California. In this paper he published correlations of different Jurassic magmatic rocks based on lithologic similarity and available U-Pb and Ar-Ar ages. He also published correlations of different facies of the McCoy Mountains Formation and similar sedimentary rocks including the Apache Wash Facies (Reynolds, Spencer and DeWitt, 1987) and Livingston Hills Formation. They concluded that there were three different pulses of magmatism during the Jurassic. There was an initial phase of volcanism beginning at 200-190 Ma. Then, there was an episode of plutonism from 175-155 Ma to which Tosdal et al. assign the name Kitt Peak-Trigo Peak Supergroup. The Kitt Peak-Trigo Peak Supergroup is divided into three main members: hornblende-bearing diorite, porphyritic granodiorite, which contains euhedral lavender feldspar phenocrysts, gray granite and leucocratic granite. The age of the granodiorite is ~160 Ma

(U-Pb whole rock L.T. Silver written communication to W.B. Hamilton, 1982) and the age of the granite is ~150 Ma. The diorite has not been dated, but is presumed to be no more than 15 Ma older than the granodiorite. The third pulse of magmatism was another, younger episode of volcanism that is ~160-150 Ma, represented by rocks to which Tosdal assigns the name Dome Rock Group. These rocks include ash flow tuffs and the enigmatic quartz porphyry unit exposed in the Plomosa, Dome Rock, McCoy and Palen Mountains. The quartz porphyry is interpreted as a hypabyssal magmatic rock and is the substrate for the McCoy Mountains Formation throughout most of the McCoy Basin. Tosdal concludes that these magmatic rocks constitute part of a Jurassic magmatic arc that stretched from northern Sonora all the way to British Columbia.

Stone and Kelley (1989) published a 1:24,000 scale map of the Palen Pass 7.5' quadrangle, which includes the southern Granite Mountains, Palen Pass and the northern Palen Mountains using the recently recognized regional stratigraphy. They separated out individual Paleozoic and Mesozoic units that had been previously assigned to the Maria and Palen Formations respectively and recognized that all of the Mesozoic stratigraphy in nearby mountain ranges are preserved at Palen Pass. They recognized the presence of a syncline with an overturned limb in the footwall of a major thrust fault that involved overturned Kaibab Formation and Triassic and Jurassic metasedimentary rocks. This syncline, like most structures in the Maria Fold and Thrust Belt is southwest-vergent fold. At least the lower part of the McCoy Mountains Formation is also involved in this syncline but only the south dipping limb of the syncline is preserved.

Ballard (1990) examined the geology of the Little Maria Mountains, and remapped at 1:24,000 scale the geology of the entire range plus the northwestern Big Maria Mountains. He concluded that there were three Mesozoic deformation events in the region and designated these events D₁, D₂ and D₃. D₁ structures formed as the result of top-to-the-southeast reverse shear and formed isoclinal folds and southeast-directed shear zones. Ballard concluded that the timing of this event must be constrained between 160-90 Ma. Based on the kinematics of D₁ he concluded that these structures might have formed during the Sevier Orogeny. D₂ is characterized by southwest-vergent folds and

reverse shear zones. These shear zones emplaced Jurassic and Proterozoic crystalline rocks over Paleozoic and Mesozoic cratonal strata and imbricated and attenuated Paleozoic and Mesozoic strata. He concluded that the timing of D_2 was constrained between 90-80 Ma. D_3 structures formed as the result of northeast-directed normal shear and are characterized by northeast vergent folds and shear zones. He concluded that the timing of D_3 was constrained between 80 and 52 Ma. These conclusions were in overall agreement with conclusions about polyphase deformation in western Arizona advanced by Laubach et al. (1989).

Knapp and Heizler (1990), using Ar-Ar analysis, examined thermal uplift history of the region. They concluded that there were three stages of syn-post kinematic uplift in the region: at 60 Ma, 30 Ma and 15 Ma respectively. The 60 Ma event would have been initial uplift related to gravitational collapse at the end of the Cretaceous. Likewise the 30 Ma and 15 Ma events would have been two stages of uplift and exhumation related to Oligocene and Miocene magmatic and extension events.

Work done as part of the Collaborative Old Woman and Piute Investigations and Explorations (COWPIE), and later efforts in the region, sought to unravel middle crustal deformation and metamorphism in the nearby Old Woman, Piute Mountains and Iron Mountains and Kilbeck Hills. The geology of these ranges shares similarities with the Maria Fold and Thrust Belt to the southeast. In this region, Cambrian through Triassic age metasedimentary rocks metamorphosed at greenschist to amphibolite facies are intruded by Jurassic and Late Cretaceous granitic rocks (Wells and Hoisch, 2008). Two deformation events are recognized in the region; D_1 is characterized by southeast-directed shortening and basement-involved nappe formation (Fletcher and Karlstrom, 1990). D_2 is characterized by northeast-southwest directed extensional deformation associated with synextensional magmatism and peak metamorphic conditions. Jurassic and older rocks exhibit extensive Mesozoic ductile deformation, mostly along the NE-striking Scanlon thrust and associated basement-cored nappes (Miller et al., 1982; Howard et al., 1987). This older deformation event is overprinted extensively by top-southwest-directed extensional deformation, which has been associated with emplacement of the Late

Cretaceous Old Woman pluton (74 +/- 3 Ma; Foster et al., 1989). Intrusion pressure accompanying pluton emplacement was on the order of 4-5 kbar, following crustal thickening associated with initial nappe emplacement (Foster et al., 1992; Rothstein and Hoisch, 1994). Given the synextensional nature of the Old Woman pluton (McCaffrey et al., 1999), extension was active at intrusion from ~74 Ma to <68 Ma (Carl et al., 1991; Foster et al., 1992).

Amphibolite grade metamorphism is associated with pluton emplacement (Miller and Barton, 1990). Ar-Ar analysis, combined with zircon crystallization ages from the same plutons consistently demonstrates that pluton emplacement took place between 90-70 Ma (Wells et al., 2002; 2005; Kula et al., 2002; Foster et al., 1989; 1992; Kidder et al., 2005; Barth et al., 2004). This was followed by cooling through ~550°C between 74-67 Ma. Regional metamorphic grades were between 3-5 kbar with peak temperatures reaching ~600°C (Hoisch et al., 1988). Therefore, it is likely that Ar-Ar ages of hornblendes would constrain the timing of peak metamorphism, which took place during the late stages of pluton emplacement and shortly afterwards.

Tosdal and Stone (1994) published a synthesis paper on the McCoy Mountains Formation (MMF) and summarized the internal stratigraphy and regional correlations. They concluded that the MMF could be divided into an upper and lower member, with an intraformational unconformity between the Mudstone Member and Conglomerate Member of Harding (1982) or Member E and Member F of Stone and Pelka (1989). Numerous lines of evidence including ash fall tuffs in the upper MMF dated at ~78 Ma by U-Pb and Cretaceous fossil wood suggest a Late Cretaceous age for the upper MMF. However the age of the lower MMF was poorly constrained. The lower bound constraint for the age of the MMF is the age of the Jurassic volcanic rocks (~160 Ma) and the upper bound constraint for the MMF is the Albian (Late Cretaceous) age of the fossil wood found in the upper MMF. In their paper Tosdal and Stone (1994) contend that the outcrop belt of the McCoy Basin spatially overlaps the MFTB in the east and diverts from it in the east. Furthermore, they point out that while the intraformational unconformity is obvious in the Plomosa and Dome Rock Mountains, that the unconformity becomes less apparent

in the McCoy and Palen Mountains and is not apparent at all in the Coxcomb Mountains. Based on these lines of evidence, they argue that the McCoy Basin actually “youngs” westward; i.e., the age of deposition of the MMF becomes younger to the west.

Later work focused on refining understanding the basic geologic framework of the region. Fackler-Adams et al. (1997) did U-Pb geochronology studies of the Jurassic volcanic units. They determined that Jurassic volcanic rocks and interbedded sandstones had an age of ~200 Ma. Based on this correlation, they interpreted that Jurassic sandstones previously correlated with the Early Jurassic Aztec/Navajo Sandstone of the Colorado Plateau might be better correlated with the Mt. Carmel Sandstone of Middle Jurassic age in Utah. Also, they determined that the contact between the lower MMF and the Jurassic volcanics was gradational, with Jurassic volcanic rocks interfingering with the lower MMF. Therefore, the lower MMF must have a Middle Jurassic age. Hargrave (1997) examined Mesozoic stratigraphy in the Little Maria Mountains and established correlations between Mesozoic rocks observed in the Little Maria Mountains with stratigraphy exposed in the Buckskin Mountains. Dupuis and Walker (1996) examined the nature and timing of deformation in the Arica Mountains. Stern (1998) examined the timing of deformation events in the Riverside Mountains. Significantly, she established a correlation between sedimentary rocks exposed there with the McCoy Mountains Formation. Thus, the Riverside Mountains are the most northwestern exposure of the MMF. Morrissey (1999) examined the attenuation of Paleozoic rocks and structural geometries of portions of the Big Maria Mountains through application of TIMS remote sensing data. The TIMS images proved extremely useful in this area due to lack of vegetation, with different minerals showing up as different colors in thermal infrared. More on the use of TIMS data will be discussed in the methods section of this paper. Svihla (2003) studied the structural geology of a portion of the southeastern Big Maria Mountains and concluded that there were three stages of progressive deformation, characterized by the S_1 fabric, formed primarily as the result of top-southeast deformation and a fourth deformation event, D_4 characterized by brittle south-directed thrust faults and drag folds.

Barth et al. (2004) did a detrital zircon study of the entire MMF from the type section. Based on the detrital zircon analysis, they assign an age of deposition for the MMF between 116-85 Ma, thus making the entire formation late Cretaceous. Additionally, detrital zircons as young as 109 Ma were found in Basal Sandstone 2 in the McCoy Mountains, below the recognized intraformational unconformity, thus indicating a Late Cretaceous age for most of the MMF. Based on the detrital zircon data, they concluded that the MMF represents sediment deposited in a Cretaceous retroarc foreland basin, existing between the rising MFTB to the north and the Cretaceous magmatic arc to the south and west. This in contrast with the traditional interpretation advanced by several workers that the MMF was deposited in a rift basin and that the McCoy Basin represents a westward continuation of the Bisbee Trough (Dickinson, 1981; Harding and Coney, 1985; Laubach et al., 1989; Spencer et al., 2005). These workers propose that the Bisbee-McCoy Basin formed as a result of rifting related to the opening of the Gulf of Mexico beginning in the Late Jurassic. Spencer et al. (2005) published detrital zircon data from the MMF in the New Water and Plomosa Mountains in Arizona and found zircons as young as ~150 Ma, indicating the maximum age for the MMF.

Salem (2005) mapped the Big Maria syncline, exposed in the southwest portion of the Big Maria Mountains at 1:24,000 scale, focusing primarily on the Paleozoic stratigraphy and structures defined by Paleozoic metasedimentary rocks. He concluded that the degree of Paleozoic attenuation varied from 11% to less than 3% of original thickness and, in general, confirmed stratigraphic correlations of Paleozoic rocks advanced by Hamilton (1982, 1987) and Stone et al. (1983). Salem concluded that there were at least two recognizable deformation events, D₁ and D₂ based on differing geometries. D₁ is characterized by a pervasive north-dipping fabric, S₁, which is axial planar cleavage to isoclinal folds. D₂ is characterized by NE-vergent tight, upright folds that refolds S₁ and a weakly expressed cleavage, southwest dipping cleavage, S₂.

Salem et al. (Chapter 1) completely expanded on this earlier work, adding new geologic mapping, integrating field data, previous geologic mapping (Hamilton, 1982, 1984), TIMS data, and more detailed and comprehensive structural analysis. As a result

of this expanded investigation, the model advanced in Salem (2005) was refined to now include three deformation events, which Salem et al. (Chapter 1) designated D_1 , D_2 and D_3 . D_1 is characterized by a pervasive, north-dipping fabric, S_1 , which is axial plane cleavage to subrecumbent isoclinal (F_1) folds. S_1 is subparallel to original bedding planes and contacts, indicating that bedding and contacts have been transposed into the S_1 fabric. Based on various kinematic indicators, including a pervasive stretching lineation, S-C fabrics, and sigmoidal quartz grains, D_1 structures were formed by top-to-the-east or southeast reverse and dextral shear. D_2 is characterized by south or southwest-vergent F_2 folds, which are tight, inclined to the north, and are west or northwest plunging. An axial plane cleavage, S_2 , is weakly expressed and generally dips to the north. The Big Maria syncline and similar folds are interpreted as D_2 structures. The timing of D_1 and D_2 are broadly constrained between 160-79 Ma. It is unclear whether D_1 and D_2 are two discrete chapters of deformation or if they represent two stages of the same progressive deformation event. This question might be constrained through new geochronology data. D_3 is characterized by NE-vergent folds and a steeply dipping SW-dipping cleavage (S_3) that is variably expressed but is mostly observed in micaceous rocks in the western most part of the range near the Cretaceous leucogranite dike swarm. Salem et al. (Chapter 1) concluded that timing of D_3 is constrained between 79-60 Ma and that these structures might have formed as a result of top-northeast shear during the Mule Mountains Thrust event (78 and 70 Ma, Tosdal, 1990). This event temporally overlaps the D_3 event described by Ballard (1990) and has parallel but opposite sense (i.e., northeast-directed shortening vs. northeast-directed extension). Salem et al. concluded that this deformation likely represents synorogenic contraction and extension, similar to the regional hypothesis proposed by Hodges and Walker (1992). In general, deformation events observed in the Big Maria Mountains are similar to those observed by other workers (Ballard, 1990; Laubach et al., 1989).

Regional stratigraphy and chronologic framework

The stratigraphy of rocks of Paleoproterozoic through Early Jurassic age found in the MFTB/McCoy Basin terrane is similar to that observed in the western Grand Canyon region of the Colorado Plateau. Above the Jurassic Aztec Quartzite, the rocks of the region are similar to those observed throughout the Mojave Desert region and in southern Arizona. This section provides descriptions of rocks observed in the area using field descriptions and geochemical/petrologic data reported from other workers and summarizes the regional stratigraphy. Figure 4 shows a generalized stratigraphic column for the region.

Proterozoic crystalline rocks

The oldest rocks observed in the area are gneisses of Paleoproterozoic age. These rocks are considered part of the Chuckwalla Complex (Ellis, 1982) and have been assumed to range in age from 1800-1700 Ma (Hamilton, 1982). These rocks are presumed to be associated with the Yavapai-Mazatzal Proterozoic province (Wooden and Miller, 1990; Whitmeyer and Karlstrom, 2007).

The most common Proterozoic lithology in the area are megacrystic feldspar granites, likely correlative to the ~1400 Ma type A granites that form a NE-trending belt across North America (Anderson, 1989). These granites consist chiefly of plagioclase, potassium feldspar, quartz and biotite, with accessory hornblende and oxides. These granites, like the older Proterozoic gneisses are characterized by an augen texture. These granites are useful for studying polyphase deformation in the region as the megacrystic feldspars form beautiful sigma and delta clasts that are useful for analyzing shear sense. These granites are believed to have originally been emplaced during a late Paleoproterozoic orogenic event (Karlstrom and Williams, 1998) that post-dated the Yavapai-Mazatzal Orogeny. Most of the Proterozoic rocks observed in this area have all been subjected to polyphase deformation and high grade metamorphism (upper greenschist to lower amphibolite grade). Although Paleoproterozoic basement rocks throughout the southwestern U.S. have been deformed and metamorphosed, it is unlikely that any of the observed metamorphism and deformation of these rocks is Proterozoic in.

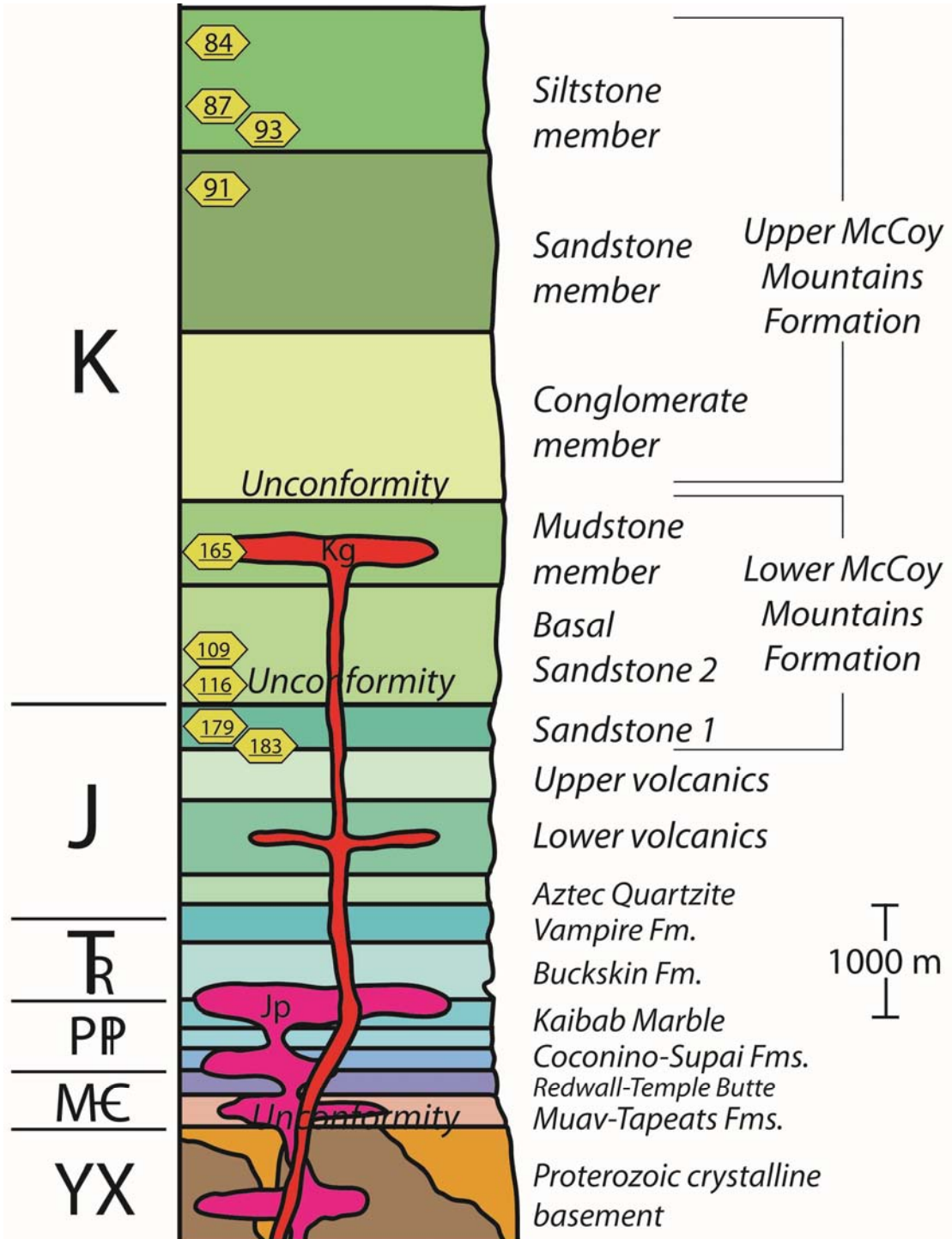


Figure 2.4: Generalized stratigraphic column of pre-Tertiary rocks for the Maria Fold and Thrust Belt/McCoy Basin region. Yellow hexagons show published detrital zircon ages and approximate stratigraphic position for the McCoy Mountains Formation from Barth et al. (2004). Thicknesses of Paleozoic rocks are from Salem (2005); Triassic and Jurassic sedimentary rocks are from Stone and Kelly (1989) and Reynolds et al. (1989); Jurassic and Cretaceous McCoy Mountains Formation are from Harding and Coney (1985). Abbreviations: Jp = Jurassic plutonic rocks; Kg = Cretaceous granitoids.

age. The closest correlatives to these rocks are observed in the Transition Zone of central Arizona.

Meso- and Neoproterozoic sedimentary rocks correlative to sequences observed in the eastern Grand Canyon, east-central Arizona and Death Valley regions are not documented in the Maria Fold and Thrust Belt or McCoy Basin.

Cambrian Tapeats Quartzite

Paleozoic rocks in the region are particularly useful for recognizing Mesozoic structures and for palinspastic reconstruction of the Maria-McCoy terrane. The stratigraphy of Paleozoic rocks is correlative to the classic cratonal sequence of the western Grand Canyon region (Noble, 1923). These correlations were first recognized by Hamilton (1964, 1982) and later expounded upon and confirmed by Stone et al. (1983) and Salem (2005). All Paleozoic rocks exposed in the Maria-McCoy terrane have been subjected to polyphase deformation and high grade metamorphism, except for an isolated fault block in the Plomosa Mountains (Miller and McKee 1971). As such, Paleozoic rocks are strongly foliated, with foliation subparallel to original bedding and unit contacts.

The oldest Paleozoic rocks observed in the region belong to the Cambrian Tapeats Quartzite, named for the Tapeats Sandstone of the Grand Canyon. This unit is a dirty maroon quartzite, characterized by dark layers of oxides, that consists chiefly of quartz with accessory muscovite, biotite, magnetite and other oxides. The Tapeats Quartzite is fine grained and quartz grains have been extensively recrystallized. Relict bedding structures, such as laminar bedding, are visible in the Tapeats Quartzite. This unit is exposed chiefly in the Big Maria Mountains, but is also exposed in the Little Maria Mountains (Ballard, 1990) and the Arica Mountains (Baltz, 1982). Maximum tectonic thickness for the Tapeats Quartzite is ~50 m.

The Tapeats Quartzite contains a basal quartzite near the contact with Proterozoic crystalline basement rocks. This contact is recognized here as the Great Unconformity (Walcott, 1894) of the Grand Canyon region, which is a regional unconformity that is

widespread throughout the western United States. The Great Unconformity marks a significant erosional period following uplift of Paleoproterozoic basement rocks to near sea level and represents a time gap of almost 1 billion years. The Tapeats Quartzite is also correlative to the Bolsa Quartzite in southeastern Arizona (Middleton and Elliot, 2003)

The initial depositional environment for the Tapeats Quartzite/Sandstone is interpreted to be an ancient beach in a passive margin off the coast of Laurentia that formed as the result of rifting of Rodinia (Middleton and Elliot, 2003). The Tapeats Sandstone represents the beginning of a marine transgression onto Laurentia during Cambrian time and is widespread throughout western North America.

Cambrian Bright Angel Schist

The next oldest Paleozoic unit is the Cambrian Bright Angel Schist, named for the Bright Angel Shale. The Bright Angel Schist is a silvery green micaceous schist that contains muscovite, chlorite and quartz, with accessory biotite, garnet and magnetite. Mica grains are generally fine grained and range in size between 1-3 mm on their long axes. Polyphase deformation fabrics show up particularly well in the Bright Angel Schist, due to its high mica content. In addition, the Bright Angel Schist is a useful unit to examine shear sense indicators in the field, such as mica “fish flash” (Reynolds and Lister, 1987). Like the Tapeats Quartzite, the Bright Angel Schist is exposed chiefly in the Big Maria Mountains but is also present in the Little Maria and Arica Mountains. Maximum tectonic thickness for the Bright Angel Schist is ~120 m. Of all the Paleozoic units exposed in the Big Maria Mountains, the Bright Angel Schist has been attenuated to the greatest degree in high strain zones, such as the Big Maria Shear Zone, defined by the attenuated limb of the Big Maria-Little Maria syncline.

The contact between the Tapeats Quartzite and Bright Angel Schist is gradational, as observed between their sedimentary correlatives in the Grand Canyon. In addition, the contact is further complicated due to the presence of intrafolial isoclinal folds that juxtapose quartzite next to schist layers. A calcareous sandstone layer is observed about halfway through the Bright Angel Schist in the Big Maria Mountains (Morrisey, 1999;

Salem, 2005). The depositional environment for the Bright Angel Shale at the Grand Canyon is interpreted to be a shallow marine setting as the Cambrian sea transgressed further onto the western margin of Laurentia during Cambrian time (Middleton and Elliott, 2003). This unit is correlative to the lower member of the Abrigo Formation in southern Arizona.

Cambrian Muav Marble

The Muav Marble is named for the Cambrian Muav Limestone in the Grand Canyon. The Muav Marble consists of coarse-grained calcitic marble characterized by light gray and whitish bands with minor amounts of chert. Minerals present include calcite and muscovite with accessory quartz, epidote, wollastonite and garnet. Polyphase deformation fabrics show up well in the Muav Marble due to this banded texture (Figure 12). Also, locally present wollastonite and muscovite help to define a mineral elongation lineation on the main foliation fabric, S_1 . Calcite in this unit has been extensively recrystallized, rendering microstructural analysis of this unit difficult despite the expression of mesoscopic folds in the field. The Muav Marble, like other Cambrian units is exposed chiefly in the central Big Maria Mountains. Maximum tectonic thickness for the Muav Marble is ~100 m. Numerous mining claims are observed near skarn zones where Jurassic (and possibly Cretaceous) plutonic rocks have intruded the Muav near the contact with the Bright Angel Schist.

In the Grand Canyon, the contact between the Muav Limestone and Bright Angel Shale is gradational, though in the Maria-McCoy terrane the contact is more abrupt. However, this could be due to the striking contrast between the silvery-green micaceous schist and the banded marble. Workers in the Grand Canyon region (Middleton & Elliott, 2003) interpret the Muav Limestone to be the top of a transgressive sequence and that the depositional setting of the limestone was a shallow sea as sea level rose during Cambrian time. The Muav Marble is also correlative to the Bonanza King Formation of the Mojave Desert region and to the upper member of the Abrigo Formation of southern Arizona.

Devonian Temple Butte Formation

Stratigraphically above the Muav Marble is a thick massive sequence of metamorphosed dolomite and dolomitized marble. For mapping purposes and based on its stratigraphic position, we have named this unit the Devonian Temple Butte Formation, after a sequence of dolomite in the Grand Canyon. The dolomite weathers to buff or light orange and is usually eggshell white on fresh surfaces and consists of fine-grained recrystallized dolomite and calcite with minor oxide impurities. The Temple Butte Formation tends to weather into steep cliffs and forms an erosional surface defined by “tear pants” weathering and has a massive texture. Mesoscopic folding is well expressed Temple Butte Formation, though lack of mica or other elongate minerals, such as wollastonite, make it difficult to see small-scale mesoscopic structures in this unit. Extensive recrystallization of dolomite and calcite render seeing microscopic structures extremely difficult. Maximum tectonic thickness for the Temple Butte Formation is ~180 m.

In reality, given the lack of internal bedding structures in the Temple Butte Formation, it is difficult to determine whether the Temple Butte in the Maria-McCoy terrane is Devonian, Cambrian or Mississippian in age. Based on its stratigraphic position, the metadolomite here could be correlative to the Cambrian Grand Wash Dolomite (Brathvode, 1986), a sequence of dolomite recognized only in the western Grand Canyon, as suggested by Hamilton (1982). A key observation that refutes this correlation is the presence of a green quartzite that fills in channels at the contact between the Muav Marble and the metadolomite. This indicates that there is an unconformity between these two units. The Cambrian-Devonian unconformity is recognized throughout much of the southwestern United States, so it stands to reason that at least the lower part of the metadolomite is of Devonian age. In the Grand Canyon, the Temple Butte tends to fill channels and lenses in the underlying Muav Limestone in the east and gradually thickens to a massive, laterally continuous cliff forming unit in the west (Beus, 2003a).

The upper part of the massive metadolomite formation in the Big Maria-Little Maria Mountains could be dolomitized Redwall Marble (Spencer et al., 1985). Lack of

internal stratigraphy within the metadolomite makes it difficult to directly test this observation. However, stratigraphic observations lend support to this possibility. In the Grand Canyon region, the Redwall Limestone varies in thickness between 150-200 m. As observed below, the Redwall Marble as recognized in the Maria-McCoy terrane reaches a maximum tectonic thickness of only ~ 40 m, an attenuation to ~20 to 25% of original stratigraphic thickness. However, the Temple Butte Formation in the Grand Canyon Region is approximately 100 m thick, so if the Devonian and Mississippian sections are combined, then the amount of tectonic thinning (~75% of original thickness) of the Devonian and Mississippian formations is equivalent to that of the rest of Paleozoic rocks in the region.

Mississippian Redwall Marble

Stratigraphically above the metadolomite is a bright white marble assigned to the Mississippian Redwall Marble, named for the Redwall Limestone of the Grand Canyon. The Redwall is a coarse grained calcitic marble consisting mostly of calcite and metamorphosed chert with minor amounts of wollastonite and epidote. It may be a dull brown where weathered and is bright white on fresh surfaces. In the attenuated section, isoclinal folds maybe defined by alternating calcite and chert layers but overall the rock appears to have a massive texture. The Redwall is exposed in Big and Little Maria, Riverside, Arica and Palen Mountains, along with all other younger Paleozoic units. Maximum tectonic thickness for the Redwall Marble is ~40 m.

Massive gray cherty cliff-forming limestone of Mississippian age is common throughout the western United States. The Redwall Limestone is stratigraphically correlative with the Escabrosa Limestone of southern Arizona. In the Grand Canyon, the Redwall Limestone lies disconformably on top of Temple Butte Formation in the west and directly on the Cambrian Muav Limestone in the east. The Redwall and correlative formations are interpreted to have been deposited in a widespread equatorial sea (Beus, 2003b).

Pennsylvanian-Permian Supai Formation

Above the Redwall Marble is a distinctive unit consisting of alternating layers of calc-silicate rocks, quartzite and marble that has been correlated with the Pennsylvanian-Permian Supai Group of the Grand Canyon. In general, the Supai Formation consists chiefly of coarse grained wollastonite, calcite and quartz with minor diopside, vesuvianite and oxides. The compositional variation between the more resistant calc-silicate and quartzite layers and the less resistant calcite marble layers, gives the Supai Formation a characteristic ledge and slope forming morphology in outcrop. The more resistant layers also are coated with dark brown desert varnish, which gives the Supai Formation a distinct light and dark banded appearance in outcrop, making this formation the most easily recognizable of all the Paleozoic units in the region and an important marker unit. On fresh surface, the Supai Formation may be either almond or light brown color. The alternating calcite and calc-silicate layers also allow for easy recognition of polyphase deformation fabrics and the banded texture shows up well even at the microscopic scale. Also, the easy recognition and mineral assemblage of the formation make it ideal for assessing T-X conditions of metamorphism (e.g., Hoisch et al., 1988). In the Big Maria Mountains, the contact between the Supai Formation and Redwall Marble is locally marked by metamorphosed terra rosa, metamorphosed red shale that filled in karst pits on top of the eroding Redwall Marble prior to deposition of the Supai Formation (Morrissey, 1999). Maximum tectonic thickness for the Supai Formation is approximately 200 m.

The Supai Group at the Grand Canyon consists of red sandstone and shale beds interbedded with limestone at its base, with the formation becoming less calcareous and more siliciclastic further up-section, suggesting a marine regression during deposition (Blakey, 2003). In contrast, the Supai Formation in the Maria Fold and Thrust Belt contains calcite and calc-silicate layers throughout the section, suggesting that it was deposited in a more marine setting than the Supai Formation of the Grand Canyon area. The ledge and slope morphology and the composition suggest that the Supai Formation as it is called here might more likely be correlative with the Naco Limestone of southeastern

Arizona. The Supai Formation in California is also correlative with the Pennsylvanian Bird Spring Formation of the Mojave Desert region (Stone et al., 1983).

Permian Hermit Formation

Stratigraphically above the Supai Formation are pale green quartzite and shale assigned to the Permian Hermit Formation. The Hermit Formation consists chiefly of fine-grained quartz, muscovite, epidote and minor tremolite, actinolite and oxides. The Hermit locally contains bustamite (Hoisch, personal comm. 2009) The Hermit Formation is pale green on fresh surface and is coated with a thin veneer of desert varnish on weathered surface and weathers recessively into shallow slopes. Maximum tectonic thickness of the Hermit Formation is approximately 50 m.

In the attenuated limb of the Big Maria syncline, the Hermit Formation is mapped together with the Coconino Quartzite. Some workers (e.g. Emerson, 1982) map the Hermit Formation as the green member of the Coconino Quartzite. In the Grand Canyon, the designation Hermit Shale is assigned to red shale beds that overlie the Esplanade Sandstone, the stratigraphic top member of the Supai Group although it is likely that the Hermit Shale was deposited in a similar deposition environment as the rest of the Supai Group. In the Maria Fold and Thrust Belt, the contact between the Hermit and Supai Formations is also gradational, indicating a gradual change from a marine to a non-marine depositional setting.

Permian Coconino quartzite

The Hermit Formation is overlain by a light gray to reddish pink vitreous quartzite designated the Coconino Quartzite. The Coconino Quartzite consists almost entirely of quartz (~98%) with minor amounts of muscovite, biotite and oxides. The Coconino Quartzite weathers into jagged and steep cliffs. Because it is composed almost entirely of quartz, ductile deformation fabrics are not well preserved in this formation; however, relict bedding structures, such as tabular cross beds are locally preserved. Maximum tectonic thickness of the Coconino Quartzite is approximately 130 m.

The Coconino Quartzite is correlative with the Coconino Sandstone of the Grand Canyon area, which is also correlative with the Glorieta Sandstone of New Mexico. The contact between the Coconino Quartzite and underlying Hermit Formation is abrupt, suggesting a change in depositional setting but due to intrafolial folds in the Maria Fold and Thrust Belt, it is sometimes difficult to separate these two units, especially in the attenuated limb of the Big Maria syncline. The sandstone is eolian and was likely deposited as one of several ergs of late Permian age that are found scattered across the western U.S. as far north as Montana (Morales, 2003). The Coconino represents a marked change in depositional environment during the Permian from a fluvial setting to a more desert-like setting.

Permian Kaibab Marble

The thickest and the most aerially extensive of Paleozoic rocks in the region are marble, calc-silicate and siliciclastic rocks assigned to the Permian Kaibab Marble, named for the Kaibab Limestone of the Grand Canyon region. The Kaibab Marble consists of coarse-grained marble consisting of calcite, tremolite, wollastonite, epidote and abundant metamorphosed chert nodules. At the base of the Kaibab Marble are green siliciclastic rocks consisting chiefly of epidote, quartz and calcite that may be correlative to the Permian Toroweap Formation of the Grand Canyon (Hamilton, 1982) but for mapping purposes are grouped together with the rest of the Kaibab Marble. The interbedding of resistant chert and calc-silicate layers with recessive calcite marble layers allows for easy recognition of polyphase deformation fabrics. Also, the abundance of calc-silicate minerals and the widespread distribution of the formation make this unit important for assessing P-T conditions of metamorphism. Finally, this unit is important for palinspastic reconstruction, as it is the oldest unit that appears on both sides of the tectonic contact between the middle crustal Maria Fold and Thrust Belt in the north and supracrustal McCoy Basin to the south. The Kaibab Marble is exposed in the overturned limb of the Palen Pass syncline, where it is in fault contact with Jurassic plutonic rocks (Figure 2.5) and sits on top of overturned Mesozoic strata. Thus, the Kaibab Marble is an

important unit for palinspastic reconstruction. Maximum tectonic thickness for the Kaibab Marble is approximately 300 m.

The Kaibab Marble is correlative with the Kaibab Limestone of the Grand Canyon, which is also correlative with the San Andres Limestone of New Mexico. In the Grand Canyon, the Kaibab Limestone overlies the Toroweap Formation, which consists of calcareous sandstone and dolostone that is interpreted as being deposited in a sabkha environment, similar to the modern Dead Sea. At the Grand Canyon the contact between the Toroweap Formation and overlying Kaibab marble is gradational, indicating a gradual change from dry evaporate lakes to more marine conditions. These limestone deposits are confined to local marine basins flanked by uplifts related to late Permian tectonism in the region (Blakey, 2003). The abundance of chert nodules and fossils in unmetamorphosed sections indicate that limestone was deposited in a shallow marine environment, representing a marine transgression toward the end of Permian (Mather, 1970).

Triassic Buckskin Formation

Triassic and Early Jurassic metasedimentary rocks are a record that stable cratonal conditions existed in the region during this time, except for a localized uplift event recorded in conglomerates of the Vampire Formation (Reynolds et al., 1989). Mesozoic rocks north of the boundary between the Maria Fold and Thrust Belt (MFTB) and McCoy Basin are highly deformed and metamorphosed. Like the Paleozoic rocks below them, Mesozoic metasedimentary rocks in the MFTB are strongly foliated, with foliation parallel to original bedding and unit contacts. In contrast, Mesozoic metasedimentary rocks in the McCoy Basin, though directly correlative with counterparts in the MFTB, are weakly and (mostly) brittlely deformed, contain a foliation fabric at high angles to bedding and exhibit lower degree of metamorphism. The oldest Mesozoic sedimentary rocks in the area are micaceous anhydrite-bearing schists and calcareous sandstones of the Buckskin Formation (Reynolds et al., 1987) named for the Buckskin Mountains of

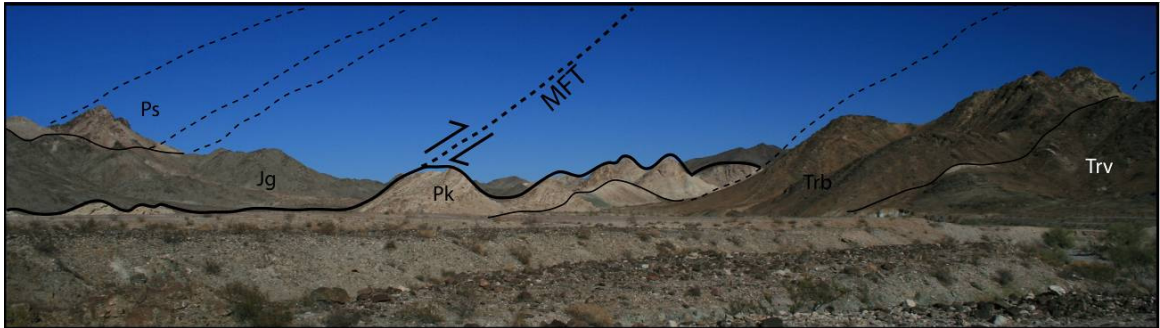


Figure 2.5: Looking northeast toward Palen Pass. The north-dipping Maria Frontal Thrust (MFT) thrusts Jurassic granitoid rocks over Kaibab Marble (Pk). In the upper plate of the MFT upright metamorphosed Supai (Ps) and Redwall Formations are intruded by the granitoids. In the lower plate, Kaibab, Buckskin formation (Trb) and Vampire Formation (Trv) are in a north-dipping, inverted sequence. Photo: L.J. Crossey.

western Arizona. The basal Buckskin Formation consists of green gypsiferous schist and sandstone and tends to weather into distinctive, low-relief green slopes. Principle minerals present include quartz, feldspar, muscovite, chlorite, biotite and minor epidote. The next member is greenish and orangish calcareous sandstone that tends to form more resistant ledges. The green schist and calcareous sandstone are present in Palen Pass and the Little Maria Mountains and in the northwestern Big Maria Mountains. A large gypsum mine is active in the Little Maria Mountains and numerous small gypsum prospects and mines are found there and at Palen Pass and the Big Maria Mountains. Most of these mines and prospects are usually located at or around the contact between the green schist member of the Buckskin Formation and Kaibab Marble. The presence of gypsum is likely due to secondary hydrothermal alteration of the Kaibab Marble and anhydrite-bearing schist during metamorphism, but some of the gypsum may represent primary deposition during evaporation of shallow marine deposits and subsequent erosion of the Kaibab Marble before deposition of the Buckskin Formation. Maximum thickness for the Buckskin Formation is approximately 600 m at Palen Pass.

The Buckskin Formation is correlated with the Triassic Moenkopi Formation of the Colorado Plateau and southwestern U.S. on the basis of similarities in lithology and stratigraphic position (Reynolds et al., 1989). The Moenkopi Formation on the Plateau disconformably overlies the Kaibab Limestone, indicating an erosional period at the end of the Permian. The Moenkopi Formation was deposited in a fluvial environment and is widespread through the Colorado Plateau/Rocky Mountain region. The Buckskin Formation is also correlative to the lower two members of the Palen Formation (Pelka, 1973; Stone and Kelly, 1989).

Triassic-Jurassic Vampire Formation

The Vampire Formation (Reynolds et al., 1987) is the name assigned to a sequence of conglomerate and volcanoclastic sandstone. The conglomerate consists of clasts of primarily Proterozoic crystalline rocks. Clasts are angular to rounded and are

heterogeneous, indicating input from a lithologically diverse nearby source (Reynolds et al., 1989). In the Big Maria Mountains, the Vampire Formation contains angular feldspar clasts that have been sheared and attenuated. The Conglomerate Member of the Vampire Formation consists of a green angular matrix consisting of biotite, epidote and chlorite and contains large quartz and feldspar clasts. At Palen Pass, the formation consists of sub-angular to rounded quartzite and granite clasts, is matrix supported, and is poorly sorted. Above the conglomerate is a light gray to grayish green sandstone unit, with volcanically derived clasts. In the Big Maria Mountains, this unit is represented by a fine-grained grayish-green micaceous schist. Maximum thickness for the Vampire Formation is approximately 400 m.

In the Big Maria Mountains this unit has been subjected to polyphase deformation and amphibolite grade metamorphism. Because of this, this unit has been tectonically thinned when compared with its relatively unmetamorphosed correlative unit in the Palen Mountains. The large feldspar clasts make useful kinematic indicators for unraveling polyphase deformation events (Chapter 1). In contrast, in the Palen Pass area, metamorphism of this unit is lower greenschist grade and there is no observable evidence of high ductile strain (e.g., stretched pebble clasts, mineral lineation, etc.). The Vampire Formation, as described here, includes the middle two members of the Palen Formation. The Vampire Formation is correlative to the Chinle Group of the Colorado Plateau (Reynolds et al., 1989). Throughout the Maria-McCoy terrane, the Vampire Formation is observed to unconformably overlie units ranging in age from Proterozoic through Triassic, indicating a widespread uplift event that took place from Late Triassic through Early Jurassic time, sedimentary evidence of which may also exist in deposits in the Chinle Group (Reynolds et al., 1989; Stewart et al., 1972). One possibility for this uplift event is the onset of active margin tectonics further west with the initiation of the Cordilleran magmatic arc during Late Triassic time (Asmerom, 1988). Evidence for this in the sedimentary record on the Colorado Plateau is observed in widespread influx of volcanic ash detritus in the Chinle Group, volcanic rocks of Triassic age in southeastern

Arizona (Asmerom et al., 1988) and with plutons of Triassic age reported in southwestern Arizona and southeastern California (Busby-Spera, 1988).

Jurassic Aztec Quartzite

An eolian quartzite that overlies the Vampire Formation is designated the Aztec Quartzite, named for the Aztec Sandstone of southern Nevada, which is correlative with Jurassic Navajo Sandstone of the Colorado Plateau. At Palen Pass, the quartzite is tan to buff, forms low relief slopes and resembles a friable sandstone. In contrast, in the Big Maria Mountains, where the quartzite has been metamorphosed at amphibolite grade, the quartzite is a competent, extensively recrystallized resistant quartzite. This quartzite consists almost entirely of quartz (~96%) with minor amounts of muscovite and oxides. The quartzite in the Big Maria Mountains forms resistant, yet low-relief jagged slopes and contains concretions and relict bedding structures, such as tabular crossbeds. Similar bedding structures are observed with the quartzite at Palen Pass. Maximum thickness for the Aztec Quartzite is approximately 300 m.

The contact between the Aztec and the underlying volcanic sandstone appears to be abrupt, indicating a change from an area of localized uplift and sedimentary infilling during Late Triassic to Early Jurassic time to stable cratonal conditions in the Early Jurassic. The Aztec Quartzite was likely deposited in a vast erg, which is similar to other widespread sandstone deposits of Jurassic age throughout the southwestern U.S. The Aztec Quartzite is correlative to the upper part of the Vampire Formation (Reynolds et al., 1989) and to the upper member of the Palen Formation (Pelka, 1973). In the Big Maria Mountains, concretions present in the Aztec Quartzite are also useful strain kinematic indicators. The correlation between this quartzite and the Navajo/Aztec quartzite is based primarily on stratigraphic position and similarity in lithology. However, contact relationships between the Aztec Quartzite and overlying Jurassic volcanic rocks is gradational and quartzite is interbedded with volcanic layers observable in the Big Maria Mountains and at Palen Pass (Fackler-Adams et al., 1997). In addition, U-Pb dates on volcanic rocks at Palen Pass yield a U-Pb age of 174 +/- 8 Ma, giving a Middle Jurassic

age for the quartzite and indicating that is more likely correlative to Middle Jurassic sandstones of the Colorado Plateau, such as the Page or Carmel Sandstones (Fackler-Adams et al., 1997).

Jurassic volcanic rocks

Stratigraphically above the Aztec Quartzite are volcanic rocks of Jurassic age. These rocks are part of the Dome Rock Group of Tosdal et al. (1989). In the Big Maria Mountains, Jurassic volcanic rocks may be divided into two members, the lower and the upper. The lower volcanic unit consists of greenish gray micaceous schist. Like the older rocks below, metavolcanic rocks in the MFTB are ductilely deformed, contain a strongly developed foliation fabric parallel to unit contacts and are highly metamorphosed. Likewise, in the McCoy Basin, Jurassic volcanic rocks exhibit low grade metamorphism, weakly developed foliation and mostly brittle deformation. The principal mineral assemblage includes quartz, muscovite, plagioclase, potassium feldspar, epidote and biotite. Accessory minerals include magnetite and other oxides. The upper volcanic unit consists of off-white to light tan micaceous schist. The principal mineral assemblage includes quartz, muscovite and potassium feldspar, with minor plagioclase, biotite and oxides. The lower volcanic unit likely corresponds to units Jdr1 and 2 of Stone and Pelka (1989) in the Palen Mountains, which consists of rhyodacite tuffs and tuffaceous sedimentary rocks. The upper volcanic unit likely corresponds to unit Jdr3 of Stone and Pelka (1989), which consists of rhyolite ignimbrite, lava and hypabyssal rocks. The hypabyssal rocks are widespread throughout the region and are locally referred to as the quartz porphyry (Tosdal et al., 1989; Reynolds, Spencer and DeWitt, 1987). Maximum thickness of the volcanic units exposed in the northern Palen Mountains is approximately 1260 m (Stone and Pelka, 1989). The quartz porphyry has been extensively prospected and mined in several mountain ranges in the area including the Palen, McCoy, Dome Rock and Plomosa Mountains.

Volcanic rocks of Jurassic age are widespread throughout the Mojave and Sonoran Deserts and constitute part of a large magmatic arc that extended from northern

Sonora to British Columbia (Tosdal et al., 1989). Reported U-Pb ages for rocks of the Dome Rock Group in the Palen Mountains include 174 +/- 8 Ma for the basal part of the section and 155 +/- 8 Ma and 162 +/- 3 Ma for rocks from the upper part of the Dome Rock Group (Fackler-Adams et al., 1997). Therefore, these rocks are Middle to Late Jurassic age. These ages indicate that upper portion of the Dome Rock Group in the Palen Mountains is broadly correlative with the Planet Volcanics of the Buckskin Mountains (Reynolds et al., 1987) and other parts of the Dome Rock Group (Tosdal et al., 1989). The types of volcanic rocks observed in the area, e.g. tuff and rhyolite-dacite flows indicate that this area of southeastern California was the site of explosive volcanism during the Middle and Late Jurassic. A possible ring structure for a Jurassic age caldera is identified in the Palen Mountains (Pelka, 1973). Explosive volcanic deposits potentially correlative to those observed in southeastern California and west-central Arizona are observed in southeastern Arizona, e.g. the Mount Wrightson Formation (Riggs and Busby-Spera, 1998).

Jurassic plutonic rocks

By far the most aerially extensive of all rock formations in the area are plutonic rocks of Jurassic age. These rocks vary significantly in composition, from mafic to felsic, and texture, from hypabyssal to porphyritic. However, these plutonic rocks may be classified broadly into three members: dark green hornblende-bearing diorite, light gray granodiorite that contains large (~1 cm. diameter) euhedral lavender feldspar crystals, and leucocratic granite. In addition, there are strongly foliated hypabyssal mafic rocks in the Big Maria Mountains that are presumed here to be part of the Jurassic suite. The hypabyssal mafic rocks are fine-grained, consisting chiefly of biotite, chlorite, hornblende, plagioclase, pyroxene, olivine and epidote. In large outcrops, these rocks are mapped as part of the diorite member, though are distinguishable from diorite by both grain size and composition. The diorite member consists principally of plagioclase, potassium feldspar, hornblende and biotite with minor quartz, pyroxene and oxides. The diorite member is aphanitic, with average grain size approximately 2-3 mm. On weathered surfaces, the diorite may contain a thin veneer of desert varnish and tends to

weather into gravelly and rugged slopes. The granodiorite consists principally of quartz, potassium feldspar, plagioclase and biotite with minor hornblende and oxides. Of the three plutonic rocks the granodiorite is the most aeri ally extensive. The granodiorite is light to dark grey in color, with lavender feldspar phenocrysts. Crystal size varies from 1-3 mm for crystals in the matrix and up to 1 cm for phenocrysts. Like the Proterozoic granite described above, highly strained granodiorite exhibits an augen texture and feldspar phenocrysts make for useful kinematic indicators of polyphase deformation. Because of these compositional and textural similarities, and because the granodiorite intrudes Proterozoic granitic rocks, it is often difficult to distinguish these two rocks in the field. The granodiorite forms most of the high craggy peaks of the Big and Little Maria Mountains and is also the chief Jurassic plutonic lithology exposed at Palen Pass. The granodiorite is observed to intrude the Paleozoic section as a series of sills and is observed to intrude the section as high up as the Kaibab Marble. On the basis of contact relations in the field and composition, the granodiorite is inferred to be younger than the diorite. The leucocratic granite is the youngest and most felsic in composition of the suite of plutonic rocks. The leucocratic granite consists principally of quartz, plagioclase and potassium feldspar, with minor biotite, hornblende, garnet and oxides. In outcrop, the granite is whitish with black flecks of biotite and hornblende. Based on contact relations in the field and composition, the leucocratic granite is inferred to be the youngest member of the plutonic rocks.

This suite of plutonic rocks is common throughout southwestern North America. Tosdal et al. (1989) broadly correlate this suite of plutonic rocks to the Kitt Peak-Trigo Peak Supergroup. U-Pb ages of ~160 Ma have been reported for the granodiorite (L.T. Silver to Hamilton, 1982; Tosdal et al., 1989). Geochronology data for these plutonic rocks is sparse, but the diorite is assumed to be no older than ~178 Ma (Tosdal et al., 1989). Not much data is available for the leucocratic granite. In addition, given the paucity of geochronology for the Big and Little Maria Mountains, it is possible that at least some plutonic rocks inferred to be Jurassic age are actually Cretaceous age and may represent continuous magmatism related to development of the Cordilleran (Sierra

Nevada) magmatic arc through Jurassic to Early Cretaceous time. Based on geochemical analysis, these plutonic rocks are likely not the source magma chambers for the Jurassic volcanic rocks in the area (Tosdal et al., 1989), but instead represent different episodes of deep-seated magmatism that temporally overlap emplacement of the Jurassic volcanic rocks based on available age constraints.

Jurassic-Cretaceous McCoy Mountains Formation

One of the key units to understanding the Mesozoic tectonic evolution of the region is the Jurassic-Cretaceous McCoy Mountains Formation (MMF), a >7 km thick siliciclastic wedge consisting of sandstone, siltstone and conglomerate that is observed throughout the region. This unit is key to understanding deformation in the region as it is the youngest unit to have experienced all episodes of polyphase deformation; therefore it is useful in providing upper and lower bound constraints on the timing of deformation. In the study area, the MMF is exposed in the Coxcomb, Palen, McCoy and Riverside Mountains. Exposures of the MMF and equivalent strata are documented as far east as the Little Harquahala Mountains (Reynolds et al., 1986) and as far south as the Castle Dome Mountains (Tosdal and Stone, 1994) in Arizona. Like all older rock units, in the MFTB the MMF is strongly foliated, with foliation parallel to original bedding and unit contacts, has been subjected to high grade metamorphism and high strain ductile deformation. In contrast, in the McCoy Basin the formation dips predominately southward, exhibits a north-dipping foliation at high angles to bedding and mostly shows brittle deformation.

Although the MMF has been subdivided differently by various workers (e.g. Pelka, 1973; Stone and Pelka, 1989; Harding and Coney, 1985; Stone, 2006) in this study we use the stratigraphy of Harding and Coney (1985). These workers divide the MMF into six broadly correlated members: Basal Sandstone 1, Basal Sandstone 2, Mudstone Member, Conglomerate Member, Sandstone Member and Siltstone Member. The names of these members refer to the dominant lithology present in each package of rocks and each member contains a variety of sedimentary lithologies. For example, Basal Sandstone 1 contains sandstone, siltstone and conglomerate layers as well as limestone beds and

calcareous pods. However, members in the field may be distinguished by overall grain size of the main rock type present as well as the composition of the matrix.

Sediments derived from quartz porphyry and Basal Sandstone 1

Stratigraphically below Basal Sandstone 1 in the McCoy and Palen Mountains, but resting on Jurassic quartz porphyry, is a sedimentary unit consisting of light gray sandstone, siltstone and pebble conglomerate. Because of the lithologic affinity of the matrix with the underlying quartz porphyry, this unit is simply referred to as sediment derived from quartz porphyry. Based on contact relations observed in the McCoy Mountains, this unit appears to represent a horizon of reworking of the quartz porphyry prior to deposition of the MMF. Thus, we interpret that in the McCoy Mountains the MMF rests nonconformably on top of the Jurassic quartz porphyry, however this unconformity is depositional, as opposed to faulted, in nature. This contact relation is also observed in the Dome Rock Mountains to the east, with sediments derived from quartz porphyry observed at the base of the MMF (Tosdal and Stone, 1994). In the Palen Mountains, this contact is noted as being gradational, with volcanic rocks interfingering with Basal Sandstone 1 (Fackler-Adams et al., 1997).

Basal Sandstone 1 consists of gray to tan arkosic sandstone and siltstone interbedded with pebble conglomerate. The formation also contains maroon sandstone and siltstone beds. The conglomerate is matrix supported, with pebbles ranging in size from 2-3 mm to ~10 cm in diameter. Pebbles in conglomerate layers are predominately rounded quartzite and chert clasts, with marble and sandstone clasts present in the conglomerate, reflecting a heterogeneous source terrane of cratonal affinity (Harding and Coney, 1985). Limestone beds are observed at the base and calcareous pods and lenses are observed throughout the section. At the top of Basal Sandstone 1 are maroon and gray sandstone and siltstone interbedded with brown recrystallized limestone layers (Member B of Stone, 2006). In general, grain size in the formation fines upward and the formation consists of fining upward sequences. Total thickness of Basal Sandstone 1 is approximately 450 m in California; thicknesses of 1000 m are reported in the Livingston

Hills/New Water Mountains (Harding and Coney, 1985). Basal Sandstone 1 is correlative to the Apache Wash Facies in western Arizona (Harding and Coney, 1985; Reynolds et al., 1989; Tosdal and Stone, 1994) and the lower part of the Livingston Hills Formation.

The depositional nature of the contact and observed interbedding of the MMF with the underlying quartz porphyry indicates that Basal Sandstone 1 is likely Late Jurassic age. A Late Jurassic age interpretation for Basal Sandstone 1 and equivalent facies is supported by detrital zircon U-Pb age analysis done rocks in the McCoy Mountains by Barth et al. (2004), who report zircons as young as 179 Ma from Basal Sandstone 1 and the age of an andesitic lava flow near the top of the MMF section in the New Water Mountains reported by Spencer et al. (2005) of 154 +/- 2.1 Ma. Broad correlations of the MMF and equivalent strata, their exposure and lateral extent, are illustrated in Figure 2.2. Deposition in a rift basin is supported by ϵ_{Nd} values of +4 to +6 reported for basaltic sills and lava flows from MMF sections in the Granite Wash, New Water and Southern Plomosa Mountains at $t = 150$ Ma by Spencer et al. (2005). Some workers (e.g. Fackler-Adams et al., 1997; Spencer et al., 2005) have proposed that the lower MMF might actually be correlative with the lower part of the Bisbee Group of southeastern Arizona, which was also determined to have been deposited in a rift setting. The likely source terrane for sediments deposited in Basal Sandstone 1 was to the north, based on paleo-current indicators (Harding and Coney, 1985). Clast composition, predominately well rounded quartzite, suggests transport from a faraway source consisting primarily of Proterozoic rocks including quartzite, most likely the Mogollon Highlands. Volcanic sediments that constitute the matrix of Basal Sandstone 1 most likely were derived from underlying Jurassic rocks. The similarity in composition of the matrix of Basal Sandstone 1 and the underlying quartz porphyry, combined with the provenance of Late Jurassic detrital zircons in the formation confirms this idea. The presence of fining upward sequences suggests that Basal Sandstone 1 was deposited in a fluvial setting, probably as a series of alluvial fan deposits. Based on the presence of limestone layers, as well as calcareous pods and lenses, sediments may have been deposited in a rift setting at or near sea level. Alternatively, limestone and calcareous

pods may represent lacustrine deposition and that limestone deposits might represent times when there was standing water filling in the basin.

Basal Sandstone 2

Basal Sandstone 2 consists of dark green to greenish-gray massive arkosic sandstone, siltstone and mudstone with minor conglomerate layers. Minor purplish sandstone and siltstone beds are also found in the formation. Conglomerate layers are matrix supported, with pebbles as large 10-15 cm. The top of Basal Sandstone 2 is a maroon-purplish sandstone interbedded with shale and minor conglomerate (Member D, Stone, 2006). In the McCoy Mountains, clasts in the conglomerate chiefly include quartzite, granite and volcanic rocks. However, in the Palen Mountains, clasts in Basal Sandstone 2 conglomerates also include sandstone, marble, and schistose rocks, suggesting a heterogeneous source terrane (Harding and Coney, 1985). Orangish-brown and tan calcareous pods and lenses are found throughout the lower portion of the formation in the type section in the McCoy Mountains. Volcanically derived clasts constitute the matrix of the rock. Paleocurrent indicators in Basal Sandstone 2, like Basal Sandstone 1, suggest a northern source terrane. Basal Sandstone 2 is approximately 1500 m in the McCoy Mountains (Stone, 2006), approximately 600 m in the Dome Rock Mountains (Harding and Coney, 1985) and, in general, thins eastward.

The overall change in color from Basal Sandstone 1 to Basal Sandstone 2, from a predominately pinkish red and light gray matrix to dark green and greenish gray matrix suggests a marked composition change of the source terrane for sediments. In the field, this contact between Basal Sandstone 1 and Basal Sandstone 2 is sharp, suggesting a disconformable contact. A disconformity between Basal Sandstone 1 and Basal Sandstone 2, at least in the McCoy Mountains, is further indicated by reported U-Pb detrital zircon ages of as young as 116 Ma near the base of Basal Sandstone 2 and as young as 109 Ma (Barth et al., 2004) toward the top. Based on geochronology from Basal Sandstone 1 equivalent facies in western Arizona, if there is an unconformity between Basal Sandstone 1 and Basal Sandstone 2 it would be no less than 45 million years.

Alternatively, the preponderance of Jurassic age zircons in the McCoy Mountains section could be simply due to the proximity of the Jurassic quartz porphyry substrate, although based on regional correlations with MMF-equivalent strata in Arizona, this alternative seems unlikely. The presence of Cretaceous detrital zircons indicates that the Cretaceous magmatic arc was nearby during deposition of Basal Sandstone 2 of the MMF. The source for these zircons most likely came from the south and west. The size of cobbles in conglomerate layers and the degree of rounding observed in these clasts suggests a high degree of transport from a low relief source terrane. The composition of clasts and paleo-current indicators suggests that these came from a heterogeneous source terrane to the north that contained both Paleozoic and Proterozoic source rocks, likely the Mogollon Highlands. The presence of calcareous pods suggests that these sediments were deposited at or near sea level or in a lacustrine setting or both. Structural data from the study area might confirm the presence or absence of an unconformity. If there is a significant difference in the mean orientation of Basal Sandstone 1 from Basal Sandstone 2, then that would indicate an unconformity. If, however, they were similar within uncertainty of measurement then it would remain ambiguous.

Mudstone Member

The Mudstone Member generally consists of light tan and light to dark gray phyllitic shale and bluish-gray slaty shale interbedded with ledge-forming sandstone and minor conglomerate layers. Near the top of the section are orangish calcareous layers and minor limestone ledges. The Mudstone Member generally tends to form recessive slopes, but with more resistant units weathering into steep cliffs and ledges. In general, conglomerate clasts tend to include volcanic rocks, quartzite and granite as well as phyllitic mudstone rocks. The contact with underlying Basal Sandstone 2 member appears to be gradational and, in general, the whole sequence tends to fine upward from the base of Basal Sandstone 2 toward the top of the mudstone layer. The Mudstone Member is approximately 1500 m thick in the McCoy Mountains (Stone, 2006).

The gradational nature of the contact with the underlying Basal Sandstone 2 member tends to support the idea that these two units represent continuous sedimentation within a subsiding basin. The thickness of the two units, both 1500 m, suggests that the basin was subsiding tectonically during deposition. The similarity of clasts in the Mudstone Member with those in underlying units suggests that conglomerate clasts are far traveled, from an area of low relief, with a diverse lithologic suite. Paleo-current indicators are similar to those observed in Basal Sandstone 1, indicating the main source for MMF deposition is in the north and is likely the Mogollon Highlands. Detrital zircons in the Mudstone Member have reported U-Pb ages as young as 165 Ma (Barth et al., 2004). This lack of Cretaceous zircons could represent a period of volcanic quiescence from the Cretaceous arc or could be the result of low flow regime represented by the mudstone layer, therefore sourcing small sediments from relatively nearby. In any case, the overall fining of grain size from Basal Sandstone 2 the mudstone layer and the dominance of shale as a lithology suggests quiet water deposition, possibly in a lacustrine setting at or near sea level and may represent the distal facies of an alluvial fan sequence.

Conglomerate Member

The Conglomerate Member is the thickest member of the McCoy Mountains Formation, though is not the most aerially extensive, and is correlative to the lower part of Stone's (2006) Unit F. The Conglomerate Member is laterally continuous (though broken up by Cenozoic faults) from the Palen Mountains to the Livingston Hills (Harding and Coney, 1985). The Conglomerate Member consists of conglomerate of variable composition and clast size. The Conglomerate Member coarsens upward from the base of the unit, with clasts as large as boulders, some as large as 0.3 m (Figure 2.6). The conglomerate typically has a gray matrix and varies from matrix to clast supported. The basal part of the Conglomerate Member is typically brown consisting of interbedded sandstone and conglomerate with only minor siltstone. Harding and Coney (1985) attribute the brown color to presence of limonite after pyrite concentrated along bedding planes and fractures. The upper part of the conglomerate is bluish gray and may be interbedded with tuff. Harding and Coney (1985) also note that major petrologic and

lithologic changes occur between the conglomerate and Mudstone Members, as indicated by the change in clast size and by the presence of microcline, suggesting exhumation of deep crustal rocks to the north. Clasts in the conglomerate include well rounded elliptical quartzite, granite, sandstone, marble and volcanic clasts. The Conglomerate Member varies in thickness from 1600 – 2000 m (Harding and Coney, 1985). Pelka (1973) reports a Late Cretaceous age for fossil wood found in the Conglomerate Member, which is confirmed by Stone et al. (1987).

There is little doubt that the rapid change in size from fine-grained mud to coarse-grained conglomerate clasts indicates a significant change in flow regime as well as in the tectonic setting of the formation. Unlike the three lower members, there are no documented calcareous layers or pods throughout most of the formation. However, the abrupt unconformity, as documented in the Dome Rock and Plomosa Mountains (Tosdal and Stone, 1994) is not apparent in the McCoy Mountains. The presence of calcareous layers near the top of the Mudstone Member and in the lower part of the Conglomerate Member, suggests that the rate of basin infilling rapidly became greater than the rate of



Figure 2.6: Rounded to sub-rounded pebble to boulder size clasts in the Conglomerate Member of the McCoy Mountains Formation (Kmc). Geologist H. Johnston for scale.

basin subsidence, suggesting significant increased sediment input during deposition of the conglomerate layer and a change in tectonic setting. The absence of an apparent unconformity, at least in the McCoy Mountains, however, means that there was no temporal break between deposition of the Mudstone Member and deposition of the Conglomerate Member. A similar contact relationship is observed in the nearby Palen Mountains. One possibility for this is a rapid increase in elevation and proximity of the source terrane. This could signify a change in the tectonic setting of the McCoy Basin, which we will discuss later. However, this contact has been recognized as an intraformational unconformity in the nearby Dome Rock and Plomosa Mountains. Assuming the Conglomerate Member is the same age everywhere it is exposed, it is possible that the underlying mudstone and Basal Sandstone 2 members may have been deposited earlier in western Arizona and later in eastern California, such that there is a temporal break in deposition in Arizona and a record of continuous deposition in California though the tectonic setting of the basin changed. This contact, however, is useful for dividing the MMF into an upper and lower member. In subsequent sections, lower MMF will refer to the three units below the Conglomerate Member and upper MMF will refer to the conglomerate, sandstone and Siltstone Members. Detrital zircon from the base of the Conglomerate Member has reported ages as young as 97 Ma (Barth et al., 2004).

Sandstone Member

The Sandstone Member consists of gray siltstone, sandstone, orangish calcareous mudstone and conglomerate. The Sandstone Member is exposed in the McCoy, Dome Rock and Plomosa Mountains and the Livingston Hills. Conglomerate clasts are highly variable in composition, consisting of siliceous volcanic rocks, quartzite, sandstone, marble and phyllitic mudstone (Harding and Coney, 1985). Harding (1982) reports fossil wood found in the Sandstone Member. The sandstone unit varies in thickness from 1000-1500 m thick. The Sandstone Member is correlative to the upper part of Unit F of Stone (2006).

The contact between the Sandstone Member and the Conglomerate Member is gradational, with the conglomerate fining upward into the sandstone (Harding and Coney, 1985). Harding and Coney (1985) interpret that sandstone was deposited as alluvial fans reworked by fluvial processes. The gradation from conglomerate to sandstone indicates that the sandstone could represent the medial facies of an overall large alluvial fan sequence. Barth et al. (2004) report U-Pb detrital zircon ages as young as 91 Ma for the Sandstone Member, indicating, along with the fossil wood observed, that the member is Late Cretaceous age. These Late Cretaceous detrital zircons must have sourced from the Cretaceous magmatic arc and come in from the south and west. This supports the idea that, at least during deposition of the upper MMF, the basin was bounded by a highland of cratonal affinity in the north and by the Cretaceous magmatic arc to the south.

Siltstone Member

The Siltstone Member is lithologically diverse, so much so that Stone (2006) divides it into six units in addition to the top of Unit F. The Siltstone Member consists of gray sandstones and siltstones, cross-bedded sandstone with fossil wood logs 0.5-3 m in length and 0.5-1 m in diameter (Pelka, 1973), and conglomerate layers. Conglomerate predominately is deposited in cut-and-fill channels and clasts in conglomerate are chiefly quartzite, granite and volcanic rocks (Stone, 2006). Paleo-current indicators indicate south-southwest flowing currents. The Siltstone Member is reported as much as 500-1800 m thick (Harding and Coney, 1985; Stone, 2006).

The Siltstone Member likely represents the distal facies of an alluvial fan sequence, based on grain size, large fossil wood logs, cross beds and recognizable point bar sequences. Overall, from the Conglomerate Member to the Siltstone Member the fining upward of the sequence is best understood as an alluvial fan sequence. The Siltstone Member is recognized in the McCoy, Dome Rock and Plomosa Mountains and Livingston Hills, but there is ~900 m of section that is exposed only in the southern McCoy Mountains (Harding and Coney, 1985). U-Pb detrital zircon ages as young as 84

Ma are reported for the Siltstone Member by Barth et al. (2004) indicate that the upper MMF is entirely Cretaceous in age.

The stratigraphic top of the MMF is not exposed anywhere. In the Dome Rock and McCoy Mountains and Palen Mountains, the contact has been folded into a northeast-vergent syncline in the footwall of the Mule Mountains thrust (Pelka, 1973; Harding and Coney, 1985; Tosdal and Stone, 1994). Timing of movement on the Mule Mountains thrust, based on cross-cutting relations of tuff layers and Cretaceous magmatic rocks, took place at approximately 70 Ma (Tosdal, 1990). Additionally, in the Coxcomb Mountains, the MMF is intruded by a late Cretaceous pluton broadly correlative with the Cadiz Valley Batholith (Howard, 2002) with a reported U-Pb age of 73.5 +/- 1.3 Ma (Barth et al., 2004).

Cretaceous plutonic rocks

In the study area there is a wide variety of plutonic rocks of Late Cretaceous age. These rocks represent plutonism in the region that began as early as ~90 Ma (e.g., Wells et al., 2005), with peak plutonism at 82-72 Ma (Wells et al., 2002, Foster et al., 1992; Kula et al., 2002). Some of these plutons, like the 85 Ma East Piute Mountains Pluton (Fletcher et al., 1988) have been subjected to high grade deformation and metamorphism. However, most of these plutons have experienced little or no deformation and/or metamorphism. Most of these plutons are felsic in composition. In the Granite, Coxcomb and northwestern Little Maria Mountains are plutons that vary in composition from granite to granodiorite. These rocks contain phenocrysts of potassium feldspar approximately 1-5 cm long and are distinctly to indistinctly foliated. These plutonic rocks are broadly correlated as part of the Cadiz Valley Batholith (Howard, 2002). Plutons of the Cadiz Batholith were emplaced elongated NW-SE are distinctly or indistinctly foliated and contain mineral lineations that plunge either NE or SW (Stone and Kelly, 1989; Ballard, 1990; Howard, 2002). Geobarometric studies done by Anderson (1988) indicate that the Cadiz Valley Batholith was emplaced at depths of ~6-8 km. Some of

these plutons, such as the Old Woman Pluton, have been subjected to pressures of 4-5 kbar (Foster et al., 1992).

Sense of shear in mylonitized plutons throughout southeastern California is determined to be top-ENE (Miller et al., 1981; Miller and Howard, 1985), which is down-dip with NE-plunging lineations. Most of these plutonic rocks intruded into older rocks between 79-70 Ma (Hoisch et al., 1988; Calzia, 1982; Barth et al., 2004). A leucogranite dike swarm exposed in the western Big Maria Mountains is inferred to have been emplaced during this episode of Cretaceous magmatism. K-Ar dating of one of these pegmatites yields an age of 79 Ma (Martin et al., 1982). These granites and pegmatites are observed to cross-cut D_1/D_2 fabrics (Hamilton, 1982; Hoisch et al., 1988; Salem, 2005). However, Salem et al. (2006) note that these dikes do locally record D_3 deformation fabrics and that these dikes were emplaced syn- or post-kinematically with D_3 fabric development. An analysis of the dike swarm indicates that the dike swarm was emplaced in a stress field with least principal stress directed ENE-WSW, consistent with that observed for other plutons associated with the Cadiz Valley Batholith (Howard, 2002). Ballard (1990) also noted that the Little Maria pluton also contains normal-sense shear bands at its margin but is relatively undeformed otherwise and that it cross-cuts earlier south-vergent deformation fabrics. To the north in the Old Woman Mountains, local development of Late Cretaceous mylonite fabrics immediately followed plutonism and were associated with extensional unroofing and rapid cooling (Foster et al., 1992). Therefore, it is likely that emplacement of the Cadiz Valley Batholith suite of plutons was emplaced during and after D_3 deformation, which is broadly associated with widespread NE-directed extension in middle crustal level rocks. This episode of Cretaceous magmatism was likely coeval with the change in geometry of the subducting Farallon slab off the west coast of North America to a flat slab geometry during the Laramide Orogeny (Saleeby, 2003).

Cenozoic sedimentary and volcanic rocks

The youngest rocks in the area consist primarily of surficial sedimentary and volcanic rocks of Miocene (perhaps Oligocene) age and younger (Stone, 2006). The oldest of these include Oligocene-Miocene volcanic rocks ranging in composition from rhyolite to basalt. An undeformed andesite flow in the Riverside Mountains has a whole rock K-Ar age of 23.5 Ma (Martin et al., 1982). Younger than these rocks are Oligocene-Miocene hypabyssal rhyolite and dacite hypabyssal intrusive rocks; a dacite plug in the Big Maria Mountains has a hornblende K-Ar age of ~22 Ma (Martin et al., 1982). Volcanic rocks were coeval with widespread crustal extension following the end of subduction of the Farallon slab and the development of the San Andreas transform margin.

Sedimentary rocks include fault and slide-block related breccia deposits, including a widespread “mega breccia” conglomerate exposed in the Palen Pass area, northernmost McCoy Mountains and in the upper plate of the Riverside Detachment in the southern Riverside Mountains. Other Miocene sedimentary rocks include limestone and fine-grained sedimentary deposits of the marine Bouse Formation, that contain freshwater fossils, such as ostracodes, barnacles, snails and clams (Hamilton, written comm. to Stone, 2006). The Bouse Formation and associated rocks are interpreted to have been deposited in a marine embayment of the ancestral Gulf of California (Busing, 1990) or a lacustrine deposit (Spencer et al., 2001). The Bouse Formation ranges in age from Miocene to early Pliocene. A tuff exposed in the formation further south has an Ar-Ar age of 5.0 Ma (Spencer et al., 2001). These Miocene and Pliocene rocks are overlain by Neogene surficial deposits including basin-fill, desert pavement and calcareous pediment and eolian sand dune deposits (Stone, 2006).

Structural geology

Overview

Structural investigations in the study area are primarily focused on Mesozoic deformation events in the region associated with convergent margin tectonics during Jurassic, Cretaceous and early Tertiary time. The overall goal of this structural analysis is to characterize, compare and contrast structural styles and fabrics across the tectonic boundary between the Maria Fold and Thrust Belt and McCoy Basin and to establish regional correlations.

For this paper, two areas were selected for detailed structural analysis: the northern McCoy Mountains and Palen Pass (outlined in Figure 2.2). The northern McCoy Mountains were selected because of their proximity to the Big and Little Maria Mountains and because they contain the best exposures of the lower McCoy Mountains Formation (MMF) and the contact between the lower and upper MMF. The Palen Pass area was selected because it is the only place on the California side of the Maria Fold and Thrust Belt where the tectonic boundary between the MFTB and McCoy Basin is exposed at the surface.

Results of this structural analysis will be integrated with results of detailed structural analysis from the Big Maria Mountains (Chapter 1) to develop a regional model for deformation.

Methods

High resolution geologic mapping (1:12,000 scale) of the northern McCoy Mountains and Palen Pass were done in order to provide spatial context for structural analysis. Structural analysis was done at all scales from macroscopic regional folds and faults, to mesoscopic structures depicted in annotated field photographs, to microstructures depicted as annotated thin sections, utilizing methods of structural analysis outlined in Hobbs et al. (1976), Means (1981), Ramsay (1967), Ramsay and Huber (1987) and Davis and Reynolds (1996). Microstructural analysis methods are after

Hirth and Tullis (1991) and Passchier and Trouw (2004) and references cited therein. Abbreviations chosen for structural elements include S for planar cleavage fabrics, D for deformation event, L for lineation fabrics and F for folds. Subscripts designate the relative order of structural elements, i.e. S_1 being first generation cleavage fabric. For original depositional bedding or volcanic layering, the designation S_0 is assigned. Geologic maps of inset areas were produced in Adobe Illustrator and ArcGIS and maps were compiled, along with measurements and sample locations in ArcGIS (CD attached). The interpretive cross sections from the Granite Mountains through the Palen Mountains and from the Little Maria through the McCoy Mountains were produced from our compilation tectonic map of the Western Maria Fold and Thrust Belt (1:100,000; Plate 2. The geologic cross sections are represented by lines B-B' and C-C' (Figure 2, Plates 3 and 4). Stereonet plots were produced using the program GEOrient. Measurement data used in GEOrient are tabulated and attached as data appendices and are shown, wherever possible, on inset geologic maps.

McCoy Mountains

Structural overview

The McCoy Mountains represent a NW-trending extensional fault block mountain range located in the southwestern Basin and Range province in California (Figure 2.2) approximately 10 miles west of Blythe. The McCoy Mountains are separated from the Big Maria Mountains to the northeast by the McCoy Wash, which is filled in with sediments covering up an extensional valley. The Little Maria Mountains are adjacent to the range to the northwest. Approximately 10 miles further west are the Granite-Palen Mountains, which are separated from the McCoy Mountains by another extensional valley. The Mule Mountains lie due south of the McCoy Mountains, the Little Chuckwalla Mountains to the southwest and the Dome Rock Mountains in Arizona to the southeast. The general architecture of the McCoy Mountains consists of Jurassic volcanic rocks at the north end of the range overlain by >7 km of Jurassic-Cretaceous McCoy Mountains Formation (MMF). At the south end of the range, the Cretaceous Mule

Mountains thrust system emplaces Jurassic volcanic and the Basal Sandstone 1 member of the McCoy Mountains Formation northward over uppermost MMF and folds the upper MMF into a north-vergent overturned syncline in the footwall of the thrust (Plate 2).

Figure 2.7 shows a 1:12,000 inset map of the north-central McCoy Mountains. Units from the Jurassic volcanics through the Cretaceous Conglomerate Member of the McCoy Mountains Formation are exposed in the map area. Analysis and mapping were done in the vicinity of a large, fault controlled wash that bisects the northern part of the range. The wash allowed easy access to the interior of the range. Most of the Jurassic volcanic suite at the north end of the range consists of quartz porphyry, which lacks any primary depositional or magmatic fabric. However, layered volcanic deposits at the north end of the range, documented by Pelka (1973) and shown in the attached CD, dip to the south. This orientation is similar to the overlying McCoy Mountains Formation,

which consistently dips southward in the McCoy Mountains as well as everywhere else it is exposed in the McCoy Basin (Harding and Coney, 1985; Tosdal and Stone, 1994), indicating that the entire McCoy Basin has been tilted to the south. All units in the McCoy Mountains record a pervasive north-dipping cleavage fabric, which strikes subparallel with bedding in the McCoy Mountains, but intersects bedding at high angles (Figure 2.8). The exception to the north dipping cleavage rule exists at the south end of the range, where cleavage is observed to be dipping south, sympathetic with the south dip of the Mule Mountains thrust fault. Pervasive south-dipping cleavage is observed almost exclusively near the Mule Mountains thrust fault (Figure 2.9).

Overall, deformation in the McCoy Mountains is best characterized as brittle in nature. Pervasive isoclinal folding, unit attenuation and ductile shearing, as observed in the nearby Big and Little Maria Mountains to the north and east are not observed at all in the McCoy Mountains. The one exception is in the area of the Mule Mountains Thrust at the south end of the range, which shows ductile strain fabrics, such as stretched pebble conglomerate (Figure 2.10). In the case of the Mule Mountains thrust, the orientation of the stretched pebble shown in Figure 2.10 records top-northeast-directed reverse shear sense. Units in the range have been cut by numerous faults and fractures at various orientations. Typically, most faults in the range trend NNW-SSE and exhibit east-side down and west-side down normal sense movement. One such fault is observed to bisect the field area in the McCoy Mountains from north to south and records west-side down directed extension (Figure 2.7 and 2.11). Slickenlines associated with fault movement are also observed on fracture surfaces. It is possible that some fractures might have formed during brittle deformation events in Mesozoic time, but this is speculation at the present time. Minor south-vergent folds are observed at the north end of the range in Basal Sandstone 1, but none are observed any further upsection. Pelka (1973) documented north-trending 100s of meter scale anticlines and synclines in the middle of the mountain range (Plate 2), but none were observed in the north part of the range.

Qualitatively, rocks in the McCoy Mountains have experienced low grade metamorphism (lower greenschist facies) and rocks in the range typically resemble their



Figure 2.8: Field photograph looking west at south-dipping bedding (S_0) vs. north-dipping spaced cleavage (S_1) in Jurassic Basal Sandstone 1 member of the McCoy Mountains Formation. Geologist A. Salem for scale. Photo: M.A. Tyra.

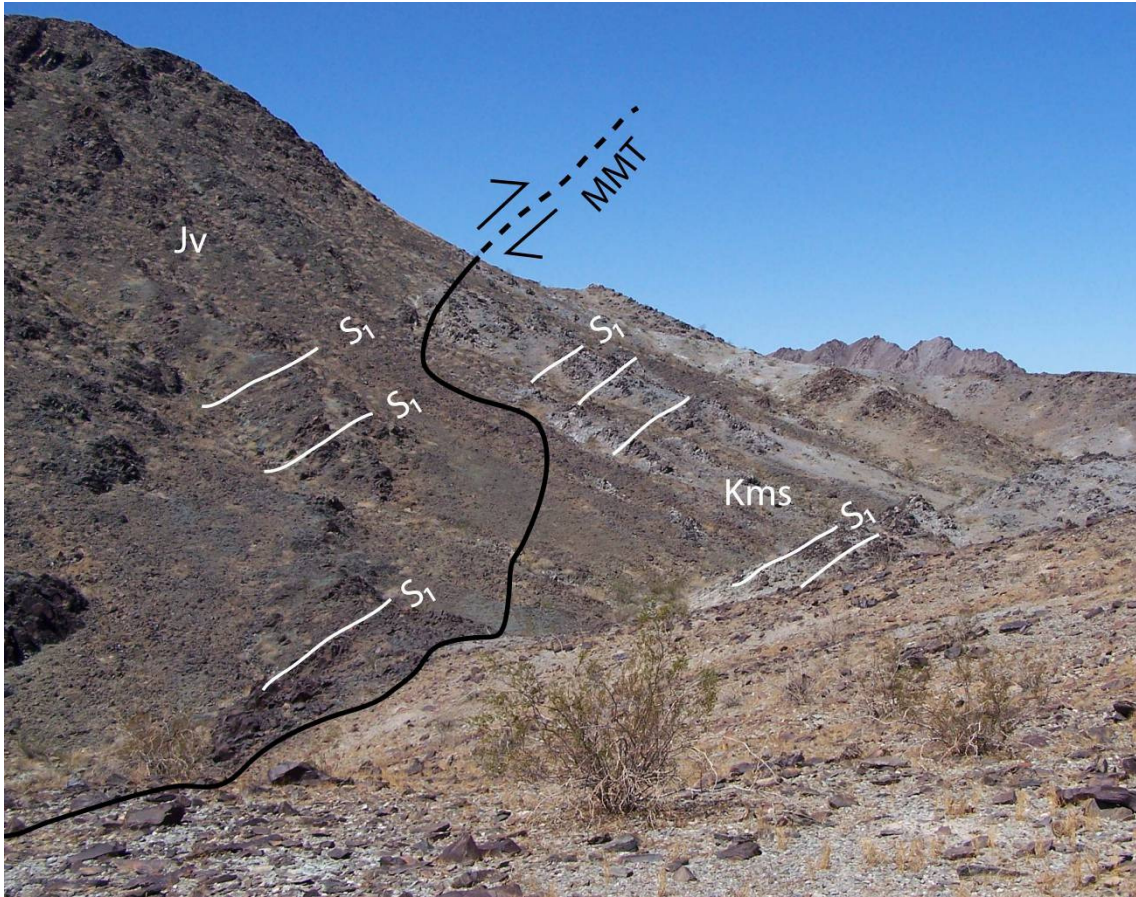


Figure 2.9: Field photograph taken looking west at the south-dipping Mule Mountains Thrust (MMT) in the southern Palen Mountains. S_1 is a south-dipping cleavage sympathetic with the dip of the fault and is subparallel with bedding. The thrust fault emplaces Jurassic volcanic rocks (Jv) northward over the Cretaceous Sandstone Member of the McCoy Mountains Formation (Kms).



Figure 2.10: Field photograph taken looking east at stretched pebble clast with strain tails near the foot of the Mule Mountains Thrust, southern McCoy Mountains. South-dipping S_1 cleavage represents shear planes. Stretched-pebble clast shows reverse shear sense. Photo: L.J. Crossey.



Figure 2.11: Field photograph looking north at west-side down directed normal fault in the McCoy Mountains. The fault offsets the Cretaceous Mudstone Member of the McCoy Mountains Formation.

protoliths in texture and composition, so much so that rocks in the range are typically referred to by their protolith name (e.g. sandstone instead of quartzite). Most primary sedimentary structures, such as laminar beds and crossbeds, have been preserved. The mineral assemblage in these rocks includes predominately sericite and epidote, with minor amounts of quartz and albite (Pelka, 1973; Harding and Coney, 1985). Based on detrital zircon analysis, peak metamorphism and most deformation in the McCoy Mountains must be constrained between 84 Ma (the youngest detrital zircon ages from Barth et al., 2004) and 73 Ma, the age of the Coxcomb Mountains pluton (Barth et al., 2004). A zone of hydrothermal alteration is observed in the northern end of the McCoy Mountains around the St. John's Mine, a smaller copper prospect. Rocks around the mine typically exhibit more fracturing and have been intruded by quartz veins. However, quartz veins are prevalent throughout the mountain range, decreasing in size and spatial frequency from the north to south end of the range.

Domain analysis

In the McCoy Mountains, structural domains are defined by contacts between members of the McCoy Mountains Formation, the stratigraphy and lithology of which was described in the previous section. Basal Sandstone 1, sediments derived from quartz porphyry and the Jurassic volcanic suite were grouped together. Figure 2.12a shows an equal area lower hemisphere projection point density contour plot of poles to S_0 from Basal Sandstone 1 (See Table 2.1 for data). The mean orientation of bedding is 105, 54° S, corresponding to a single maximum in the point density contour plot. In the study area, bedding is observed to dip predominately southward from as shallow as 25° to as steep near vertical orientation (88°). This variation in dips is shown graphically by the contour plot and is also witnessed in the field (Figure 2.13). In the field, dips of bedding in Basal Sandstone 1 are highly variable and locally folds are observed. This suggests that Basal



Figure 2.12: Equal area lower hemisphere stereonet point density contour plots of A) poles to S_0 in Jurassic Basal Sandstone 1 member of the McCoy Mountains Formation ($N = 52$) and B) poles to S_1 in Jurassic volcanic rocks and Basal Sandstone 1 ($N = 89$). S_0 has a statistically significant mean orientation of $105, 54^\circ\text{S}$ (shown as blue star). S_1 point density contour plot shows two maxima, one at $270, 50^\circ\text{N}$ and the other at $215, 58^\circ\text{W}$ (shown as blue stars). Statistically determined mean orientation is $249, 60^\circ\text{N}$ (shown as green rectangle)

Table 2.1: Structural data for Jurassic volcanics and Jurassic Basal Sandstone 1 member of the McCoy Mountains Formation. Plane data reported as strike, dip and dip direction

S0 Original bedding		S1 Cleavage		
290,55,S	285,40,S	072,85,N	060,40,N	030,55,W
330,70,S	322,54,S	072,86,N	260,70,N	050,56,W
335,55,S	100,45,S	085,50,N	085,55,N	033,45,W
310,54,S	055,42,N	092,41,N	070,55,S	030,43,W
035,85,S	292,83,S	280,42,N	080,55,N	032,59,W
130,52,S	085,51,S	045,40,N	288,50,N	302,60,N
265,55,S	294,75,S	080,85,N	280,56,N	090,58,N
290,88,S	280,53,S	035,68,W	270,48,N	090,50,N
280,45,S	265,42,S	040,70,W	020,25,W	300,50,N
302,65,S	308,40,S	087,80,N	285,55,N	297,55,N
080,60,S	288,60,S	095,83,S	300,53,N	080,51,N
070,75,S	300,53,S	274,76,S	100,50,N	310,65,N
100,63,S	315,74,S	262,80,S	030,63,N	320,55,N
095,36,S	293,62,S	085,85,N	252,83,S	262,57,N
285,55,S	280,64,S	245,75,N	275,80,S	286,51,N
098,58,S	290,51,S	240,60,N	085,74,N	268,61,N
115,55,S	280,26,S	010,30,W	244,82,S	277,54,N
295,50,S	070,35,S	165,28,W	200,60,W	070,61,N
305,60,S	285,64,S	230,74,N	210,50,W	270,53,S
280,56,S	295,43,S	185,65,W	245,90,N	095,66,N
080,40,S	085,35,S	205,52,W	200,50,W	210,72,W
070,32,S	084,75,S	200,53,W	045,70,W	060,70,N
105,43,S	095,60,S	070,65,N	045,83,W	035,60,W
275,80,S	085,75,S	127,64,N	235,65,N	016,69,W
090,65,S	320,50,W	300,82,N	090,84,S	000,77,S
045,24,S	290,75,S	085,60,N	030,82,W	055,58,N
		080,64,N	035,58,W	055,80,W
		070,35,N	029,65,W	038,83,W
		083,86,N	271,21,N	045,52,N
		304,32,N	300,58,N	

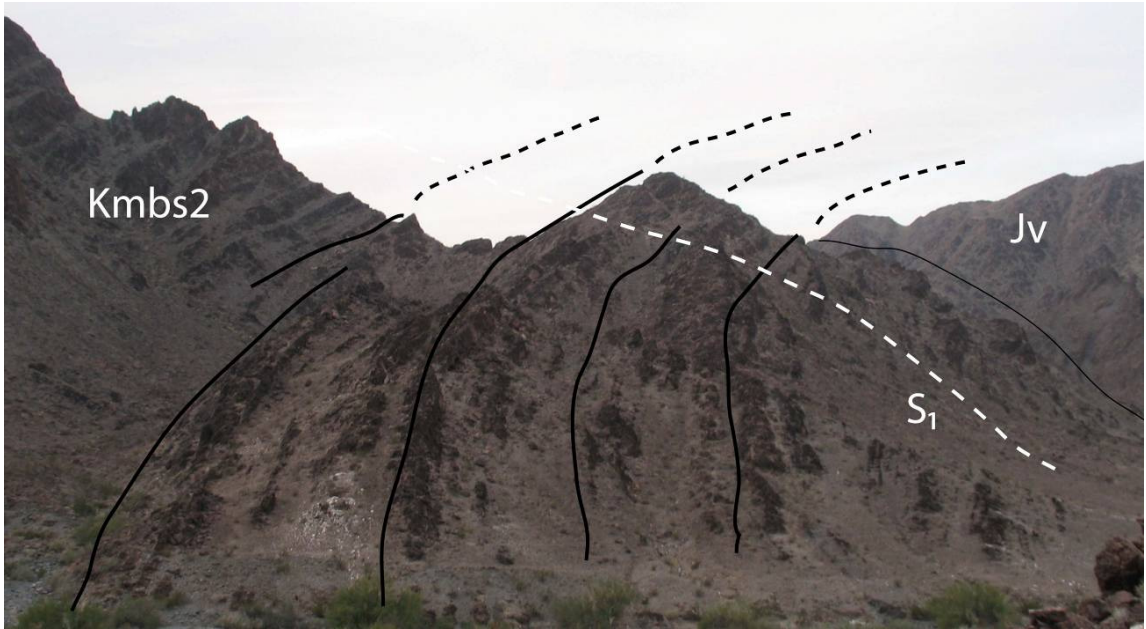


Figure 2.13: Field photograph taken looking west at bedding in Jurassic Basal Sandstone 1 of the McCoy Mountains Formation. Bedding highlighted by black lines. North-dipping S_1 is axial plane cleavage to buckling fold defined by bedding. Basal Sandstone 1 depositionally overlies the Jurassic volcanics (Jv) and is underneath Cretaceous Basal Sandstone 2 member (Kmbs2)

Sandstone 1 has experienced a significant amount of internal deformation. Folds observed in Basal Sandstone 1 seem to confirm this idea. Figure 2.12b shows an equal area lower hemisphere projection point density contour plot of poles to S_1 from Jurassic volcanic rocks and Basal Sandstone 1 of the McCoy Mountains Formation. S_1 cleavage typically dips northward, as shallow as 20° and as steep as vertical orientation. The mean orientation of S_1 is $249, 60^\circ\text{N}$. The point density contour plot shows two defined maxima, the major one at $270, 50^\circ\text{N}$ and the other at $215, 58^\circ\text{W}$. These two maxima could correspond to two observed cleavages in the field, which are variably expressed (Figure 2.14). These cleavages could be conjugate fabrics, as they intersect at approximately 60° . The mean cleavage orientation bisects these two maxima almost perfectly. If the mean S_1 orientation is perpendicular to the shortening direction during D_1 deformation in the McCoy Mountains, then shortening would be the pole to mean S_1 , 30° toward 159 or SSE-directed shortening. Alternatively, the major maximum at $270, 50^\circ\text{N}$ could represent the actual orientation of S_1 , with the second maximum representing a localized deflection of cleavage around the St. John's Mine (Figure 2.7) hydrothermal alteration zone, or a weakly expressed ancillary cleavage fabric. If this is the case, then the shortening direction would be the pole to $270, 50^\circ\text{N}$, which is 40° toward 180 , or top-south-directed shortening. This shortening direction is also consistent with folds observed in the area, which have axial plane cleavages similar to S_1 . Finally, the second maximum point density orientation could actually be recording a cleavage fabric from a kinematically different event. In this case, the pole to the mean orientation of $215, 58^\circ\text{W}$, which is 32° toward 125 , would represent the shortening direction during emplacement of this cleavage. In this case, this represents top-southeast directed shortening.

Figure 2.15a shows an equal area projection point density contour plot for poles to S_0 in Basal Sandstone 2 (see Table 2.2. for data). The mean orientation of bedding is $082, 43^\circ\text{S}$, which is defined by a maximum point density at that orientation. The contour interval is larger, and in general S_0 measurements in Basal Sandstone 2 seem to have a tighter distribution than those observed in Basal Sandstone 1, which could indicate that this unit has experienced less internal deformation. S_0 measurements dip consistently



Figure 2.14: Field photograph taken looking north at two intersecting cleavages (highlighted in white) in the Jurassic volcanic upper member. Cleavages intersect at $60/120^\circ$ and dip north (into the picture).

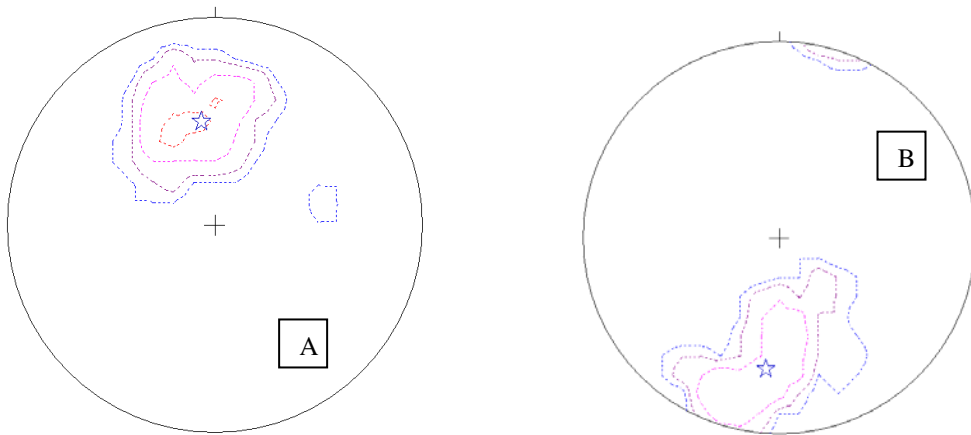


Figure 2.15: Equal area lower hemisphere point density contour plots of A) poles to S_0 ($N = 36$) and B) Poles to S_1 ($N=35$) from Cretaceous Basal Sandstone 2 member of the McCoy Mountains Formation. S_0 has a statistically significant mean orientation of $082, 43^\circ\text{S}$ (shown as blue star). S_1 has a statistically significant mean orientation of $276, 56^\circ\text{N}$.

Table 2.2: Structural data from Cretaceous Basal Sandstone 2 member, McCoy Mountains Formation

S0 Original Bedding	S1 Cleavage
260,65,S	290,74,N
028,25,S	318,83,N
075,36,S	053,30,N
282,54,S	090,78,N
045,45,S	095,33,N
065,45,S	267,41,N
355,50,W	302,70,N
080,50,S	285,78,N
152,43,S	065,66,N
265,42,S	285,88,N
280,30,S	285,55,N
250,65,S	303,68,N
245,46,S	280,64,N
258,63,S	280,70,N
063,46,S	285,49,N
065,36,S	270,54,N
280,55,S	085,52,N
086,36,S	290,85,N
275,44,S	283,69,N
093,44,S	090,60,N
250,62,S	118,72,N
287,60,S	285,70,N
055,50,S	282,81,N
067,55,S	040,32,N
095,62,S	025,75,E
070,46,S	060,56,N
060,38,S	090,61,N
102,32,S	085,48,N
273,53,S	038,16,W
080,30,S	065,39,N
085,44,S	088,34,N
279,19,S	080,50,N
045,32,S	270,26,N
062,30,S	108,80,N
100,42,S	285,32,N
290,48,S	

southward as shallow as 19° and as steep as 65° . An unconformity between Basal Sandstone 1 and Basal Sandstone 2 is suggested by detrital zircon analysis presented by Barth et al. (2004) and Spencer et al. (2005). This unconformity could be no more than 45 million years, based on the age of detrital zircons present in Basal Sandstone 2 in the McCoy Mountains as young as 109 Ma (Barth et al., 2004) and the age of a lava flow found near the top of Basal Sandstone 1 in the New Water Mountains of 154 Ma (Spencer et al., 2005). The statistically significant difference in mean orientation of bedding uncovered by structural analysis here seems to support an interpretation of a significant intraformational unconformity between these two members.

Figure 2.15b shows a lower hemisphere equal area projection point density contour plot of poles to S_1 from Basal Sandstone 2. The mean orientation of S_1 is $276, 57^\circ\text{N}$, which is in excellent agreement with the mean orientation of S_1 determined from the Jurassic volcanic units and Basal Sandstone 1. Based on this, we interpret that the pole to S_1 represents the shortening direction during regional deformation. In this case, the pole to S_1 is 33° toward 186, or top-south-directed shortening.

Figure 2.16a shows a lower hemisphere equal area projection point density contour plot of poles to S_0 from the Mudstone Member. Mean orientation of bedding is $079, 38^\circ\text{S}$, which is in excellent agreement with bedding from Basal Sandstone 2. Values of bedding dips vary from 22 to 60°S , which is also in good agreement with the range of measurements from Basal Sandstone 2. The gradational nature of the contact between Basal Sandstone 2 and the Mudstone Member and the similarity in orientation in bedding indicates that the transition from Basal Sandstone 2 to the Mudstone Member represents continuous deposition and a decrease in the flow regime during deposition within the same depositional setting, such as the change from medial to distal facies in an alluvial fan sequence. Figure 2.16b shows a lower hemisphere equal area projection point density contour plot of poles to S_1 from the Mudstone Member. In the Mudstone Member, S_1 varies a great deal in orientation, with dips ranging from 15° to 70° and with observed dip directions ranging from due east to due west. The variability in development of the



Figure 2.16: Lower hemisphere equal area point density contour plots of A) poles to S_0 ($N = 31$) and B) poles to S_1 ($N = 52$) for the Cretaceous Mudstone Member of the McCoy Mountains Formation. Statistically determined mean orientation of S_0 is $079, 38^\circ\text{S}$. Mean orientation of S_1 is $295, 28^\circ\text{N}$. Mean orientations shown as blue stars

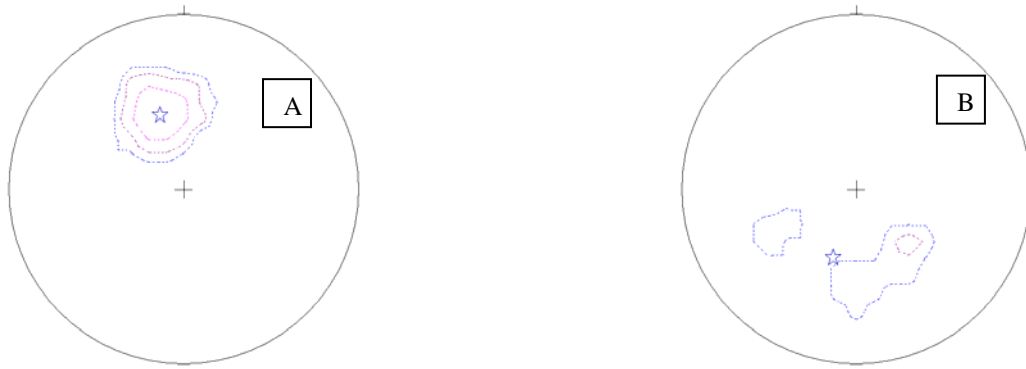


Figure 2.17: Equal area lower hemisphere point density contour plots of A) poles to S_0 ($N = 16$) and B) poles to S_1 ($N = 11$) from Cretaceous Conglomerate Member of the McCoy Mountains Formation. S_0 has statistically determined mean orientation of $072, 37^\circ\text{S}$. S_1 has a mean orientation of $288, 35^\circ\text{N}$. Mean orientations shown as blue stars.

Table 2.3: Structural data from Cretaceous mudstone (Kmm) and conglomerate (Kmc) members of the McCoy Mountains Formation

Kmm			Kmc	
S0 Original bedding	S1 Cleavage		S0 Original Bedding	S1 Cleavage
075,59,S	295,66,N	337,29,E	064,51,S	280,30,N
325,50,S	090,70,N	010,35,E	040,34,S	012,55,E
300,70,S	300,45,S	010,23,E	070,36,S	335,50,E
087,40,S	308,58,S	337,29,E	078,43,S	328,30,E
310,80,W	059,45,N	010,35,E	072,38,S	330,43,E
085,40,S	305,14,N	010,23,E	074,56,S	061,38,N
275,40,S	315,30,N	112,51,N	076,40,S	034,31,W
055,39,S	300,20,N	029,21,E	065,47,S	053,41,N
025,31,S	305,28,N	068,38,N	065,40,N	090,48,N
040,44,S	313,35,N	298,40,N	064,26,S	304,85,W
062,30,S	300,30,N	292,43,N	068,35,S	270,50,N
030,31,S	298,32,N	069,40,N	055,41,S	
042,35,S	290,30,N	052,40,N	075,24,S	
093,40,S	295,27,N	023,20,N	280,42,S	
060,39,S	308,23,N	294,39,N	276,40,S	
295,44,S	295,62,N	315,53,N	085,32,S	
050,30,S	320,55,E	295,45,N		
095,45,S	304,36,N	308,20,N		
088,59,S	304,50,N	010,30,W		
274,28,S	055,55,N	308,42,N		
270,45,S	000,23,W	065,37,N		
068,41,S	010,22,W			
045,38,S	315,54,N			
045,45,S	090,41,N			
045,38,S	286,30,N			
045,45,S	292,30,N			
280,53,S	289,19,N			
041,23,S	065,16,N			
320,47,S	048,15,N			
265,38,S	342,47,E			
300,45,S	330,34,E			

cleavage fabric could be governed by lithology. The relatively high mica content and fine grain size prevalent in the phyllitic Mudstone Member might allow for cleavage fabrics to be more diffuse, and thus be at different orientations, throughout the rock. However, S_1 predominately dips north and the mean orientation is $295, 28^\circ\text{N}$. This orientation is significantly different from S_1 measurements observed further north in the range. One possibility is that the mudstone event is recording a kinematically different deformation event, though this seems unlikely given that the Mudstone Member is younger and, therefore, cleavages observed in the younger Mudstone Member should also be recognized further down-section. Alternatively, it is more likely that the overall orientation of cleavage is becoming shallower and less expressed further away from a major south-vergent thrust. This thrust fault represents a major structural discontinuity that emplaces the middle crustal Maria Fold and Thrust Belt up over the supracrustal McCoy Basin. This south-vergent thrust has been proposed by other workers (Harding and Coney, 1985; Yeats, 1985) and is designated here as the Maria Frontal Thrust (Figure 2.2, Plate 2).

Figures 2.17a and b show lower hemisphere equal area projection point density contour plots of poles to S_0 and S_1 respectively for the Conglomerate Member of the McCoy Mountains Formation. The contact between the Conglomerate Member and the underlying Mudstone Member has been recognized as a major intraformational unconformity and separates what is recognized as the lower MMF from the upper MMF. Therefore, characterizing the nature of the contact and looking for structural discontinuities between these two members was an important goal of this study. The mean orientation of bedding in the Conglomerate Member is $072, 37^\circ\text{S}$, which in excellent agreement with the orientation of the mudstone and Basal Sandstone 2 members. The mean orientation of S_1 cleavage observed in the lower part of the Conglomerate Member is $288, 35^\circ\text{N}$, which is in excellent agreement with S_1 observed in the Mudstone Member. Additionally, S_1 crosscuts the contact between the conglomerate and mudstone layer. Finally, S_1 is not as strongly expressed in the conglomerate as it is in lower layers.

The close agreement in bedding between the Conglomerate Member and the Mudstone Member, combined with the gradational nature of the contact between the Mudstone Member observed in the field (see previous section), tends to refute the idea that this contact represents a major intraformational unconformity as suggested by Harding and Coney (1985). Additionally, the close agreement between the mean orientation of S_1 from the Conglomerate Member and S_1 from the Mudstone Member, and the observation that S_1 crosscuts the contact, indicate that units above and below the contact between the mudstone and Conglomerate Member underwent D_1 deformation. This confirms that S_1 becomes shallower further upsection and becomes a less developed deformation fabric. Overall, degree of internal deformation in the formation decreases further up section. However, the significant change in clast size indicates that, at least in the McCoy Mountains there was a significant change in the flow regime and depositional setting of the McCoy Basin marked by the change from the mudstone to the Conglomerate Member. Further west in the Dome Rock and Plomosa Mountains, this contact is recognized clearly as an unconformity, suggesting that there was a temporal break between deposition of the lower and upper McCoy Mountains Formation in western Arizona. However, the unconformity is not apparent in the McCoy Mountains, confirming observations by Tosdal and Stone (1994), who also note that the unconformity is not apparent in the Palen Mountains to the west. In the Coxcomb Mountains, the westernmost extent of exposures of the McCoy Mountains Formation, the Mudstone Member is intruded by the Coxcomb Mountains pluton. Therefore, we conclude that there was in fact a regional change in the tectonic setting of the McCoy Mountains Formation based on change in clast size and composition from the mudstone to Conglomerate Members. However, we also conclude that there was a temporal break in deposition in western Arizona coinciding with the change in depositional/tectonic setting of the McCoy Basin, but that the change in tectonic setting of the McCoy Basin in eastern California was marked by continuous deposition. As such, we conclude that exposures of Basal Sandstone 2 and Mudstone Member in Arizona are older than exposures of their correlatives in California, meaning westward progression of the depositional center

during Basal Sandstone 2 and Mudstone Member time. Implications for the tectonic setting of the McCoy Basin based on these observations and conclusions will be elaborated on later.

Microstructures

Samples from the volcanic units from the northern edge of the range were selected for microstructural analysis. Figure 2.18 shows two photomicrographs of sample M07 KS03 collected from the quartz porphyry of the upper Jurassic volcanics. The quartz porphyry consists of ~90% quartz, with minor plagioclase, potassium feldspar, muscovite, garnet and oxides. The thin section was made cut perpendicular to S_1 foliation. Two cleavage fabrics are observed to intersect each other at $\sim 60^\circ$. Euhedral oxide grains with sharp grain boundary edges indicate that these rocks have not undergone high strain ductile deformation. In addition, quartz and feldspar grains, while fractured, do not exhibit rim alteration or recrystallization, indicating that peak temperature conditions did not exceed the temperature conditions necessary for plastic deformation of quartz, approximately 400°C (Passchier and Trouw, 2004), confirming observations on metamorphic grade advanced by Pelka (1973) and Harding and Coney (1985). Based on the stereonet analysis of cleavages in the area, we interpret that each of these cleavages corresponds to each of the maxima displayed in the stereonet plot in Figure 2.12.

Quartz vein analysis

Figure 2.19 shows an equal area lower hemisphere projection plot of poles to quartz vein orientations from the northern McCoy Mountains (see Table 2.4 for data). Quartz veins are interpreted to represent hydrothermal veins emplaced during widespread regional metamorphism and Cretaceous magmatism. However, exact timing of the emplacement of quartz veins is unknown as it is difficult to precisely date pure quartz veins. If the quartz veins have a statistically significant mean orientation, then measurements of the quartz veins should help quantify the strain and paleo-stress field during emplacement and, consequently, during regional metamorphism. The point density contour plot shows two maxima, one at $022, 86^\circ\text{E}$ and the other at $272, 35^\circ\text{N}$. In the field,

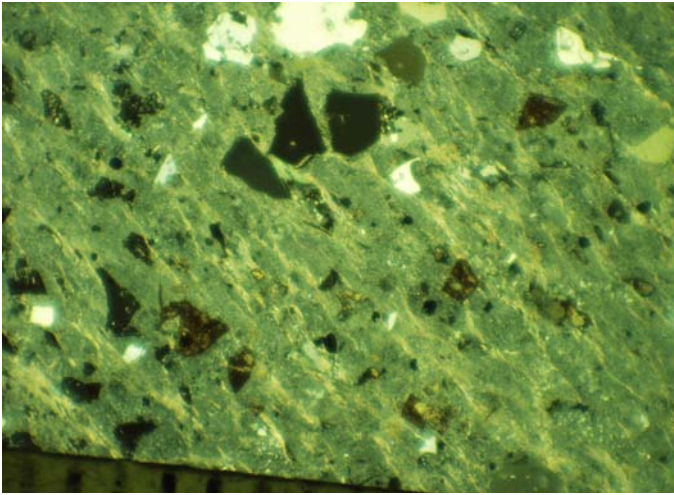
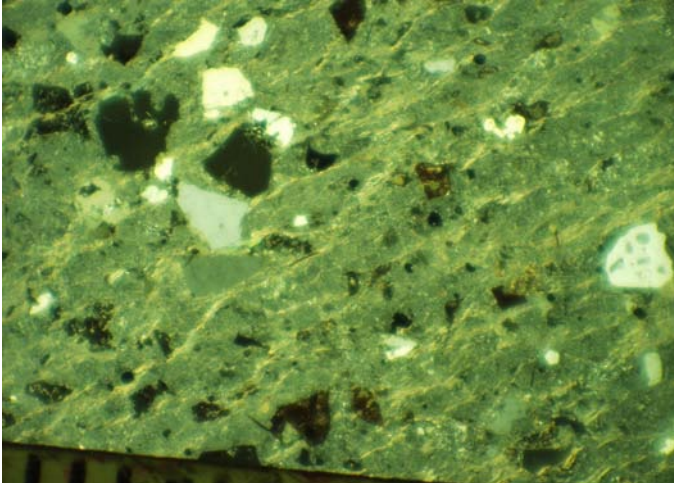


Figure 2.18: Photomicrographs in cross-polarized light of sample M07 KS03 from Jurassic quartz porphyry (volcanics upper member). Thin section was made cut perpendicular to S_1 foliation. **A)** S_1 main cleavage fabric defined by white micas (slide rotated 20° counterclockwise from E-W orientation to show cleavage). **B)** S_2 cleavage defined by white micas (slide rotated 34° clockwise from E-W orientation to show cleavage)

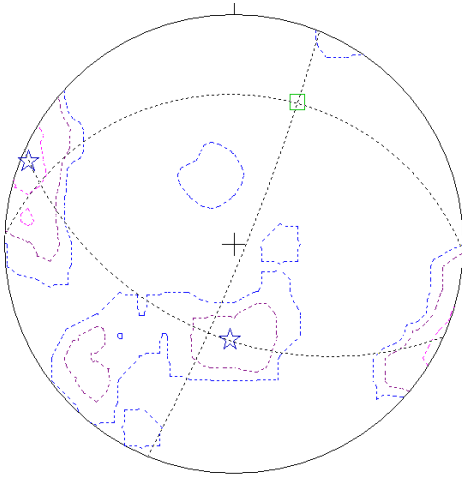


Figure 2.19: Equal area lower hemisphere point density contour plot of poles to quartz vein orientations, northern McCoy Mountains (N = 37). Point density contour plot shows two maxima for orientations, one at 022, 86°E the other at 272, 35°N (shown as blue stars). Pole to 022, 86°E (blue star on left) is determined to be direction of maximum extension, σ_3 , during quartz vein emplacement. Intersection of two mean orientations gives σ_1 , direction of maximum compressive stress, which is determined to be 33° toward 024 (green rectangle)



Figure 2.20: Looking north at network of quartz veins cross-cutting Basal Sandstone 1, northern McCoy Mountains (geologist H. Johnston for scale). Major quartz veins are observed to have subvertical orientation.

Table 2.4: Strike and dip of quartz veins from northern McCoy Mountains

**Quartz
veins**

004,90,E
035,82,W
088,36,N
019,60,W
000,75,E
027,78,E
030,90,E
075,27,S
025,80,E
025,15,W
070,25,S
018,77,E
085,34,N
045,71,W
325,40,N
292,37,N
020,88,W
290,50,N
030,83,W
296,30,N
306,74,N
015,86,W
324,68,E
005,78,E
304,85,W
350,63,E
076,46,N
290,82,N
073,32,N
060,32,N
345,20,W
012,85,E
014,75,E
029,88,W
321,54,E
319,80,E
322,72,E

intersecting quartz veins are common (Figure 2.20), with one vein being larger than the other. The larger veins commonly strike north or northeast and dip steeply either west or east. The smaller veins commonly strike east-west and dip shallow to moderately to the north. Based on these field observations, we conclude that quartz veins with orientation at or around the statistical mean orientation of 022, 86°E record σ_3 , or the direction of least compressive stress, during emplacement of the veins. The pole to this plane, 4° toward 292, represents the direction of σ_3 , horizontal northwest-directed extension. The minor set of quartz veins, with orientation 272, 35°N, record σ_2 , the direction of intermediate compressive stress, during emplacement of the quartz veins. The pole to this plane, 55° toward 182, is the direction of σ_2 . The intersection of these two planes, which are perpendicular to each other, gives the direction of σ_1 , which is the direction of maximum compressive stress. This line is 33° toward 024, or NE-directed shortening.

Based on regional tectonic events, we interpret that the stress field obtained from this analysis is consistent with the NE-directed Mule Mountain Thrust System. The frontal thrust of the Mule Mountain Thrust is located at the southeastern tip of the range (Figure 2, Plate 3). Therefore, we interpret that the quartz veins were emplaced during Mule Mountains Thrust deformation, the timing of which is constrained to ~70 Ma (Tosdal, 1990). Consequently, the veins were emplaced during the late stages of Late Cretaceous deformation and metamorphism in the region and were coeval with peak metamorphism.

Regional analysis – Little Maria Mountains to McCoy Mountains

Cross section B-B' (Plate 3) was drafted along a north-south line through the northwestern Little Maria Mountains through the McCoy Mountains to the southern terminus of the range where the Mule Mountains Thrust is exposed. The geology of the Little Maria Mountains represents a westward continuation of the main geologic features observed in the Big Maria Mountains (Figure 2 Hamilton, 1982, 1987; Ballard, 1990; Stone, 2006; Chapter 1). Ballard (1990) notes that the architecture of the range consists of

three plates: the lower plate, which contains the Big Maria-Little Maria syncline and the high strain Big Maria shear zone; a middle plate, which consists of high grade metamorphosed Mesozoic and Proterozoic age gneissic rocks; and the upper plate, which consists chiefly of Paleozoic and Mesozoic metasedimentary rocks extensively intruded by Jurassic granites. These rocks contain a pervasive north-dipping foliation fabric, S_1 , which is subparallel to unit contacts and original bedding. This fabric is directly correlative to S_1 in the Big Maria Mountains (Hamilton, 1982; Chapter 1).

Middle crustal polyphase deformation fabrics recorded in rocks in the Little Maria Mountains are similar to those observed in the Big Maria Mountains. D_1 is characterized by isoclinal folds and shear zones that formed as a result of top-southeast-directed (reverse and dextral) shear. We interpret that these structures, based on kinematics and timing, formed as the result of southeast-directed transport during the Sevier Orogeny. D_2 is characterized by southwest-vergent folds that refold S_1 foliation and shear zones that emplace Jurassic and Proterozoic crystalline rocks over Paleozoic and Mesozoic metasedimentary units and imbricate and attenuate Paleozoic sections. However, we interpret D_2 structures to be the result of continued refolding and shearing of earlier fabrics as part of a progressive deformation event related to southeast-directed ductile channel flow during the Sevier Orogeny as opposed to a distinctly separate kinematic event as suggested by Ballard (1990). Evidence for this includes preponderance of west and northwest plunging stretching lineation with reverse shear sense indicators throughout most of the Little Maria and Big Maria Mountains (Ballard, 1990; Salem et al., 2006). Ballard's Domain 4, located in the eastern part of the range, is one of only two major areas in the Big Maria-Little Maria Mountains where the Big Maria-Little Maria syncline plunges eastward and where northeast plunging lineations are documented. The other place is in the hanging wall of the down-to-the-east Quien Sabe Fault, which is part of the breakaway to the Colorado River Extensional Corridor (Figure 2.2), in the east central Big Maria Mountains. Additionally high strain zones, such as the Maria shear zone (Chapter 1), with high degrees of stratal attenuation (to less than 1% of original stratigraphic thickness), also contain kinematic indicators that indicate top-SE directed

reverse and ductile shear. Based on similarities with high grade nappe assemblages as described by Williams and Jiang (2005), such high strain zones might represent earlier structural discontinuities, such as high angle normal faults, that were rotated into the direction of channel flow during ductile crustal scale shearing. Given the hypothesis advanced by several workers, that the McCoy Basin originated as a Jurassic-Cretaceous rift basin prior to Late Cretaceous deformation and metamorphism, such high angle normal faults might have existed prior to MFTB deformation. D_1/D_2 deformation in the Maria Fold and Thrust Belt might be coeval with sedimentation in the upper McCoy Mountains Formation. The contact between the mudstone and Conglomerate Members has been interpreted by several workers to represent an intraformational unconformity, based on a significant upward increase in clast size and a change in clast provenance. Although we do not interpret a temporal unconformity in the McCoy Mountains, based on lack of an erosional surface or structural evidence, we agree that the change in clast size represents a change in tectonic setting of the McCoy Basin. Paleocurrent indicators indicate that most McCoy Mountains Formation sediments were sourced from the north (Harding and Coney, 1985). The appearance of large rounded cobbles above a fine grained horizon is laterally continuous for tens of kilometers, indicating that a major uplift must have taken place to the north concomitant with sedimentation in the McCoy Basin to the south. This hypothesis has been suggested by other workers (Spencer et al., 2005; Barth et al., 2004). If this interpretation is correct, then the onset of D_1/D_2 deformation would have begun ~97 Ma, based on the detrital zircon analysis of Barth et al. (2004).

Salem et al. (Chapter 1) determined that late stage D_3 deformation in the Big Maria and Little Maria Mountains contains evidence of both NE-directed shortening, evidenced by N and NE-vergent F_3 folds *and* E or NE-directed extension, evidenced by the dike swarm, wherein dikes are refolded about F_3 folds and weakly record S_3 cleavage. Ballard (1990) documents shear-sense indicators from the Little Maria pluton that show NE-directed extensional shear. In turn, we interpret that D_3 is contemporaneous with Late Cretaceous magmatism, based on local mylonitization of the Little Maria pluton (Ballard,

1990) and similar granitoid rocks (Howard, 2002) and overprinting of the Cretaceous leucogranite dike swarm by D_3 deformation fabrics documented in the Little Maria Mountains (Salem et al., 2006). This interpretation that widespread shortening and synconvergent extension was coeval with magmatism is consistent with findings of many other workers (e.g. Hodges and Walker, 1992; Howard, 2002; Wells et al., 2005). We also interpret that D_3 deformation significantly modified earlier structures in the Maria Fold and Thrust Belt and that this event is responsible for exhumation of MFTB middle crustal terrane, indeed lower crustal rocks of the Sevier hinterland itself.

In the supracrustal McCoy Mountains to the south, we interpret that the pervasive north-dipping cleavage fabric was formed by south-directed shortening. Furthermore, we interpret that the Maria Frontal Thrust, which separates the Little Maria from the McCoy Mountains, is a major D_3 south-directed thrust. Initial fabric development may have begun with the onset of D_1/D_2 deformation (southeast-directed transpression). Intensity of deformation in the McCoy Mountains is observed to decrease south and further away from the proposed location of the Maria Frontal Thrust. Stone (2006) interpreted that there was no major tectonic contact that separated rocks in the Little Maria Mountains and Palen Pass area from supracrustal rocks exposed in the McCoy and Palen Mountains to the south. Instead, he interprets that the Big Maria-Little Maria syncline and an anticline pair are correlative to a syncline-anticline pair observed in the Palen Pass area. We argue, however, that Big Maria-Little Maria syncline cannot be the same syncline as observed in the Palen Pass area based on different kinematics of formation of the Big Maria-Little Maria syncline compared with fabric development in the McCoy Mountains and in contrasting style of deformation and degree of metamorphism. We present our data and discuss these lines of evidence in more detail in the next section. All rocks in the Big Maria-Little Maria syncline have been subjected to polyphase deformation and amphibolite grade metamorphism. In contrast, rocks in the McCoy Mountains are characterized by predominately brittle deformation and are observed to passively record a pervasive north-dipping cleavage that dips at high angles opposite to bedding, in contrast with rocks in the Big Maria and Little Maria Mountains, in which foliation is subparallel

with original bedding and that contain evidence of high degrees of ductile deformation. We further interpret that D_3 deformation represents exhumation of the middle crustal MFTB channel over the supracrustal McCoy Basin. Most regional evidence indicates that D_3 deformation, which contains evidence of synconvergent extension, exhumed the middle crustal Sevier hinterland and was coeval with peak metamorphic conditions in the region and widespread Cretaceous magmatism. Analysis of the quartz veins from the northern McCoy Mountains indicate a strain field that has been rotated clockwise from the D_3 stress field indicated by the leucogranite dikes in the Big Maria Mountains. We interpret that this stress field was formed as a result of Mule Mountains thrusting, which in all likelihood represents a late stage backthrust during D_3 deformation.

Palen Pass

Structural overview

Figure 2.21 shows our inset map at 1:12,000 scale of the Palen Pass area. Here one can observe the supracrustal McCoy Basin juxtaposed across high-angle faults with the middle crustal Maria Fold and Thrust Belt and a large Late Cretaceous granitic pluton, all in an area less than 5 km wide north to south. These Mesozoic tectonic features are overprinted by numerous brittle Cenozoic normal and right lateral faults. The Palen Pass area separates the Granite Mountains in the north from the Palen Mountains in the south. Plate 4 is a cross section from the middle of the Granite Mountains to the southern end of the range. Figure 2.22 is a field photograph taken looking east that shows the basic architecture of the southern Granite-northern Palen Mountains. The basic architecture of the Granite-Palen Mountains consists of the Late Cretaceous Granite Mountains pluton at the north end that is separated from Palen Pass by the Riverside-Maria-Granite (RMG) detachment fault. Part of this fault constitutes the Breakaway to the Colorado River Extensional Corridor (Howard and John, 1987; Wells et al., 2005). Total displacement on

this fault is unknown, but is assumed to be on the order of kilometers (Hamilton, 1987). The Granite Mountains Foliation is observed to strike generally NNW and dip ENE or WSW (Stone and Kelly, 1989) and represents local mylonitization of the Granite Mountains pluton. From the southwestern end of the Granite Mountains, the Palen Mountains, including the pass, trend almost due south for another 20 km, where they are detached from the McCoy Mountains from the east and the Coxcomb Mountains in the west by large extensional grabens. The Palen Mountains have an unusual “gourd shape” morphology. They are approximately 15 km wide at the southern end and narrow to less than 5 km wide in the central part of the range before widening again at the Palen Pass area to approximately 10 km (Figure 2.2). Palen Pass consists primarily of Paleozoic and Mesozoic metasedimentary rocks that have been intruded by Jurassic plutons. Numerous gypsum prospects may be found in the area of Palen Pass near the contact between the upper Buckskin Formation and the Kaibab Marble. A kilometers long fault zone that trends roughly east-west through Palen Pass separates two distinctly different structural domains. We interpret here that this fault represents the Maria Frontal Thrust. However, resolving kinematics on this fault proved to be difficult due to extensive overprinting of the fault by Cenozoic normal and right lateral faults (Figure 2.21). North of the fault, Paleozoic and Triassic metasedimentary rocks are intruded extensively by Jurassic plutons. Paleozoic rocks are preserved as roof pendants are expressed as pods and lenses rather than as laterally continuous units. However, Paleozoic and Mesozoic rocks are observed to be preserved in their correct stratigraphic order, defining a domain of ghost stratigraphy, with Paleozoic rocks “swimming” in a sea of Jurassic plutonic rocks (Figure 2.23). These rocks are characterized by a pervasive north-dipping foliation, S_1 , which trends subparallel with unit contacts and relict sedimentary structures (i.e., original bedding) and crosscuts contacts between Paleozoic rocks and Jurassic plutons (Figure 2.24). This north-dipping foliation is similar to that observed in the Big Maria and Little Maria Mountains and represents transposed bedding.

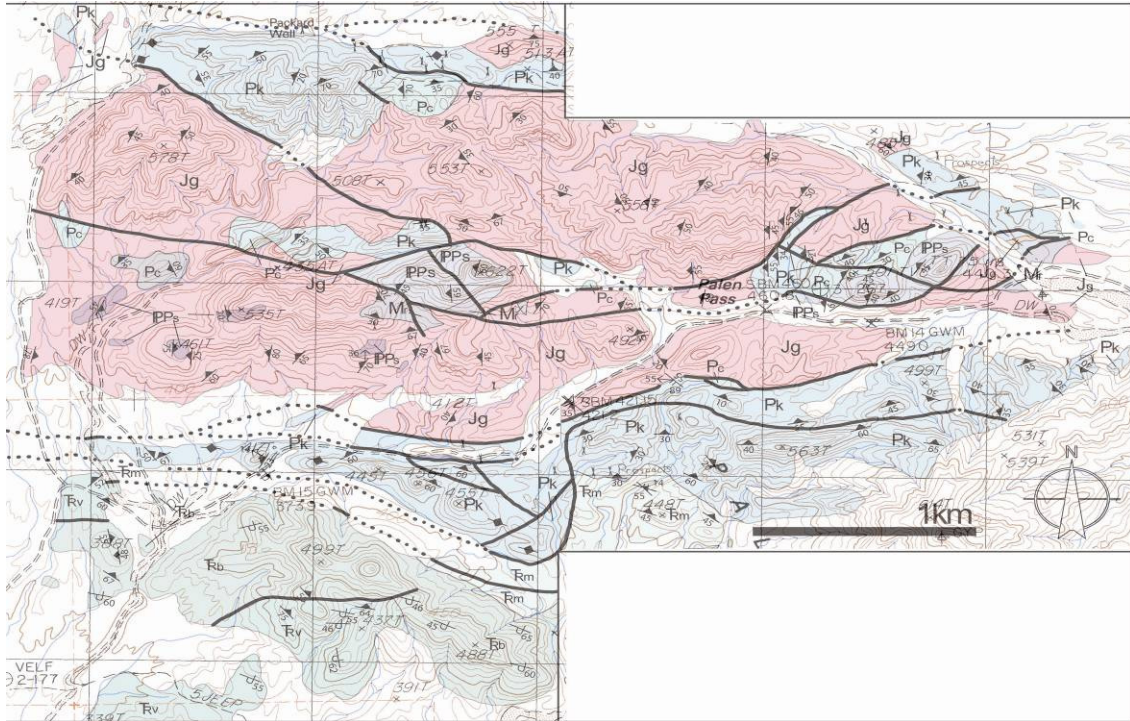


Figure 2.21: Inset geologic map of the Palen Pass area, originally mapped at 1:12,000 scale. Structural domains II and III shown on map.

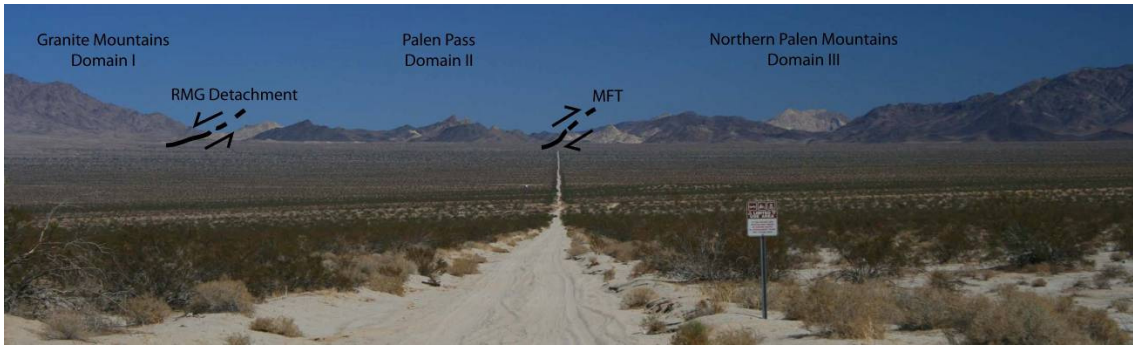


Figure 2.22: Field photograph looking east toward Palen Pass showing the basic architecture of the northern Palen Mountains and spatial location of structural domains. Abbreviations: RMG (Riverside-Maria-Granite), MFT (Maria Frontal Thrust). Photo: L.J. Crossey.



Figure 2.23: Field photograph taken looking north at Jurassic granite (Jg) intruding Kaibab Marble (Pk) and Supai Formation (Ps). Units are offset by northwest-trending normal fault (heavy black line). Photo: L.J. Crossey.



Figure 2.24: Field photograph taken looking northwest at intrusive contact between foliated Jurassic granite (Jg) and Supai Formation (Ps). Dikes from granite have been involved in isoclinal F_1 folds. Photo: L.J. Crossey.



Figure 2.25: Field photograph taken looking north at F_1 isoclinal folds with S_1 axial plane cleavage (shown in white) from the Supai Formation, Domain II, Palen Pass area. Photo: L.J. Crossey.

S_1 is axial plane cleavage to isoclinal F_1 folds (Figure 2.25); similar to what is observed in the Big Maria Mountains. Mesoscopic F_1 folds are best expressed in the Kaibab Marble, as alternating chert, calc-silicate and carbonate layers help to define structures. Also, elongate minerals, such as wollastonite and muscovite, define a mineral lineation on S_1 , which is also similar to what is observed in the Big Maria Mountains. The stratigraphic order of these rocks is right side up, with the Mississippian Redwall Marble, the oldest unit, found in the south and the Triassic Moenkopi Formation observed in the north just below the RMG detachment. These observations are similar to what is observed in the Big and Little Maria Mountains, confirming that the Maria Fold and Thrust Belt extends out to the Palen Mountains. However, the Palen Pass area represents the western terminus of the Maria Fold and Thrust Belt. The Coxcomb Mountains pluton intrudes into the McCoy Mountains Formation in the Coxcomb Mountains and likely overprints earlier structures and rocks from the Maria Fold and Thrust Belt.

South of the fault, Late Permian through Jurassic rocks are observed in a continuous north-dipping stack in inverted, stratigraphic order. The Permian Kaibab Marble is the oldest unit exposed south of the fault and is immediately adjacent to it. The Kaibab Marble and Moenkopi Formation resemble their counterparts observed north of the fault. These formations contain an S_1 fabric that is subparallel to original bedding and isoclinal folds are expressed well in the Kaibab Marble (Figure 2.26). Additionally, the Kaibab records brittle compressive deformation as well. Figure 2.27 shows a series of imbricate, brittle, minor south-vergent thrusts that overprint earlier ductile fabrics. These rocks also contain a well expressed, second north-dipping cleavage fabric. However, continuing upsection Mesozoic rocks begin to resemble their respective protoliths further to the south.

Additionally, with the exception of the Moenkopi and Kaibab Formations, most deformation observed in Mesozoic sedimentary rocks may be characterized as brittle in nature. Furthermore, these rocks record a pervasive north-dipping cleavage, similar to that observed in the McCoy Mountains to the east.



Figure 2.26: Field photograph looking northwest at complex F_1 isoclinal folds with northwest-dipping S_1 axial plane cleavage in the Kaibab Marble, Domain III, Palen Pass area. Photo: L.J. Crossey



Figure 2.27: Field photograph looking west at imbricate set of minor, brittle, south-vergent thrust faults offsetting folded layers in the Kaibab Marble, Domain III, Palen Pass area. Geologist B. MacFarlane for scale. Photo: L.J. Crossey.

Rocks are folded in a major syncline-anticline pair. On the southern limb of the anticline rocks are folded around into a right side up, south dipping stratigraphic succession. Jurassic-Cretaceous McCoy Mountains Formation is deposited on top of Jurassic volcanic substrate. All formations, from Late Triassic through Cretaceous, are observed to dip south and contain a pervasive north-dipping cleavage.

There is approximately 4500 m of McCoy Mountains Formation exposed in the Palen Mountains, unlike >7300 m exposed in the type section. The entire Siltstone Member is missing in the southern Palen Mountains, perhaps due to truncation by the Mule Mountains Thrust at the south end of the basin. Similarly, more of the underlying substrate of the McCoy Basin, including sedimentary rocks of Triassic and Permian age, is exposed in the northern Palen Mountains, whereas these rocks are not exposed in the northern McCoy Mountains due to truncation by the Maria Frontal Thrust at the north end of the basin. Like the McCoy Mountains, the southern end of the Palen Mountains contains the leading thrust of the Mule Mountains Thrust. Also, like the McCoy Mountains, rocks in the footwall of the Mule Mountains Thrust are folded into a north vergent syncline and a south-dipping cleavage is locally expressed at the southern end of the range. Finally, volcanic rocks and lower McCoy Mountains Formation, contained in the hanging wall of the thrust, have been emplaced over upper McCoy Mountains Formation.

Domain analysis

The Palen Pass area is divided into three structural domains. Domain I encompasses the Granite Mountains north of the RMG detachment fault (not to be confused with the Granite Mountains northwest of the Coxcomb Mountains). Domain II encompasses the Palen Pass area north of the Maria Frontal Thrust. Domain III encompasses the area south of the Maria Frontal Thrust to the south end of the Palen Pass 7.5' quadrangle. Data from Domain I and III were sourced from the published map of the Palen Pass 7.5' quadrangle (Stone and Kelly, 1989).

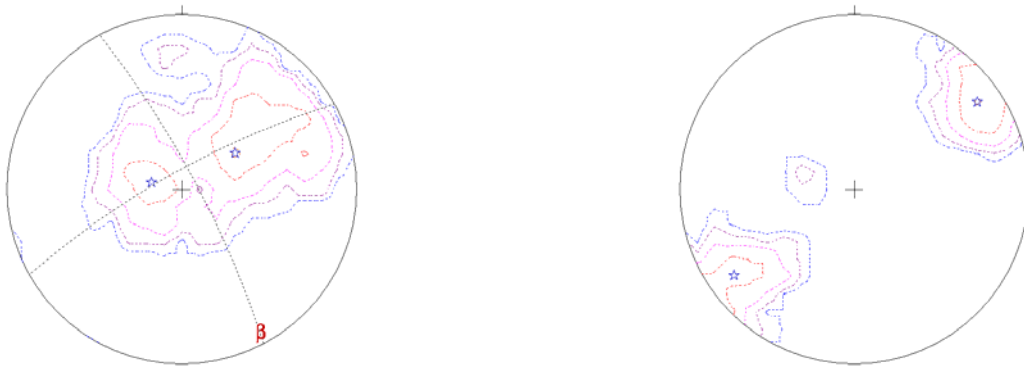


Figure 2.28: Equal-area lower hemisphere projection stereonet point density contour plots of A) poles to S_1 ($N = 132$) and B) mylonitization lineation ($N = 57$) from the southern Granite Mountains, Domain I, Palen Pass area. Point density contour plot of S_1 shows two maxima, one at $146, 30^\circ\text{W}$ and the other at $010, 16^\circ\text{E}$ (blue stars, fig. A), which are interpreted to be two limbs of a broad antiform. Poles to S_1 define a best-fit great circle girdle of a macroscopic fold plunging 8° toward 151 (red letter beta, fig. A). Fold axial plane determined manually to have an orientation of $330, 83^\circ\text{W}$. Point density contour plot of lineation shows two maxima, one at 17° toward 235 and the other at 14° toward 055 (blue stars, fig. B).

Figure 2.28 shows a lower hemisphere equal area point density contour plot of poles to S_1 foliation from the Granite Mountains pluton in Domain I (see Table 2.5 for data). The point density contour plot shows two maxima for S_1 orientation, one at 146, 30°W and the other at 010, 16°E. We interpret that these two maxima represent the mean orientations of two limbs of a broad, northwest trending antiformal dome (Figure 2.29), which is asymmetric, nearly upright, and has an interlimb angle of ~130°. The fold is asymmetric with respect to the western limb being slightly more inclined than the eastern limb. Poles to S_1 define a best-fit great circle girdle with a macroscopic fold axis that plunges shallowly to the southeast (8° toward 151). To determine the axial plane of the fold, a great circle was manually fit to the stereonet plot that passes through the statistically determined beta axis and intersects the great circle girdle at 90°. The orientation of the axial plane was determined to be 330, 83°W. Figure 2.28b shows an equal area point density contour plot of mineral lineation from the pluton. The contour plot defines two maxima for orientation of the stretching lineation (shown as blue stars), one at 17° toward 235 and the other at 14° toward 055. These lineation maxima are nearly equal and opposite to each other and are oriented symmetrically on a NE-SW trending axis and are depicted schematically on Figure 2.29. Lineations are down-dip on their respective limbs.

We interpret the Granite Mountains pluton to represent a Cretaceous metamorphic core complex, based on our interpretation of the structural data compiled by Stone and Kelly (1989). The lineation measurements show low angle extension directed along a NE-SW axis and both lineation and S_1 are associated with mylonitization of the pluton (Stone and Kelly, 1989). This low angle extension allowed for unroofing and exhumation of the pluton. The Granite Mountains pluton is part of a belt of Late Cretaceous magmatism observed in the region. The leucogranite dike swarm of the western Big Maria Mountains is broadly correlative with the Granite Mountains pluton and other Late Cretaceous plutons in the area, which were largely emplaced beginning at ~90 Ma and reaching a peak between 82-72 Ma (Barth et al., 2004; Miller et al., 1982; Foster et al., 1992, Wells et

Table 2.5: Structural data from Domain I, southern Granite Mountains, Palen Pass area. From Stone and Kelly (1989)

S1 Foliation				L1 Lineation	
272,65,S	315,35,S	340,35,W	322,70,W	00,060	70,284
340,45,W	300,60,S	310,35,S	327,40,W	05,053	70,270
060,35,S	295,45,S	327,35,W	313,45,W	05,050	45,220
084,70,S	330,20,W	303,70,S	340,65,W	20,032	45,225
035,10,E	280,25,S	330,55,W	305,25,N	5,062	10,230
060,30,S	286,20,S	338,60,W	335,60,W	30,057	15,242
060,40,S	348,25,W	325,70,W	345,55,W	15,057	10,060
033,10,E	315,20,S	315,70,S	340,30,W	15,050	30,230
030,15,E	325,25,S	315,25,S	325,60,W	20,052	30,225
015,35,E	322,40,S	325,75,W	315,45,W	10,233	15,070
045,25,S	035,25,E	324,50,S	359,10,W	35,050	5,048
009,35,E	307,30,S	322,65,S	325,40,W	30,049	5,238
038,25,S	050,45,N	320,55,S	023,25,W	5,229	10,053
320,15,E	290,30,S	325,30,S	300,10,N	20,060	5,033
358,25,E	336,40,W	334,40,W	007,45,W	10,056	15,055
085,15,S	290,15,S	322,70,W	345,35,W	5,049	5,045
040,25,S	320,30,S	355,65,W	040,35,E	5,046	15,060
352,40,E	067,40,S	345,55,W	022,25,E	30,235	20,060
342,35,E	087,40,S	320,70,W	045,20,N	30,235	25,065
355,05,W	315,20,S	310,45,S	017,15,E	15,215	5,055
010,30,E	320,55,S	345,30,W	015,15,E	20,260	10,045
346,15,E	338,75,W	340,50,W	090,25,N	15,240	15,065
018,15,E	352,65,W	300,80,S	018,20,N	15,235	10,045
020,10,E	340,85,W	060,20,N	060,25,N	20,232	25,060
038,15,E	330,70,W	340,65,W	030,35,E	25,235	10,063
339,30,W	305,70,S	325,40,W	330,20,N	30,230	
325,30,S	300,80,S	310,45,W	305,25,N	15,245	
356,20,W	343,75,W	315,45,W	020,10,E	25,230	
305,60,S	350,70,W	312,60,S	357,15,E	40,230	
292,55,S	307,70,S	008,35,W	335,15,E	10,234	
285,65,S	350,65,W	308,50,S	315,10,E	25,230	
294,35,S	340,70,W	357,50,W	317,25,E	55,288	
086,65,S	310,55,S	313,55,S	300,10,N		

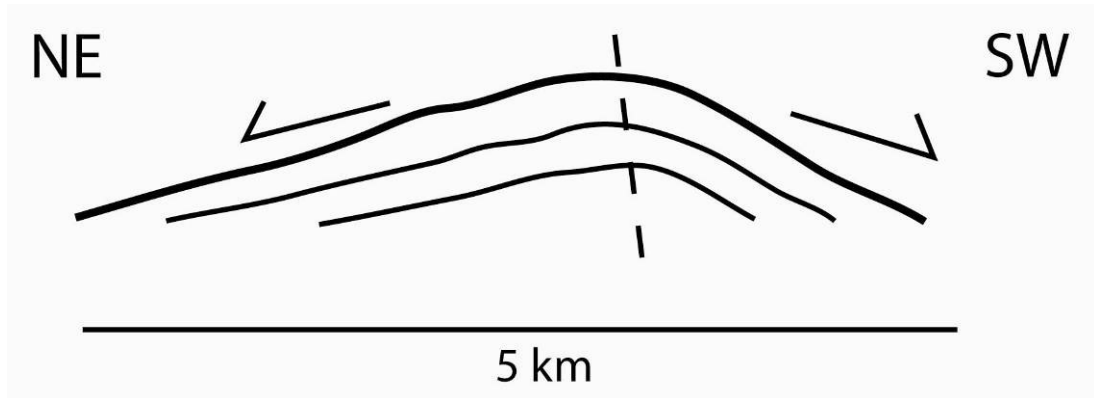


Figure 2.29: Schematic cross-sectional sketch looking down-plunge at broad antiform in the Cretaceous granite in the southern Granite Mountains, Domain I, Palen Pass area. Geometry of the antiform is constrained by structural data plotted graphically in Figure 28. Arrows show orientation of mylonitization lineation. We interpret the Granite Mountains antiform to represent the lower plate of a Cretaceous metamorphic core complex formed by NE-SW-directed extension.

al, 2002; 2005). Since the dike swarm and the pluton were emplaced during the same episode of magmatism, it is expected that they should share common structural features. An analysis of the dike swarm done by Salem et al. (Chapter 1) indicates that the direction of maximum tensional stress, σ_3 , was 29° toward 258, or ENE-directed extension, during emplacement of the dike swarm. This is in good agreement with the extension direction determined for the Granite Mountains metamorphic core complex and tends to support the hypothesis that widespread Cretaceous plutonism was accompanied by east or northeast-directed extension in the Sevier hinterland. Additionally, Salem et al. (Chapter 1) determined that the dikes were weakly refolded about a southeast plunging fold axis (25° toward 153), which is also in good agreement with the plunge of the Granite Mountains antiform. Finally, Salem et al. (Chapter 1) documented that development of a southwest-dipping cleavage (S_3 in the Big Maria Mountains) is more strongly expressed in proximity to the leucogranite dike swarm. This observation plus the observation that the leucogranite dikes locally record the S_3 fabric in the Big Maria Mountains indicated that D_3 deformation in the Big Maria Mountains and emplacement of the dike swarm were coeval. In the Big Maria Mountains, the determined mean orientation of S_3 from direct measurement was $328, 66^\circ W$. This is in excellent agreement with the determined orientation of the axial plane of the Granite Mountains antiform. We therefore conclude that the Granite Mountains metamorphic core complex formed during Late Cretaceous northeast directed extension and is correlative with plutonism associated with D_3 deformation in the Big Maria Mountains.

Domain II consists of the area in the footwall of the RMG detachment and in the hanging wall of the Maria Frontal Thrust. In this area, structures correlative to Maria Fold and Thrust Belt style deformation are confined in a narrow zone (see Figure 2.2). This is likely due to intrusion of the Granite Mountains pluton, which overprints the northern portion of the Maria Fold and Thrust Belt. This area represents the western terminus of the MFTB. The belt of deformed middle crustal Paleozoic and Mesozoic strata is picked up again further northwest in the Old Woman and Piute Mountains (Figure 2.1). In Domain II, Paleozoic and Mesozoic metamorphic rocks, correlative to those observed in

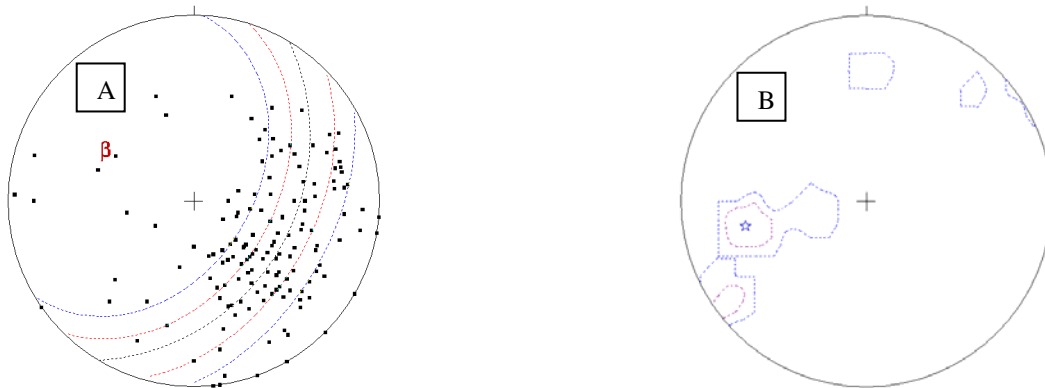


Figure 2.30: Equal area lower hemisphere projection stereonet plots of A) poles to S_1 ($N = 161$) and B) point density contour plot of mineral elongation lineation ($N = 13$) from Domain II, Palen Pass area. Poles to S_1 define a best-fit great circle girdle of a macroscopic F_2 fold axis that plunges 43° toward 302 (red letter beta). Red and blue small circles are 10 and 20° from best-fit girdle. Folding is non-cylindrical. Point density contour plot shows a maximum orientation of lineation plunging 34° toward 259 (blue star).

Table 2.6: Structural data from Domain II, above Maria Frontal Thrust, Palen Pass area. Some data from Stone and Kelly (1989)

S1/S2 Composite Foliation				L1 Lineation
075,25,N	040,50,N	330,40,W	080,85,N	25,045
350,30,E	045,55,N	022,60,W	315,50,N	5,240
043,25,N	090,75,N	060,30,N	330,50,W	10,050
055,45,N	012,50,W	042,30,N	352,65,W	65,265
042,35,N	000,45,W	330,35,W	030,40,E	20,260
038,35,N	005,90,W	295,50,N	282,30,N	10,235
090,20,N	030,90,W	070,55,N	040,65,N	40,258
055,55,N	305,45,S	070,50,S	335,75,W	65,250
070,25,N	040,30,N	063,55,N	003,80,W	36,000
053,35,N	045,70,N	335,50,W	016,78,E	21,005
032,15,N	050,40,N	322,45,W	043,67,W	24,230
053,40,N	035,45,W	011,40,W	055,77,W	37,260
060,30,N	030,50,N	010,40,W	082,90,N	35,250
027,65,W	060,40,N	015,50,W	060,90,N	
005,50,W	070,90,N	035,40,W	030,70,W	
020,45,W	040,55,N	358,55,W	021,40,W	
330,50,S	343,35,W	010,40,W	347,67,W	
330,45,S	055,50,N	000,45,W	010,90,W	
015,35,W	020,20,W	042,50,W	035,65,N	
340,65,W	062,75,N	310,60,N	340,70,W	
015,20,W	035,55,N	008,30,W	030,40,W	
030,30,N	045,35,N	075,45,N	077,60,N	
075,40,N	335,60,W	330,35,W	282,58,N	
050,25,N	018,45,E	030,40,W	002,86,E	
060,25,N	000,75,E	055,30,N	245,30,N	
040,55,N	008,25,W	032,45,W	205,50,N	
320,65,W	072,40,S	015,20,W	005,70,W	
310,55,S	045,90,N	347,70,W	044,46,N	
330,45,W	043,60,N	325,90,N	014,55,W	
340,65,W	000,15,W	317,40,W	355,34,W	
350,50,W	347,20,W	010,80,W	352,55,W	
350,50,W	065,50,N	327,20,E	354,27,W	
290,50,W	048,35,N	070,40,N	040,70,N	
315,45,S	070,50,N	030,65,W	070,40,N	
040,40,N	072,50,N	015,70,W	027,40,W	
050,50,N	355,70,W	030,70,W	345,70,W	
050,55,N	078,35,N	342,50,W	334,70,W	
043,30,N	084,90,N	020,60,W	354,72,W	
047,60,N	090,75,N	355,65,W	055,74,N	
047,55,N	080,70,N	000,50,W	225,70,N	
070,40,N	292,70,N	000,45,W	169,70,W	

the Big and Little Maria Mountains, are highly deformed and metamorphosed. Figure 2.30a shows a lower hemisphere equal area projection plot of poles to S_1 from Domain II. Poles to S_1 define a best-fit great circle girdle of a mesoscopic F_2 fold axis that plunges 44° toward 302 (see Table 2.6 for data). Small circles in red and blue show small circle plots 10 and 20° from the best-fit great circle girdle. Based on this analysis, folding in this particular area might be classified as non-cylindrical (Ramsay and Huber, 1987), as less than 90% of points fall within 20° from the best-fit girdle. Mean orientation of S_1 from the stereonet plot is $206, 24^\circ W$. Figure 2.30b shows a lower hemisphere equal area point density contour plot of mineral elongation lineation (L_1) from Domain II. The contour plot shows a maximum concentration of lineation measurements plunging 34° toward 259 .

We interpret the mesoscopic F_3 fold at Palen Pass defined by refolding of S_1/S_2 composite foliation to be equivalent to folds formed during D_3 deformation in the Big and Little Maria Mountains based on similar fold geometry. Salem et al. (Chapter 1) determined F_3 fold axes plunge predominately to the northwest (28° toward 301) which, while somewhat shallower, is in excellent agreement with the beta axis determined for Domain II in the Palen Pass area. It is also noted that in the western Big Maria Mountains (Area C of Chapter 1), F_3 folds are apparently non-cylindrical. This is likely because D_3 deformation is non-coaxial and because the aerial extent of domains selected for analyzing F_3 refolds is too large. Thus, several F_3 folds could be represented on a single stereonet plot, thus creating sufficient interference as to make F_3 folds appear non-cylindrical. Ultimately, the similarity of the trend and plunge of F_3 fold axes in two different areas approximately 50 km away from each other is clear indication that D_3 deformation is pervasive and covers a large aerial extent. Since mesoscopic folds are correlative with D_3 structures in the Big Maria Mountains and because the Granite Mountains antiform and refolding of the leucogranite dikes in the Big Maria Mountains are also interpreted as being D_3 structures, an important problem to address is the difference in plunge direction. Recall that the Granite Mountains antiform and the leucogranite dikes are folded about shallowly SE-plunging fold axes, whereas F_3 folds in

Paleozoic and Mesozoic metasedimentary rocks in Palen Pass and the Big Maria Mountains and Palen Pass are refolded about NW-plunging axes. To account for this, we submit that the geometry of D_1/D_2 deformation in Paleozoic and Mesozoic rocks controlled the geometry of subsequent F_3 refolding; this hypothesis is suggested for similar refolding geometries observed in the Old Woman and Piute Mountains (Fletcher and Karlstrom, 1990). We submit that prior to F_3 refolding, Paleozoic and Mesozoic rocks were already dipping $\sim 30^\circ$ to the north as the result of progressive, polyphase non-coaxial deformation as the result of SE-directed reverse and dextral shear (Salem et al., 2006; Chapter 1). This refolding accounts for variability in the orientation of S_1 in the Palen Pass area. Dip values for S_1 which range in value from $15-90^\circ$ and generally dip north and west and strike values are locally highly variable. As discussed above, we interpret that D_3 deformation in the Maria Fold and Thrust Belt is associated with Late Cretaceous plutonism and that these structures formed as a result of east or northeast directed extension.

Domain III consists of the area south of the Maria Frontal Thrust to the southern edge of the Palen Pass 7.5' x 7.5' quadrangle. Data for domain analysis were collected in the field and joined with previously published map data (Stone and Kelly, 1989). The Permian Kaibab Marble is the oldest unit exposed in this domain and volcanic rocks of the Jurassic Dome Rock Sequence are the youngest. The Maria Frontal Thrust strikes through a complicated and heavily fractured fault zone. The frontal thrust is observed to strike east west. Two measurements along the thrust indicate that the fault dips north at about 40° . Vertical displacement along the Maria Frontal thrust is estimated to be approximately 1 km at Palen Pass, with sense of motion top-south. Also present is one of the most complete, weakly deformed and metamorphosed sections of Mesozoic stratigraphy anywhere in the Maria Fold and Thrust Belt-McCoy Basin terrane. The area is dominated by the roughly east-west trending Palen Pass syncline (Stone and Kelly, 1989). Based on differences in overall structural styles as described above and in the previous section on the northern McCoy Mountains, we interpret that Domain III encompasses the supracrustal McCoy Basin tectonic province. Figure 31a shows an equal

area lower hemisphere plot of poles to S_0 from Domain III from the Triassic upper Buckskin and Vampire Formations and the Jurassic Aztec Quartzite (see Table 2.7 for data). Poles to S_0 define a best-fit great circle girdle for a mesoscopic fold axis that plunges 4° degrees toward 295 . The mean orientation of S_0 is $293, 57^\circ\text{N}$. Although the direction of plunge is nearly similar to the mesoscopic F_2 fold axis observed in Domain II, the fold is nearly horizontal. Based on the stereonet plot, folding is non-cylindrical. Figure 31b shows an equal area lower hemisphere plot of poles to S_1 , which represents transposed bedding in the Permian Kaibab Marble and from the Triassic lower Buckskin Formation from Domain III. Poles to S_1 define a best-fit great circle girdle for a mesoscopic fold axis that plunges 16° toward 293 . Although slightly steeper, this fold axis has a similar orientation to the refolding of S_0 and likely represents the same structure. The mean orientation of S_1 determined from the plot is $273, 40^\circ\text{N}$, which is shallower than and strikes 20 degrees counterclockwise from S_0 . This can be accounted for because these are measurements taken in different formations. Overall, both S_0 and S_1 strike roughly east-west and dip northward and are folded around a sub-horizontal to slightly northwest plunging fold axis.

The mean orientation of S_1 is consistent with observed measurements of the Maria Frontal Thrust at Palen Pass, with both the fault and the overturned Kaibab and Buckskin Formations dipping approximately 40° to the north, sympathetic with the dip of the fault. As such, we interpret that the Palen Pass syncline is a south-vergent syncline that formed as the result of drag at the foot of the ductile Maria Frontal Thrust, which is a south-directed reverse fault. The syncline thus formed as a result of south-directed shortening, and has a fold axis that is nearly perpendicular to shortening, based on the composite orientation of S_0/S_1 . In contrast, the Big Maria-Little Maria syncline, which was formed as the result of top-southeast directed shortening (Salem and Reynolds, 2005; Chapter 1), has a fold axis that has been rotated nearly parallel with the direction of tectonic transport as the result of simple shear and ductile crustal flow. Also, we do not observe moderately northwest-plunging folds correlative to those observed in Domain II. Furthermore, there

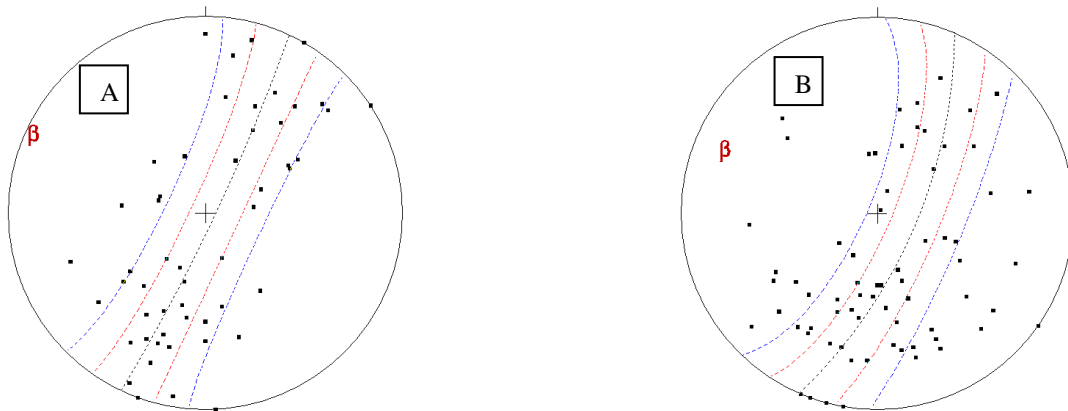


Figure 2.31: Lower hemisphere equal area projection stereonet plot of A) poles to S_0 ($N = 54$) and B) poles to S_1 ($N = 72$) from Domain III, Palen Pass area. Poles to S_0 define a best-fit great circle girdle for a macroscopic F_2 fold axis that plunges 4° toward 295 . Red and blue small circles are 10° and 20° from best-fit girdle. Folding is sub-cylindrical. Poles to S_1 define a best-fit great circle girdle for a F_2 fold axis that plunges 16° toward 293 . Folding is non-cylindrical.

Table 2.7: Structural data from Domain III, south of Maria Frontal Thrust, Palen Pass area. Some data from Stone and Kelly (1989)

S0 Original bedding		S1 Foliation		L1 Lineation
075,55,N	005,35,E	300,40,S	312,60,S	43,215
075,55,N	015,20,E	322,30,W	295,40,S	13,005
055,40,N	290,70,N	070,25,N	315,40,S	53,001
090,80,S	290,70,N	020,35,W	295,65,S	25,300
320,70,W	285,80,S	300,40,S	282,45,S	10,282
320,60,E	300,60,S	290,30,S	290,50,S	20,115
020,20,E	070,25,S	065,55,N	320,45,E	24,330
300,25,S	317,70,W	075,60,N	330,50,E	26,247
070,20,N	310,50,S	280,65,N	315,60,E	24,320
090,55,N	300,90,S	075,65,N	300,20,N	33,243
320,45,N	327,90,W	085,40,N	082,25,S	
295,25,N	080,40,N	295,40,N	043,52,N	
310,25,N	285,60,N	322,20,N	315,75,W	
287,30,N	340,62,N	090,30,N	305,60,N	
322,40,E	090,46,N	300,60,N	294,10,S	
284,40,N	173,20,W	020,30,W	225,58,S	
280,45,N	294,84,N	070,30,N	312,02,W	
293,45,N	280,84,N	087,30,N	030,23,N	
300,65,N		310,45,N	280,90,N	
290,60,N		292,45,N	065,65,N	
289,55,N		285,60,N	325,50,W	
300,50,N		286,30,N	065,60,N	
087,90,N		280,45,N	020,64,W	
295,60,N		273,35,N	355,55,E	
280,50,S		293,90,N	350,49,W	
330,45,W		290,90,N	080,47,N	
337,25,W		290,60,N	300,57,N	
300,40,S		300,60,N	083,57,N	
310,60,S		080,60,N	070,38,N	
310,40,N		282,35,N	352,67,W	
290,90,N		088,25,S	040,66,N	
280,70,S		285,60,N	048,68,N	
295,50,S		285,90,N	318,75,E	
330,40,W		030,40,N	327,53,E	
045,30,E		035,90,N	285,42,N	
332,40,W		040,50,E	274,64,N	

is no evidence to suggest that the Palen Pass syncline has been refolded by later deformation events in contrast with rocks in the Maria Fold and Thrust Belt. The mean orientation of S_1 is in good agreement with S_1 from the northern McCoy Mountains. Additionally, in contrast with the Big Maria-Little Maria syncline, most rocks involved in the Palen Pass syncline did not undergo polyphase deformation and high grade metamorphism. Rocks in both the upper and lower limb of the Big Maria-Little Maria syncline record evidence of 1) southeast-directed reverse and ductile shear, 2) upper greenschist-lower amphibolite grade metamorphism and 3) extensive refolding of earlier ductile deformation fabrics. In contrast, most rocks in Domain III, except for the Kaibab and lower Buckskin Formation are weakly metamorphosed, do not contain evidence for crustal scale southeast-directed shearing and only exhibit one generation of folding. Thus the interpretative cross section made by Stone (2006), which suggests that the Big Maria-Little Maria syncline and the Palen Pass syncline are the same structure, and which does not depict the Maria Frontal Thrust is refuted by our observations. The two synclines have clearly different kinematic origins and each deformed rocks at different crustal levels.

If it is not the same structure as the Big Maria syncline, then what generation of folding does the Palen Pass syncline represent? Here we make the case that the Palen Pass syncline formed in the same strain field as the north-dipping S_1 cleavage in the McCoy Mountains to the west. The inferred axial plane of the syncline and the orientation of S_1 from the northern McCoy Mountains are in excellent agreement with each other and represent structures/fabrics formed as a result of south-directed shortening. As discussed in the previous section on the McCoy Mountains, structures formed by north-south directed shortening are consistent with the strain field determined for D_3 deformation by analysis of the leucogranite dikes in the Big Maria Mountains. Therefore, we determine that the Palen Pass syncline, likewise the Maria Frontal Thrust, formed as the result of D_3 deformation on a regional scale. Based on this, formation of the Palen Pass syncline must post-date D_1/D_2 deformation exhibited in rocks in Domain II and must instead have formed syntectonically with Cretaceous plutonism and with peak metamorphism in the

southern Mojave Desert region. This also constrains timing of formation of the Palen Pass syncline and the Maria Frontal Thrust to Late Cretaceous based on regional observations.

Regional analysis – Granite Mountains to southern Palen Mountains

Plate 4 shows a true-scale cross section line that extends from the central Granite Mountains to the southern end of the Palen Mountains, constructed from map data from Stone and Kelly (1989) and Pelka (1973) and incorporating our interpretation of deformation events in the region. The Granite Mountains pluton represents a Late Cretaceous metamorphic core complex and thus supports the hypothesis discussed above that exhumation of middle crustal rocks in the Sevier hinterland was the result of synconvergent extension that was coeval with peak metamorphism and plutonism in the area. Structural analysis of the Granite Mountains antiform and correlation of the pluton allows for correlation of this structure with D₃ deformation in the Big Maria Mountains indicating that D₃ was a significant regional deformation event. Although the Granite Mountains pluton contains a foliation fabric and zones of mylonitization, the pluton clearly crosscuts a significant portion of the Maria Fold and Thrust Belt and, based on regional correlation with the leucogranite dike swarm in the Big Maria Mountains, the Granite Mountains pluton must post-date earlier deformation fabrics observed in the northern part of Palen Pass (Domain II). These earlier deformation fabrics are correlative with those observed in the Little Maria and Big Maria Mountains to the east and indicate that these rocks were deformed by southeast-directed reverse and ductile shear and then were later refolded about folds with northwest-plunging axes related to northeast or east vergent extension that was syntectonic with peak metamorphism and Late Cretaceous plutonism. The Maria Frontal Thrust, a significant tectonic contact, places amphibolite grade polyphase deformed Paleozoic and Mesozoic sedimentary and Jurassic plutonic rocks over greenschist grade, weakly deformed and Mesozoic rocks of the McCoy Basin. This contact relationship is covered between the Little Maria and McCoy Mountains, but is exposed in the Palen Pass area, though the Maria Frontal Thrust is in an area riddled with faults, most of which are Cenozoic in age. The Palen Pass syncline is a south-

vergent drag fold that formed in the footwall of the Maria Frontal thrust and is a structure that was likely formed synkinematically with fabric development in the McCoy Mountains Formation. Although the Palen Pass syncline is not directly observed in the McCoy Mountains, the similarity in fabric orientation in the McCoy Mountains with that in the Palen Mountains suggests that at least the lower part of the McCoy Mountains Formation might be involved in the syncline and that all rocks in the McCoy Mountains Formation record at least evidence of this south-directed shortening deformation event. The direction of shortening of this south-directed deformation event is consistent with that predicted by pale strain field determined by analysis of the Granite Mountains antiform and the Cretaceous leucogranite dike swarm in the Big Maria Mountains. Therefore, the Maria Frontal Thrust and the Palen Pass syncline are D_3 structures. In the next section, we summarize structural findings for the region and discuss how folds with opposite apparent vergence can form in the same temporal strain field.

Geochronology

Overview

In this section, we present new geochronology data obtained from deformed plutonic and magmatic rocks from the Big Maria Mountains. As discussed above, geochronology data for the western half of the Maria Fold and Thrust Belt is sparse and would be useful in order to constrain the kinematics and timing of deformation in the Maria Fold and Thrust Belt. In particular, testing the hypothesis that sedimentation in the McCoy Basin represents synorogenic response to deformation in the Maria Fold and Thrust Belt would be more conclusive with better geochronologic constraints. As such, a reconnaissance study to obtain crystallization ages and cooling ages from magmatic rocks to test these hypotheses was undertaken. Initially, five samples for U-Pb zircon analysis were selected from deformed plutonic rocks assumed to be Jurassic (~160 Ma) in age and from undeformed dikes from the leucogranite dike swarm previously dated with K-Ar as 79 Ma. Because the Jurassic rocks are deformed and metamorphosed, the age of these rocks would provide lower-bound ages on the timing of D_1/D_2 deformation in the region.

Next, we selected eight samples for Ar-Ar thermochronology analysis of biotite and hornblende grains from Jurassic plutonic and volcanic rocks. Hornblende and biotite were chosen in order to constrain timing of peak metamorphic conditions (and thus synchronous D₃ deformation) in the region and ascertain the early cooling history of the rocks. Based on regional studies (Foster et al., 1992; Knapp and Heizler, 1990; Wells et al., 2002), and on Ar-Ar thermochronology from the western Big Maria Mountains (Hoisch et al., 1988), we expected that the hornblende analyses would yield Late Cretaceous (75-65 Ma) ages and that biotite analyses would yield Paleocene-Eocene ages (60-50 Ma). Figure 32 shows sample locations in the Big Maria Mountains.

Methods

Samples were collected from the Big Maria Mountains. Samples for U-Pb analysis were selected from the central part of the range in the vicinity of the Big Maria syncline. Samples for Ar-Ar analysis were collected along a northwest-southeast transect along the southwestern front of the range. Ar-Ar samples and sample clusters were spaced approximately 2-3 km apart (Figure 2.32). This was done to ascertain if there was a spatial relationship to cooling ages. A specific hypothesis we wanted to test was if there was significant variance in thermal history from rocks in the northwestern part of the range, close to the leucogranite dike swarm and in the vicinity of a proposed buried pluton (Hoisch, 1987) versus rocks further south in the range. The metamorphic isograd map of the range (Hoisch et al., 1988) shows increasing metamorphic grade from SE-NW so we expected that cooling ages of hornblendes and biotites might be older in the south and younger farther north because higher temperatures were reached during peak metamorphism.

Mineral separates for U-Pb and Ar-Ar analysis were obtained using standard heavy liquid, magnetic and hand picking methods. After mineral separation, two of the five original samples selected for U-Pb analysis had sufficient zircon content. Of the ten samples selected for Ar-Ar analysis, six had sufficient biotite and four had sufficient amounts of hornblende.

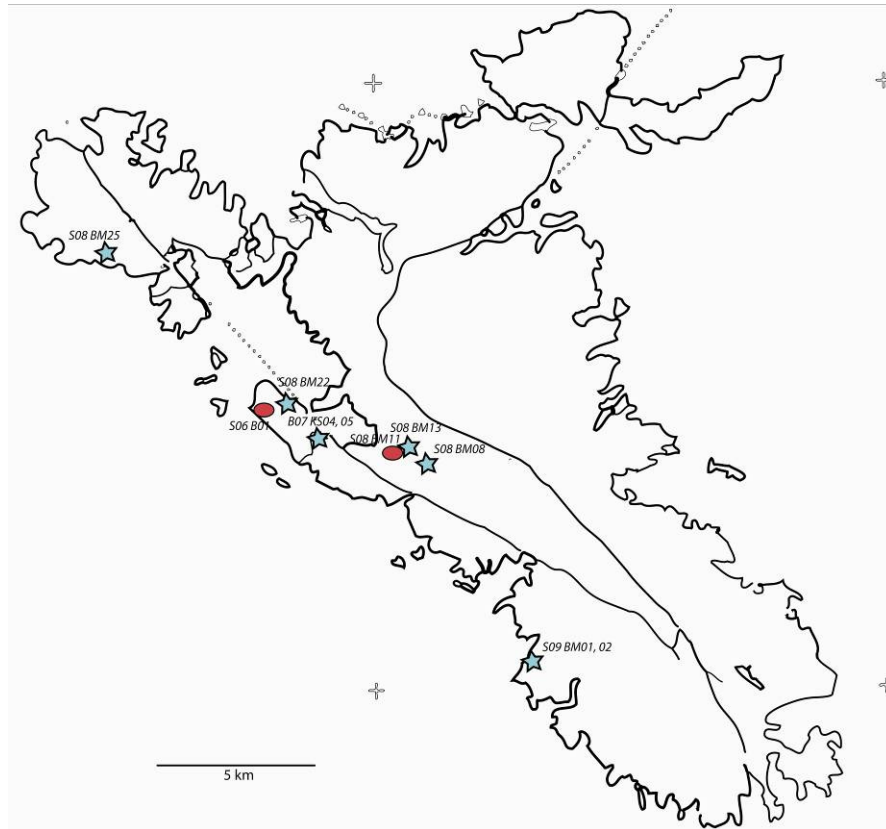


Figure 2.32: Index map of the Big Maria Mountains showing the location of U-Pb (red filled circles) and Ar-Ar (blue filled stars) samples

U-Pb zircon analysis was done using the Laser Ablation Multi Collector Inductively Coupled Mass Spectrometer (LA-MC-ICPMS) at the LaserChron Facility of the Department of Geosciences at the University of Arizona, Tucson, under the supervision of George Gehrels. This facility was selected because reliable U-Pb zircon ages (within 2σ precision or 1-2% analytic error) for magmatic samples could be acquired quickly and cost effectively. Zircon grains were hand picked and mounted for analysis following protocol described in Gehrels et al. (2008). Laser ablation of grains released U, Th and Pb from the sample and isotope analysis was done using the ICPMS. Data reduction for U-Pb samples was done using AgeCalc, an Excel spreadsheet equipped with VBA macros developed by George Gehrels. This system is fully automated to import data from Isoprobe files, perform all necessary corrections, and calculate ages, uncertainties, and error correlations. Following extraction from a set of Isoprobe files, corrections were applied for fractionation, ^{204}Pb (common lead) and U and Th corrections (Gehrels et al., 2008). Additionally, analytical error with the machine is corrected for using the error correlation is calculated following Ludwig (1980, 2003). AgePick, another Excel spreadsheet developed by George Gehrels, analyzes whether U-Pb analyses have been compromised by lead loss and overgrowth/recrystallization of metamorphic zircons. AgePick will also calculate best weighted mean average ages for magmatic samples based on $^{238}\text{U}/^{206}\text{Pb}$ ratios, and these ages are reported here. This Excel spreadsheet allows the user to quickly determine whether outliers are associated with high U concentration or high U/Th ratios, which suggests metamorphic regrowth/alteration of zircons.

Ar-Ar analysis of biotite and hornblende grains was done at the New Mexico Geochronology Research Lab at New Mexico Tech, Socorro, under the supervision of Matt Heizler. For Ar-Ar sample preparation, hornblende and biotite samples were irradiated for 8.9 hours at Texas A&M University. The standard used to monitor neutron flux in the machine was the Fish Canyon Tuff sanidine, which has an assigned age of 28.02 Ma (Renne et al., 1994). Analysis was done using the Mass Analyzer Products 215-50 mass spectrometer on-line with all metal extraction system. Samples were step heated in a molybdenum double vacuum extraction furnace. In furnace analysis, reactive gases

were removed during an eight minute heating with a SAES GP-50 getter operated at ~450°C. Additional cleanup (3 minutes) of samples was done following heating with two SAES GP-50 getters, one operated at ~450°C and one at 20°C. Gas was also exposed to a cold finger, at -140°C, during heating. The Ar-Ar facility at New Mexico Tech is equipped to provide precise and reliable Ar-Ar ages, within less than 1 Ma precision for Jurassic and Cretaceous age grains, utilizing small quantities of sample (20 mg or less). Data from the mass spectrometer are used to make age spectra diagrams, which then may be analyzed to determine ages for hornblende and biotite grains for each sample.

U-Pb zircon ages of magmatic rocks of the Big Maria Mountains

U-Pb zircon ages indicate time of crystallization for deformed plutonic rocks and thus place constraints on the timing of deformation. Figure 33a shows an age vs. U concentration plot for S06 B01, a leucocratic granite sample collected from the western Big Maria Mountains. AgePick determined a final $^{238}\text{U}/^{206}\text{Pb}$ age of 144.0 ± 2.9 Ma (MSWD = 5.5), which indicates the crystallization age of the granite, indicating a latest Jurassic age for the granite. This granite is probably correlative to plutons exposed throughout mountain ranges in southern California (Barth et al., 2007), notably the Eagle Mountains pluton (Mayo and Wooden, 1993) and is related to continued arc magmatism in the Late Jurassic (Tosdal et al., 1989) in the Mojave and Sonora Desert region. Some zircon grains yielded from this sample yielded lower ages than this cluster indicates, but these grains had high extremely high U concentrations, indicating a significant amount of Pb loss from these grains during crystallization of the granite. As such, these grains are shown on the age vs. U concentration plot, but are not highlighted. Grains that also had high U/Th ratios, which indicate metamorphic regrowth of zircons, were omitted from crystallization age determination, are shown on the plot, but are not highlighted. Inherited zircons, with ages much older than the main cluster of zircons, are also shown on the plot, but are not highlighted. Table 2.8 shows LA-ICP-MS data for all zircon grains from sample S06 B01.

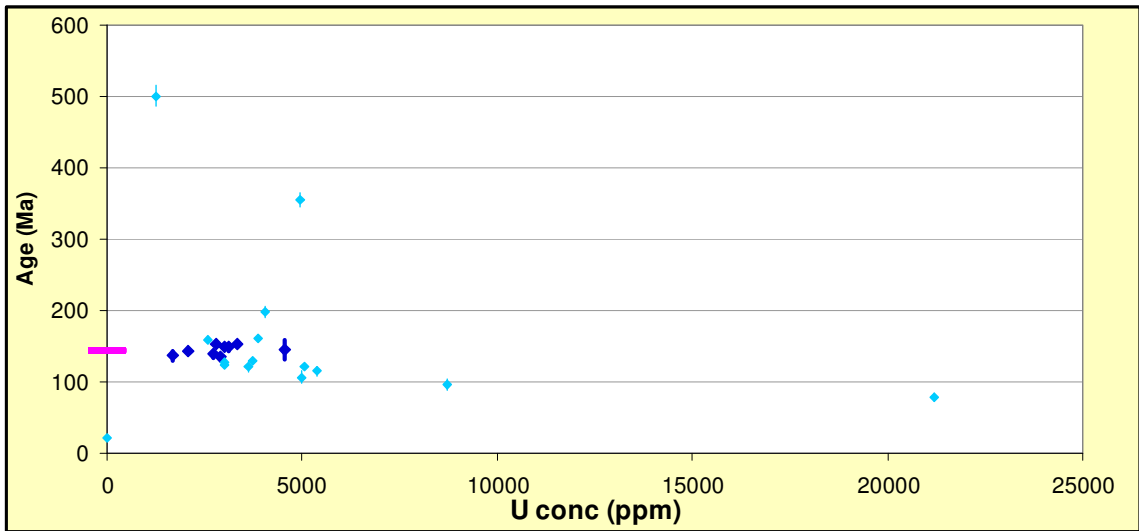


Figure 2.33: $^{238}\text{U}/^{206}\text{Pb}$ zircon ages vs. U concentration for sample S06 B01. Grains in dark blue were used for crystallization age determination. Light blue grains were omitted from age determination due to high U concentration, indicating significant Pb loss, or high U/Th concentrations, indicating metamorphic regrowth of zircons. Final age determined by AgePick = 144.0 ± 2.9 Ma (shown by heavy pink line)

Table 2.8: U-Pb geochronologic analyses for Sample S06-B01

Analysis	Isotope ratios										Apparent ages (Ma)								
	U	206Pb	U/Th	206Pb*	±	207Pb*	±	206Pb*	±	error	206Pb*	±	207Pb*	±	206Pb*	±	Best age	±	Conc
	(ppm)	204Pb		207Pb*	(%)	235U*	(%)	238U	(%)	corr.	238U*	(Ma)	235U	(Ma)	207Pb*	(Ma)	(Ma)	(Ma)	(%)
S06-B01-8TIP	42578	11868	0.5	17.6536	7.9	-0.0036	7.9	-0.0005	0.5	0.06	-3.0	0.0	-3.7	-0.3	477.7	174.0	-3.0	0.0	-0.6
S06-B01-5	21200	119412	0.2	20.4872	2.0	0.0233	5.2	0.0035	4.8	0.92	22.3	1.1	23.4	1.2	138.7	46.7	22.3	1.1	16.1
S06-B01-13	8724	6636	0.5	17.3949	3.3	0.0973	8.4	0.0123	7.8	0.92	78.6	6.1	94.3	7.6	510.3	73.3	78.6	6.1	15.4
S06-B01-21	4996	48356	0.1	19.9097	4.1	0.1034	9.1	0.0149	8.1	0.89	95.6	7.7	99.9	8.6	205.5	96.1	95.6	7.7	46.5
S06-B01-5LOW	5395	81124	1.0	20.9181	4.3	0.1099	9.0	0.0167	8.0	0.88	106.6	8.4	105.9	9.1	89.6	101.7	106.6	8.4	118.9
S06-B01-17	5075	34888	1.0	19.9780	5.0	0.1241	7.6	0.0180	5.8	0.75	114.9	6.6	118.8	8.6	197.5	116.8	114.9	6.6	58.2
S06-B01-3TIP	3628	14016	7.3	17.4218	12.7	0.1508	13.1	0.0191	3.2	0.24	121.7	3.8	142.7	17.4	506.9	280.8	121.7	3.8	24.0
S06-B01-3	3010	41000	3.3	19.8617	3.9	0.1325	7.6	0.0191	6.6	0.86	121.9	7.9	126.3	9.1	211.1	89.3	121.9	7.9	57.7
S06-B01-2	3030	55508	8.6	20.1641	2.1	0.1313	3.5	0.0192	2.8	0.81	122.6	3.4	125.2	4.1	175.9	48.1	122.6	3.4	69.7
S06-B01-9	3729	63604	12.8	20.1371	2.1	0.1360	6.4	0.0199	6.0	0.94	126.8	7.6	129.5	7.8	179.1	49.9	126.8	7.6	70.8
S06-B01-16	2905	18496	12.3	17.0752	20.9	0.1642	21.1	0.0203	2.8	0.13	129.8	3.6	154.4	30.2	550.9	460.6	129.8	3.6	23.6
S06-B01-15	1696	22860	8.6	18.8821	7.6	0.1547	7.8	0.0212	1.5	0.19	135.2	2.0	146.1	10.5	327.1	172.8	135.2	2.0	41.3
S06-B01-10	2722	72932	11.1	20.4259	4.3	0.1446	6.8	0.0214	5.3	0.77	136.6	7.1	137.1	8.8	145.8	101.8	136.6	7.1	93.7
S06-B01-20	2082	57728	8.3	19.7258	2.6	0.1519	4.5	0.0217	3.7	0.82	138.6	5.1	143.6	6.1	227.0	60.8	138.6	5.1	61.1
S06-B01-14	4538	76628	3.0	20.3285	4.5	0.1514	4.7	0.0223	1.3	0.29	142.3	1.9	143.1	6.3	157.0	105.4	142.3	1.9	90.7
S06-B01-19	3112	71896	13.0	20.1104	1.3	0.1557	9.6	0.0227	9.5	0.99	144.7	13.7	146.9	13.2	182.2	30.3	144.7	13.7	79.5
S06-B01-12	3003	100048	7.8	20.1839	2.0	0.1589	3.6	0.0233	2.9	0.82	148.2	4.3	149.7	5.0	173.7	47.6	148.2	4.3	85.4
S06-B01-18	2812	150304	2.5	20.1686	1.6	0.1598	2.2	0.0234	1.5	0.67	149.0	2.1	150.6	3.0	175.4	37.8	149.0	2.1	84.9
S06-B01-1	3340	122612	0.1	20.5123	1.7	0.1611	3.4	0.0240	3.0	0.88	152.7	4.6	151.7	4.9	135.9	39.0	152.7	4.6	112.4
S06-B01-19TIP	2573	62836	6.8	20.1015	1.1	0.1651	2.1	0.0241	1.8	0.86	153.3	2.7	155.1	3.0	183.2	24.5	153.3	2.7	83.7
S06-B01-8	3881	87320	18.9	20.2158	1.3	0.1692	2.7	0.0248	2.4	0.88	158.0	3.7	158.8	4.0	170.0	30.6	158.0	3.7	93.0
S06-B01-11	4043	131340	6.9	20.0624	1.6	0.1743	2.0	0.0254	1.2	0.61	161.5	1.9	163.1	3.0	187.7	37.3	161.5	1.9	86.0
S06-B01-4	4966	65972	1.0	12.9855	2.1	0.3308	4.9	0.0312	4.4	0.90	197.7	8.5	290.1	12.3	1121.4	42.7	197.7	8.5	17.6

Figure 2.34 shows a $^{238}\text{U}/^{206}\text{Pb}$ age vs. U concentration for sample S08 BM11, collected from a deformed diorite sill that intrudes the attenuated limb of the Big Maria syncline. AgePick determined a final age of 86.3 ± 2.1 Ma (MSWD = 3.8), which is the crystallization age of the diorite, indicating a Late Cretaceous age. This diorite might have been emplaced during the same magmatic event as the ~85 Ma Piute Mountains Pluton (Fletcher et al., 1988), which is documented to have undergone polyphase deformation and metamorphism (Fletcher and Karlstrom, 1990) and the ~90 Ma Mid Hills monzogranite from the New York Mountains (Wells et al., 2005). Table 2.9 shows all LA-ICP-MS data for zircons from sample S08 BM11.

Ar-Ar hornblende and biotite ages of magmatic rocks of the Big Maria Mountains

Figure 2.35 shows Ar-Ar age spectra plots of hornblende for samples from the western Big Maria Mountains. Samples B07 KS04, B07 KS05 and S08 BM13 were collected from Jurassic diorite rocks above the attenuated limb of the Big Maria syncline. Hornblende Ar-Ar ages indicate when rocks cooled through 500°C and would thus constrain timing of peak metamorphism in the range. Sample S08 BM22 was collected from Jurassic diorite in the west central part of the range. Sample B07 KS04 (Figure 2.35a) is assigned a spectrum plateau age of 70.6 ± 0.5 Ma. Sample S08 BM13 (Figure 2.35b) is assigned a spectrum plateau age of $69.0 \text{ Ma} \pm 0.4$ Ma. Sample B07 KS05 (Figure 2.35c) indicates a Late Cretaceous cooling age, based on its age spectrum analysis, but is not assigned a cooling age due to the complexity of the age spectrum. The hornblende age for S08 BM22 (Figure 2.35d) is much younger than the other three samples and is considered meaningless, due to likely contamination by biotite evidenced by the high K/Ca ratio. Overall, these ages suggest that these rocks in the region cooled through 550°C during Late Cretaceous time (~70 Ma), suggesting that peak metamorphic conditions were reached in the area at around 70 Ma.

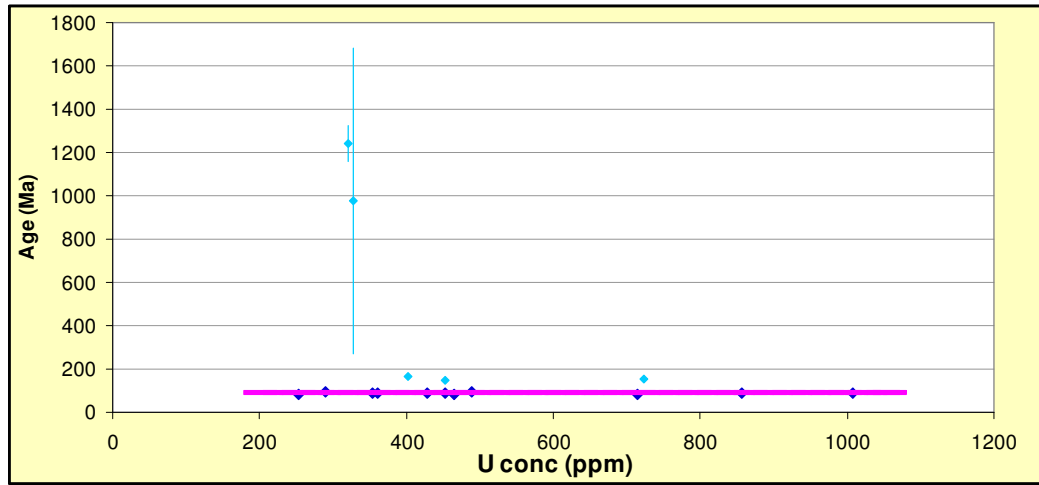


Figure 2.34: $^{238}\text{U}/^{206}\text{Pb}$ zircon ages vs. U concentration for sample S08 BM11. Grains in dark blue were used for crystallization age determination. Light blue grains were omitted from age determination due to high U concentration or high U/Th ratios. Final age determined by AgePick = 86.3 ± 2.1 Ma (shown by heavy pink line)

Table 2.9: U-Pb geochronologic analyses for Sample S08 BM11

Analysis	Isotope ratios										Apparent ages (Ma)						Best age (Ma)	± (Ma)	Conc (%)
	U (ppm)	206Pb/204Pb	U/Th	206Pb*/207Pb*	± (%)	207Pb*/235U*	± (%)	206Pb*/238U*	± (%)	error corr.	206Pb*/238U* (Ma)	± (Ma)	207Pb*/235U* (Ma)	± (Ma)	206Pb*/207Pb* (Ma)	± (Ma)			
S08-BM11-2TIP	714	15452	4.9	21.2688	6.6	0.0819	6.9	0.0126	1.9	0.28	80.9	1.5	79.9	5.3	50.1	157.2	80.9	1.5	161.5
S08-BM11-7	465	16064	1.7	20.3652	4.5	0.0886	4.8	0.0131	1.5	0.31	83.9	1.2	86.2	3.9	152.7	106.1	83.9	1.2	54.9
S08-BM11-9	252	4300	1.7	19.6089	15.7	0.0923	16.7	0.0131	5.6	0.33	84.1	4.7	89.7	14.3	240.7	363.8	84.1	4.7	34.9
S08-BM11-2C	1007	19020	2.8	21.2432	3.4	0.0866	6.6	0.0133	5.7	0.86	85.4	4.8	84.3	5.4	52.9	81.7	85.4	4.8	161.4
S08-BM11-7TIP	428	7980	3.3	21.9638	6.4	0.0844	7.5	0.0134	3.8	0.51	86.1	3.3	82.3	5.9	-27.3	155.1	86.1	3.3	-315.8
S08-BM11-6	452	13608	1.8	22.0567	7.3	0.0842	8.0	0.0135	3.2	0.41	86.2	2.8	82.1	6.3	-37.5	177.1	86.2	2.8	-230.2
S08-BM11-2	353	11560	6.2	22.3114	11.8	0.0833	12.1	0.0135	2.6	0.21	86.3	2.2	81.2	9.4	-65.4	289.5	86.3	2.2	-131.9
S08-BM11-6TIP	857	7028	1.8	20.1181	4.4	0.0948	7.5	0.0138	6.1	0.81	88.5	5.4	92.0	6.6	181.3	101.8	88.5	5.4	48.8
S08-BM11-4C	360	7876	2.3	20.9783	18.4	0.0932	18.7	0.0142	3.2	0.17	90.7	2.9	90.5	16.2	82.8	440.3	90.7	2.9	109.6
S08-BM11-4	289	9324	2.6	23.2551	12.7	0.0850	12.8	0.0143	1.5	0.12	91.8	1.4	82.9	10.2	-167.6	317.6	91.8	1.4	-54.8
S08-BM11-4RTIP	489	9832	3.2	22.4066	8.2	0.0890	8.9	0.0145	3.5	0.39	92.6	3.2	86.6	7.4	-75.8	200.1	92.6	3.2	-122.1
S08-BM11-5	453	16188	1.3	20.1497	4.3	0.1593	5.6	0.0233	3.6	0.64	148.4	5.2	150.1	7.8	177.6	100.7	148.4	5.2	83.5
S08-BM11-3TIP	723	22648	1.3	21.0872	3.7	0.1597	4.4	0.0244	2.4	0.53	155.6	3.6	150.5	6.2	70.5	89.0	155.6	3.6	220.6
S08-BM11-3	402	18588	0.9	20.8516	8.6	0.1727	8.6	0.0261	0.8	0.09	166.2	1.2	161.7	12.9	97.2	204.2	166.2	1.2	171.0
S08-BM11-5TIP	327	2764	1.3	13.9604	33.7	0.2060	34.0	0.0209	4.6	0.14	133.1	6.1	190.2	59.0	975.5	706.1	975.5	706.1	13.6
S08-BM11-1	321	28948	3.2	12.2224	4.3	0.5766	7.4	0.0511	6.0	0.81	321.4	18.8	462.3	27.5	1241.1	84.8	1241.1	84.8	25.9

Figure 2.36 shows Ar-Ar age spectra plots of biotite for samples from the western Big Maria Mountains. All samples except for S08 BM08 were collected from Jurassic plutonic rocks. S08 BM08 (Figure 2.36a) was collected from the lower member of the Jurassic volcanic unit in the upright limb of the Big Maria syncline. This sample has a total gas age of 55.36 ± 0.13 Ma. Sample S08 BM13 (Figure 2.36b), which had a hornblende plateau age of 69.0 ± 0.4 Ma, has total gas age for biotite of 59.6 ± 0.2 Ma, which indicates that the sample cooled from 500°C to $\sim 350^{\circ}\text{C}$ in approximately 12 million years. Sample S08 BM22 (Figure 2.36c), collected from a diorite located in the west central part of the range, has a total gas age of 53.56 ± 0.16 Ma. Sample S08 BM25 (Figure 2.36d), collected from a diorite located in the northwest part of the range, has a total gas age of 58.3 ± 0.2 Ma. Sample S09 BM01 (Figure 2.36e), collected from a fine-grained metagabbro at the southeast part of the range, has a total gas age of 48.5 ± 0.2 Ma. This sample is an outlier compared to the rest of the sample set and although the age is considered reliable, we interpret that these biotites may have undergone a later thermal event. Biotite hand picked from this sample was different in composition from biotites collected in the other sample, based on a marked color difference. Finally, sample S09 BM02 (Figure 2.36f), which was collected from a rock similar in composition and texture to S09 BM01, yields a total gas age of 57.94 ± 0.12 Ma, which is good agreement with ages from the other four samples. For the most part, biotite samples record that rocks in the Big Maria Mountains were cooled below 350°C during Paleocene time between 60-54 Ma. This is consistent with Paleocene ages obtained for cooling published in Knapp and Heizler (1990), Foster et al. (1992) and Kula et al. (2002). All Ar-Ar geochemical data is tabulated in Table 2.10.

Discussion

The U-Pb zircon data, while limited, gives us geochronologic information about magmatism and deformation in the Big Maria Mountains that was previously unknown. Although the felsic granite from the Big Maria Mountains is Late Jurassic in age (~ 144 Ma), it is clear that plutonism in the mountains did not occur as the result of a single

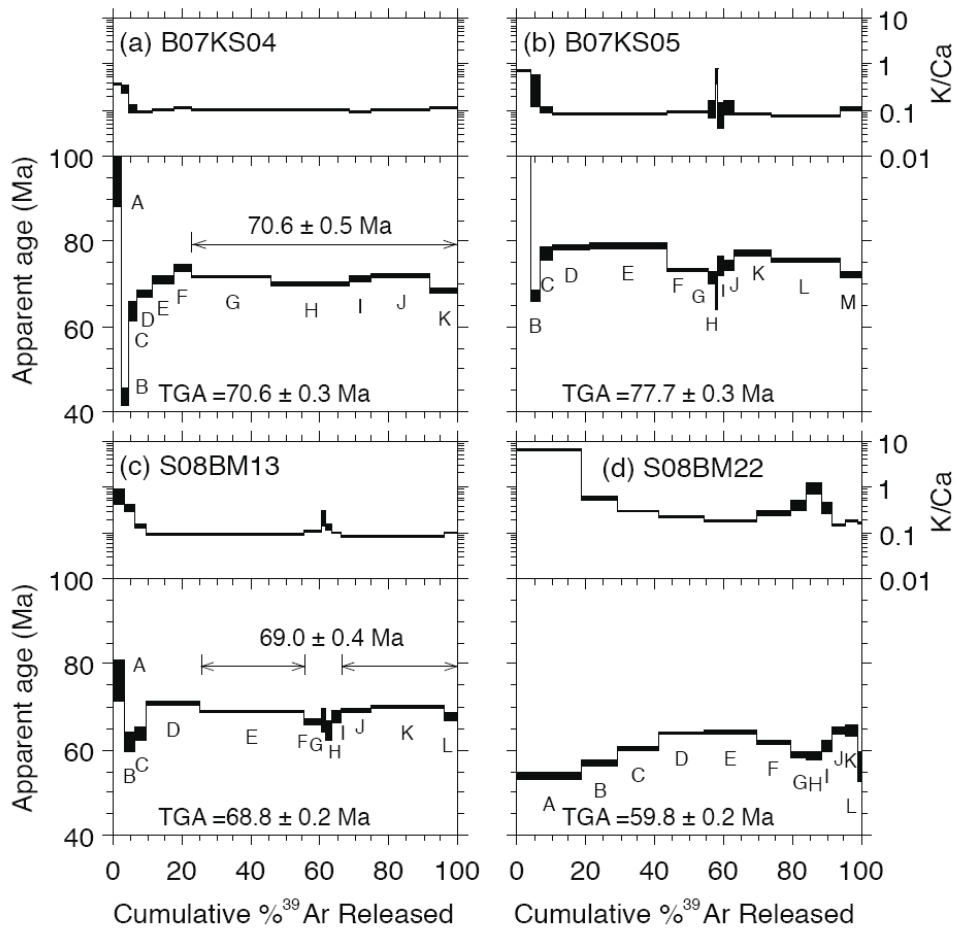


Figure 2.35: Hornblende age spectra plots from four magmatic samples from the western Big Maria Mountains. Except for sample S08 BM22, age spectra analysis of hornblende indicate that samples cooled through 550°C at ~70 Ma. B07 KS05 indicates Late Cretaceous cooling, but is not assigned a specific age due to complex age spectrum. These samples constrain timing of peak metamorphism in the area to ~70 Ma. S08 BM22 cooling age is considered meaningless due to contamination by biotite, evidenced by high K/Ca ratios.

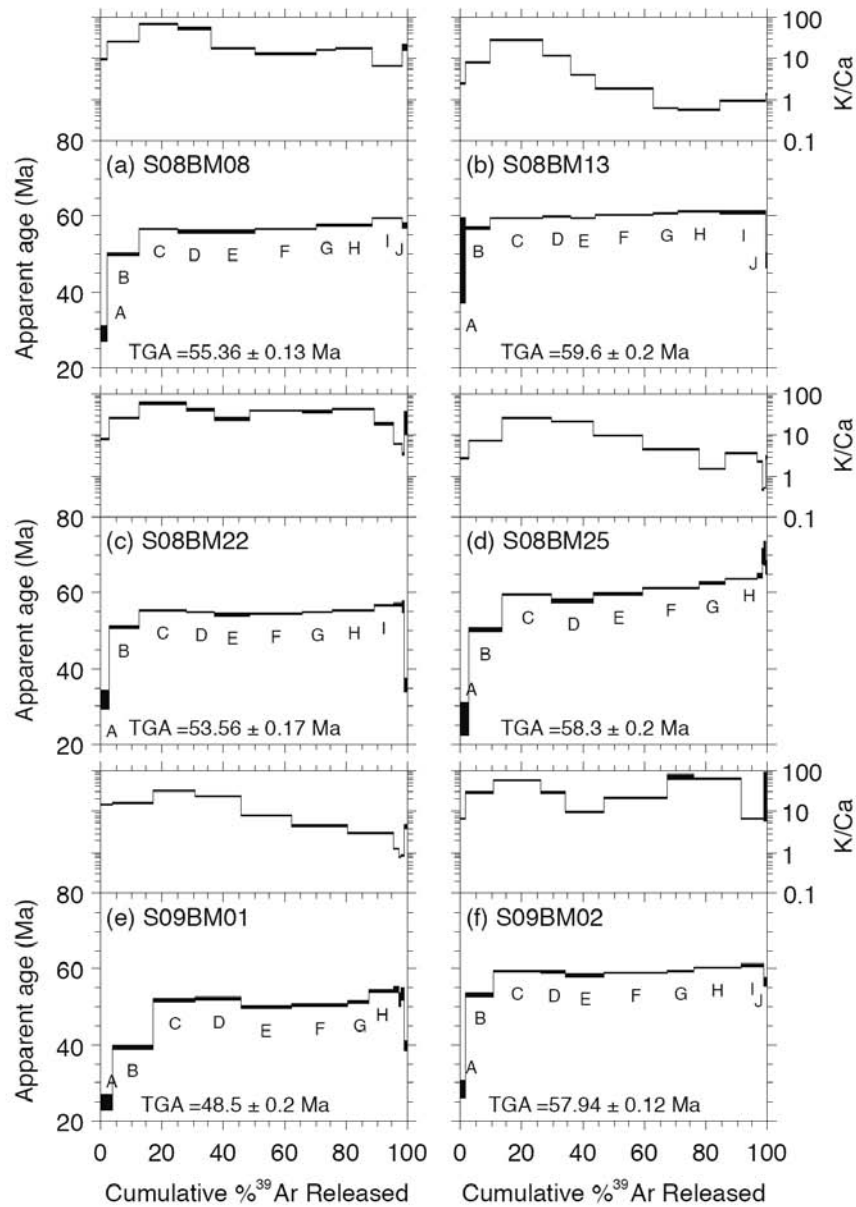


Figure 2.36: Biotite age spectra from magmatic rocks from the Big Maria Mountains. Except for S09 BM01, the biotite age spectra show that samples cooled through 350°C between 54-60 Ma, suggesting a regional cooling event during Paleocene to early Eocene time.

Table 2.10: Ar-Ar geochemical data for biotite and hornblende samples

ID	Temp (°C)	⁴⁰ Ar/ ³⁹ Ar	³⁷ Ar/ ³⁹ Ar	³⁶ Ar/ ³⁹ Ar (x 10 ⁻³)	³⁹ Ar _K (x 10 ⁻¹⁵ mol)	K/Ca	⁴⁰ Ar* (%)	³⁹ Ar (%)	Age (Ma)	±1σ (Ma)
S08BM08 , Biotite, 9.83 mg, J=0.0010224±0.09%, D=1.0014±0.001, NM-222J, Lab#=58837-01										
# A	650	121.4	0.0565	357.4	4.88	9.0	13.0	2.6	28.8	1.0
# B	750	38.73	0.0193	38.70	19.0	26.5	70.5	12.7	49.65	0.20
# C	850	35.80	0.0074	15.85	24.2	68.8	86.9	25.5	56.49	0.16
# D	920	37.32	0.0096	22.44	20.2	53.3	82.2	36.3	55.74	0.16
# E	1000	37.80	0.0285	23.96	26.8	17.9	81.3	50.5	55.79	0.17
# F	1075	35.78	0.0390	15.61	37.6	13.1	87.1	70.5	56.60	0.15
# G	1110	34.60	0.0320	10.24	12.0	16.0	91.3	76.9	57.33	0.14
# H	1180	34.00	0.0286	7.982	23.0	17.8	93.1	89.1	57.44	0.14
# I	1300	34.36	0.0752	6.196	18.2	6.8	94.7	98.8	59.04	0.13
# J	1680	38.28	0.0288	22.77	2.32	17.7	82.4	100.0	57.28	0.40
								K2O=7.20		
Integrated age ± 1σ			n=10		188.3	16.8		%	55.36	0.13
Plateau ± 1σ			no plateau							
S08BM13 , Biotite, 13.34 mg, J=0.0010084±0.10%, D=1.0014±0.001, NM-222J, Lab#=58836-01										
# A	650	146.9	0.2157	406.3	3.54	2.4	18.3	2.1	48.3	5.7
# B	750	38.54	0.0631	23.32	12.9	8.1	82.1	9.7	56.68	0.19
# C	850	35.30	0.0182	7.094	28.9	28.1	94.1	26.9	59.42	0.12
# D	920	36.59	0.0449	10.96	15.8	11.4	91.2	36.3	59.68	0.19
# E	1000	39.44	0.1230	21.52	13.7	4.1	83.9	44.4	59.23	0.14
# F	1075	35.76	0.2807	7.363	31.6	1.8	94.0	63.2	60.14	0.12
# G	1110	35.25	0.8188	4.708	13.6	0.62	96.2	71.3	60.72	0.13
# H	1180	35.01	0.8994	3.235	23.2	0.57	97.5	85.1	61.08	0.13
# I	1300	34.89	0.5693	3.093	24.5	0.90	97.5	99.6	60.88	0.18
# J	1680	42.73	0.4050	53.95	0.685	1.3	62.8	100.0	48.2	1.1
								K2O=4.82		
Integrated age ± 1σ			n=10		168.6	1.4		%	59.62	0.17
Plateau ± 1σ			no plateau							

Table 2.10 Cont.

1σ

S08BM22, Biotite, 5.08 mg, J=0.0010132±0.22%, D=1.0014±0.001, NM-222J, Lab#=58833-01

#	A	650	146.1	0.0673	435.3	3.54	7.6	11.9	3.3	31.6	1.2
#	B	750	37.61	0.0202	32.10	10.0	25.3	74.8	12.7	50.70	0.20
#	C	850	33.78	0.0086	10.80	16.3	59.4	90.6	28.1	55.06	0.11
#	D	920	37.01	0.0131	22.38	9.9	38.9	82.1	37.4	54.73	0.16
#	E	1000	38.88	0.0213	30.28	11.9	24.0	77.0	48.6	53.90	0.17
#	F	1075	33.42	0.0135	11.39	18.3	37.9	89.9	65.9	54.13	0.14
#	G	1110	32.42	0.0144	6.716	10.5	35.6	93.9	75.8	54.80	0.13
#	H	1180	31.99	0.0127	4.433	14.5	40.3	95.9	89.5	55.23	0.11
#	I	1210	32.37	0.0284	3.178	6.82	17.9	97.1	95.9	56.56	0.14
#	J	1250	32.65	0.0903	3.937	3.01	5.6	96.5	98.8	56.68	0.25
#	K	1300	34.93	0.1532	13.05	0.590	3.3	89.0	99.3	55.95	0.88
#	L	1680	40.70	0.0236	71.27	0.717	21.6	48.3	100.0	35.56	0.87
									K2O=7.91		
									%	53.56	0.17
	Integrated age ± 1σ			n=12		106.0	25.6				
	Plateau ± 1σ			no plateau							

S08BM25, Biotite, 6.8 mg, J=0.0010035±0.11%, D=1.0014±0.001, NM-222JJ, Lab#=58835-01

#	A	650	211.2	0.1950	664.5	3.69	2.6	7.0	3.2	26.6	2.2
#	B	750	50.33	0.0730	75.52	12.6	7.0	55.7	14.0	50.02	0.27
#	C	850	42.54	0.0194	31.40	18.6	26.4	78.2	30.1	59.24	0.21
#	D	920	43.83	0.0249	38.90	15.4	20.5	73.8	43.4	57.60	0.20
#	E	1000	44.33	0.0532	37.14	18.9	9.6	75.3	59.7	59.41	0.23
#	F	1075	42.62	0.1195	28.12	21.5	4.3	80.5	78.3	61.10	0.19
#	G	1110	39.80	0.3268	16.33	9.9	1.6	87.9	86.8	62.29	0.17
#	H	1180	38.69	0.1378	10.22	11.3	3.7	92.2	96.6	63.47	0.15
#	I	1210	39.41	0.2454	11.30	2.30	2.1	91.6	98.6	64.19	0.30
#	J	1250	45.24	1.093	21.20	0.667	0.47	86.4	99.1	69.43	0.99
#	K	1300	48.56	1.034	31.16	0.339	0.49	81.2	99.4	70.1	1.6
#	L	1680	56.34	0.1817	64.07	0.646	2.8	66.4	100.0	66.52	0.96
									K2O=6.52		
									%	58.27	0.20
	Integrated age ± 1σ			n=12		115.8	4.7				
	Plateau ± 1σ			no plateau							

Table 2.10 Cont.

1σ plateau

S09BM01, Biotite, 5.76 mg, J=0.0010272±0.24%, D=1.0014±0.001, NM-222J, Lab#=58831-01

#	A	650	132.3	0.0356	402.7	4.19	14.3	10.1	4.0	24.5	1.0
#	B	750	41.98	0.0329	69.69	13.9	15.5	50.9	17.3	39.21	0.27
#	C	850	40.21	0.0173	40.43	14.8	29.5	70.3	31.4	51.64	0.22
#	D	920	41.02	0.0222	42.12	15.0	23.0	69.7	45.8	52.20	0.21
#	E	1000	41.51	0.0667	48.13	17.4	7.7	65.8	62.5	49.89	0.20
#	F	1075	40.50	0.1209	44.44	19.1	4.2	67.6	80.8	50.05	0.23
#	G	1110	39.25	0.1665	38.26	7.54	3.1	71.2	88.0	51.09	0.24
#	H	1180	38.60	0.1809	30.62	8.05	2.8	76.6	95.7	53.97	0.21
#	I	1210	40.24	0.4317	35.40	1.72	1.2	74.1	97.3	54.43	0.53
#	J	1250	39.46	0.7104	38.04	0.830	0.72	71.7	98.1	51.68	0.86
#	K	1300	40.54	0.6166	38.97	0.91	0.83	71.7	99.0	53.12	0.75
#	L	1680	39.76	0.1211	61.38	1.07	4.2	54.4	100.0	39.65	0.70
									K2O=6.78		
Integrated age ± 1σ				n=12		104.5	5.7		%	48.49	0.22

Plateau ± 1σ no plateau

S09BM02, Biotite, 5.74 mg, J=0.0010224±0.09%, D=1.0014±0.001, NM-222JJ, Lab#=58838-01

#	A	650	130.9	0.0838	391.0	2.65	6.1	11.7	2.2	28.1	1.2
#	B	750	37.74	0.0191	28.80	10.7	26.8	77.5	11.1	53.12	0.19
#	C	850	35.60	0.0096	10.34	19.0	53.4	91.4	26.8	59.04	0.14
#	D	920	36.78	0.0181	14.24	9.3	28.2	88.6	34.5	59.10	0.17
#	E	1000	36.80	0.0510	16.26	15.4	10.0	87.0	47.2	58.08	0.15
#	F	1075	36.07	0.0239	12.60	24.7	21.3	89.7	67.7	58.71	0.14
#	G	1110	35.46	0.0073	9.306	10.5	70.0	92.2	76.4	59.35	0.15
#	H	1180	35.31	0.0084	7.631	18.4	60.4	93.6	91.6	59.96	0.13
#	I	1300	35.65	0.0786	7.054	9.1	6.5	94.2	99.2	60.89	0.15
#	J	1680	39.05	0.0110	26.83	1.01	46.6	79.7	100.0	56.52	0.62
									K2O=7.92		
Integrated age ± 1σ				n=10		121.0	19.8		%	57.94	0.12

Plateau ± 1σ no plateau

Table 2.10 Cont.

B07KS04 , Hornblende, 17.68 mg, J=0.0010316±0.16%, D=1.004±0.001, NM-222M, Lab#=58863-01											
#	A	900	807.0	1.357	2542.2	1.23	0.38	6.9	2.5	101.2	6.7
#	B	1000	60.51	1.827	125.7	1.18	0.28	38.9	4.9	43.3	1.0
#	C	1050	62.92	4.966	97.83	0.99	0.10	54.7	7.0	63.2	1.1
#	D	1080	47.94	5.563	39.00	2.35	0.092	76.9	11.8	67.61	0.48
#	E	1090	45.60	5.175	25.06	3.07	0.099	84.7	18.1	70.73	0.45
#	F	1100	45.66	4.908	20.20	2.54	0.10	87.8	23.3	73.37	0.45
	G	1120	42.20	5.159	12.29	11.2	0.099	92.4	46.3	71.39	0.17
	H	1180	40.84	5.122	10.64	11.0	0.100	93.3	68.8	69.81	0.18
	I	1220	43.39	5.559	17.62	3.23	0.092	89.1	75.4	70.78	0.37
	J	1260	42.23	5.341	12.15	8.34	0.096	92.5	92.5	71.57	0.22
	K	1650	41.72	4.865	16.92	3.66	0.10	89.0	100.0	68.02	0.36
									K2O=1.03		
						48.8	0.10		%	70.57	0.30
	Integrated age ± 1σ		n=11								
	Plateau ± 1σ	steps G-K	n=5	MSWD=28.3	2	37.433			76.7	70.64	0.534
B07KS05 , Hornblende, 22.08 mg, J=0.0010321±0.12%, D=1.0014±0.001, NM-222J, Lab#=58839-01											
#	A	900	308.5	0.6959	808.2	1.78	0.73	22.6	4.1	125.5	2.7
#	B	1000	53.78	1.551	58.67	1.44	0.33	68.0	7.3	66.91	0.72
#	C	1050	55.03	5.204	45.34	1.38	0.098	76.4	10.5	76.93	0.74
#	D	1080	48.29	6.351	20.33	4.74	0.080	88.6	21.3	78.32	0.28
#	E	1100	47.22	6.476	15.93	9.7	0.079	91.2	43.4	78.77	0.23
#	F	1110	42.00	5.901	9.099	5.31	0.086	94.8	55.6	72.92	0.25
#	G	1120	42.13	4.634	12.12	1.06	0.11	92.4	58.0	71.30	0.65
#	H	1130	44.75	0.8919	25.34	0.314	0.57	83.4	58.7	68.3	2.2
#	I	1140	45.90	5.837	20.00	0.618	0.087	88.2	60.1	74.1	1.2
#	J	1180	45.67	4.498	18.88	1.40	0.11	88.6	63.3	74.03	0.58
#	K	1220	46.30	6.606	16.21	4.71	0.077	90.8	74.1	77.00	0.31
#	L	1260	44.08	6.740	11.72	8.7	0.076	93.4	94.0	75.42	0.22
#	M	1650	44.15	4.997	18.24	2.61	0.10	88.7	100.0	71.75	0.40
									K2O=0.74		
						43.8	0.088		%	77.74	0.24
	Integrated age ± 1σ		n=13								
	Plateau ± 1σ	no plateau									

Table 2.10 Cont.

Notes:

Isotopic ratios corrected for blank, radioactive decay, and mass discrimination, not corrected for interfering reactions.

Errors quoted for individual analyses include analytical error only, without interfering reaction or J uncertainties.

Integrated age calculated by summing isotopic measurements of all steps.

Integrated age error calculated by quadratically combining errors of isotopic measurements of all steps.

Plateau age is inverse-variance-weighted mean of selected steps.

Plateau age error is inverse-variance-weighted mean error (Taylor, 1982) times root MSWD where MSWD>1.

Plateau error is weighted error of Taylor (1982).

Decay constants and isotopic abundances after Steiger and Jäger (1977).

symbol preceding sample ID denotes analyses excluded from plateau age calculations.

Weight percent K₂O calculated from ³⁹Ar signal, sample weight, and instrument sensitivity.

Ages calculated relative to FC-2 Fish Canyon Tuff sanidine interlaboratory standard at 28.02 Ma

Decay Constant (LambdaK (total)) = 5.543e-10/a

Correction factors:

$$({}^{39}\text{Ar}/{}^{37}\text{Ar})_{\text{Ca}} = 0.00068 \pm 5\text{e-}05$$

$$({}^{36}\text{Ar}/{}^{37}\text{Ar})_{\text{Ca}} = 0.00028 \pm 2\text{e-}05$$

$$({}^{38}\text{Ar}/{}^{39}\text{Ar})_{\text{K}} = 0.0125$$

$$({}^{40}\text{Ar}/{}^{39}\text{Ar})_{\text{K}} = 0 \pm 0.0004$$

discreet pulse of magmatism, but suggests rather that arc magmatism was continuous in the area throughout the Jurassic and Cretaceous and was thus related to the Sierra Nevadan and Peninsular Range magmatic events. This observation is confirmed by ~86 Ma age obtained for a deformed diorite in the range. Not only does this deformed diorite indicate that magmatism in the Maria Fold and Thrust Belt was active from Jurassic through Cretaceous time, it is also the first documented example of a Late Cretaceous rock that underwent all stages of deformation in the range and significantly changes the lower bound timing of D₁/D₂ deformation. Based on the age of this diorite, all episodes of deformation observed in the Maria Fold and Thrust Belt must be Late Cretaceous in age. However, it is not the only example of a deformed Late Cretaceous pluton in the Sevier hinterland of southeastern California. The ~85 Ma Piute Mountains granodiorite (Fletcher et al., 1988) is documented as having undergone polyphase deformation and amphibolite grade metamorphism (Fletcher and Karlstrom, 1990). This correlation provides direct evidence that all deformation in the Sevier hinterland in southeastern California is Late Cretaceous in age and establishes a temporal and magmatic link between deformation in the Maria Fold and Thrust Belt and in the Old Woman-Piute Mountains area, thus confirming the hypothesis that Maria Fold and Thrust Belt is an eastward extension of the Sevier hinterland as suggested in Figure 2.1. The Late Cretaceous age and Late Jurassic age for magmatic rocks in the Big Maria Mountains calls for further study of plutonic rocks in the range. It is more than likely that some rocks mapped in the range as Jurassic are actually Cretaceous in age and that there may be a complex history of arc magmatism in the range. Finally, the 86 Ma age for the deformed diorite in the range temporally overlaps with the 97-84 age for sedimentation in the McCoy Mountains Formation. Timing of plutonism deformation in the Maria Fold and Thrust Belt coincides with timing of late stage sedimentation in the McCoy Mountains Formation, thus establishing a link between southeast-directed contractile shortening in the Maria Fold and Thrust Belt and development of the Late Cretaceous McCoy retroarc foreland basin.

The Ar-Ar analyses taken from the range do not show any significant spatial relationship for hornblende and biotite cooling ages. However, the data does indicate that

rocks in the Big Maria Mountains cooled through $\sim 550^{\circ}\text{C}$ at ~ 70 Ma, which places constraints on the timing of metamorphism and is in overall general agreement with timing of metamorphism in the region by other workers as discussed earlier. Based on the timing of emplacement of peraluminous granites between 74-67 Ma, latest Cretaceous plutonism in the region was coeval with metamorphism. Finally, structural observations in this study confirm that Late Cretaceous plutons were syn- and post-kinematic with extensional (east or northeast-directed) deformation and thus it is likely the timing hornblendes in the Big Maria Mountains corresponds to the timing of peak metamorphism and D_3 deformation in the Maria Fold and Thrust Belt. Meanwhile, biotite Ar-Ar ages indicate that rocks cooled through $\sim 350^{\circ}\text{C}$ during a Paleocene cooling event between 60-54 Ma. This cooling event seems to correspond with the timing of cessation of magmatism in this region during this time and is similar to Ar-Ar ages for biotite as cited by other workers. We note that Paleocene cooling ages for rocks in the Maria Fold and Thrust Belt coincides with the timing of ultrahigh pressure metamorphism of the Pelona-Rand-Orocopia schist, which suggests that even though magmatism waned in this area during the Paleocene, active margin tectonism persisted at least through Eocene time. Paleocene-Eocene cooling of these rocks could correspond to conductive cooling of rocks through 350°C or to initial uplift of middle crustal rocks in response to synorogenic collapse during Paleocene-Eocene time.

Discussion of tectonic evolution

In this section we synthesize the structural and geochronology observations and interpretations from the western Maria Fold and Thrust Belt and McCoy Basin to discuss the Mesozoic tectonic history of this important part of the Cordillera. We present revised interpretations of the tectonic setting of the Maria Fold and Thrust Belt and present figures that show the temporal tectonic evolution of the region, utilizing constraints obtained from data in this study integrated with regional observations discussed in the previous section. For each time slice we present a simplified tectonic map and schematic cross section through the basin. We discuss how structures in the region developed in

response to convergent tectonics at the plate boundary. We illustrate how the pre-existing geometry of the McCoy rift basin may have influenced the later geometry of the Maria Fold and Thrust Belt and synorogenic McCoy retroarc foreland basin. We show how sedimentation in the McCoy Basin relates to synorogenic deformation in the Maria Fold and Thrust Belt. Finally, we place deformation events in the Maria Fold and Thrust Belt in the context of regional tectonics of the southwestern U.S. We begin our discussion of Mesozoic tectonic events in the Late Jurassic, and conclude in Eocene time, which marks the end of contractile deformation in the region.

Late Jurassic to Early Cretaceous: Development of the McCoy rift system and synchronous widespread magmatism (170-100 Ma)

Jurassic volcanic rocks of the Dome Rock Sequence and plutonic rocks of the Kitt Peak-Trigo Peaks Supergroup mark the onset of active margin tectonism in the region beginning around 170 Ma (Tosdal et al., 1989). Although the Dome Rock Sequence and Kitt Peak-Trigo Peaks Supergroup are magmatic rocks that temporally overlap, they are not chemically related. That is, plutons from the Kitt Peak-Trigo Peaks Supergroup do not represent source magmas for the Dome Rock Sequence rocks. However, both of these groups of rocks were likely formed in the same tectonic setting. During Late Jurassic time, the Kula-Farallon plate was being subducted beneath North America, leading to the creation of the Jurassic magmatic arc contemporaneous with the opening of the Gulf of Mexico (Dickinson et al., 1987; Saleeby and Busby, 1992). The McCoy-Bisbee Basin is interpreted by several workers (Dickinson et al., 1987; Bilodeau, 1982; Spencer et al., 2005) to have formed in response to opening of the Gulf of Mexico, which was accompanied by transtensional faulting in west. Rift formation in the southwestern U.S. was aided by thermally softened lithosphere due to presence of the magmatic arc. Evidence of this early stage of rift formation in the Maria Fold and Thrust Belt region are sedimentary deposits of Basal Sandstone 1 of the McCoy Mountains Formation. Basal Sandstone 1 represents deposition in a fluvial sedimentary basin. The contact between Basal Sandstone 1 of the McCoy Mountains Formation and the underlying Jurassic quartz

porphyry observed in the McCoy Mountains indicates reworking of the Jurassic volcanics by erosional processes followed by deposition of Basal Sandstone 1, suggesting an unconformity between Jurassic volcanic rocks and Basal Sandstone 1. Detrital zircon from the McCoy Mountains constrains the age of Basal Sandstone 1 to no older than 179 Ma (Barth et al., 2004). However, the contact is observed to interfinger with Jurassic volcanic rocks in the Palen Mountains (Fackler-Adams et al., 1997), which would constrain the formation to no younger than ~154 Ma, which is consistent with the age of a 155 Ma lava flow found near the top of Basal Sandstone 1 correlative rocks in western Arizona (Spencer et al., 2005). Therefore, we conclude that Basal Sandstone 1 is Jurassic in age and that the erosional unconformity observed in the McCoy Mountains represents at most ~5 million years prior to deposition of Basal Sandstone 1 of the McCoy Mountains Formation. The Late Jurassic McCoy-Bisbee Basin extended at least as far as the Coxcomb Mountains, based on exposures of Basal Sandstone 1, trended west-northwest and was approximately 50 km wide through western Arizona and eastern California. The Late Jurassic McCoy rift basin was bounded in the north by the Mogollon Highlands, which served as a source area for sedimentation in the rift. The spatial extent and geometry of this rift basin would greatly influence the spatial extent and geometry of later tectonic provinces, as we will demonstrate.

Deposition in the McCoy-Bisbee Basin waned in southern California and western Arizona between ~150-110 Ma, based on an unconformity between Basal Sandstone 1 and Basal Sandstone 2 suggested by detrital zircon analysis of Basal Sandstone 2 of the McCoy Mountains Formation and correlative rocks in western Arizona (Barth et al., 2004; Spencer et al., 2005). However, deposition continued throughout most of the McCoy-Bisbee Basin further to the southeast (Dickinson and Lawton, 2001). Comparison of mean orientation of bedding obtained from Basal Sandstone 1 compared with Basal Sandstone 2 suggests a shallow angular unconformity between the two members. A marked compositional change between Basal Sandstone 1 and Basal Sandstone 2 and a sharp depositional contact observed between the two units in the northern McCoy Mountains also bolsters the interpretation of an unconformity between the two members.

The depositional hiatus in the McCoy Basin during this time is coeval with an observed lull in tectonic activity in the Sevier hinterland, a westward retreat of the magmatic arc by several hundred kilometers (Christiansen et al., 1994) and a reduction in arc magmatism during the Early Cretaceous (DeCelles, 2004). During this time period, however, the McCoy Basin region was still a site of active, albeit deep-seated, magmatism as indicated by plutonic rocks of Latest Jurassic age (~145 Ma) documented in the Big Maria Mountains in this study.

Figure 2.37 shows a tectonic map of the southwestern U.S. during 110-100 Ma, during which time deposition in the northwestern McCoy-Bisbee Basin resumed. This is coeval with resumed arc magmatism and crustal shortening in the Sevier hinterland (Smith et al., 1993). The magmatic arc overlapped the basin during this time. The rift basin established during the Late Jurassic continued to serve as an area of deposition for sediments deposited during marine inundation in the southeast (Dickinson and Lawton, 2001; Spencer et al., 2005) and fluvial deposition in the northwest. Figure 2.37 also shows a schematic cross section from the submarine trench through the magmatic arc and across the McCoy-Bisbee Basin. The essential geometry of the rift basin likely remained unchanged during this time. We assume a classic rift geometry for the basin, with normal faults dipping toward the center of the rift on either side. The Mogollon highlands to the north continued to be a source area for sediments based on clast composition and paleo-current indicators (Harding and Coney, 1985). The composition of Basal Sandstone 2 and the Mudstone Member of the McCoy Mountains Formation indicates deposition in a fluvial setting during this time period that was at or near sea level, based on the presence of calcareous pods and lenses and limestone beds. Volcanically derived sand and silt clasts in Basal Sandstone 2 and the Mudstone Member also indicates that volcanism resumed during this time period; this is also supported by Cretaceous detrital zircons found in the formation, which must have sourced from the Cretaceous magmatic arc surrounding the basin to the north, south and west. Farther to the east, the Colorado

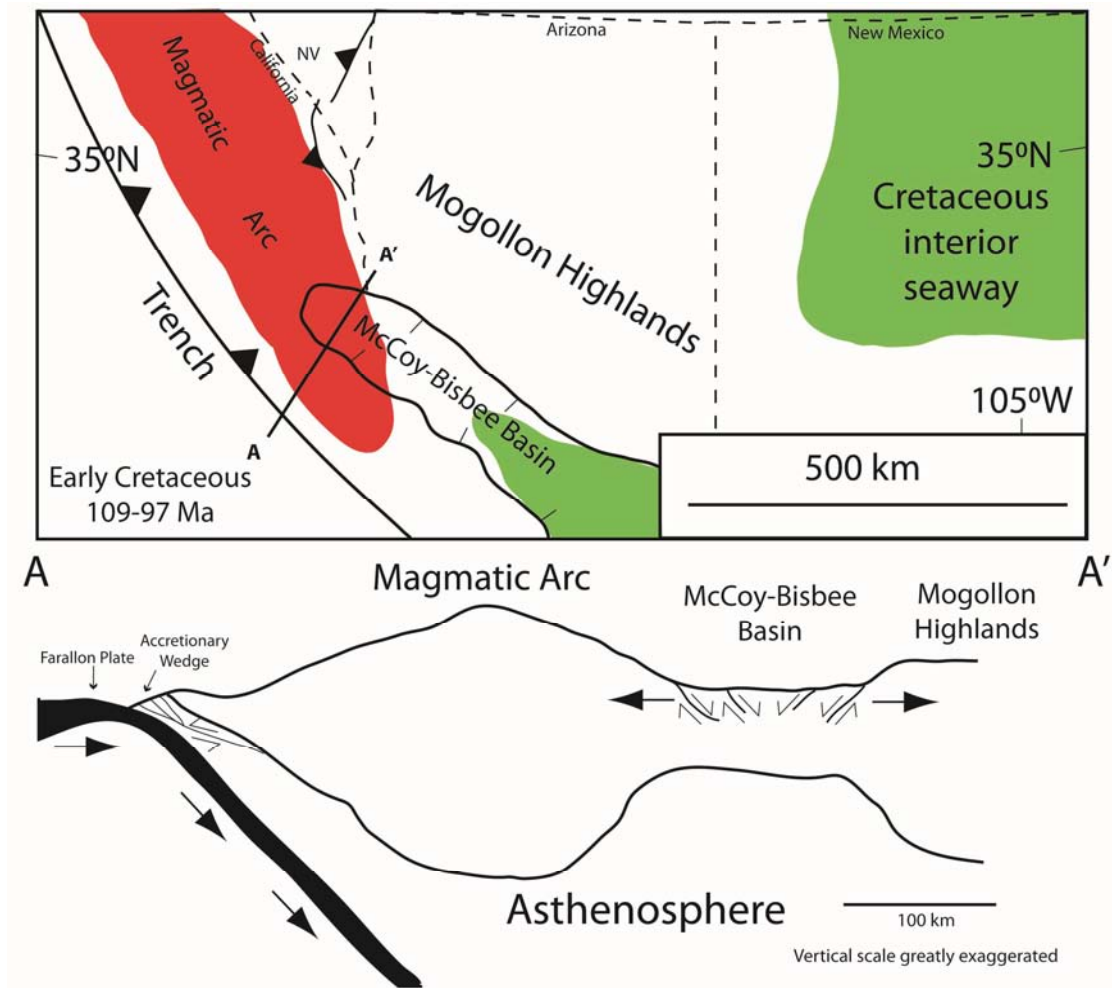
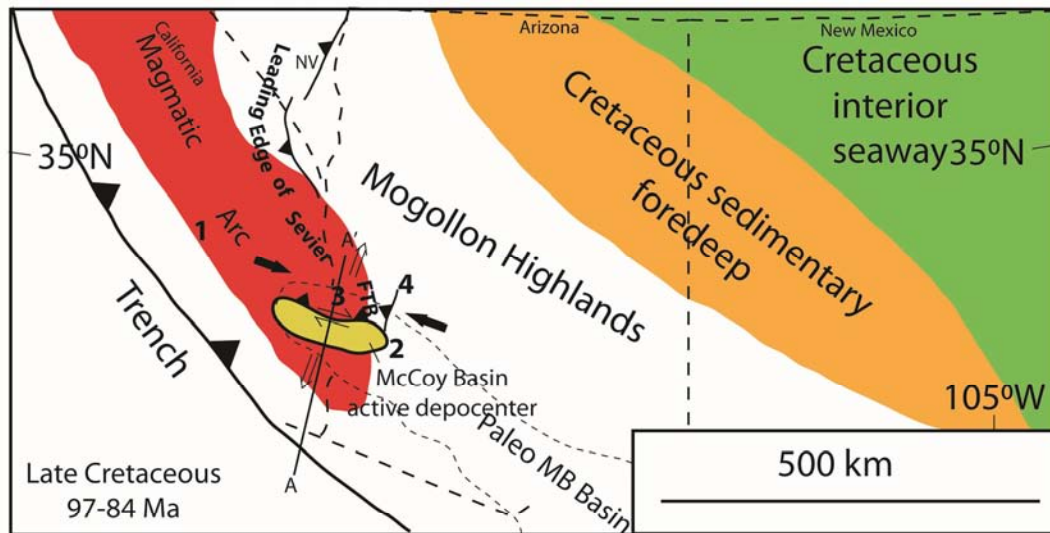


Figure 2.37: Simplified tectonic map of the southwestern U.S. during Early Cretaceous time. Map created from palinspastic reconstruction by DeCelles (2004) and references therein and from interpretation by Spencer et al. (2005)

Plateau continued to remain a depositional area for sediments close to sea level, as indicated by the presence of the Cretaceous Interior Seaway observed in northeastern New Mexico. To the north, the clastic foredeep in front of the Sevier Foreland Thrust Belt extended as far south as southern Utah and extended across central Colorado.

Late Cretaceous: Northwest-directed underthrusting of the miogeocline marking the onset of Sevier tectonism (100-80 Ma)

Figure 2.38 shows our tectonic map and schematic cross section for the time period between 100-80 Ma. In this tectonic snapshot, the Farallon Plate is being subducted underneath the west coast of North America and the Cretaceous magmatic arc covers the same aerial extent in the southwestern U.S. but has shifted eastward (Smith et al., 1993). The clastic foredeep in front of the leading edge of the Sevier Fold and Thrust Belt has now increased substantially in area in the southwestern U.S. and stretches into northwestern Arizona and northern New Mexico. In addition, marine transgression of the Cretaceous Interior Seaway has spread westward into northeastern Arizona. The strain ellipse shown on the map indicates the paleo strain field for rocks in the Maria Fold and Thrust Belt for D_1/D_2 time. During this time, the tectonic setting of the McCoy Basin is inferred to change from a rift basin into a transpressional (dextral and reverse) retroarc foreland basin in southeastern California and western Arizona, though deposition in the Bisbee rift basin to the southeast continued during this time (Dickinson and Lawton, 2001). We interpret that this change in tectonic setting is marked by an abrupt change in depositional setting suggested by the contact between the Mudstone Member and Conglomerate Member in the northern McCoy Mountains. This change is characterized by a substantial increase in clast size. The sequence coarsens upward at the base of the Conglomerate Member and large, boulder size clasts are observed in the basal 200 m of the Conglomerate Member. In the McCoy Mountains, this contact is interpreted to be gradational, suggesting gradual infilling of the basin prior to increased rate of tectonic subsidence and basin infill. Paleocurrent indicators from the Conglomerate Member still indicate that the source terrane is to the north, but the increase in tectonic subsidence and



- 1 SE-directed reverse and dextral shear constrained by strain markers in field and microstructural indicators
- 2 Extent of McCoy Basin depocenter inferred from exposures of upper McCoy Mountains Formation
- 3 Basin boundary type inferred from tectonic transport direction determined from future Maria Fold and Thrust Belt
- 4 Front of Sevier Fold and Thrust Belt inferred from lateral extent of future Maria Fold and Thrust Belt

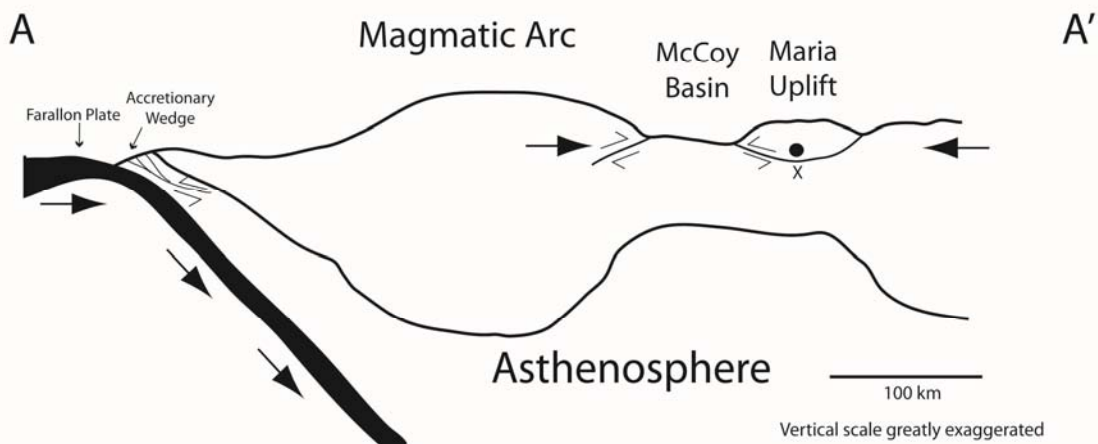


Figure 2.38: Late Cretaceous tectonic map of the southwestern U.S. Cretaceous retroarc transpressive McCoy Basin shown in yellow. Sediments are being deposited in the McCoy Basin at this time. Strain ellipse constrained by kinematic indicators from Big and Little Maria Mountains. Strain ellipse for McCoy Basin area only. Prior extent of McCoy-Bisbee Basin outlined with dashed lines. Modified from DeCelles (2004) and Spencer et al. (2005).

basin infill by large clasts in the conglomerate indicates possibly that there was uplift to the north.

We propose here that this uplift was caused by northwest-directed underthrusting of the Cordilleran miogeocline to the north of the McCoy Basin. The locus of this uplift, which we designate the Maria Uplift, is defined by the spatial area of rocks that would later become part of the middle crustal Maria Fold and Thrust Belt. We propose that tectonic burial of these rocks to 12-15 km depth as indicated by metamorphic mineral assemblages (Hoisch et al., 1988) was accomplished during this underthrusting event, which was synchronous with sedimentation in the McCoy Basin. Three lines of evidence support these conclusions. First, kinematic indicators in the western Maria Fold and Thrust Belt show that rocks were deformed by top-southeast directed reverse and ductile shear at middle crustal levels (12-15 km). Geochronology and observed field relationships from the Big Maria Mountains indicate that this deformation must have taken place after 86 Ma, the age of a deformed diorite obtained from this study, but prior to 79 Ma the K-Ar age of the leucogranite dikes (Martin et al., 1982). Second, rocks in the McCoy and Palen Mountains do not record any structures related to this deformation event, so there must be a structural discontinuity along which rocks in the Maria Fold and Thrust Belt were buried to and deformed at middle crustal levels while rocks in the McCoy Basin were not. One possibility is that a right lateral transpressive fault as a structure that could have accommodated this. Such a structure is consistent with inferred sense of tectonic transport in the Maria Fold and Thrust Belt. Another possibility is that the present day erosion surface; faults do not necessarily control the present day exposure of outcrops. Third, detrital zircon work from the McCoy Mountains Formation (Barth et al., 2004) constrains the age of the upper McCoy Mountains Formation (conglomerate through Siltstone Member) to 97-84 Ma. The timing of sedimentation of the upper McCoy Mountains Formation thus temporally overlaps emplacement and deformation of the deformed diorite, thus establishing a link between southeast-directed deformation in the Maria Fold and Thrust Belt and sedimentation in the McCoy Basin. In other words,

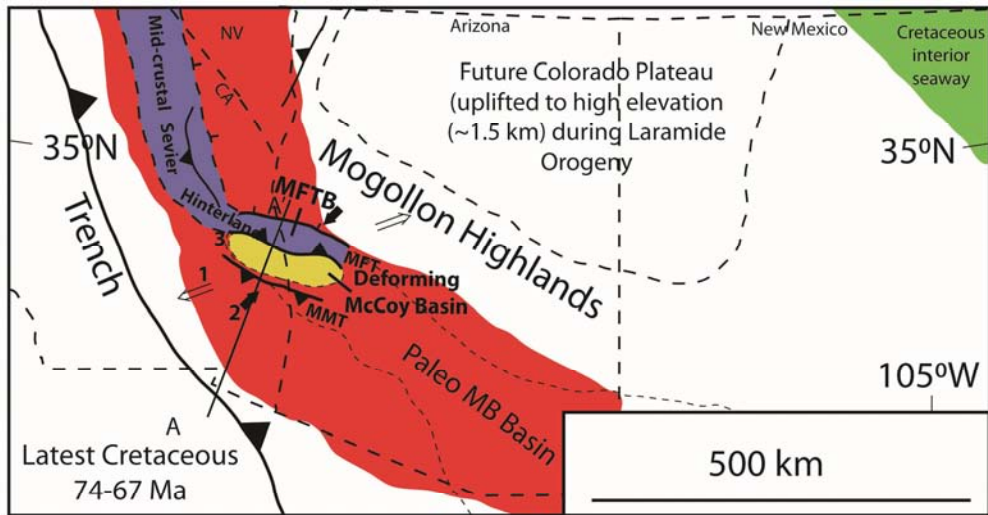
while sediments were being deposited at the surface in the McCoy transpressive retroarc basin, rocks in the Maria Fold and Thrust Belt to the north (and at deeper levels) were being deformed at middle crustal depths. Furthermore, this link effectively rules out any penetrative Jurassic deformation in the western Maria Fold and Thrust Belt (Hamilton, 1982). It is likely that the right lateral transpressive fault between the McCoy Basin and the Maria Fold and Thrust Belt to the north represents an accommodation zone for southeast-directed thrusting during the Sevier Orogeny as shown in our map. This transpressional accommodation zone may have exploited a previously established McCoy rift east-west trending normal fault but we cannot demonstrate this conclusively. Figure 2.38 takes our interpretation into account and shows the geometry through the Maria Fold and Thrust Belt and McCoy Basin along a north-south axis. Our interpretation refines current models of Mesozoic tectonism by accounting for how rocks in the Maria Fold and Thrust Belt reached middle crustal depths and why rocks in the McCoy Basin did not, explains contrasting styles of deformation from the Maria Fold and Thrust Belt to the McCoy Basin, precisely constrains timing of D_1/D_2 deformation and confirms the hypothesis that sedimentation in the McCoy Basin can be linked temporally to deformation in the Maria Fold and Thrust Belt.

Late Cretaceous to Eocene: Laramide tectonism, widespread magmatism, deformation and metamorphism and rapid cooling (80-55) Ma

Figure 2.39 shows a tectonic map of the southwestern U.S. with accompanying schematic cross section during Latest Cretaceous time. By this time, middle crustal rocks in the Sevier hinterland region have begun to be exposed and the frontal thrusts of the Sevier Fold and Thrust Belt and the associated foreland basin have extended farther east. The magmatic arc reaches its greatest lateral extent, spreading across into southern Arizona and into southwestern New Mexico. Uplift of the Colorado Plateau and Laramide foreland uplifts is observed to take place at this time, and the westward limit of the Cretaceous Interior Seaway has regressed into northeasternmost New Mexico. As discussed earlier, regional observations and studies of the Maria Fold and Thrust Belt and

surrounding areas indicate that peak metamorphism and deformation in the Sevier hinterland were coeval with this stage of Cretaceous plutonism (Hoisch et al., 1988; Carl et al., 1991; Foster et al., 1992; Wells et al., 2002; Wells and Hoisch, 2008). This investigation indicates that in the western Maria Fold and Thrust Belt, deformation caused by NE-SW directed shortening refolded earlier fabrics and that emplacement of Late Cretaceous plutons was coeval with this stage of deformation. The inferred strain field for Late Cretaceous time is shown on Figure 2.39. For this strain field the shortening direction has rotated significantly counterclockwise from the D_1/D_2 strain field. Evidence exists that demonstrates extension nearly parallel to shortening toward the late stages of D_3 , consistent with regional observations that there was synconvergent extension in the Sevier Hinterland, including the Maria Fold and Thrust Belt. This interpretation is constrained by (1) analysis of the leucogranite dike swarm in the Big Maria Mountains, indicating that extension during emplacement of the dikes was ENE-WSW directed, (2) the Cretaceous Granite Mountains metamorphic core complex, which, based on available kinematic data, formed as a result of NE-directed extension, and (3) shear bands documenting northeast-directed ductile extension in the Little Maria Mountains (Ballard, 1990). Northeast-vergent folds in the Big Maria Mountains that refold earlier fabrics also document reorientation of the strain field but demonstrate that D_3 (Laramide) deformation in this area was both contractile and extensional. We interpret that northeast-directed compression overthickened cratonic crust to the point where it collapsed during orogenesis. Crustal collapse removed supracrustal rocks from above the Maria Fold and Thrust Belt and led to extrusion and exhumation of these middle crustal rocks.

The strain field determined for this time period also predicts continued north-south directed shortening, which explains the apparently anomalous south-vergence of structures in the Maria Fold and Thrust Belt compared to the rest of the Cordillera. South-vergent structures are anomalous because they indicate transport *away* from the continent, unlike most structures from the Sevier Fold and Thrust Belt and Andean Cordillera, which show vergence toward the continent. Our tectonic map for this time period shows that Maria Fold and Thrust Belt inherited its anomalous (in respect to cutting across the



- 1 Extension direction determined from analysis of dike swarm, quartz veins and Granite Mtns. core complex
- 2 Shortening direction inferred from orientation of S_3 Foliation plane
- 3 Maria Frontal Thrust inferred based on juxtaposition of middle crustal rocks next to supracrustal rocks

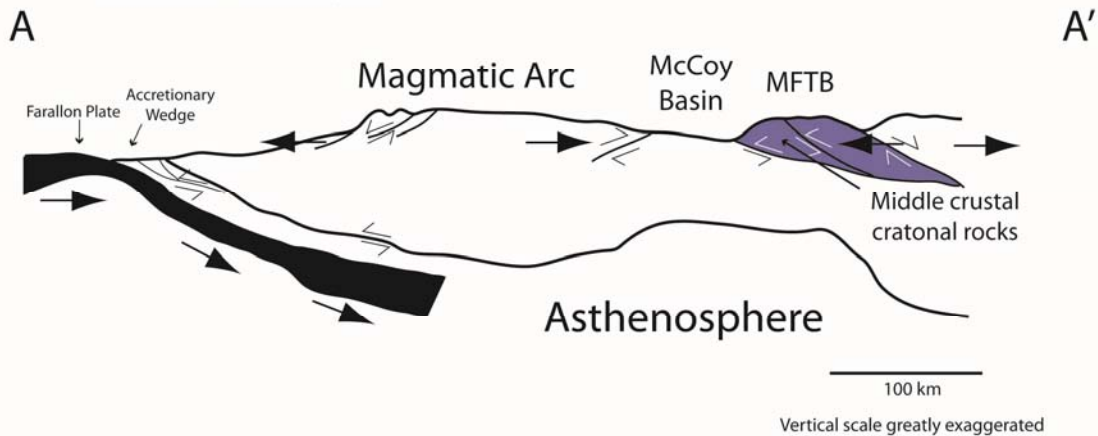


Figure 2.39: Latest Cretaceous tectonic map of the southwestern U.S. Maria Fold and Thrust Belt (MFTB) exhumed during this time. No further sedimentation in the McCoy Basin. Rocks throughout the region experience deformation and peak metamorphic conditions. Strain ellipse for MFTB region constrained by Granite Mountains core complex analysis, dike and quartz vein field analyses, fold geometry and kinematic indicators in the MFTB and south-vergent shortening structures in the McCoy Basin. Modified from DeCelles (2004) and Spencer et al. (2005)

grain of the Cordillera) geometry from the initial configuration of the McCoy-Bisbee rift basin. The Maria Fold and Thrust Belt and Cretaceous McCoy Basin are shown to spatially overlap the original McCoy-Bisbee rift basin. Since the Maria Fold and Thrust Belt is oriented east-west, it would be aligned perpendicular to the shortening direction for the latest Cretaceous paleo strain field, and thus would be pushed northward up over the Cretaceous McCoy Basin along the Maria Frontal Thrust. This would also account for south-vergent ductile thrusts present in the Maria Fold and Thrust Belt. Additionally, this strain field explains south-vergent structures in the McCoy Basin. Examples of these types of structures observed in southeastern California include the south vergent Palen Pass syncline (in the footwall of the thrust), and the north-dipping cleavage observed in the northern McCoy Mountains. We also interpret that the north-vergent Mule Mountains thrust also formed in this strain field, though analysis of quartz veins in the northern McCoy Mountains indicate that the Mule Mountains thrust was slightly more northeast than north-vergent, but the north-directed shortening direction indicated by the Mule Mountains thrust fits in with this overall strain field.

Timing of peak metamorphic conditions is inferred to be syntectonic with emplacement of Cretaceous plutons (Wells and Hoisch, 2008) in southeastern California as indicated by regional thermochronology studies. Ar-Ar thermochronology of hornblende crystals in this study shows that rocks in the Big Maria Mountains cooled below 500°C at ~70 Ma by this time, indicating that peak metamorphism took place at around this time. This is in excellent agreement with timing of the emplacement of Late Cretaceous plutons. Based on peak metamorphic conditions determined for the region by Hoisch et al. (1988), rocks in the Maria Fold and Thrust Belt were metamorphosed at amphibolite grade. Thus, hornblende ages indicate timing of peak metamorphism. Our data confirms the hypothesis that peak metamorphism was coeval with emplacement of Late Cretaceous plutons. Field observations indicate that D₃ deformation in the area took place syntectonically with emplacement of the plutons. Therefore, northeast-directed extension, Cretaceous plutonism and peak metamorphic conditions were all coeval. This event also coincides with deposition of the Pelona-Rand-Orocopia schist (Grove et al.,

2003), which is inferred to represent an accretionary wedge complex related to a northeast-dipping subducting slab during the Laramide Orogeny.

Ar-Ar ages from biotite grains in this age indicate that rocks in this area cooled through $\sim 350^{\circ}\text{C}$ by Paleocene time (between 60-54 Ma). This is consistent with observations in the area made from other workers (e.g. Knapp and Heizler, 1990; Foster et al., 1992). The cooling of rocks through this time coincides with a wane in magmatism in the area and provides an upper bound constraint for the timing of D_3 deformation, thus indicating that this is a Late Cretaceous-Paleocene deformation event.

Summary

The main conclusions of our investigation are as follows: 1) The Maria Fold and Thrust Belt-McCoy Basin region records a complex history of deformation in response to convergent margin tectonism off the west coast of North America. The McCoy Basin originated as a WNW-trending rift basin during the Late Jurassic. Rift formation was coeval with Late Jurassic magmatism in the region. The geometry of this basin greatly influenced the later geometry of the Maria Fold and Thrust Belt. An unconformity in the rift basin deposits indicated by detrital zircon data and confirmed by structural analysis is concomitant with a wane in magmatism. Early Late Cretaceous sedimentation in the McCoy Basin was deposited in the pre-existing McCoy Basin and timing of deposition is coeval with a revival in magmatic activity in the region. Rift faults in the McCoy Basin likely were reactivated during southeast-directed thrusting during the Sevier Orogeny forming the Cretaceous McCoy retroarc foreland basin. 2) Three regional Late Cretaceous deformation events are recognized in the Maria Fold and Thrust Belt and McCoy Basin region. Structures in the Maria Fold and Thrust Belt correlated to D_1/D_2 deformation in the Big and Little Maria Mountains formed as the result of northwest-directed underthrusting of the Cordilleran miogeocline during the Sevier Orogeny. Onset of this deformation event occurred at ~ 97 Ma and is linked to deposition of the upper McCoy Mountains Formation in a retroarc foreland basin during Late Cretaceous time. The timing of middle crustal deformation in the Maria Fold and Thrust Belt is constrained to

after ~86 Ma based on the age of a diorite sample in the Big Maria Mountains. In the Maria Fold and Thrust Belt to the north, deformation is characterized by isoclinal folding and high strain ductile shear zones formed as a result of progressive southeast-directed reverse and ductile shear. D_1/D_2 deformation continued until at least 84 Ma based on detrital zircon ages from the upper McCoy Mountains Formation. 3) D_3 deformation is coeval with peak metamorphism at ~70 Ma and is characterized by both northeast-directed shortening and extension, which led to synorogenic collapse and unroofing of the Sevier hinterland during the Laramide Orogeny. Late Cretaceous plutons are observed to be emplaced coeval with D_3 deformation and widespread Late Cretaceous metamorphism between 75-67 Ma. Structures associated with northeast-southwest directed shortening are observed in the Maria Fold and Thrust Belt and McCoy Basin. Structures correlative to this event are the Maria Frontal Thrust, which emplaces the middle crustal Maria Fold and Thrust Belt over the supracrustal McCoy Basin, the south-vergent Palen Pass syncline and the north-dipping cleavage in the McCoy Basin. Ar-Ar analysis of hornblende grains at ~70 Ma constrains timing of metamorphism. 4) Our study confirms that rotation of the strain field from D_1/D_2 to D_3 deformation records evolving stress fields from the Sevier to Laramide Orogeny from top-southeast directed reverse and dextral shear to northeast-southwest-directed shortening and later extension in the Maria Fold and Thrust Belt. 5) Deformation and metamorphism likely ended by Late Paleocene to Early Eocene time (60-54 Ma) as indicated by Ar-Ar ages for biotite in the Big Maria Mountains. This is coincident with the end of the Laramide Orogeny in the southwestern Cordillera.

Chapter 3 : A new geologic map of the Maria Fold and Thrust Belt, southeastern California: A digital repository for multiple integrated datasets

Salem, A.C and Karlstrom, K.E.

Introduction

With this report we present a new geologic map of the western half of the Maria Fold and Thrust Belt, southeastern California. The Maria Fold and Thrust Belt (Reynolds et al., 1986) is characterized by primarily south and southeast-vergent isoclinal folds and ductile shear zones found in an area approximately 150 km long east-to-west and approximately 50 km. wide north-to-south that trends roughly east-west across Arizona and California. The geology of the Maria Fold and Thrust Belt consists of highly deformed and metamorphosed Proterozoic, Paleozoic and Mesozoic cratonal rocks correlative to rocks observed in the Colorado Plateau region and in southeastern Arizona. The Maria Fold and Thrust Belt is flanked to the south and trends subparallel with the McCoy Basin (Harding and Coney, 1985), which is defined by exposures of Jurassic-Cretaceous McCoy Mountains Formation. The McCoy Mountains Formation is > 7 km thick sedimentary unit consisting primarily of sandstone, siltstone and conglomerate variably interbedded with calcareous rocks and limestone. Although rocks in the McCoy Basin also have been deformed and metamorphosed, in contrast with the Maria Fold and Thrust Belt, rocks in the McCoy Basin have experienced low grade metamorphism and deformation may mostly be characterized as brittle. In the McCoy Basin, McCoy Mountains Formation is deposited primarily on Jurassic volcanic rocks. Highly deformed and metamorphosed rocks in the Maria Fold and Thrust Belt have weakly deformed and metamorphosed correlatives in the McCoy Basin, thus establishing a geologic link between the two provinces.

Recent advances in thinking about structural geology and tectonics, as well as new methods of structural analysis and geochronology, have greatly improved our understanding of this important and enigmatic part of the North American Cordillera. However, obtaining geologic data upon which to base effective future investigations in

the region is difficult. Published geologic maps from the area currently include a 1:24,000 map of the Big Maria Mountains NE Quadrangle (Hamilton, 1964), a 1:48,000 map of the Big Maria Mountains (Hamilton, 1984), a 1:24,000 map of the Palen Pass Quadrangle (Stone and Kelly, 1989), the 1:250,000 compilation map of the Salton Sea sheet (Jennings, 1967) and the recently compiled 1:100,000 map of the western half of the Blythe sheet (Stone, 2006). Most of the excellent geologic mapping done by workers in the region, especially in the California half of the Maria Fold and Thrust Belt and McCoy Basin remains unpublished and may currently only be accessed from master's theses or doctoral dissertations. Thus, there is a need for a data repository that is easily accessible by the geologic community at large for this region. The Maria Fold and Thrust Belt makes a good test case for developing a digital geologic map archive. With so much data scattered throughout many sources it would be ideal to gather these data sets and store them all in one place. Additionally, an area as structurally complex as the Maria Fold and Thrust Belt needs to be examined at a variety of scales. It is with these reasons in mind that we undertook compilation of a new geologic map of the western portion of the Maria Fold and Thrust Belt and McCoy Basin. We utilized the powerful spatial capabilities of ArcGIS to compile geologic maps from a wide range of data sources. The results are a published 1:24,000 tectonic map of the Big Maria Mountains and a published 1:48,000 scale tectonic map of the western Maria Fold and Thrust Belt. These paper maps will be made available for publication and dissemination to the scientific community at large and the map file compiled in ArcGIS will serve as a digital archive for geologic, geophysical and geochemical data that can be shared among geologists interested in the area, as well one that can be added to as data becomes available. Although our work primarily focuses on Mesozoic tectonism, important major Cenozoic tectonic features are noted as well. Finally, geologic cross sections through the Big Maria Mountains, the Little Maria and McCoy Mountains and the Granite and Palen Mountains were generated from these maps, which provide a comprehensive overview of Mesozoic and Cenozoic deformation events in the region.

Datasets used

Creation of a digital archive in the form of a personal geodatabase using ArcGIS allows the geologist unprecedented capability for working with, storing and studying geospatial datasets at a variety of scales. The advantages of using ArcGIS include: 1) georeferencing capability that allows for all images to be referenced to an actual part of the earth's surface, 2) each geologic map or remote sensing image or other data set can be a separate layer in the same file, eliminating the need to flip back and forth between one map or another, 3) maps and images can be scaled to any scale the user wishes, allowing for easy integration of maps and images originally produced at different scales, 4) spatial analysis tools allow for quick analysis of area and distances on the earth's surface, which aid in palinspastic reconstruction of deformed terranes, 5) drafting of lines and polygons can be traced right over any dataset the user wishes, 6) sample locations can be easily input either by hand from the user or downloaded directly from a GPS and 7) maps can be printed at any scale the user wishes directly from the geodatabase, including or excluding any data layer the user sees fit.

In this investigation, we worked with high resolution mapping done as part of a doctoral dissertation by Salem (2009) at 1:12,000 and 1:6,000 scale, the published geologic maps described above and previously unpublished mapping as described below, digital orthophotoquads (DOQQ), aerial photographs and satellite images, TIMS remote sensing images and a metamorphic isograd map from the Big Maria Mountains. In the past, trying to work with all of these different datasets would have required tedious copying and scaling by hand, being careful to make sure all the different maps were copied to the exact scale and project correctly. In addition, working with more than two datasets at any given time would have been extremely cumbersome. ArcGIS allowed us to work quickly and easily with all of these datasets to produce a robust, spatially accurate geologic map.

New high resolution mapping done from 2004-09

Previously unpublished field mapping at a variety of scales done by us from 2004-09 in the Big Maria, McCoy and Palen Mountains was compiled in the geodatabase. These maps include a 1:24,000 map of the Big Maria syncline from a master's thesis (Salem, 2005), 1:6,000 mapping of three structural domains from the same area mapped during 2006-08, and 1:12,000 mapping from Palen Pass mapped during Spring 2007 and the northern McCoy Mountains, mapped in Spring 2007 and Winter 2009. Sample locations were recorded using a handheld GPS unit in the field, which was also used to assist in accurately mapping contact lines and recording measurement locations.

Pre-existing published and unpublished geologic mapping

A compilation effort of this magnitude relies heavily on contributions made by other workers. For the Big Maria Mountains, we used Hamilton's unpublished 1:24,000 map of the entire mountain range. For the Little Maria Mountains, we used Ballard's (1990) unpublished 1:24,000 scale map from his doctoral dissertation. For the McCoy and Palen Mountains, we used Pelka's 1:31,250 mapping from his doctoral dissertation (1973). For Palen Pass and the southern Granite Mountains, we used Stone and Kelly's (1989) 1:24,000 map of the Palen Pass Quadrangle. For the Arica and Riverside Mountains, we used maps from master's theses by Baltz (1982) and Lyle (1982) respectively. For the rest of the northwest portion of the map area, we used Howard's (2002) published 1:100,000 map of the Sheep Hole Mountains sheet.

TIMS and other remote sensing data

Aerial photographs aided in mapping the swarm of leucogranite pegmatites in the west-central Big Maria Mountains. Also, images from the Thermal Infrared Multispectral Scanner (TIMS) from NASA (1995) aided in mapping portions of the Big Maria Mountains. The TIMS is a multispectral scanner system using a dispersive grating and a six element mercury cadmium to produce six discrete channels in the 8.2 to 12.2 micron region. Using an airborne geologic remote sensing tool, the TIMS acquires mineral

signature data that permits the discrimination of silicate, carbonate and hydrothermally altered minerals (<http://www.nasa.gov/centers/dryden/research/AirSci/ER-2/tims.html>). The data are then calibrated and atmospherically corrected, and emissivity variations in the form of alpha residuals are extracted from which color composite images can be made (Hook et al., 1994). In these color composite images, for example, quartz shows up as red, feldspar and mica as purple, calc-silicate minerals as blue and carbonates as green. These images had been used successfully by Morrissey (1999) in a study of the range and in the Piute Mountains to the northwest (Hook et al., 1994). These images are high quality and have a resolution of ~3 m per pixel. In areas of minimal vegetation and excellent bedrock exposure, like southeastern California, TIMS data is highly applicable in a setting like this, as these mountains contain little vegetation and have almost 100% exposure of bedrock. Therefore, in the TIMS images, mappable units of different lithologies starkly contrast with each other, e.g. the Kaibab Marble shows up as green with blue streaks and is contact with the Coconino Quartzite, which shows as a red or reddish orange unit. Therefore, it is possible to accurately map portions of the mountain range that the TIMS image covers with a reasonable amount of accuracy. In addition, in the TIMS images vegetation also shows up as green and it is often easy to identify washes on the TIMS images as green dotted lines. The washes aided in georeferencing the TIMS images, as bends in washes and stream confluences were useful registration points when compared with the base topographic map. However, georeferencing the TIMS images presented a challenge, due to distortion of the images during the collection process and the large aerial extent of the images. Despite this, the TIMS images provided an invaluable guide in mapping units and in identifying mesoscopic and macroscopic folds and faults.

Metamorphic isograd map

The metamorphic isograd map from Hoisch et al. (1988) for the Big Maria Mountains was georeferenced and added to the 1:24,000 geologic map of the Big Maria

Mountains. This map shows zones of different metamorphic grade. This map is useful for showing spatial trends in metamorphic grade of rocks in the range.

Digitization and compilation methods

Except for the 1:100,000 scale maps of the Blythe sheet (Stone, 2006), the Sheep Hole Mountains sheet (Howard, 2000) and the TIMS images, most other maps had to be digitally scanned. Once maps were in digital format, they then had to be georeferenced in ArcGIS. The projection system used was Universal Transverse Mercator (UTM), North American Datum 1927 (NAD 27), which was selected because this is the projection system used for topographic base maps from the area. Sample locations in the field were recorded in the GPS as UTM readings in NAD 27. Topographic maps, digital elevation models and DOQQ of the region were acquired from the USGS Seamless Server (http://www.usgs.gov/seamless_server). These files already contain spatial information and are georeferenced in UTM NAD27, allowing for easy importation into ArcGIS. Georeferencing most of the unpublished geologic maps was relatively easy, as these maps consisted of geologic mapping overlain over topographic base maps. This provided several registration points that could be used for georeferencing. Georeferencing the metamorphic isograd map involved using the outline trace of the mountain range as registration points. Finally, the method of and difficulties with georeferencing the TIMS images is described above.

Once these maps and images were georeferenced, the master map was by drawing geologic formations as polygons with different colors and assigning attributes to the polygons. These attributes include the formation name, age and map symbol, for example Kaibab Marble, Permian, Pk. Formations were assigned colors based on their stratigraphic ages. For example, Paleozoic units are depicted in shades of blue, Mesozoic sedimentary units in shades of green, Proterozoic crystalline rocks as brown and so on. Color selection was based primarily on USGS standard colors for published geologic maps, as outlined in USGS Open File Report 99-430. Some exceptions include lower Paleozoic units, which were assigned shades of red to make them stand out more, Tertiary

sedimentary deposits, which were assigned subdued shades of pink and Quaternary surficial deposits were left white, in order that Mesozoic and older bedrock units would stand out in contrast. Structural measurements were plotted on the map as point features and assigned attributes, though. For example, strike and dip measurements were assigned strike, dip and dip direction values using azimuth notation, whereas linear features, such as fold axes, were assigned trend and plunge. Linear features, such as faults and fold axes were assigned attributes such as name, type of fault or fold and so on. All of these features are saved in data tables that are automatically referenced to the personal database and can be updated as necessary by the user. Symbology for features, such as folds, faults and other structural measurements were after the symbols shown in the digital cartographic standards as outlined in USGS Open File Report 99-430.

For the 1:24,000 geologic map of the Big Maria Mountains, units were assigned names and ages after the stratigraphy for the range outlined in Hamilton (1982) and Salem (2005); stratigraphic names for Mesozoic metasedimentary units are after Reynolds et al. (1987). For the 1:100,000 map of the western Maria Fold and Thrust Belt and McCoy Basin, unit name and age assignment is after Stone (2006) and Harding and Coney (1985).

Future directions and summary

As more geologic investigations are conducted in the region, data can easily be added to the personal geodatabase digital archive. We envision that eventually, georeferenced field photos, thin sections, geophysical data, metamorphic data and geochronologic data (as well as other forms of geologic data) will be added to the digital archive. It is our hope that this new detailed geologic map will spur future workers to continue investigations in this interesting, yet poorly understood part of the North American Cordillera and that this map will be consulted often as a reference for future investigators to base their studies on. In particular, we hope that more detailed studies of pressure-temperature conditions of metamorphism and detailed structural analysis will be

conducted in the region. The published paper maps and the digital archive of the area should serve as a springboard and a guide for these future investigations.

In conclusion, we have compiled all of the existing published and unpublished geologic mapping in the region into a master map of the western Maria Fold and Thrust Belt and McCoy Basin. We have added our own detailed geologic mapping of key locales in the region and have annotated the map based on our interpretations of the data in accordance with local and regional constraints. The map was augmented with remote sensing data, including TIMS images, to make the most robust and current tectonic map of the region. This map was a necessary compilation of multiple datasets scattered throughout a variety of published and unpublished sources. It is our hope that this map will act as a springboard and as a guide for future investigations in this important part of the Cordillera.

References

- Anderson, J.L., 1988, Core complexes of the Mojave-Sonoran Desert: Conditions of plutonism, mylonitization and decompression, *in* Ernst, W.G., ed., *Metamorphism and crustal evolution of the western United States (Rubey volume 7)*: Englewood Cliffs, New Jersey, Prentice Hall, p. 502–525.
- Anderson, P., 1989, Proterozoic plate tectonic evolution of Arizona, *in* Jenney, J.P., and Reynolds, S.J., eds., *Geologic evolution of Arizona: Tucson, Arizona*, Arizona Geological Society Digest, vol. 17, p. 17-55.
- Applegate, J.D.R., Walker, J.D., and Hodges, K.V., 1992, Late Cretaceous extensional unroofing in the Funeral Mountains metamorphic core complex, California: *Geology*, v. 20, p. 519–522, doi: 10.1130/0091-7613(1992)020 <0519:LCEUIT>2.3.CO;2.
- Asmerom, Y., 1988, Mesozoic igneous activity in the southern Cordillera of North America: Implications for tectonics and magma genesis [Ph.D. thesis]: University of Arizona, Tucson, 232 p.
- Asmerom, Y., Zartman, R.E., Damon, P.E. and Shafiqullah, M., 1988, U-Th-Pb zircon ages from the Santa Rita Mountains, SE Arizona: Implications for timing of early Mesozoic magmatism: *Geological Society of America Abstracts with Programs*, v. 20, p. 140
- Ballard, S.N., 1990, The Mesozoic structural evolution of the Little Maria Mountains, Riverside County, California [Ph.D. dissertation]: University of Southern California, Santa Barbara.
- Baltz, R., 1982, Late Mesozoic folding and thrusting and Tertiary extensional faulting in the Arica Mountains, Riverside County, California, *in* Frost, E.G., and Martin, D.L., eds., *Mesozoic-Cenozoic tectonic evolution of the Colorado River region, California, Arizona, and Nevada: Cordilleran Publ.*, San Diego, California, p. 582-596
- Banakar, V.K., Galy, A., Sukamaran, N.P., Parthiban, G., and Volvaiker, A.Y., 2003, Himalayan sedimentary deposits recorded by silicate detritus within a ferromanganese crust from the central Indian Ocean, *Earth and Planetary Science Letters*, vol. 205, no. 3-4, p. 337-348.
- Barth, A.P., and Schneiderman, J.S., 1996, A comparison of structures in the Andean Orogen of northern Chile and exhumed midcrustal structures in southern California, USA: An analogy in tectonic style?: *International Geology Review*, v. 38, p. 1075–1085.

- Barth, A.P., Wooden, J.L., Grove, M., Jacobson, C.E., and Pedrick, J.N., 2003, U-Pb zircon geochronology of rocks in the Salinas Valley region of California: A reevaluation of the crustal structure and origin of the Salinian block: *Geology*, v. 31, p. 517–520
- Barth, A.P., Wooden, J.L., Jacobson, C.E. and Probst, K., 2004, U-Pb geochronology and geochemistry of the McCoy Mountains Formation, southeastern California: A Cretaceous retroarc foreland basin: *Geological Society of America Bulletin*, v. 116, p. 142-153.
- Beaumont, C., Jamieson, R.A., Nguyen, M.H., Lee, B., 2001, Mid-Crustal channel flow in large hot orogens: results from coupled thermalmechanical models. In: Cook, F., Erdmer, P. (Eds.), *Slave—Northern Cordillera Lithospheric Evolution (SNORCLE) and Cordilleran Tectonics Workshop; Report of 2001 Combined Meeting Lithoprobe Report*, 79, p. 112–170.
- Beus, S.S. and Morales, M., 2003, *Grand Canyon Geology*, 2nd edition: Oxford Press, New York, 432 p.
- Beus, S.S., 2003a, Temple Butte Formation, *in* Beus, S.S., and Morales, M., eds., *Grand Canyon Geology*, 2nd edition: Oxford Press, New York, p. 107-114.
- Beus, S.S., 2003b, Redwall Limestone and Surprise Canyon Formation, *in* Beus, S.S., and Morales, M., eds., *Grand Canyon Geology*, 2nd edition: Oxford Press, New York, p. 115-135
- Beus, S.S., and Morales, M., 2003, *Grand Canyon Geology*, 2nd edition: Oxford Press, New York, 432 p.
- Blakey, R.C., 2003, Supai Group and Hermit Formation, *in* Beus, S.S., and Morales, M., eds., *Grand Canyon Geology*, 2nd edition: Oxford Press, New York, p. 136-162.
- Boggs, S., 2000, *Principles of Sedimentology and Stratigraphy*, 3rd edition: Prentice Hall, New York, 770 p.
- Boettcher, S.S., Mosher, S. and Tosdal, R.M., 2002, Structural and tectonic evolution of Mesozoic basement-involved fold nappes and thrust faults in the Dome Rock Mountains, Arizona; *Geological Society of America Special Paper*, vol. 365, pp. 73-97.
- Brathvode, J.R., 1986, *Stratigraphy of the Grand Wash Dolomite (Upper? Cambrian), Western Grand Canyon, Mohave County, Arizona [M.S. thesis]: Northern Arizona University, Flagstaff, 140 p*

- Buising, A.V., 1990, The Bouse Formation and bracketing units, southeastern California and western Arizona—implications for the evolution of the proto-Gulf of California and the lower Colorado River: *Journal of Geophysical Research*, v. 95, no. B12, p. 20,111–20,132
- Burchfiel, B.C., Chen, Z., Hodges, K.V., Liu, Y., Royden, L.H., Deng, C. and Xu, J., 1992, The South Tibetan detachment system Himalayan Orogen: extension contemporaneous with and parallel to shortening in a collisional mountain belt, *Geological Society of America Special Paper*, vol. 269, 41 p.
- Burchfiel, B.C., and Davis, G.A., 1981, Mojave desert and environs, *in* Ernst, W.G., ed., *The Geotectonic development of California: Englewood Cliffs, New Jersey, Prentice-Hall*, p. 217-252.
- Burchfiel, B.C., and Davis, G.A., 1975, Nature and controls of Cordilleran orogenesis, western United States: Extensions of an earlier synthesis: *American Journal of Science*, 275-A, p. 363-396.
- Busby-Spera, C.J., 1988, Speculative tectonic model for the early Mesozoic arc of the Southwestern Cordilleran United States, *Geology*, vol. 16, no. 12, pp. 1121-1125
- Calzia, J.P., 1982, Geology of granodiorite in the Coxcomb Mountains, southeastern California, *in* Frost, E.G. and Martin, D.L, eds., *Mesozoic-Cenozoic tectonic evolution of the Colorado River region, California, Arizona, and Nevada (Anderson-Hamilton volume): San Diego, Cordilleran Publishers*, p. 173–181
- Carl, B.C., Miller, C.F., and Foster, D.A., 1991, Western Old Woman Mountains shear zone: Evidence for latest Cretaceous core complex development in southeastern California: *Geology*, v. 19, p. 893–896
- Christiansen, E.H., Kowallis, B.J., and Barton, M.D., 1994, Temporal and spatial distribution of volcanic ash in Mesozoic sedimentary rocks of the western interior: an alternative record of Mesozoic magmatism, *in* Caputo, M.V., Peterson, J.A. and Franczyk, K.J., eds.. *Mesozoic systems of the Rocky Mountain region, USA: Denver, Colorado, Rocky Mountain Section SEPM*, p. 73-94
- Coney, P.J., and Harms, T.A., 1984, Cordilleran metamorphic core complexes: Cenozoic extensional relics of Mesozoic compression: *Geology*, v. 12, p. 550–554
- Cloetingh, S., Cornu, T., Ziegler, P.A., and Beekman, F., 2003, Neotectonics and intraplate continental topography of the northern Alpine Foreland, *Earth Science Reviews*, vol. 74, no. 3-4, pp. 127-196

- Dahlen, F.A., 1990, Critical taper model of fold and thrust belts and accretionary wedges, *Annual Review of Earth and Planetary Sciences*, vol. 18, 55-99
- Davis, G.H. and Reynolds, S.J., 1996, *Structural Geology of Rocks and Regions*, 2nd edition: John Wiley and Sons, Inc., New York, 776 p.
- DeCelles, P.G., 2004, Late Jurassic to Eocene evolution of the Cordilleran thrust belt and foreland basin system, western USA: *American Journal of Science*, vol. 304, p. 105–168
- Demaree, R.G., 1981, *Geology of Palen Pass, Riverside County, California*, MS Thesis: San Diego State University, San Diego, CA
- Dickinson, W.R., 1981, Plate tectonics and the continental margin of California, *in* Ernst, W.G., ed., *The geotectonic development of California (Rubey Volume I)*: Englewood Cliffs, New Jersey, Prentice-Hall, p. 1–28.
- Dickinson, W.R., Fiorillo, A.R., Hall, D.L., Monreal, R., Potochnik, A.R., and Swift, P.N., 1989, Cretaceous strata of southern Arizona, *in* Jenney, J.P., and Reynolds, S.J., eds., *Geologic evolution of Arizona: Arizona Geological Society Digest*, v. 17, p. 447–461.
- Dickinson, W.R., and Lawton, T.F., 2001, Carboniferous to Cretaceous assembly and fragmentation of Mexico: *Geological Society of America Bulletin*, v. 113, p. 1142–1160, doi: 10.1130/0016-7606(2001)113<1142: CTCAAF>2.0.CO;2.
- Dupuis, C.A. and Walker, J.D., 1996, Deformation history of the Arica Mountains southeastern California: *Geological Society of America Abstracts with Programs*, vol. 28, no. 7, p. 115
- Ehlig, P.L., 1981, Origin and tectonic history of the basement terrane of the San Gabriel Mountains, central Transverse Ranges, *in* Ernst, W.G., ed., *The geotectonic development of California; Rubey Volume 1*: Englewood Cliffs, New Jersey, Prentice-Hall, p. 253–283
- Ellis, M.J., 1982, Structural analysis of the Big Maria Mountains, Riverside County, California, *in* Frost, E.G., and Martin, D.L., *Mesozoic-Cenozoic tectonic evolution of the Colorado River region, California, Arizona, and Nevada: Cordilleran Publ.*, San Diego, CA, United States, p. 222-233.

- Emerson, W.S., 1981, Geological and deformational characteristics of the Little Maria Mountains, Riverside County, California [M.S. thesis]: San Diego State University, San Diego, CA, 98 p
- Fackler-Adams, B.N., Busby, C.J., and Mattinson, J.M., 1997, Jurassic magmatism and sedimentation in the Palen Mountains, southeastern California: Implications for regional tectonics on the Mesozoic continental arc: Geological Society of America Bulletin, v. 109, 1464-1484
- Fletcher, J.M., Bartley, J.M., Martin, M.W., Glazner, A.F., and Walker, J.D., 1995, Large magnitude continental extension: An example from the central Mojave metamorphic core complex: Geological Society of America Bulletin, v. 107, p. 1468–1483
- Fletcher, J.M. and Karlstrom, K.E., 1990, Late Cretaceous ductile deformation metamorphism and plutonism in the Piute Mountains, eastern Mojave Desert, Journal of Geophysical Research, vol. 95, no. B1, p. 487-500
- Fletcher, J.M., Karlstrom, K.E., Ring, T.E., Wooden, J.E. and Foster, D.A., 1988, Tectonic style and timing of deep-seated Mesozoic crustal shortening: Piute Mountains, eastern Mojave Desert, Geological Society of America Abstracts with Programs, vol. 20, A272-273
- Flowers, R.M., Wernicke, B.P. and Farley, K.A., 2008, Unroofing, incision and uplift history of the southwestern Colorado Plateau from apatite (U-Th-He) thermochronology, Geological Society of America Bulletin, vol. 120, no. 5-6, p. 571-587
- Foster, D.A., Harrison, T.M., and Miller, C.F., 1989, Age, inheritance, and uplift history of the Old Woman–Piute batholith, California, and implications for K-feldspar age spectra: Journal of Geology, v. 97, p. 232–243.
- Foster, D.A., Miller, C.F., Harrison, T.M., and Hoisch, T.D., 1992, $^{40}\text{Ar}/^{39}\text{Ar}$ thermochronology and thermobarometry of metamorphism, plutonism, and tectonic denudation in the Old Woman Mountains area, California: Geological Society of America Bulletin, v. 104, p. 176–191
- Gehrels, G. E., V. A. Valencia, and J. Ruiz (2008), Enhanced precision, accuracy, efficiency, and spatial resolution of U-Pb ages by laser ablation–multicollector–inductively coupled plasma–mass spectrometry, *Geochem. Geophys. Geosyst.*, 9, Q03017, doi:10.1029/2007GC001805.
- Godin, L., Grujic, D., Law, R.D. and Searle, M.P., 2006, Channel flow, ductile extrusion and exhumation in continental collision zones; an introduction, *in* Law, R.D., Searle,

- M.P. and Godin, L. (eds.) *Channel Flow, Ductile Extrusion and Exhumation in Continental Collision Zones*, Geol. Soc., London Special Pubs. 268, 1-23
- Grove, M., Jacobson, C.E., Barth, A.P., and Vucic, A., 2003b, Temporal and spatial trends of Late Cretaceous–early Tertiary underplating of Pelona and related schists beneath southern California and southwestern Arizona, *in* Johnson, S.E., et al., eds., *Tectonic Evolution of Northwestern Mexico and Southwestern USA: Geological Society of America Special Paper 374*, p. 381–406
- Hamilton, W.B., 1987, Mesozoic geology and tectonics of the Big Maria Mountains region, southeastern California, *in* Dickinson, W.R., and Klute, M.A, eds., *Mesozoic rocks of southern Arizona and adjacent areas: Arizona Geological Society, Tucson, Arizona* p. 33-47.
- Hamilton, W., 1984, Generalized geologic map of the Big Maria Mountains region, northeastern Riverside County, southeastern California: Open-File Report – U.S. Geological Survey, 1 sheet, U.S. Geological Survey., Reston, VA, United States, pg. 8.
- Hamilton, W., 1982, Structural evolution of the Big Maria Mountains, northeastern Riverside County, southeastern California, *in* Frost, E.G., and Martin, D.L., eds., *Mesozoic-Cenozoic tectonic evolution of the Colorado River region, California, Arizona, and Nevada: Cordilleran Publ., San Diego, CA, United States*, p. 1-27.
- Hamilton, W.B., 1964, Nappes in southeastern California [abs.]: *Geological Society of America Abstracts with Programs*, p. 274.
- Harding, L.E., 1982, Tectonic significance of the McCoy Mountains Formation, southeastern California and southwestern Arizona [Ph.D. Dissertation]: University of Arizona, Tucson, 197 p.
- Harding, L.E., and P.J. Coney, 1985, The geology of the McCoy Mountains Formation, southeastern California and southwestern Arizona: *Geological Society of America Bulletin*, 96, p. 755-769.
- Hargrave, E.V., 1999, Stratigraphy and correlation of Triassic and Jurassic rocks in west-central Arizona and southeastern California [M.S. thesis]: Arizona State University, Tempe
- Hirth, G. and Tullis, J., 1992, Dislocation creep regimes in quartz aggregates; *Journal of Structural Geology*, vol. 14, p. 145-159

- Hilley, G.E., and Strecker, M.R., 2005, Processes of oscillatory basin filling and excavation in a tectonically active orogen; Quebrada del Toro Basin, NW Argentina, *Geological Society of America Bulletin*, vol. 117, no. 7-8, p. 887-901.
- Hobbs, B.E., Means, W.D., Williams, P.F., 1976. *An Outline of Structural Geology*. Wiley, New York.
- Hodges, K.V., and Walker, J.D., 1992, Extension in the Cretaceous Sevier orogen, North American Cordillera; With Suppl. Data 92-13, *Geological Society of America Bulletin*, vol. 104, no. 5, pp. 560-569
- Hoisch, T.D., 1985, Conditions of metamorphism determined from low-grade metagranites, Big Maria Mountains, SE California: AGU 1985 spring meeting, American Geophysical Union, Washington, D.C., p. 385
- Hoisch, T.D., Miller, C.F., Heizler, M.T., Harrison, T.M., and Stoddard, E.F., 1988, Late Cretaceous regional metamorphism in southeastern California, *in* Ernst, W.G., ed., *Metamorphism and crustal evolution of the Western United States*: Prentice-Hall, Englewood Cliffs, NJ, United States, p. 539-571.
- Hook, S. J., Karlstrom, K. E., Miller, C. F., and McCaffrey, K. J. W., 1994, Mapping the Piute Mountains, California, with thermal infrared multispectral scanner (TIMS) images, *Journal of Geophysical Research*, vol. 99 (B8), 15,605–15,622
- Horton, B.K., 2005, The role of sedimentary basins in orogenic belts, *Geological Society of America Abstracts with Programs*, vol. 37, no. 7, p. 313
- Howard, K.A., 1986, Evolution of crustal layering in southeastern California: *Geological Society of America Abstracts with Programs*, 18, p. 119.
- Howard, K.A., 2002, Geologic Map of the Sheep Hole Mountains 30' x 60' quadrangle, USGS Miscellaneous Field Studies, MF-2344, 2 sheets
- Howard, K.A., and John, B.E., 1987, Crustal extension along a rooted system of imbricate low-angle faults: Colorado River extensional corridor, California and Arizona, *in* Coward, M.P., et al., eds., *Continental Extensional Tectonics*: Geological Society [London] Special Publication 28, p. 299–312
- Howard, K.A., John, B.E., and Miller, C.F., 1987, Metamorphic core complexes, Mesozoic ductile thrusts, and Cenozoic detachments: Old Woman Mountains–Chemehuevi Mountains transect, California and Arizona, *in* Davis, G.A., and VanderDolder, E.M., eds., *Geologic Diversity of Arizona and Its Margins: Excursions*

- to Choice Areas: Arizona Bureau of Geology and Mineral Technology Special Paper 5, p. 365–382.
- Humphreys, E.D., 1995, Post-Laramide removal of the Farallon slab, western United States: *Geology*, v. 23, p. 987–990
- Jacobson, C.E., 1997, Metamorphic convergence of the upper and lower plates of the Vincent thrust, San Gabriel Mountains, southern California, USA: *Journal of Metamorphic Petrology*, v. 15, p. 155–165.
- Jacobson, C.E., and Dawson, M.R., 1995, Structural and metamorphic evolution of the Orocochia Schist and related rocks, southern California: Evidence for late movement on the Orocochia fault: *Tectonics*, v. 14, p. 933–944.
- Jacobson, C.E., Grove, M., Vucic, A., Pedrick, J.N. and Ebert, K.A., 2007, Exhumation of the Orocochia Schist and associated rocks of southeastern California; relative roles of erosion, synsubduction tectonic denudation, and middle Cenozoic extension, *Geological Society of America Special Paper*, vol. 419, p. 1-37
- Jacobson, C.E., Oyarzabal, F.R., and Haxel, G.B., 1996, Subduction and exhumation of the Pelona-Orocochia-Rand schists, southern California: *Geology*, v. 24, p. 547–550
- Jamieson, R.A., Beaumont, C., Nguyen, M.H., Lee, B., 2002. Interaction of metamorphism, deformation and exhumation in large convergent orogens. *Journal of Metamorphic Geology* 20, 9–24.
- Jennings, C.W., 1967, Salton Sea sheet, Geologic Map of California: California Division of Mines and Geology, 1:250,000
- Karlstrom, K.E. and Bowring, S.A., 1993, Proterozoic orogenic history in Arizona, *in* Van Schmus, W.R. and Brickford M.E., eds. *Transcontinental Proterozoic Provinces, The Geology of North America*, vol. c-2: Precambrian of the Conterminous U.S., Geological Society of America (DNAG), p. 188-228
- Karlstrom, K.E., Ilg, B.R., Williams, M.L., Hawkins, D.P., Bowring, S.A., and Seaman, S.J., 2003, Paleoproterozoic rocks of the Granite Gorges, *in* Beus, S.S., and Morales, M., eds., *Grand Canyon Geology*, 2nd edition: Oxford Press, New York, p. 9-38.
- Karlstrom, K.E. and Williams, M.L., 1998, Heterogeneity of the middle crust; implications for strength of continental lithosphere, *Geology*, vol. 26, no. 9, p. 815-818.

- Kassem, O.K., and Ring, U., 2004, Underplating-related finite strain pattern in the Gran Paradiso Massif, Western Alps, Italy; heterogeneous ductile strain superimposed on a nappe stack, *Journal of the Geological Society of London*, vol. 161, part 5, p. 875-884.
- Kidder, S., Ducea, M., Gehrels, G., Patchett, J., and Vervoort, J., 2005, Tectonic and magmatic development of the Salinian Coast Ridge Belt, California: *Tectonics*, v. 22, 1058, doi: 10.1029/2002TC001409.
- Klepeis, K.A., Clarke, G.L., Gehrels, G.E., and Vervoort, J.D., 2004, Processes controlling vertical coupling and decoupling between the upper and lower crust of orogens; results from Fiordland, New Zealand, *Journal of Structural Geology*, vol. 26, no. 4, p. 765-791.
- Knapp, J.H., and Heizler, M.T., 1990, Thermal history of crystalline nappes of the Maria Fold and Thrust Belt, west central Arizona: *Journal of Geophysical Research*, 95 (B12), 20049-20073
- Kula, J.L., Spell, T.L., and Wells, M.L., 2002, Syntectonic intrusion and exhumation of a Mesozoic plutonic complex in the Late Cretaceous, Granite Mountains, southeastern California: *Geological Society of America Abstracts with Programs*, v. 34, no. 6, p. 249
- Laubach, S.E., Reynolds, S.J., Spencer, J.E., and Marshak, S., 1989, Progressive deformation and superposed fabrics related to Cretaceous crustal underthrusting in western Arizona, U.S.A.: *Journal of Structural Geology*, 11, no. 6, p. 735-749.
- Livaccari, R.F., and Perry, F.V., 1993, Isotopic evidence for preservation of Cordilleran lithospheric mantle during the Sevier-Laramide Orogeny, Western United States: *Geology*, v. 21, p. 719-722
- Ludwig, K., 1980, Calculation of uncertainties of U-Pb isotope data, *Earth Planet. Sci. Lett.*, 46, 212-220.
- Ludwig, K., 2003, *Isoplot 3.00*, Spec. Publ. 4, 70 pp., Berkeley Geochron. Cent., Berkeley, Calif.
- Lyle, J.H., 1982, Interrelationship of late Mesozoic thrust faulting and mid-Tertiary detachment faulting in the Riverside Mountains, southeastern California, *in* Frost, E.G., and Martin, D.L., eds., *Mesozoic-Cenozoic tectonic evolution of the Colorado River region, California, Arizona, and Nevada: Cordilleran Publ.*, San Diego, CA, p. 470-491.

- Martin, D.L., Krummenacher, D., and Frost, E.G., 1982, K/Ar geochronologic record of Mesozoic and Tertiary tectonics of the Big Maria-Little Maria-Riverside Mountains terrane, *in* Frost, E.G., and Martin, D.L., Mesozoic-Cenozoic tectonic evolution of the Colorado River region, California, Arizona, and Nevada: Cordilleran Publ., San Diego, CA, United States, p. 518-549.
- Mather, T., 1970, Stratigraphy and paleontology of Permian Kaibab Formation, Mogollon Rim region, Arizona [Ph.D. Dissertation]: University of Colorado, Boulder, 164 p.
- Mayo, D.P. and Wooden, J.L., 1993, Mingled mafic and felsic magmas in the Jurassic Eagle Mountain Pluton, southeastern California; Geological Society of America Abstracts with Programs, vol. 25. no. 5. pp. 116
- McCaffrey, K.J.W., Miller, C.F., Karlstrom, K.E., and Simpson, C., 1999, Synmagmatic deformation patterns in the Old Woman Mountains, SE California: Journal of Structural Geology, v. 21, p. 335–349
- Means, W.D., 1981. The concept of steady state foliation. Tectonophysics 78, 179–199
- Middleton, L.T., and Elliott, D.K., 2003, Tonto Group, *in* Beus, S.S., and Morales, M., Grand Canyon Geology, 2nd edition: Oxford Press, New York, p. 90-106
- Miller, C.F., and Barton, M.D., 1990, Phanerozoic plutonism in the Cordilleran interior, USA, *in* Kay, M.S., and Rapela, C.W., eds., Plutonism from Antarctica to Alaska: Geological Society of America Special Paper 241, p. 213–231.
- Miller, C.F., and Bradfish, L.J., 1980, An inner Cordilleran belt of muscovite-bearing plutons: Geology, vol. 8, p. 412–416
- Miller, C.F., Howard, K.A., and Hoisch, T.D., 1982, Mesozoic thrusting, metamorphism, and plutonism, Old Woman–Piute Range, southeastern California, *in* Frost, E.G., and Martin, D.L., eds., Mesozoic–Cenozoic Tectonic Evolution of the Colorado River Region, California, Arizona, and Nevada: San Diego, California, Cordilleran Publishers, p. 561–581
- Miller, D.M., and Howard, K.A., 1985, Bedrock geologic map of the Iron Mountains Quadrangle, San Bernardino and Riverside Counties, California: U.S. Geological Survey MF-1736, scale 1:62,500
- Miller, D.M., Howard, K.A., and Anderson, J.L., 1981, Mylonitic gneiss related to emplacement of a Cretaceous batholith, Iron Mountains, southern California, *in* Howard, K.A., Carr, M.D., and Miller, D.M., eds., Tectonic framework of the Mojave

- and Sonoran Deserts, California and Arizona: U.S. Geological Survey Open-file Report 81-503, p. 73-75
- Miller, F.K., and McKee, E.D., 1971, Thrust and strike-slip faulting in the Plomosa Mountains, southwestern Arizona: Geological Society of America Bulletin, 82, p. 717-722
- Miller, W.J., 1944, Crystalline rocks of southern California: *Geological Society of America Bulletin*, 57, p. 457-502.
- Morrissey, G.E., 1999, Structural attenuation in the Big Maria Mountains: A study with the thermal infrared multispectral scanner [M.S. Thesis]: Arizona State University, Tempe, 220 p.
- NASA, 1995, A.R.C., C-130 Flight Summary Report: NASA, Moffett Field, California, 13 p.
- Noble, L.F., 1923, A section of the Paleozoic formations of the Grand Canyon at the Bass trail, *in* Shorter contributions to general geology 1922: U.S. Geological Survey Professional Paper 131, p. 23-73.
- Passchier, C.W. and Trouw, R.A.J., 2004, *Microtectonics*, 2nd edition: Springer, Verlag Berlin Heidelberg, Germany, 322 p.
- Pederson, J.L., Mackley, R.D., and Eddleman, J.L., 2002, Colorado Plateau uplift and erosion evaluated using GIS, *GSA Today*, August, pp. 4-10
- Pelka, G.J., 1973, Geology of the McCoy and Palen Mountains, southeastern California [Ph.D. Dissertation]: University of California, Santa Barbara, 160 p.
- Ramsay, J.G., 1967, *Folding and Fracturing of Rocks*: McGraw-Hill Book Co., New York, 568 p.
- Ramsay, J.G. and Huber, M.I., 1987, *The Techniques of Modern Structural Geology*, 3rd edition: Academic Press, London, 392 p.
- Rehrig, W.A. and Reynolds, S.J., 1980, Geologic and geochronologic reconnaissance of a northwest-trending zone of metamorphic core complexes in southern and western Arizona, *Geological Society of America Memoir*, no. 153, p. 131-157.
- Renne, P.R., Deino, A.L., Walter, R.C., Turrin, B.D., Swisher, C.C., Becker, T.A., Curtis, G.H., Sharp, W.D., Jaouni, A., 1994, Intercalibration of astronomical and radioisotopic time; *Geology*, vol. 22, no. 9, pp. 783-786

- Reynolds, S.J. and Lister, G.S., 1987, Structural aspects of fluid rock interactions in detachment zones, *Geology*, vol. 15, no. 4, p. 362-366
- Reynolds, S.J., Spencer, J.E., Richard, S.M., and Laubach, S.E., 1986, Mesozoic structures in west-central Arizona: *Arizona Geological Society Digest*, 16, p. 35-51.
- Reynolds, S.J., Spencer, J.E., and DeWitt, E., 1987 Stratigraphy and U-Th-Pb geochronology of Triassic and Jurassic rocks in west-central Arizona, *in* Dickinson, W.R., and Klute, M.A., eds., *Mesozoic rocks of central and southern Arizona and adjacent areas: Arizona Geological Society Digest*, vol. 18, p. 65-80.
- Reynolds, S.J., Spencer, J.E., Asmerom, Y., DeWitt, E. and Laubach, S.E., 1989, Early Mesozoic uplift in west-central Arizona and southeastern California, *Geology*, vol. 17, no. 3, p. 207-211
- Richard, S.M., Stanton N., Boettcher, S.S., Hamilton, W.B., Hoisch, T.D., and Tosdal, R.M., 1994, Mesozoic tectonics of the Maria belt, west-central Arizona and southeastern California, *in* McGill, S.F. and Ross, T.M., *Geological investigations of an active margin: Geological Society of America, 27th Annual Meeting Cordilleran Section Guidebook*, p. 272–291.
- Riggs, N.R., and Busby-Spera, C.J., 1990, Evolution of a multi-vent volcanic complex within a subsiding arc graben depression; Mount Wrightson Formation, Arizona, *Geological Society of America Bulletin*, vol. 102, no. 8, p. 1114-1135
- Rothstein, D.A., and Hoisch, T.D., 1994, Multiple intrusions and low-pressure metamorphism in the central Old Woman Mountains, southeastern California: Constraints from thermal modeling: *Journal of Metamorphic Geology*, v. 12, p. 723–734
- Royse, F., Warner, M.A. and Reese, D.L., 1977 Thrust belt of Wyoming, Idaho and northern Utah: Structural geometry and related stratigraphic problems, *AAPG Bulletin*, vol. 61, no. 8, pp. 1389
- Saleeby, J., 2003, Segmentation of the Laramide Slab — Evidence from the southern Sierra Nevada region: *Geological Society of America Bulletin*, vol. 115, p. 655–668,
- Salem, A.C., 2005, Structural geology and stratigraphy of Paleozoic rocks of the Big Maria syncline, MS thesis, Arizona State University, Tempe, 168 p.
- Salem, A.C., Reynolds, S.J., Geier, J. and Karlstrom, K.E., 2006, Structural evolution of the Big Maria syncline, southeastern California, *Backbone of the Americas* –

- Patagonia to Alaska, Geological Society of America Abstracts with Programs Specialty Meeting no. 2, p. 25
- Salem, A.C, Karlstrom, K.E., Williams, M.L. and Koning, D., 2007, Insights from recent mapping in the Ojo Caliente and La Madera Quadrangles, Tusas Mountains, New Mexico; kinematics, timing and rheology of Proterozoic deformation and fault reactivation: *New Mexico Geology*, vol. 29, no. 2, pp. 58
- Shklanka, R., 1963, Repeated metamorphism and deformation of evaporate-bearing sediments, Little Mara Mountains, California, PhD thesis, Stanford University, Stanford, California, 127 p.
- Simpson, C., 1990, Microstructural evidence for northeastward movement on the Chocolate Mountains fault zone, southeastern California: *Journal of Geophysical Research*, v. 95, p. 529–537
- Simpson, C. and Schmidt, S., 1983, An evaluation of criteria to deduce the sense of movement in sheared rocks: *Geological Society of America*, 94, p. 1281-1288
- Smith, D.L., Miller, E.L., Wyld, S.J. and Wright, J.E., 1993, Progression and timing of Mesozoic crustal shortening in the northern Great Basin, western U.S.A., *in* Dunn, G., and McDougall, K., eds., *Mesozoic Paleogeography of the Western United States – II Pacific section*: Society of Economic Paleontologists and Mineralogists, Book 71, p. 389-406
- Spencer, J.E., 1996, Uplift of the Colorado Plateau due to lithospheric attenuation during Laramide low-angle subduction: *Journal of Geophysical Research*, v. 101, p. 13595–13609
- Spencer, J.E., Peters, L., McIntosh, W.C., and Patchett, P.J., 2001, $^{40}\text{Ar}/^{39}\text{Ar}$ geochronology of the Hualapai Limestone and Bouse Formation and implications for the age of the lower Colorado River, *in* Young, R.A., and Spamer, E.E., eds., *Colorado River—origin and evolution*: Grand Canyon, Ariz., Grand Canyon Association, p. 89–91
- Spencer, J.E., and Reynolds, S.J., 1990, Relationship between Mesozoic and Cenozoic tectonic features in west-central Arizona and adjacent southeastern California: *Journal of Geophysical Research*, vol. 95, no. B1, pp. 539-555
- Spencer, J.E. and Richard, S.M., 2008, Influence of the Maria Fold and Thrust Belt on styles of Oligo-Miocene extension in western Arizona; application of critical taper theory, *Geological Society of America Abstracts with Programs*, vol. 40, no. 1, p. 76

- Spencer, J.E., Richard, S.M., Gehrels, G., Gleason, J.D., and Dickinson, W.R., 2005, Geochronologic and geochemical evidence for extension of the Bisbee Trough to the lower part of the McCoy Mountains Formation in southwestern Arizona, Geological Society of America Abstracts with Programs, GSA National Meeting, Salt Lake City, Utah, Oct. 2005.
- Spencer, J.E., Richard, S.M., and Reynolds, S.J., 1985, Geologic map of the Little Harquahala Mountains, west-central Arizona: Arizona Bureau of Geology and Mineral Technology Open-File Report 85-9, 18 p.
- Stern, S.M., 1998, Timing and nature of deformation in the Riverside Mountains, southeastern California, [Ph.D. thesis]: University of Kansas, Lawrence, 84 p.
- Stewart, J.H., Poole, F.G., Ketner, K.B., Madrid, R.J., Roldán-Quintana, J., and Amaya-Martínez, R., 1990, Tectonics and stratigraphy of the Paleozoic and Triassic southern margin of North America, Sonora, Mexico, *in* Gehrels, G.E. and Spencer, J.E., eds., Geologic excursions through the Sonoran Desert Region, Arizona and Sonora: Arizona Geological Survey Special Paper 7, p. 183-202.
- Stewart, J.H., Poole, F.G. and Wilson, R.F., 1972, Stratigraphy and origin of the Chinle Formation and related Upper Triassic strata in the Colorado Plateau region: USGS Professional Paper 690, 336 p.
- Stock, J.M. and Atwater, T., 1997, Revised Pacific-North America plate reconstructions; implications for Neogene tectonics and volcanism in northwestern Mexico and southern California, *Eos, Transactions, American Geophysical Union*, vol.78, no.46, Suppl., pp.842
- Stone, P., 2006, Geologic map of the west half of the Blythe 30' x 60' quadrangle, Riverside County, California and La Paz County, Arizona, USGS Scientific Investigations Map, Report SIM-2922, 22 p., 1 sheet, 1:100,000
- Stone, P., Howard, K.A., and Hamilton, W., 1983, Correlation of metamorphosed Paleozoic strata of the southeastern Mojave Desert region, California and Arizona: *Geological Society of America Bulletin*, 94 (10), p. 1135-1147.
- Stone, P. and Kelly, M.M., 1989, Geologic map of the Palen Pass quadrangle Riverside County, California, USGS Miscellaneous Field Studies Map, Report MF-2070, 1 sheet, 1:24,000
- Stone, P., Page, V.M., Hamilton, W., and Howard, K.A., 1987, Cretaceous age of the upper part of the McCoy Mountains Formation, southeastern California and

- southwestern Arizona, and its tectonic significance: Reconciliation of paleobotanical and paleomagnetic evidence: *Geology*, 15, p. 561-564.
- Stone, P., and Pelka, G.J., 1989, Geologic map of the Palen-McCoy Wilderness Study Area and vicinity, Riverside County, California: U.S. Geological Survey Miscellaneous Field Studies Map MF-2092, scale 1:62,500
- Svihla, V., 2003, Structural evolution of the east central Big Maria Mountains, Maria fold and thrust belt, southeastern California [M.S. Thesis]: University of Texas, Austin, 134 p.
- Timmons, J. M., Karlstrom, K. E., Heizler, M. T., Bowring, S. A., Gehrels, G. E., and Crossey, L.J., 2005, Tectonic inferences from the ca. 1254–1100 Ma Unkar Group and Nankoweap Formation, Grand Canyon: Intracratonic deformation and basin formation during protracted Grenville orogenesis, *Geological Society of America Bulletin*, v.117, no.11/12, p. 1573 - 1595.
- Tosdal, R.M., 1990, Constraints on the tectonics of the Mule Mountains thrust system, southeast California and southwest Arizona: *Journal of Geophysical Research*, 95, p. 20,025-20,048
- Tosdal, R.M., Haxel, G.B., and Wright, J.E., 1989, Jurassic geology of the Sonoran Desert region, southern Arizona, southeastern California, and northernmost Sonora: Construction of a continental-margin magmatic arc, *in* Jenney, J.P., and Reynolds, S.J., *Geologic evolution of Arizona: Tucson, Arizona, Arizona Geological Society Digest*, vol. 17, p. 397-434.
- Tosdal, R.M., and Stone, P., 1994, Stratigraphic relations and U-Pb geochronology of the Upper Cretaceous upper McCoy Mountains Formation, southwestern Arizona, *Geological Society of America Bulletin*, vol. 106, no. 4, p. 476-491.
- Tucker, R.S., 1980, A reconnaissance study of metamorphism in the Big Maria Mountains, Riverside County, California, MS thesis: San Diego State University, San Diego, CA, 124 p.
- Verges, J., Ramos, E., Seward, D., Busquets, P. and Colombo, F., 2001, Miocene sedimentary and tectonic evolution of the Andean Precordillera at 31 degrees S, Argentina; *Journal of South American Earth Sciences*, vol. 14, no. 7, pp. 735-750.
- Walcott, C.D., 1894, Precambrian igneous rocks of the Unkar Terrane, Grand Canyon of the Colorado in northern Arizona: U.S. Geological Survey 14th Annual Report for 1892/3, part 2, p. 497-519.

- Wells, M.L., Beyene, M.A., Spell, T.L., Kula, J.L., Miller, D.M. and Zanetti, K.A., 2005, The Pinto Shear Zone: A Laramide synconvergent extensional shear zone in the Mojave Desert Region of the southwestern United States, *Journal of Structural Geology*, vol. 27, p. 1697-1720
- Wells, M.L. and Hoisch T.D., 2008, The role of mantle delamination in widespread Late Cretaceous extension and magmatism in the Cordilleran orogen, western United States, *Geological Society of America Bulletin*, vol. 120, no. 5-6, p. 515-530
- Wells, M.L., Spell, T.L., and Grove, M., 2002, Late Cretaceous intrusion and extensional exhumation of the Cadiz Valley batholith, Iron Mountains, southeastern California: *Geological Society of America Abstracts with Programs*, v. 34, no. 6, p. 178.
- Whitmeyer, S.J. and Karlstrom, K.E., 2007, Tectonic model for the Proterozoic growth of North America, *Geosphere*, vol. 3, no. 4, pp. 220-259
- Williams, P.F. and Jiang, D., 2005, An investigation of lower crustal deformation: Evidence for channel flow and its implications for tectonics and structural studies, *Journal of Structural Geology*, vol. 27, p. 1486-1504
- Wooden, J.L., and Miller, D.M., 1990, Chronologic and isotopic framework for early Proterozoic crustal evolution in the eastern Mojave Desert region, SE California, *Journal of Geophysical Research, B, Solid Earth and Planets*, vol. 5, no. 12, p. 20,133-20,146.
- Yeats, K.J., *Geology and structure of the northern Dome Rock Mountains, La Paz County, Arizona [M.S. Thesis]: The University of Arizona, Tucson, 123 p.*
- Yin, A., 2002, Passive-roof thrust model for the emplacement of the Pelona-Orocopia Schist in southern California, United States: *Geology*, v. 30, p. 183–186